**Polymeric depressants for selective mineral flotation and the interaction mechanisms**

by

Duowei Yuan

A thesis submitted in partial fulfillment of the requirements for the degree of

Doctor of Philosophy

In

Chemical Engineering

Department of Chemical and Materials Engineering
University of Alberta

# Abstract

In nature, the molybdenite ores are frequently associated with copper sulfide minerals such as chalcopyrite, and the flotation separation of copper-molybdenum (Cu-Mo) sulfides largely relies on the use of toxic and hazardous depressants such as cyanides, $Na_2S$/NaHS. It is desired to replace these toxic chemicals with more environmentally benign depressants. In addition, talc, a problematic gangue mineral, also frequently occurs in the Cu-Mo sulfide ores. As an inherent hydrophobic magnesium silicate, talc can easily report to the Cu-Mo bulk concentrates in the flotation, reducing the grade of concentrates and strongly affects the subsequent smelting operations. Therefore, economic beneficiation of these Cu-Mo sulfide ores could not be achieved without proper depressants and the efficient removal of talc.

Humic acids (HA), a primary constituent of humic substances or humus (organic fraction of soil), has a wide range of technological and practical applications owing to its abundance and low-cost. In this work, humic acids and its analogues have been studied as depressants for the Cu-Mo sulfides separation and molybdenite-talc separation. The flotation results indicated that HA is a selective depressant for molybdenite while the flotation of chalcopyrite or talc is barely affected. Besides, the depression and adsorption mechanisms of HA were also investigated by a range of different techniques such as zeta potential measurements, infrared spectroscopy, Atomic force microscopy (AFM), X-ray photoelectron spectroscopy (XPS), Time-of-flight secondary ion mass spectrometry

(ToF-SIMS) and Quartz crystal microbalance with dissipation (QCM-D). The experimental results demonstrated that HA strongly adsorbs onto molybdenite basal planes through hydrophobic interaction, while chemical interactions were not involved. In contrast, the adsorption of HA on talc basal planes was hindered by electrostatic repulsion. Besides, HA could also adsorb onto chalcopyrite surfaces, and the interactions are likely to be electrostatic in nature. However, the addition of xanthate collector could potentially desorb the attached HA and restore the floatability of chalcopyrite.

In addition, O-Carboxymethyl chitosan (O-CMC), a derivative of the second most abundant natural polysaccharide—chitin, was also investigated as a depressant for the Cu-Mo sulfides separation. The flotation tests indicate that O-CMC selectively depresses molybdenite during molybdenite-chalcopyrite separation over a broad range of pH. Moreover, the adsorption characteristics and mechanisms of O-CMC on molybdenite and chalcopyrite were systematically investigated by electrokinetic study, infrared spectroscopy, AFM, XPS, and ToF-SIMS characterizations. The experimental results demonstrated that O-CMC adsorbed on both mineral surfaces. However, the interactions between O-CMC and chalcopyrite are mostly weak physical interactions such as electrostatic interaction etc., and the adsorbed O-CMC can be readily removed by rinsing or displaced by xanthate. In comparison, the adsorption of O-CMC on molybdenite basal planes is dictated by hydrophobic attraction and electrostatic repulsion and is barely affected by rinsing or xanthate addition. Therefore, the strong interaction between O-CMC and molybdenite is responsible for the depression of molybdenite and selective

separation of two minerals in the flotation. The research also showed that no strong chemical interactions were involved during the adsorption of O-CMC on both mineral surfaces.

The results of this work shed light on the fundamental understanding of the interaction mechanisms between polymeric depressants and mineral surfaces under different solution conditions, and provided valuable guidance for the selection of polymeric depressants and directions for the development of many other polymeric depressants or flocculants. This research also provides important implications for the beneficiation and separation of many other mineral systems and related technological and industrial processes such as wastewater treatment.

# Preface

Chapter 2 of this thesis has been partially published as Yuan, D.; Xie, L.; Shi, X.; Yi, L.; Zhang, G.; Zhang, H.; Liu, Q.; Zeng, H., "Selective flotation separation of molybdenite and talc by humic substances." *Minerals Engineering* 2018, 117, 34-41. I was responsible for the concept formation, experimental design, data analyses, and manuscript composition. Dr. Lei Xie assisted with AFM imaging and manuscript edits. Dr. Xingwei Shi assisted with the graphs and the manuscript edits. Dr. Longsheng Yi, Dr. Guofan Zhang and Dr. Hao Zhang provided valuable suggestions. Dr. Qi Liu and Dr. Hongbo Zeng contributed to the concept formation, experimental design, as well as manuscript edits.

Chapter 3 of this thesis has been partially published as Yuan, D.; Cadien, K.; Liu, Q.; Zeng, H., "Selective separation of copper-molybdenum sulfides using humic acids." *Minerals Engineering* 2019, 133, 43-46. I was responsible for the concept formation, experimental design, data analyses, and manuscript composition. Dr. Ken Cadien is the supervisory author and was involved in manuscript edits and composition, Dr. Qi Liu and Dr. Hongbo Zeng contributed to the concept formation, experimental design, as well as manuscript edits.

Chapter 4 of this thesis will be submitted for publication as Yuan, D.; Cadien, K.; Liu, Q.; Zeng, H., "Impact of surface hydrophobicity and salinity on the adsorption of humic acids." I was responsible for concept formation, experimental design, data

analyses, and manuscript composition. Dr. Ken Cadien is the supervisory author and was involved in concept formation, experimental design, manuscript edits and composition. Dr. Qi Liu and Dr. Hongbo Zeng contributed to the concept formation, experimental design, as well as manuscript edits.

Chapter 5 of this thesis has been published as Yuan, D.; Cadien, K.; Liu, Q.; Zeng, H., "Flotation separation of Cu-Mo sulfides by O-Carboxymethyl chitosan" *Minerals Engineering* 2019, 134, 202-205; and as Yuan, D.; Cadien, K.; Liu, Q.; Zeng, H., "Adsorption characteristics and mechanisms of O-carboxymethyl chitosan on chalcopyrite and molybdenite" *Journal of Colloid and Interface Science* 2019, 552, 659-670. I was responsible for the concept formation, experimental design, data analyses, and manuscript composition. Dr. Ken Cadien is the supervisory author and was involved in concept formation, experimental design, manuscript edits and composition, Dr. Qi Liu and Dr. Hongbo Zeng contributed to the concept formation, experimental design, as well as manuscript edits.

Chapters 1 and 6 are written by Duowei Yuan and have not been published, but may be published in the future.

# Acknowledgments

I would like to express my sincere gratitude to Dr. Ken Cadien for his inspiring encouragement, solid support, and excellent guidance. I also wish to thank Dr. Hongbo Zeng and Dr. Qi Liu for their helpful suggestions and kind support during my graduate study.

I wish to thank all my group members who helped me in different ways throughout my Ph.D. study. Special thanks are given to Dr. Lei Xie, Dr. Jing Liu, Dr. Min Wu, and Dr. Xingwei Shi for teaching me how to operate AFM. I am very grateful to Dr. Bin Yan who taught me the polymer syntheses, zeta potential measurements, and UV-Vis spectroscopy. Thank Dr. Ling Zhang, Dr. Jing Liu and Mrs. Xiaoqi Deng for the QCM-D training. Thank Dr. Jun Huang who assisted me with the surface modification and AFM force measurements.

I would like to acknowledge Mrs. Ni Yang and Mrs. Nancy Zhang for their assistance in FTIR/TOC training and XRD/XRF training, respectively. I also gratefully acknowledge Dr. Anqiang He and Dr. Shihong Xu for their assistance with XPS and ToF-SIMS measurements.

I also wish to thank the spectacular view of the Rocky Mountains and many kind people I met in Canada.

The financial support from the Natural Sciences and Engineering Research Council of Canada (NSERC) and the China Scholarship Council (CSC) are gratefully acknowledged.

Last but not least, my deepest gratitude goes to my family and my friends; I am forever grateful to my parents and my brother for their love and support.

# Table of Contents

List of Tables ..... xiv

List of Figures ..... xv

List of Acronyms ..... xxiv

Chapter 1. Introduction ..... 1

1.1 Froth flotation ..... 1

1.2 Depressants ..... 4

1.2.1 Inorganic depressants ..... 4

1.2.2 Organic/polymeric depressants ..... 5

1.3 A brief review of polymer adsorption ..... 6

1.3.1 Mechanisms of polymer adsorption ..... 6

1.3.2 Characterization of polymer adsorption ..... 8

1.4 Challenges ..... 13

1.5 Possible solutions ..... 15

1.5.1 Humic acids and its analogues ..... 15

1.5.2 Chitosan and its derivatives ..... 16

1.6 Objective ..... 18

1.7 Structure of the thesis ..... 19

1.8 References ..... 20

Chapter 2. Selective flotation separation of molybdenite and talc by humic substances ..... 30

2.1 Introduction ..... 30
2.2 Materials and methods ..... 32
2.2.1 Materials ..... 32
2.2.2 Methods ..... 34
2.3 Results and discussion ..... 39
2.3.1 Flotation ..... 39
2.3.2 Contact angle measurements ..... 45
2.3.3 Adsorption isotherms ..... 46
2.3.4 Infrared spectroscopy ..... 51
2.3.5 Electrokinetic studies ..... 53
2.3.6 AFM imaging ..... 56
2.4 Conclusions ..... 59
2.5 Acknowledgements ..... 60
2.6 References ..... 61
Chapter 3. Selective separation of copper-molybdenum sulfides using humic acids ..... 71
3.1 Introduction ..... 71
3.2 Materials and methods ..... 72
3.2.1 Materials ..... 72
3.2.2 Methods ..... 74
3.3 Results and discussion ..... 77
3.3.1 Single mineral flotation ..... 77

3.3.2 Mixed minerals flotation ..... 80

3.3.3 Adsorption isotherms ..... 82

3.3.4 Electrokinetic studies ..... 86

3.3.5 Infrared spectroscopy ..... 88

3.3.5 XPS measurements ..... 90

3.3.6 ToF-SIMS measurements ..... 93

3.4 Conclusions ..... 97

3.5 Acknowledgements ..... 99

3.6 References ..... 100

Chapter 4. Impact of surface hydrophobicity and salinity on the adsorption of humic acids ..... 105

4.1 Introduction ..... 105

4.2 Experimental section ..... 106

4.2.1 Materials ..... 106

4.2.2 Surface modification ..... 109

4.2.3 Methods ..... 109

4.3 Results and discussion ..... 113

4.3.1 Substrate Characterization ..... 113

4.3.2 QCM-D Studies ..... 115

4.3.3 Adsorbed layer thickness and contact angles ..... 133

4.4 Conclusions ..... 137

4.5 Acknowledgements ..... 138

4.6 References ..... 139

Chapter 5. Flotation separation of Cu-Mo sulfides by O-Carboxymethyl chitosan and the associated mechanisms ..... 145

5.1 Introduction ..... 145

5.2 Materials and methods ..... 147

5.2.1 Materials ..... 147

5.2.2 Methods ..... 149

5.3 Results and discussion ..... 154

5.3.1 Flotation ..... 154

5.3.2 Electrokinetic studies ..... 159

5.3.3 Infrared spectroscopy ..... 166

5.3.4 AFM imaging ..... 169

5.3.5. XPS analyses ..... 173

5.3.6 ToF-SIMS analysis ..... 183

5.4 Conclusions ..... 187

5.5 Acknowledgements ..... 189

5.6 References ..... 190

Chapter 6. Summary and Future Work ..... 200

6.1 Conclusions ..... 200

6.1.1 Conclusions about HA ..... 200

6.1.2 Conclusions about O-CMC ..... 203

6.2 Original contributions ..... 204

6.3 Future work ..... 205

Bibliography ..... 207

# List of Tables

**Table 2.1**. Adsorption parameters of HA adsorption on molybdenite and talc at T=298.15K, as determined from fitting to Langmuir-Freundlich equation. ..... 49

**Table 3.1**. Adsorption parameters for the adsorption of HA on molybdenite 1 and 2 at T=298.15K, as determined from fitting to Langmuir-Freundlich equation. ..... 85

**Table 4.1**. Adsorption kinetic parameters for HA adsorption on thiol-coated gold surfaces with varying hydrophobicity, as determined from fitting to Langmuir-Freundlich equation. ..... 125

**Table 4.2**. Adsorption kinetic parameters for HA adsorption on thiol-coated gold surfaces of varying hydrophobicity, as determined from fitting to a summation of Langmuir-Freundlich equation and linear equation. ..... 129

**Table 4.3**. Adsorbed HA layer thickness (at 4200 s) of different surfaces after treatment with 20 ppm HA in 0.001 M or 0.1 M KCl solution at pH 3 or pH 9. ..... 134

**Table 4.4**. Contact angles of thiol-coated gold surfaces before and after treatment with 20 ppm HA in 0.001 M or 0.1 M KCl solution at pH 3 or pH 9..... 135

# List of Figures

**Figure 1.1**. Schematic of froth flotation.[6] ..... 2

**Figure 1.2**. A structure model of flotation reagents.[6, 10] ..... 3

**Figure 1.3**. Classification of adsorption isotherms.[50-53] ..... 9

**Figure 1.4**. The surface coverage of a polymer depressant (guar gum) on molybdenite basal planes. (A) AFM height (left) and phase (right) image of bare molybdenite basal plane. (B) AFM height (left) and phase (right) image of molybdenite treated in 1 ppm guar gum solution, with a polymer surface coverage of ~5.6% and a water contact angle of 73°. (C) AFM height (left) and phase (right) image of molybdenite treated in 5 ppm guar gum solution, with a polymer surface coverage of ~44.5% and a water contact angle of 65°. Adapted with permission from literature.[54] Copyright 2017, American Chemical Society. ..... 11

**Figure 1.5**. Schematic of an adsorbed polymer molecule at the mineral surface (Train-loop-tail conformation).[20] ..... 13

**Figure 1.6**. Challenges in talc-molybdenite-chalcopyrite flotation separation. ..... 15

**Figure 1.7**. A hypothetical molecular structure of humic acids (sodium salts).[56] ..... 16

**Figure 1.8**. The molecular structure of (a) Cellulose (b) Chitin (C) Chitosan. ..... 17

**Figure 1.9**. The molecular structure of O-Carboxymethyl chitosan (O-CMC)..... 18

**Figure 2.1**. Schematic of a custom-made Hallimond tube..... 34

**Figure 2.2**. Recovery of talc and molybdenite in 0.001 M KCl solution at pH 9 with the addition of varying HA concentration (i.e., 0 to 20 ppm). Frother: 20 ppm MIBC. .....40

**Figure 2.3**. Recovery of talc and molybdenite with and without the addition of 5 ppm HA at varying pH in 0.001 M KCl solution. Frother: 20 ppm MIBC. .....42

**Figure 2.4**. Flotation recovery of talc and molybdenite from a 1:1 artificial mixture with the addition of 5 ppm HA at varying pH in 0.001 M KCl solution. Frother: 20 ppm MIBC. .....44

**Figure 2.5**. Contact angles of talc and molybdenite particles (size: -150+74 μm) pretreated with varying concentration of HA in 0.001 M KCl at pH 9. .....45

**Figure 2.6**. Adsorption isotherms of HA on talc and molybdenite in 0.001 M KCl at pH 9. (Initial HA concentration was 0, 10, 20, 40, 60, 80, 100, 150, 200 ppm) .....47

**Figure 2.7**. Fitted adsorption isotherms of HA on talc and molybdenite in 0.001 M KCl at pH 9. .....48

**Figure 2.8**. The DRIFT spectra of talc before and after treatment with 500 ppm HA at pH 9 in 0.001 M KCl. .....52

**Figure 2.9**. The DRIFT spectra of molybdenite before and after treatment with 500 ppm HA at pH 9 in 0.001 M KCl. .....53

**Figure 2.10**. Zeta potential of talc, talc + HA, molybdenite and molybdenite + HA at varying pH in 0.001 M KCl solution. .....55

**Figure 2.11**. AFM height images of mineral substrates: (a) freshly cleaved molybdenite surface, (b) freshly cleaved talc surface, (c) molybdenite surface treated with 5 ppm HA

in 0.001 M KCl solution at pH 9, (d) talc surface treated with 5 ppm HA in 0.001 M KCl solution at pH 9, (e) molybdenite surface treated with 5 ppm HA in 0.001 M KCl solution at pH 3, and (f) talc surface treated with 5 ppm HA in 0.001 M KCl solution at pH 3. ...58

**Figure 3.1**. XRD pattern of (a) Molybdenite sample (b) Chalcopyrite sample. .....73

**Figure 3.2**. Flotation recovery of chalcopyrite and molybdenite in 0.001 M KCl solution with various concentration (0 to 40 ppm) of HA at pH 9. Collector: 20 ppm KIBX. Frother: 20 ppm MIBC. .....78

**Figure 3.3**. Flotation recovery of chalcopyrite and molybdenite in 0.001 M KCl solution with and without 20 ppm HA at varying pH. Collector: 20 ppm KIBX. Frother: 20 ppm MIBC. .....80

**Figure 3.4**. Flotation recovery of molybdenite and chalcopyrite from a 1:1 artificial mixture in 0.001 M KCl solution with 10 ppm HA at varying pH. Collector: 20 ppm KIBX. Frother: 20 ppm MIBC. .....81

**Figure 3.5**. Adsorption isotherms of HA on chalcopyrite and molybdenite in 0.001 M KCl at pH 9 (Initial HA concentration was 0, 10, 20, 40, 60, 80, 100, 150, 200, 250 ppm). .....83

**Figure 3.6**. Fitted adsorption isotherms of HA on chalcopyrite and molybdenite in 0.001 M KCl at pH 9. .....84

**Figure 3.7**. Zeta potential of chalcopyrite, chalcopyrite + HA, HA, molybdenite and molybdenite + HA at varying pH in 0.001 M KCl. The zeta potential results of molybdenite and molybdenite + HA are from our previous work.[17] .....88

**Figure 3.8**. The DRIFT spectra of chalcopyrite before and after conditioning in 0.001 M KCl with 500 ppm HA at pH 9. ..... 89

**Figure 3.9**. The DRIFT spectra of molybdenite before and after conditioning in 0.001 M KCl with 500 ppm HA at pH 9. ..... 90

**Figure 3.10**. High-resolution XPS spectra of (a) Mo 3d and (b) S 2p of molybdenite before and after treatment by 20 ppm HA in 0.001 M KCl solution at pH 9. ..... 91

**Figure 3.11**. High-resolution XPS spectra of (a) C 1s and (b) O 1s of molybdenite before and after treatment by 20 ppm HA in 0.001 M KCl solution at pH 9. ..... 92

**Figure 3.12**. Positive-ion images of 86 × 86 $\mu m^2$ of the surface of chalcopyrite–molybdenite mixture (weight ratio of 1:1) treated with 20 ppm HA in 0.001 M KCl solution at pH 9. (a) Image of $Fe^+$ distribution; (b) Image of $Cu^+$ distribution; (c) Image of $Mo^+$ distribution; (d) Image of $C_3H_7^+$ distribution; (e) Image of $C_4H_7^+$ distribution. ..... 94

**Figure 3.13**. Positive ion ToF-SIMS spectra of chalcopyrite–molybdenite mixture (weight ratio 1:1) treated with 20 ppm HA in 0.001 M KCl solution at pH 9. ..... 95

**Figure 3.14**. A simplified schematic diagram of the surface layer composition of chalcopyrite before and after treatment with HA and xanthate. ..... 97

**Figure 4.1**. A theoretical structure of humic acids sodium salts (HA).[1] ..... 107

**Figure 4.2**. Zeta potential of 20 ppm HA in 0.001 M KCl solution at varying pH. ..... 108

**Figure 4.3**. AFM height images and corresponding water contact angles of (a) Bare gold surface (b) $M_{OH}$ =0 gold surface with a contact angle θ =106°; (c) $M_{OH}$ =0.5 gold surface with a contact angle θ =79°; (d) $M_{OH}$ =1 gold surface with a contact angle θ =22°. ..... 114

**Figure 4.4**. Influence of surface hydrophobicity on HA adsorption onto thiol-functionalized gold surfaces in 0.001 M KCl solution at pH 9 (a) $M_{OH}$ =1 gold surface with a contact angle θ =22°; (b) $M_{OH}$ =0.5 gold surface with a contact angle θ =79°; (c) $M_{OH}$ =0 gold surface with a contact angle θ =106°. Frequency change (Δf) and energy dissipation shift (ΔD) recorded at four different overtone number (3, 5, 7, and 9). (d) Summary of the adsorbed mass (at 4200s) of HA layers on gold surfaces; the error bar represents the standard deviation calculated from four different overtone numbers (3, 5, 7, and 9). ..... 117

**Figure 4.5**. Influence of surface hydrophobicity on HA adsorption onto thiol-functionalized gold surfaces in 0.001 M KCl solution at pH 3 (a) $M_{OH}$ =1 gold surface with a contact angle θ =22°; (b) $M_{OH}$ =0.5 gold surface with a contact angle θ =79°; (c) $M_{OH}$ =0 gold surface with a contact angle θ =106°. Frequency change (Δf) and energy dissipation shift (ΔD) recorded at four different overtone number (3, 5, 7, and 9). (d) Summary of the adsorbed mass (at 4200s) of HA layers on gold sensors; the error bar represents the standard deviation calculated from four overtone numbers (3, 5, 7, and 9). ..... 119

**Figure 4.6**. Influence of surface hydrophobicity on HA adsorption onto thiol-functionalized gold surfaces in 0.1 M KCl solution at pH 9 (a) $M_{OH}$ =1 gold surface with a contact angle θ =22°; (b) $M_{OH}$ =0.5 gold surface with a contact angle θ =79°; (c) $M_{OH}$ =0 gold surface with a contact angle θ =106°. Frequency change (Δf) and energy dissipation shift (ΔD) recorded at four different overtone number (3, 5, 7, and 9). (d)

Summary of the adsorbed mass (at 4200s) of HA layers on gold sensors; the error bar represents the standard deviation calculated from four overtone numbers (3, 5, 7, and 9). ..... 122

**Figure 4.7**. Adsorption isotherms (mass versus time) of 20 ppm HA on surfaces with varying hydrophobicity in 0.001 M KCl solution at pH 3. Solid lines represent fits to Langmuir-Freundlich model. The $R^2$ values for the fits are as follows: 0.993 for $M_{OH}$= 0; 0.981 for $M_{OH}$= 0.5; 0.923 for $M_{OH}$= 1 in the first 1200s of adsorption. ..... 124

**Figure 4.8**. Adsorption kinetic data for 20 ppm HA adsorption on gold surfaces with varying hydrophobicity in 0.1 M KCl solution at pH 9. Solid lines represent fits to a summation of Langmuir-Freundlich equation and linear equation. The $R^2$ values for the fits are as follows: 0.992 for $M_{OH}$= 0; 0.993 for $M_{OH}$= 0.5; 0.982 for $M_{OH}$= 1..... 128

**Figure 4.9**. Influence of surface hydrophobicity on $\Delta f/\Delta D$ recorded at overtone number n=7 in 0.001 M KCl solution with 20 ppm HA at pH 3. ..... 131

**Figure 4.10**. Influence of surface hydrophobicity on $\Delta f/\Delta D$ recorded at overtone number n=7 in 0.1 M KCl solution with 20 ppm HA at pH 9. ..... 133

**Figure 5.1**. The molecular structure of O-Carboxymethyl chitosan (O-CMC)..... 149

**Figure 5.2**. Recovery of chalcopyrite and molybdenite in 0.001 M KCl solution at pH 9 under various concentrations (i.e., 0 to 200 ppm) of O-CMC. Collector: 20 ppm KIBX. Frother: 20 ppm MIBC. ..... 155

**Figure 5.3**. Recovery of chalcopyrite and molybdenite with and without the addition of 150 ppm O-CMC at varying pH in 0.001 M KCl solution. Collector: 20 ppm KIBX. Frother: 20 ppm MIBC. ..... 157

**Figure 5.4**. Flotation recovery of chalcopyrite and molybdenite from artificial molybdenite-chalcopyrite mixtures (weight ratio: 1:1) in 0.001 M KCl solution with the addition of 150 ppm O-CMC at varying pH. Collector: 20 ppm KIBX. Frother: 20 ppm MIBC. ..... 158

**Figure 5.5**. Zeta potential of aged chalcopyrite (exposed in air for ~30 minutes after grinding), fresh ground chalcopyrite, chalcopyrite + O-CMC, O-CMC, molybdenite (data from our previous work[38]), and molybdenite + O-CMC at varying pH in 0.001 M KCl solution. ..... 161

**Figure 5.6**. A simplified depiction of the surface layer composition of chalcopyrite upon slight oxidation. ..... 163

**Figure 5.7**. The DRIFT spectra of O-CMC, O-CMC treated chalcopyrite, and chalcopyrite (chalcopyrite spectrum data from our previous work[38]). ..... 167

**Figure 5.8**. The DRIFT spectra of O-CMC, O-CMC treated molybdenite, and molybdenite (molybdenite spectrum data from our previous work[38]). ..... 168

**Figure 5.9**. AFM height, cross-section and phase images ($2 \times 2$ $\mu m^2$) of molybdenite basal planes before and after treatment with 150 ppm O-CMC in 0.001 M KCl solution at pH 9. (A) freshly exfoliated molybdenite surface; (B) cross-section line profile of fresh molybdenite surface; (C) phase image of fresh molybdenite surface; (D) molybdenite

surface treated with O-CMC; (E) cross-section line profile of molybdenite surface treated with O-CMC; (F) phase image of molybdenite surface treated with O-CMC. ..... 170

**Figure 5.10**. AFM height, cross-section and phase images (2 × 2 $\mu m^2$) of chalcopyrite surfaces before and after treatment with 150 ppm O-CMC in 0.001 M KCl solution at pH 9. (A) freshly polished chalcopyrite surface; (B) cross-section line profile of fresh chalcopyrite surface; (C) phase image of fresh chalcopyrite surface; (D) chalcopyrite surface treated with O-CMC; (E) cross-section line profile of chalcopyrite surface treated with O-CMC; (F) phase image of chalcopyrite surface treated with O-CMC..... 172

**Figure 5.11**. High-resolution (a) C 1s (b) N 1s (c) O 1s XPS spectrum of as-received O-CMC. ..... 174

**Figure 5.12**. High-resolution (a) C 1s (b) N 1s (c) O 1s XPS spectra of molybdenite before (bottom) and after O-CMC treatment (top). ..... 176

**Figure 5.13**. High-resolution (a) Mo 3d (b) S 2p XPS spectra of Molybdenum disulfide before (top) and after O-CMC treatment (bottom). ..... 177

**Figure 5.14**. High-resolution (a) C 1s (b) N 1s (c) O 1s XPS spectra of chalcopyrite before (bottom) and after O-CMC treatment (top). ..... 179

**Figure 5.15**. High-resolution (a) Cu 2p (b) Fe 2p (c) S 2p XPS spectra of chalcopyrite before (top) and after O-CMC treatment (bottom). ..... 181

**Figure 5.16**. Positive-ion images of 86 × 86 $\mu m^2$ of the surface of chalcopyrite–molybdenite mixture (weight ratio of 1:1) treated with 150 ppm O-CMC in 0.001 M KCl solution at pH 9. (A) Image of $^{56}Fe^+$ distribution; (B) Image of $^{63}Cu^+$ distribution; (C)

Image of $^{65}Cu^{+}$ distribution; (D) Image of $^{98}Mo^{+}$ distribution; (E) Image of $^{96}Mo^{+}$ distribution; (F) Image of $^{95}Mo^{+}$ distribution; (G) Image of $^{12}CH_4N^{+}$ distribution; (H) Image of $^{14}NH_4^{+}$ distribution. ..... 185

**Figure 5.17**. A simplified schematic diagram of the surface layer composition of chalcopyrite after treatment with O-CMC and water rinsing. ..... 187

# List of Acronyms

| | |
|---|---|
| **HA** | Humic acids or Humic acids sodium salts |
| **O-CMC** | O-Carboxymethyl chitosan |
| **KIBX** | Potassium isobutyl xanthate |
| **MIBC** | 4-Methyl-2-pentanol |
| **AAS** | Atomic absorption spectrometry |
| **XRD** | X-ray powder diffraction |
| **AFM** | Atomic force microscopy |
| **rms** | root-mean-square |
| **FTIR** | Fourier transform infrared spectroscopy |
| **DRIFT(S)** | Diffuse reflectance infrared Fourier transform (spectroscopy) |
| **XPS** | X-ray photoelectron spectroscopy |
| **ToF-SIMS** | Time of flight secondary ion mass spectrometry |
| **QCM-D** | Quartz crystal microbalance with dissipation |
| **IEP** | Isoelectric point |
| **PZC** | Point of zero charge |
| **Cu-Mo** | Copper-Molybdenum |
| **vdW** | van der Waals |

# Chapter 1. Introduction

## 1.1 Froth flotation

Flotation, generally referred to as froth flotation, is recognized as the most widely used and versatile mineral processing technique. Originally patented in 1906, flotation has been adopted in the beneficiation and separation of low-grade and complex ores for over a hundred years. As a selective and cost-effective process, flotation utilizes the surface property differences between valuable minerals and gangue minerals to achieve effective separation and concentration.[1-6]

Based on the differences in the interaction between mineral particles and air bubbles during flotation, the hydrophobic or hydrophobized mineral particles, usually the valuable minerals, will more readily attach to air bubbles in the mineral suspension due to the attractive hydrophobic interaction, and then transported to the froth phase for recovery. While the hydrophilic or hydrophilized mineral particles, mostly the gangue minerals, will remain in the pulp or slurry as tailings. The schematic of the flotation process is shown in **Figure 1.1**.

However, due to the hydrophilic nature of most minerals, selective separation of valuable and gangue minerals would not automatically take place without the addition of proper flotation reagents.[7] Generally, three types of flotation reagents, including collectors, frothers and regulators, are routinely used to modify the surface properties of minerals and achieve selective separation.

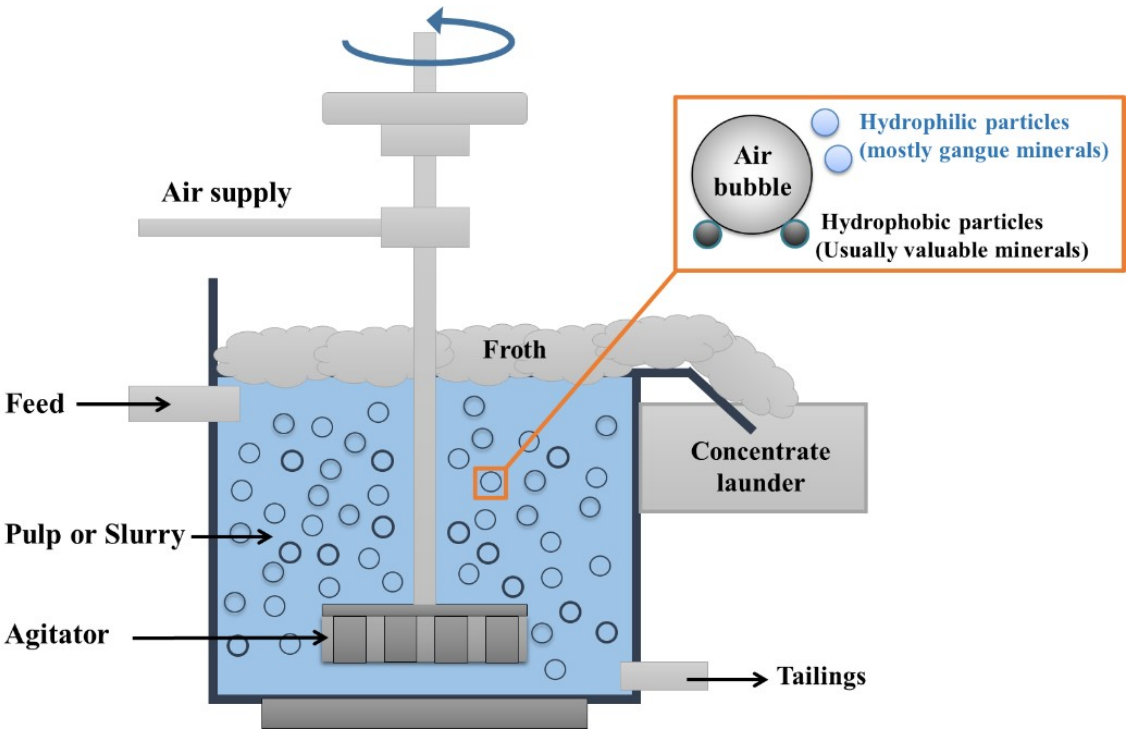


**Figure 1.1**. Schematic of froth flotation.[6]

Specifically, collectors are mostly bipolar organic compounds to induce and/or enhance the surface hydrophobicity of valuable minerals by adsorbing onto mineral surfaces. Frothers are usually heteropolar surfactants added to stabilize the air bubbles and froth layers as well as control the bubble size during flotation.[8, 9] Regulators (or modifiers) are used in flotation to modify the action of collectors and minerals, and it can be further classified into activators, depressants, and pH regulators. Activators are chemical compounds that can impart hydrophobicity to the minerals by promoting collector-mineral interactions or altering the surface chemistry of minerals, although they usually do not make the mineral surface hydrophobic themselves after adsorption. In contrast, depressants are extensively used in flotation to prevent unwanted minerals from

floating by rendering them hydrophilic, making the flotation separation more efficient and effective.[6, 8] A schematic depiction of the molecular structures of conventional flotation reagents is shown in **Figure 1.2**.

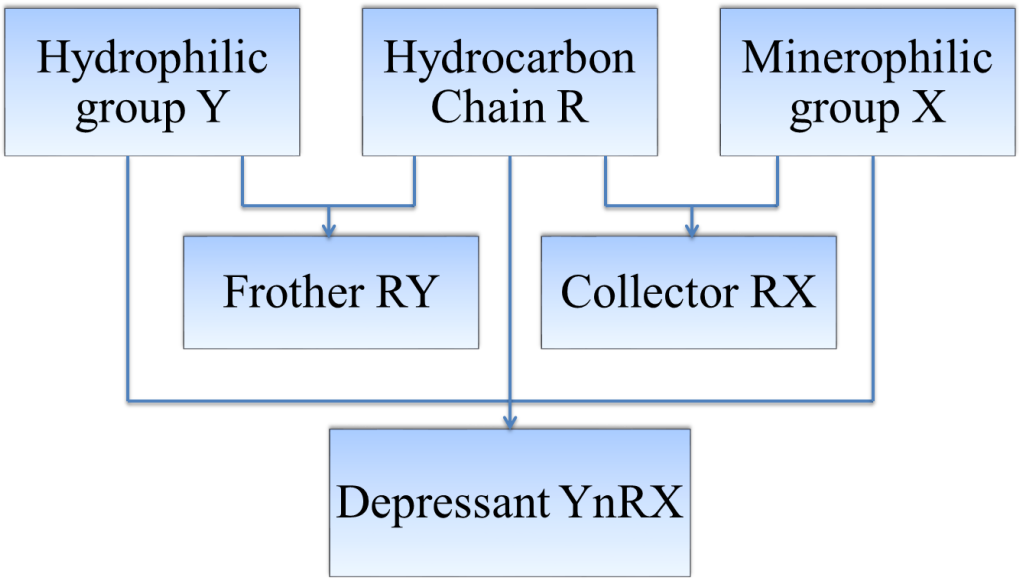


**Figure 1.2**. A structure model of flotation reagents.[6, 10]

Unfortunately, in many cases, naturally hydrophobic gangue minerals such as talc are almost inevitably floated into concentrates during the flotation process, reducing concentrate grades and significantly affects subsequent smelting operations. In extreme cases, this could render the mineral concentrates unacceptable by the smelters, resulting in significant losses to the mining companies.[11] Therefore, the efficient depression or removal of talc is critical to the economical processing of many complex sulfide ores such as the molybdenum ores, copper-molybdenum sulfide ores and the ores of platinum group metals (PGM).[12]

## 1.2 Depressants

Depressants play a principal role in the depression of gangue minerals such as talc and purification of bulk concentrates during the flotation process. Over the past several decades, a large number of depressants including inorganic[13-17] and organic/polymeric depressants[18-23] have been extensively used to remove the gangue minerals, such as talc, from the concentrates or purify the concentrates. In many cases, the cost of depressants can exceed that of any other types of flotation reagents,[22] yet the basic understanding of their depression behaviors and interaction mechanisms remains limited, making the depression of the gangue minerals more challenging to control compared with other types of processes in mineral flotation.[6, 24, 25]

### 1.2.1 Inorganic depressants

Inorganic depressants are undoubtedly the most widely used depressants in the mineral processing industry, most of which are water soluble salts such as sodium silicate or "water glass" ($Na_2SiO_3$), sodium carbonate ($Na_2CO_3$), zinc sulfate ($ZnSO_4$), and aluminum sulfate $Al_2(SO_4)_3$. Conventionally, these inorganic depressants are added in different combinations to enhance the depression effect of gangue as well as regulate the pH of the pulp.[13] However, the depression mechanisms of different combinations of inorganic depressants are still poorly understood. Some studies have shown that metal cations can depress the floatability of siliceous minerals (e.g., talc) during flotation due to their interaction with the mineral surfaces.[13-15, 17, 19] However, it should be noted that the

adsorption of metal ions on mineral surfaces is typically through the hydroxyl complexes of the metal ions due to electrostatic interactions, and then the adsorbed hydroxyl complexes render the mineral surface hydrophilic.[14, 15] However, the adsorbed metal hydroxyl complexes are also often the adsorption centers for collectors, which is why many metal ions also act as activators in mineral flotation.[26-28] Therefore, precautions should be taken when using metallic inorganic depressants in mineral flotation.

### 1.2.2 Organic/polymeric depressants

Compared with the widely used inorganic depressants, polymeric depressants have the advantage of being less toxic and environmentally friendly, therefore, their application in mineral processing industry is increasing.[6, 26] Typically, organic/polymeric depressants are more efficient than the inorganic depressants and can be used under various solution conditions,[29] or modified for selective adsorption.[20, 30]

Common organic depressants used for talc and/or other mineral depression are natural or synthetic polysaccharides such as carboxymethyl cellulose,[7, 17-19, 31-34] guar gum,[18, 21, 35, 36] dextrins,[37-42] lignosulphonates,[43] and synthetic polyacrylamides.[11, 44, 45] Natural polysaccharides have been widely used for several decades primarily because they are inexpensive and widely available.

In terms of polymeric depressants, there are several possible depression mechanisms by which they prevent unwanted minerals from floating, and some of which are listed as follows:

(1) Depressants are able to adsorb onto and/or interact with mineral surfaces directly, making the mineral surface hydrophilic and/or preventing the adsorption of collectors on the mineral surfaces, resulting in the depression of unwanted minerals.

(2) Some depressants (especially the large molecular weight polymers) can depress certain minerals regardless of how well the collectors react with minerals. By adsorbing on the mineral surfaces, these depressants can cover the collectors and create hydrophilic films on the surfaces, rendering the minerals hydrophilic.[8]

Overall, no matter what the actual depression mechanisms are, the successful adsorption of polymeric depressants onto mineral surfaces is critical to their depression performance.

## 1.3 A brief review of polymer adsorption

### 1.3.1 Mechanisms of polymer adsorption

Polymer adsorption on mineral surfaces is driven by the reduction of free energy, in other words, attractive interactions or attractive forces.[20] The interactions between polymeric depressants and mineral surfaces are comprised of physical and chemical interactions, or a combination of them. The typical interactions involved are listed as follows:

(a) Electrostatic interactions: such as the adsorption of polyelectrolytes onto surfaces of opposite charge. The electrostatic interactions can be both attractive and repulsive depending on the charge properties of polyelectrolytes and surfaces.

(b) Hydrophobic interaction: the tendency of nonpolar molecules/substances (or groups on polymers) to escape from the aqueous environment and adhere to other nonpolar species.[5, 8, 46]

The origin of hydrophobic interaction is not clearly understood and still under debate, in spite of the numerous studies carried out over the last several decades.[47] However, it is widely accepted that hydrophobic interaction has an entropic origin and typically much stronger than van der Waals force.[5, 47]

(c) Hydrogen bonding: hydrogen bonding is essentially a very strong dipole-dipole interaction or a subtype of electrostatic interaction. When a hydrogen atom is connected with a strongly electronegative atom (such as O, N, and F); the hydrogen atom is able to interact with nonbonding electron pairs on other such electronegative atoms.[5, 8]

In many early reports, hydrogen bonding has been claimed to be the primary interaction mechanism between polysaccharides and mineral surfaces without strong evidence.[8] However, it should be noted that polysaccharides could also form hydrogen bonds with surrounding water molecules in aqueous solutions. Hence, the formation of hydrogen bonds between polymers and mineral surfaces requires the breakdown of existing hydrogen bonds. It is therefore questionable to take hydrogen bonding as the dominant adsorption mechanism in aqueous solutions.[8, 48]

(d) van der Waals (vdW) forces: essentially interactions within or between dipoles and/or induced dipoles.[5] The van der Waals interactions are usually not as strong as

electrostatic or hydrophobic interactions, but they are always present in the systems and cannot be neglected under certain circumstances.[5]

(e) Chemical interactions: polymer groups react with the solid surfaces and result in the formation of covalent bonds or complex.[46] The free energy change (or heat of adsorption) of chemisorption is typically larger than 50 KJ/mol, and usually around 100~300 KJ/mol.[49, 50]

### 1.3.2 Characterization of polymer adsorption

#### 1.3.2.1 The adsorption isotherms

The adsorption isotherm is defined as the adsorption density of a polymer on the solid surface versus the equilibrium concentration of the polymer in the solution at a constant temperature. The slope and shape of the isotherms are affected by the properties of the system, and the Gibbs free energy change of adsorption can indicate the mechanisms of the adsorption process.[20]

Based on the interaction mechanisms of the adsorption process, the adsorption can be classified into two types: physical adsorption and chemical adsorption. In physical adsorption, no electrons transfer would take place, while in chemical adsorption; transfer of electrons typically occurs during the adsorption process.[50] According to Giles *et al.* (1960, 1974) classification, four classes of adsorption isotherms have been recognized based on the initial part of the isotherms, as shown in **Figure 1.3**. Each class has subgroups, which related to the behavior at higher concentrations.[50]

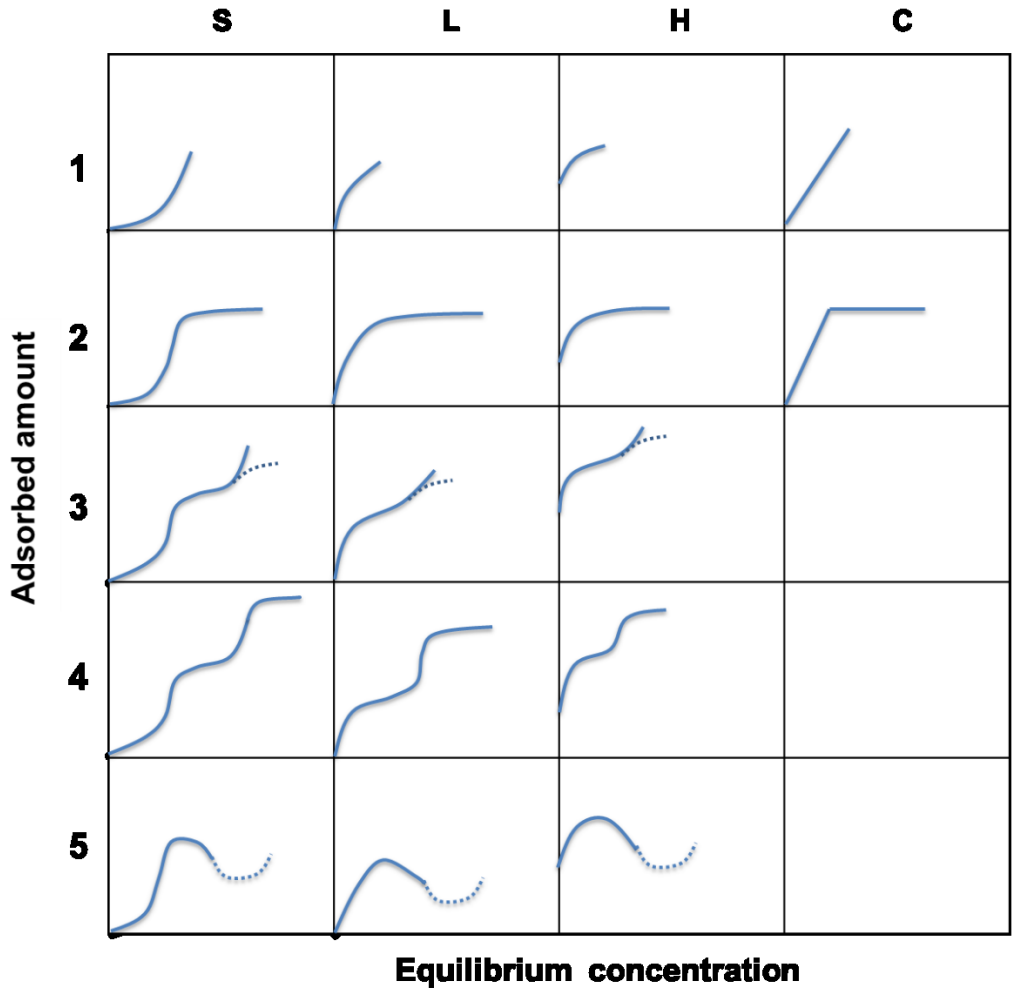


**Figure 1.3**. Classification of adsorption isotherms.[50-53]

The four main classes of adsorption isotherms as shown in **Figure 1.3** are named the S, L (Langmuir type), H (high affinity), and C (constant partition) isotherms, among which the L (Langmuir) class is the most common and best-known isotherm. The characteristic feature of Langmuir adsorption isotherms is an initial region concave to the equilibrium concentration axis. The L2 isotherm reaches a plateau when increase the

solution concentration, indeed the L2 adsorption isotherm probably represents the majority of cases of adsorption from dilute solution.[50, 51]

The H (high affinity) type of isotherms has an initial portion that almost overlaps the ordinate, showing extremely strong adsorption at low concentration,[50] which indicates chemical interactions may be involved during the adsorption process. However, it should be noted that one cannot determine if the adsorption is chemisorption or physisorption simply based on the shapes of the isotherms. The other classes of isotherms are less common and some of them have not been experimentally observed, thereby were not discussed in this work.

1.3.2.2 Polymer surface coverage

The polymer surface coverage strongly affects the depression performance of a depressant.[39] Typically, with increasing polymer surface coverage, the hydrophobicity (or water contact angle) and floatability (or flotation recovery) of minerals will decrease if the polymer chains contain a large number of hydrophilic groups such as hydroxyls. Hence, polymer depressants with larger surface coverage usually possess stronger depression effect, and this trend was observed in single and mixed mineral talc and chalcopyrite flotation,[33] as well as in the flotation of molybdenite.[54]

The morphology of mineral surfaces before and after polymer treatment and the polymer surface coverage can be determined by AFM imaging and related image processing software. **Figure 1.4** shows typical images of molybdenite basal planes before

and after polymer (guar gum) treatment and the corresponding polymer surface coverage. The Igor Pro software was used to assess the height of the polymer domains and estimate the polymer surface coverage in the AFM images.

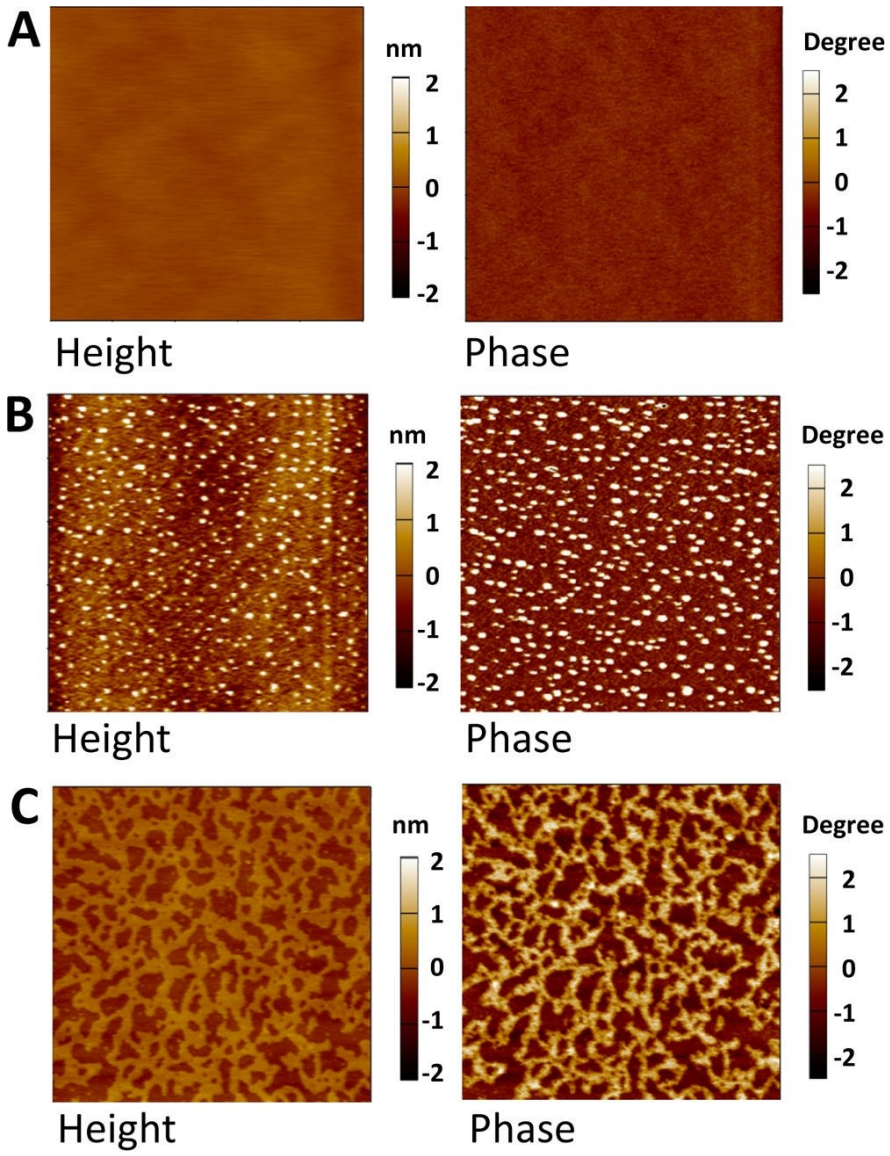


**Figure 1.4**. The surface coverage of a polymer depressant (guar gum) on molybdenite basal planes. (A) AFM height (left) and phase (right) image of bare molybdenite basal plane. (B) AFM height (left) and phase (right) image of molybdenite treated in 1 ppm guar gum solution, with a polymer surface coverage of ~5.6% and a water contact angle

of 73°. (C) AFM height (left) and phase (right) image of molybdenite treated in 5 ppm guar gum solution, with a polymer surface coverage of ~44.5% and a water contact angle of 65°. Adapted with permission from literature.[54] Copyright 2017, American Chemical Society.

As can be seen, the freshly exfoliated molybdenite basal plane is hydrophobic with a water contact angle of 75° and slightly decreased to 73° after treatment in 1 ppm polymer solution. Further increasing the polymer concentration to 5 ppm reduces the water contact angle to 65°.[54] Overall, the polymer surface coverage increased with increasing polymer concentration, and the corresponding water contact angle decreases with increasing polymer surface coverage. The Cassie−Baxter equation (equation 1.1),[5] could be employed to predict the polymer surface coverage ($\phi$) on the mineral surfaces based on the water contact angles ($\theta$) and vice versa.

$$\cos\theta = \phi \cdot \cos\theta_{\min-poly} + (1-\phi) \cdot \cos\theta_{\min} \quad (1.1)$$

Where $\theta_{min}$ and $\theta_{min\text{-}poly}$ correspond to the water contact angle of pure mineral surface and the mineral surface fully covered by polymers.[54] However, it should be noted that this equation and the above AFM imaging technique might not be applicable to certain minerals and/or depressants, due to the fact that some minerals do not have smooth cleavage planes, etc.

1.3.2.3 The adsorbed layer thickness

The adsorbed layer thickness is another important parameter to characterize the adsorbed polymer layer, which is strongly affected by the adsorbed polymer conformation. The conformation of adsorbed polymers can also influence the adsorption density of polymers and adsorption isotherms. Typically, in dilute solutions, polymer molecules tend to have relatively flat conformation with fewer loops and tails, while in concentrated polymer solutions, the adsorbed layer thickness is more likely to increase due to the formation of more loops and tails.[20, 55]

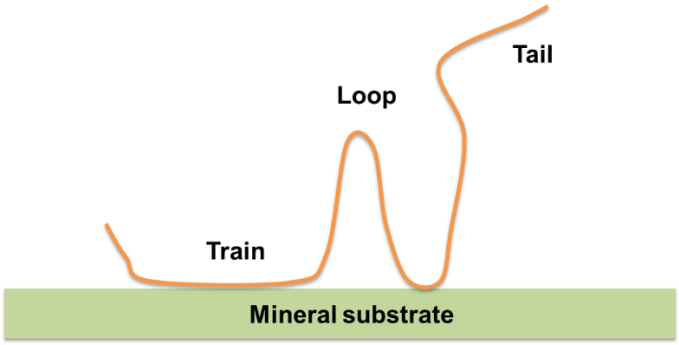


**Figure 1.5**. Schematic of an adsorbed polymer molecule at the mineral surface (Train-loop-tail conformation).[20]

## 1.4 Challenges

As shown in **Figure 1.6**, talc is one of the most common hydrophobic gangue minerals encountered in complex sulfide ores, especially in copper-molybdenum sulfide ores. Economic separation and beneficiation of these copper-molybdenum sulfide ores could not be achieved without the removal or depression of talc. In addition, the separation of copper-molybdenum sulfides is also a challenging issue in the mineral

industry. Therefore, the use of proper depressants is critical to the processing and beneficiation of these ores.

The widely used inorganic depressants for sulfides separation are toxic and hazardous; hence, the application of polymeric depressants is growing. Most of the extensively used polymeric depressants are natural polymers such as carboxymethyl cellulose, guar gum, and dextrin, mainly due to their low cost and widespread availability. However, it should be noted that these natural polysaccharides also suffer from some drawbacks, including uncertain chemical compositions depending on sources, lack of selectivity, and inconsistent performance.[20] Considering the disadvantages of natural polysaccharides, synthetic polymers have also drawn considerable attention. Correctly synthesized polymeric depressants could often show better selectivity and efficiency.

However, most of the synthetic polymers are expensive, non-biodegradable, and can make the reuse of recycled water problematic in the flotation process. Hence, new and biodegradable depressants derived or modified from natural polysaccharides for the mineral processing industry, especially for the talc-molybdenite-chalcopyrite flotation separation, are of great fundamental and practical importance. Since there are numerous natural polysaccharides or macromolecules in nature, there must be some non-toxic, biodegradable and eco-friendly polymeric depressants originate from natural polymers for the mineral flotation separation.

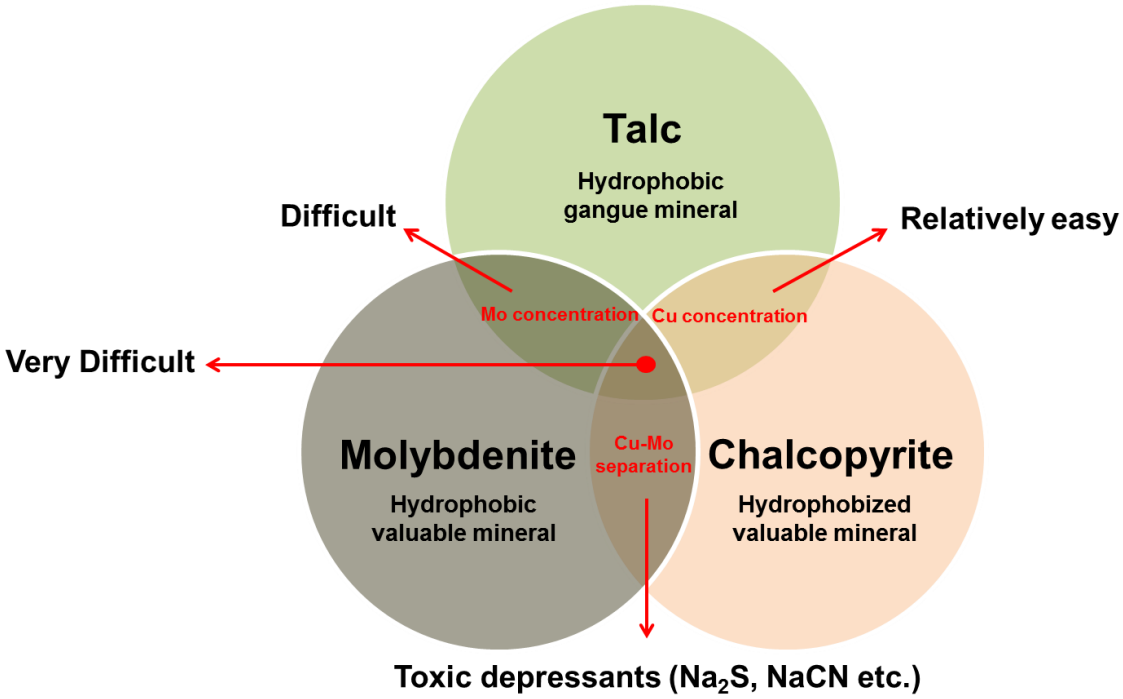


**Figure 1.6**. Challenges in talc-molybdenite-chalcopyrite flotation separation.

## 1.5 Possible solutions

### 1.5.1 Humic acids and its analogues

Humic acids (HA) are the primary organic constituents of humus or soil, and widely exist in dystrophic lakes, rivers, seawater, and even industrial process water.[56, 57] As one of the most abundant naturally occurring organic macromolecules, humic acids are produced by the microbial decomposition of vegetation, animals, and microorganisms and subsequent polymerization and condensation of the biodegradation products.[56] As a result, HA contains both aliphatic chains and aromatic rings (hydrophobic moieties), in which carboxyl groups, phenolic –OH groups and –N–, –O– bridging atoms (hydrophilic moieties) randomly distributed, as demonstrated in **Figure 1.7**.

In addition, HA is strongly negatively charged over a broad range of pH. The hydrocarbon chains and aromatic rings of HA may originate from the lignin and microbial degradation, which contribute to its hydrophobicity under a certain pH range.[56] The major advantages of HA are its low-cost, abundance, and non-toxicity, making it suitable as flotation depressants. However, the chemical composition of humic acids is uncertain and may vary from source to source.

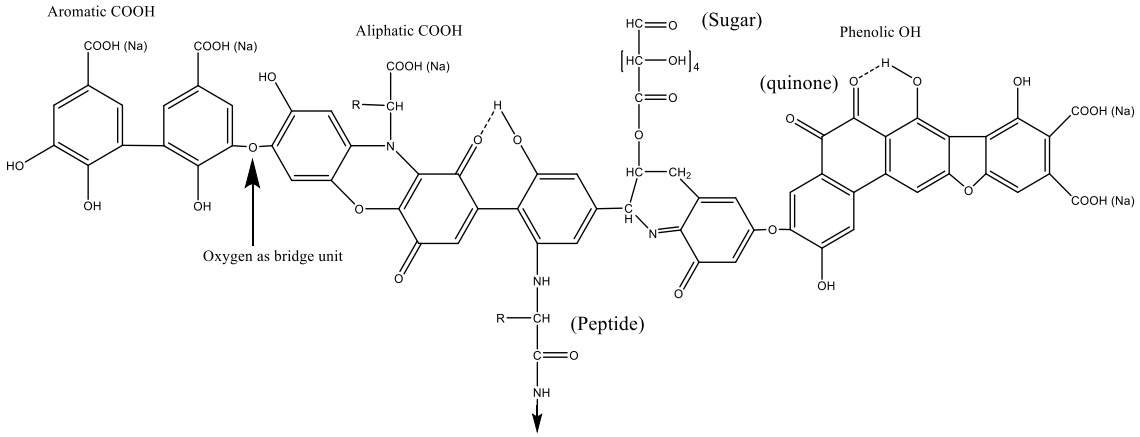


**Figure 1.7**. A hypothetical molecular structure of humic acids (sodium salts).[56]

### 1.5.2 Chitosan and its derivatives

Chitosan, a cationic copolymer of D-glucosamine and N-acetyl-D-glucosamine, is produced by the deacetylation of a natural polysaccharide—chitin.[8, 58-62] Chitin, as the second most abundant natural polymer in the world after cellulose, can be readily obtained from crab or shrimp shells and fungal mycelia.[60] The structures of cellulose, chitin, and chitosan are shown in **Figure 1.8** (a), (b), and (c), respectively.

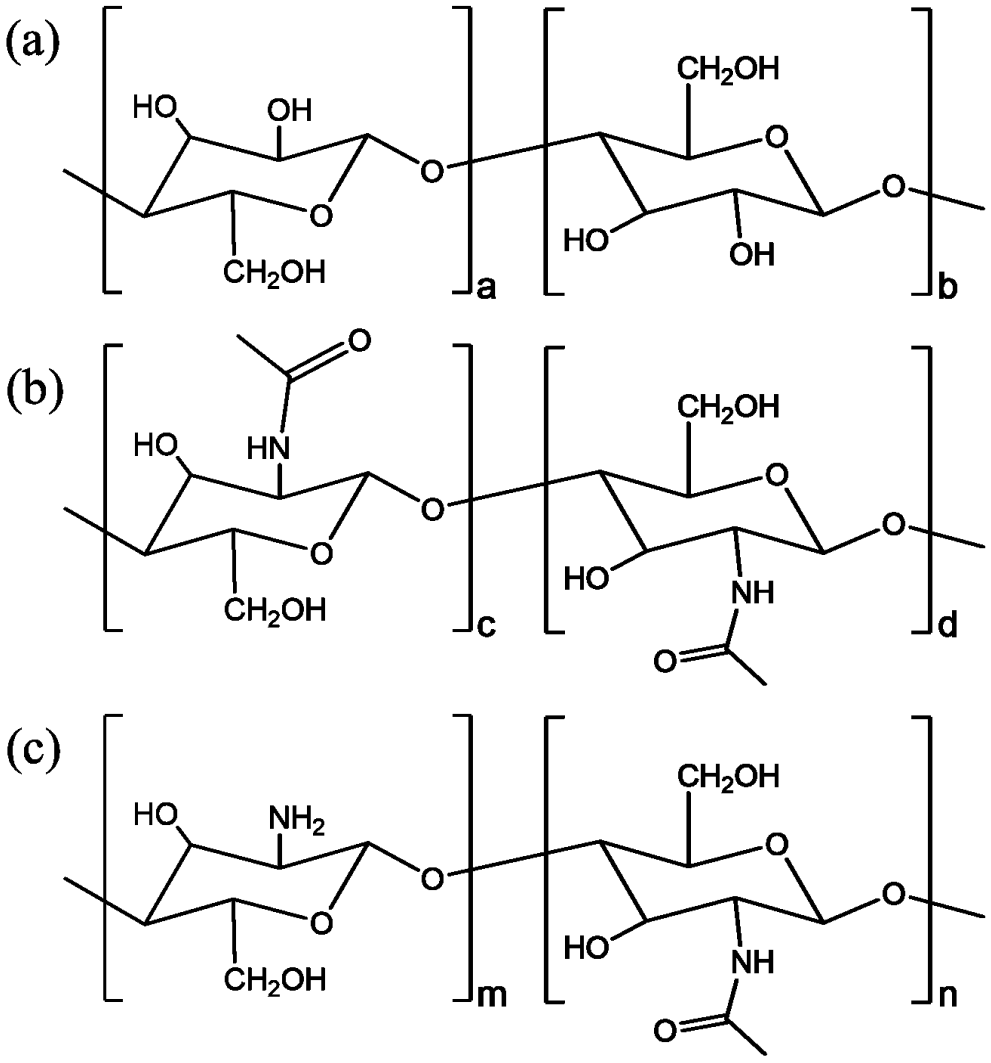


**Figure 1.8**. The molecular structure of (a) Cellulose (b) Chitin (C) Chitosan.

As can be seen, chitosan, chitin, and cellulose have similar chemical structures, and chitin can be regarded as cellulose with hydroxyl groups on C-2 replaced by acetamido group, while chitosan is the N-deacetylated derivative of chitin.[60] For chitosan, the hydroxyl groups and amino groups on the glucosamine provide possible reaction sites for the formation of metal complexes and the substitution of new functional groups,[8, 63] while

the large number of hydrophilic groups of chitosan enables it to possess adequate depression effect.

However, the polymeric depressants used for mineral flotation are typically non-ionic or anionic, while cationic polymers like chitosan are rarely directly used in the mineral processing industry owing to their poor selectivity.[20] The consideration is that most mineral particles, including valuable and gangue minerals, are negatively charged under mild alkaline conditions where industrial flotation is typically performed; thus the cationic polymers will unselectively adsorb onto negatively charged particles due to electrostatic attraction. Therefore, in this work, a novel and biodegradable anionic polymer derived from chitosan, i.e., O-Carboxymethyl chitosan (O-CMC), is investigated as a depressant. The chemical structure of O-CMC is shown in **Figure 1.9**.

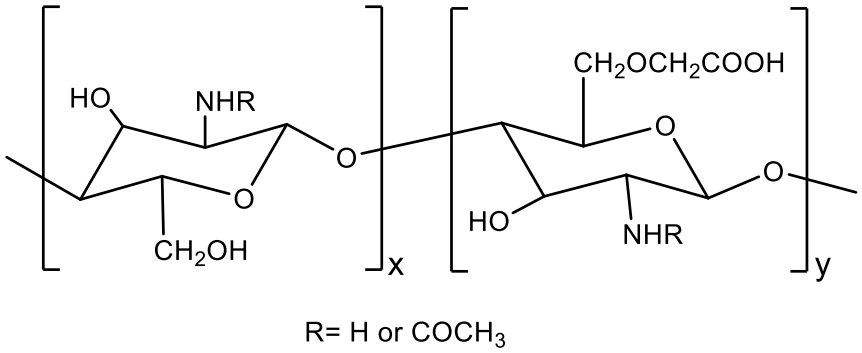


**Figure 1.9**. The molecular structure of O-Carboxymethyl chitosan (O-CMC).

## 1.6 Objective

This research is aimed at developing non-toxic, selective and biodegradable polymeric depressants derived from chitosan and/or other natural polymers or

macromolecules such as humic acids for mineral flotation, particularly for the flotation separation of talc, molybdenite, and chalcopyrite. The interaction and adsorption mechanisms between selected depressants and mineral surfaces are also investigated. The detailed objectives are listed as follows:

(1) Investigate the flotation response of single minerals (e.g., talc, molybdenite, and chalcopyrite) in the presence of various polymeric depressants, to improve the depression effect of unwanted minerals such as talc, and study the adsorption characteristics of polymeric depressants on mineral surfaces.

(2) Optimize the types of polymeric depressants and flotation conditions, and evaluate the selectivity of selected depressants towards artificial mineral mixtures (talc, molybdenite, and chalcopyrite) under different solution conditions.

(3) Elucidate the interaction mechanisms between selected polymeric depressants and mineral surfaces under various pH and ionic strength, further confirm the proposed interaction mechanisms using model hydrophobic surfaces and/or polymeric depressants.

## 1.7 Structure of the thesis

Chapter 1 introduces the basic principles and reagents in mineral flotation, especially the depressants and associated depression/adsorption mechanisms, as well as the remaining challenges. The potential polymers for the mineral flotation separation and the objectives of this research are also presented.

Chapter 2 illustrates the flotation separation of molybdenite and talc using humic acids and the adsorption mechanisms of humic acids on both minerals. The adsorption mechanisms of humic acids on both minerals were also investigated and discussed.

Chapter 3 investigates the application of humic acids in the flotation separation of copper-molybdenum sulfides. The adsorption characteristics of humic acids on molybdenite and chalcopyrite and the possible interaction mechanisms were also reported.

Chapter 4 demonstrates the impacts of surface hydrophobicity and salinity on the adsorption characteristics and kinetics of humic acids.

Chapter 5 studies the feasibility of O-CMC as a selective depressant during the flotation separation of copper-molybdenum sulfides. The adsorption characteristics and mechanisms of O-CMC on both mineral surfaces were also systematically studied.

Chapter 6 presents the major conclusions of this work and the original contributions. The directions for future work are also suggested.

## 1.8 References

1. Klassen, V. I.; Mokrousov, V. A., *An introduction to the theory of flotation*. Butterworths: 1963.

2. Fuerstenau, M. C.; Miller, J. D.; Kuhn, M. C., *Chemistry of flotation*. Society for Mining Metallurgy: 1985.

3. Fuerstenau, M. C., *Principles of mineral processing*. SME: 2003.

4. Fuerstenau, M. C.; Jameson, G. J.; Yoon, R.-H., *Froth flotation: a century of innovation*. SME: 2007.

5. Israelachvili, J. N., *Intermolecular and surface forces: revised third edition*. Academic press: 2011.

6. Wills, B. A., *Wills' mineral processing technology: an introduction to the practical aspects of ore treatment and mineral recovery*. Butterworth-Heinemann: 2011.

7. Kor, M.; Korczyk, P. M.; Addai-Mensah, J.; Krasowska, M.; Beattie, D. A., Carboxymethylcellulose adsorption on molybdenite: the effect of electrolyte composition on adsorption, bubble-surface collisions, and flotation. *Langmuir: the ACS journal of surfaces and colloids* **2014,** *30* (40), 11975-84.

8. Xiang, Y. Carboxymethyl Chitosan as a Selective Depressant in Differential Flotation of Galena and Chalcopyrite. University of Alberta, 2015.

9. Elmahdy, A. M.; Mirnezami, M.; Finch, J. A., Zeta potential of air bubbles in presence of frothers. *International Journal of Mineral Processing* **2008,** *89* (1-4), 40-43.

10. Somasundaran, P.; Wang, D., *Solution chemistry: minerals and reagents*. Elsevier: 2006; Vol. 17.

11. Beattie, D. A.; Huynh, L.; Kaggwa, G. B.; Ralston, J., Influence of adsorbed polysaccharides and polyacrylamides on talc flotation. *International Journal of Mineral Processing* **2006,** *78* (4), 238-249.

12. Yuan, D.; Xie, L.; Shi, X.; Yi, L.; Zhang, G.; Zhang, H.; Liu, Q.; Zeng, H., Selective flotation separation of molybdenite and talc by humic substances. *Minerals Engineering* **2018,** *117*, 34-41.

13. Huch, R. O.; Valles, P. Talc-molybdenite separation. 1975.

14. Fuerstenau, M. C.; Lopezvaldivieso, A.; Fuerstenau, D. W., Role of Hydrolyzed Cations in the Natural Hydrophobicity of Talc. *International Journal of Mineral Processing* **1988,** *23* (3-4), 161-170.

15. Kusaka, E.; Amano, N.; Nakahiro, Y., Effect of hydrolysed aluminum(III) and chromium(III) cations on the lipophilicity of talc. *International Journal of Mineral Processing* **1997,** *50*, 243-253.

16. Huang, P.; Fuerstenau, D. W., The effect of the adsorption of lead and cadmium ions on the interfacial behavior of quartz and talc. *Colloids and Surfaces A: Physicochemical and Engineering Aspects* **2001,** *177* (2-3), 147-156.

17. Parolis, L. A. S.; van der Merwe, R.; Groenmeyer, G. V.; Harris, P. J., The influence of metal cations on the behaviour of carboxymethyl celluloses as talc depressants. *Colloids and Surfaces A: Physicochemical and Engineering Aspects* **2008,** *317* (1-3), 109-115.

18. Steenberg, E.; Harris, P., Adsorption of carboxymethylcellulose, guar gum, and starch onto talc, sulfides, oxides, and salt-type minerals. *South African Journal of Chemistry* **1984,** *37* (3), 85-90.

19. Gomes, L.; Oliveira, J. In *The control of natural floatability of talc with carboxymethyl cellulose and aluminium chloride*, Fine Particles Processing Flotation, Proceedings of the 17th Int. Miner. Process. Congress, 1991; pp 353-364.

20. Morris, G. E. The adsorption characteristics of polymeric depressants at the talc-water interface. Ph.D. thesis, University of South Australia, 1996.

21. Rath, R. K.; Subramanian, S.; Laskowski, J. S., Adsorption of Dextrin and Guar Gum onto Talc. A Comparative Study. *Langmuir: the ACS journal of surfaces and colloids* **1997,** *13*, 6260-6266.

22. Shortridge, P. G.; Harris, P. J.; Bradshaw, D. J.; Koopal, L. K., The effect of chemical composition and molecular weight of polysaccharide depressants on the flotation of talc. *International Journal of Mineral Processing* **2000,** *59*, 215-224.

23. Morris, G. E.; Fornasiero, D.; Ralston, J., Polymer depressants at the talc–water interface: adsorption isotherm, microflotation and electrokinetic studies. *International Journal of Mineral Processing* **2002,** *67*, 211-227.

24. Shortridge, P.; Harris, P.; Bradshaw, D., The influence of ions on the effectiveness of polysaccharide depressants in the flotation of talc. *Polymers in Mineral Processing, JS Laskowski, Met Soc, Quebec* **1999**, 155-170.

25. Bradshaw, D. J.; Oostendorp, B.; Harris, P. J., Development of methodologies to improve the assessment of reagent behaviour in flotation with particular reference to collectors and depressants. *Minerals Engineering* **2005,** *18* (2), 239-246.

26. Liu, Q.; Laskowski, J. S., The interactions between dextrin and metal hydroxides in aqueous solutions. *Journal of colloid and interface science* **1989,** *130* (1), 101-111.

27. Liu, Q.; Laskowski, J. S., The role of metal hydroxides at mineral surfaces in dextrin adsorption, II. Chalcopyrite-galena separations in the presence of dextrin. *International Journal of Mineral Processing* **1989,** *27* (1-2), 147-155.

28. Liu, Q.; Laskowski, J. S., The role of metal hydroxides at mineral surfaces in dextrin adsorption, I. Studies on modified quartz samples. *International Journal of Mineral Processing* **1989,** *26* (3-4), 297-316.

29. Bakinov, K.; Vaneev, I.; Gorlovsky, S.; Eropkin, U.; Zashikhin, N.; Konev, A., New methods of sulphide concentrate upgrading. In *7th Int. Miner. Process. Congr.*, Gordon And Breach New York: 1964; pp 227-238.

30. Pugh, R. J., Macromolecular organic depressants in sulphide flotation—A review, 1. Principles, types and applications. *International Journal of Mineral Processing* **1989,** *25* (1-2), 101-130.

31. Rhodes, M. In *The effects of the physical variables of carboxymethyl cellulose reagents on the depression of magnesia bearing minerals in Western Australian nickel sulphide ores*, INTERNATIONAL MINERAL PROCESING CONGRESS, 1979; pp 346-366.

32. Cuba-Chiem, L. T.; Huynh, L.; Ralston, J.; Beattie, D. A., In situ particle film ATR FTIR spectroscopy of carboxymethyl cellulose adsorption on talc: binding mechanism,

pH effects, and adsorption kinetics. *Langmuir: the ACS journal of surfaces and colloids* **2008,** *24* (15), 8036-44.

33. Mierczynska-Vasilev, A.; Beattie, D. A., Adsorption of tailored carboxymethyl cellulose polymers on talc and chalcopyrite: Correlation between coverage, wettability, and flotation. *Minerals Engineering* **2010,** *23* (11-13), 985-993.

34. Wu, J.; Delcheva, I.; Ngothai, Y.; Krasowska, M.; Beattie, D. A., Bubble–surface interactions with graphite in the presence of adsorbed carboxymethylcellulose. *Soft matter* **2015,** *11* (3), 587-599.

35. Wang, J.; Somasundaran, P.; Nagaraj, D. R., Adsorption mechanism of guar gum at solid–liquid interfaces. *Minerals Engineering* **2005,** *18* (1), 77-81.

36. Vidal, C. A. G.; Pawlik, M., Molecular weight effects in interactions of guar gum with talc. *International Journal of Mineral Processing* **2015,** *138*, 38-43.

37. Rath, R. K.; Subramanian, S.; Laskowski, J. S., Adsorption of Dextrin and Guar Gum onto Talc. A Comparative Study. *Langmuir: the ACS journal of surfaces and colloids* **1997,** *13* (23), 6260-6266.

38. Mierczynska-Vasilev, A.; Ralston, J.; Beattie, D. A., Adsorption of modified dextrins on talc: effect of surface coverage and hydration water on hydrophobicity reduction. *Langmuir: the ACS journal of surfaces and colloids* **2008,** *24* (12), 6121-7.

39. Beaussart, A.; Mierczynska-Vasilev, A.; Beattie, D. A., Adsorption of dextrin on hydrophobic minerals. *Langmuir: the ACS journal of surfaces and colloids* **2009,** *25* (17), 9913-21.

40. Mierczynska-Vasilev, A.; Beattie, D. A., In situ atomic force microscopy of modified dextrin adsorption on hydrophobic and hydrophilic layered silicate minerals. *Journal of colloid and interface science* **2010,** *344* (2), 429-37.

41. Beaussart, A.; Parkinson, L.; Mierczynska-Vasilev, A.; Beattie, D. A., Adsorption of modified dextrins on molybdenite: AFM imaging, contact angle, and flotation studies. *Journal of colloid and interface science* **2012,** *368* (1), 608-15.

42. Braga, P. F. A.; Chaves, A. P.; Luz, A. B.; França, S. C. A., The use of dextrin in purification by flotation of molybdenite concentrates. *International Journal of Mineral Processing* **2014,** *127*, 23-27.

43. Kelebek, S.; Yoruk, S.; Smith, G. W., Wetting Behavior of Molybdenite and Talc in Lignosulphonate/Mibc Solutions and Their Separation by Flotation. *Separation Science and Technology* **2001,** *36* (2), 145-157.

44. Chiem, L. T.; Huynh, L.; Ralston, J.; Beattie, D. A., An in situ ATR-FTIR study of polyacrylamide adsorption at the talc surface. *Journal of colloid and interface science* **2006,** *297* (1), 54-61.

45. Sedeva, I. G.; Fornasiero, D.; Ralston, J.; Beattie, D. A., The influence of surface hydrophobicity on polyacrylamide adsorption. *Langmuir: the ACS journal of surfaces and colloids* **2009,** *25* (8), 4514-21.

46. Attia, Y. A., Chapter 9 - Flocculation. In *Developments in Mineral Processing*, Laskowski, J. S.; Ralston, J., Eds. Elsevier: 1992; Vol. Volume 12, pp 277-308.

47. Zeng, H.; Shi, C.; Huang, J.; Li, L.; Liu, G.; Zhong, H., Recent experimental advances on hydrophobic interactions at solid/water and fluid/water interfaces. *Biointerphases* **2015,** *11* (1), 018903.

48. Liu, Q.; Zhang, Y.; Laskowski, J. S., The adsorption of polysaccharides onto mineral surfaces: an acid/base interaction. *International Journal of Mineral Processing* **2000,** *60* (3-4), 229-245.

49. Smith, J. M., *Chemical engineering kinetics*. 1981.

50. Rao, S. R.; Leja, J., *Surface chemistry of froth flotation*. New York: Kluwer Academic/Plenum Publishers, 2nd ed. : 2004.

51. Giles, C. H.; MacEwan, T.; Nakhwa, S.; Smith, D., Studies in adsorption. Part XI. A system of classification of solution adsorption isotherms, and its use in diagnosis of adsorption mechanisms and in measurement of specific surface areas of solids. *Journal of the Chemical Society (Resumed)* **1960**, 3973-3993.

52. Giles, C. H.; D'Silva, A. P.; Easton, I. A., A general treatment and classification of the solute adsorption isotherm part. II. Experimental interpretation. *Journal of colloid and interface science* **1974,** *47* (3), 766-778.

53. Giles, C. H.; Smith, D.; Huitson, A., A general treatment and classification of the solute adsorption isotherm. I. Theoretical. *Journal of colloid and interface science* **1974,** *47* (3), 755-765.

54. Xie, L.; Wang, J.; Yuan, D.; Shi, C.; Cui, X.; Zhang, H.; Liu, Q.; Liu, Q.; Zeng, H., Interaction Mechanisms between Air Bubble and Molybdenite Surface: Impact of

Solution Salinity and Polymer Adsorption. *Langmuir: the ACS journal of surfaces and colloids* **2017,** *33* (9), 2353-2361.

55. Scheutjens, J. M. H. M.; Fleer, G. J., Statistical theory of the adsorption of interacting chain molecules. 2. Train, loop, and tail size distribution. *The Journal of Physical Chemistry* **1980,** *84* (2), 178-190.

56. Stevenson, F. J., Humus chemistry: genesis, composition, reactions. 2nd ed.; Wiley: New York, 1994.

57. Thurman, E. M., Aquatic Humic Substances. In *Organic Geochemistry of Natural Waters*, Springer Netherlands: Dordrecht, 1985; pp 273-361.

58. Mourya, V. K.; Inamdar, N. N.; Tiwari, A., Carboxymethyl chitosan and its applications. *Advanced Materials Letters* **2010,** *1* (1), 11-33.

59. Rinaudo, M., Chitin and chitosan: Properties and applications. *Progress in Polymer Science* **2006,** *31* (7), 603-632.

60. Ravi Kumar, M. N. V., A review of chitin and chitosan applications. *Reactive and Functional Polymers* **2000,** *46* (1), 1-27.

61. Dutta, P. K.; Dutta, J.; Tripathi, V., Chitin and chitosan: Chemistry, properties and applications. *Journal of Scientific and Industrial Research* **2004,** *63* (1), 20-31.

62. Huang, P. Chitosan in Differential Flotation of Base Metal Sulfides. University of Alberta, 2013.

63. Zeng, D.; Wu, J.; Kennedy, J. F., Application of a chitosan flocculant to water treatment. *Carbohydrate polymers* **2008,** *71* (1), 135-139.

# Chapter 2. Selective flotation separation of molybdenite and talc by humic substances

## 2.1 Introduction

Humic acids (HA) or more generally, humic substances are produced by the decomposition and biodegradation of organic matter. As one of the most abundant natural substances, humic substances contribute to 60-70% of natural organic materials in soil and 30-50% of organic constituents in aquatic systems,[1, 2] and can be easily found in rivers, dystrophic lakes, seawater, and even industrial process water.[1, 3] Humic acids and their analogues have been used in a wide range of biological and technological applications such as chemical engineering, healthcare, agriculture, and aquaculture, mainly because they are non-toxic, widely available, inexpensive and biocompatible. Humic acids and their analogues have also been explored in the mineral industry and have been shown to have a depressive effect on the flotation of molybdenite.[3-6]

Hoover (1980) reported that humic and tannic acids existing in recycled process water showed a detrimental effect on the flotation of molybdenite. Following this initial report, the effect of humus organics concentration on molybdenite flotation was studied, and it was found that even at a very low concentration (~1 ppm), humic acids could dramatically reduce the recovery of molybdenite. On the other hand, it was observed that clay particles (kaolinite) with adsorbed humus materials could become hydrophobic under certain solution conditions.[5, 7] As a result, humic acids and their analogues were

tested as potential selective depressants for value minerals by reverse flotation of the clay gangue, including the reverse flotation of coal,[8-10] and iron ore.[2, 11]

Talc is one of the most common hydrophobic clay minerals encountered in complex polymetallic sulfide ores, especially in complex copper/nickel sulfide ores, molybdenum ores and the ores of platinum group metals.[12-19] Economic beneficiation of these complex sulfide ores cannot be achieved without the removal of talc. In the past several decades, various depressants including inorganic[20-23] and organic/polymeric depressants[12, 24-28] have been used to depress the gangue mineral talc during sulfide flotation. Generally, organic/polymeric depressants have been proven to be more efficient, less toxic and eco-friendly as compared to inorganic depressants,[29] and can be used under various conditions, or modified for better selectivity.[25, 30]

Common polymeric depressants used for talc depression are natural or synthetic polysaccharides such as carboxymethyl cellulose,[12, 23, 24, 31-35] guar gum,[16, 17, 24, 26, 36, 37] dextrin,[14, 38-42] and synthetic polyacrylamides.[13, 43, 44] However, these depressants generally lack selectivity during the flotation separation of inherent hydrophobic minerals, e.g., molybdenite and talc, lowering molybdenite concentrate grades and causing severe problems to the subsequent smelting operations. Hence, in this study, HA was proposed as a potential depressant for molybdenite during the flotation separation of molybdenite and talc, and the adsorption characteristics of HA on these two hydrophobic minerals have been investigated through equilibrium adsorption studies, diffuse reflectance infrared Fourier transform (DRIFT) spectroscopy, and atomic force microscopy (AFM).

## 2.2 Materials and methods

### 2.2.1 Materials

2.2.1.1 Mineral samples

The mineral samples used in this study were high purity talc (Imerys Talc Group, USA) and molybdenite (Dayu, Jiangxi, China). The purity of the talc sample was reported to be > 96%, with a minor amount of chlorite (< 3%) and dolomite (< 1%). The purity of the talc sample was confirmed by X-ray diffraction (XRD) using a Rigaku Ultimate IV XRD, as no detectable impurity was observed. The mineralogical and chemical composition of the molybdenite sample was also analyzed by XRD and atomic absorption spectrometry (AAS), and the purity was found to be > 96% with $SiO_2$ (< 4%) as the major impurities. Hence, the mineral samples were used as received.

Talc is a 2:1 layer hydrated magnesium silicate which consists of two tetrahedral silica layers held together with brucite, $Mg(OH)_2$, with a formula $Mg_3(Si_2O_5)_2(OH)_2$.[20, 28, 45] The layered talc sheets are held together by weak van der Waals forces. As a result, talc is an anisotropic mineral and exhibit distinct edges and basal cleavage planes. The basal planes are naturally hydrophobic,[46, 47] and the edges of talc created by the breakage of the Si–O and Mg–O bonds are hydrophilic.[48, 49] Molybdenite is a mineral of molybdenum disulfide, $MoS_2$, which also exhibits a laminar crystal structure similar to talc. The rupture of S−Mo covalent bonds generates hydrophilic edges, while the breakage of weak van der Waals force linked S−Mo−S layers generates hydrophobic basal planes.[6, 14, 50]

The lumps of talc and molybdenite were first hammer crushed, hand sorted and then dry ground. The ground product was dry screened through Tyler standard sieves. The -150+74 μm fraction was collected and used for flotation tests, while the -37 μm fraction was used for adsorption studies, infrared spectroscopy and other surface analyses.[26] The specific surface areas of the -37 μm mineral particles, used for adsorption studies, were determined using an Autosorb Quantachrome 1MP based on Brunauer–Emmett–Teller (BET) theory. The specific surface area of the -37 μm talc and molybdenite was determined to be 2.72 $m^2/g$ and 2.02 $m^2/g$, respectively.

2.2.1.2 Reagents

Humic acid sodium salt or HA (Sigma-Aldrich, USA) was chosen as the depressant for molybdenite. HA contains both aromatic rings and aliphatic chains (hydrophobic moieties), in which –COOH groups, phenolic –OH groups and –O–, –N– bridging units (hydrophilic moieties) randomly distributed, making HA strongly negatively charged over a wide range of pH. The aromatic rings and the hydrocarbon chains of HA may originate from the lignins and microbial degradation, which may contribute to its hydrophobic characteristics under certain pH.

4-Methyl-2-pentanol (MIBC, 99+%, Acros Organics) was used as a frother in flotation. High purity water (Milli-Q, Millipore) with a resistivity of 18.2 MΩ·cm at 295K was used in the preparation of solutions. Potassium chloride (KCl, ACS reagent

grade, Fisher Scientific) was used as the background electrolyte for the experiments. The pH of all solutions was adjusted using KOH and HCl solutions.

### 2.2.2 Methods

2.2.2.1 Flotation

The single and mixed mineral flotation tests were carried out in a microflotation tube with a Siwek top as shown in **Figure 2.1**.[51] A sintered glass frit with a pore size of 1.6 μm is fitted at the base of the tube, on which a magnetic stirring bar is used to mix and agitate the pulp. The top of the tube is connected to a collection bulb by a narrow throat. Hence, the mechanical entrainment can be minimized.[51]

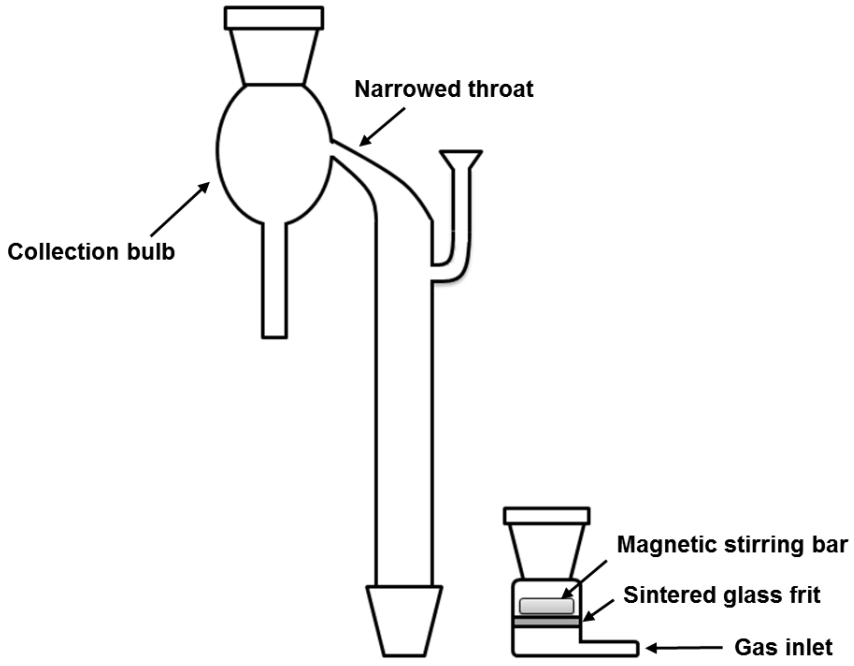


**Figure 2.1**. Schematic of a custom-made Hallimond tube.

In the single mineral flotation test, 1.5 g molybdenite or talc mineral particles (size: -150+74 μm) were added into 150 mL 0.001 M KCl solution at desired pH without or with HA at a desired concentration. In mixed mineral flotation test, 1.5 g molybdenite and talc mineral particles (size: -150 +74 μm) with a weight ratio of 1:1 were added into 150 mL 0.001 M KCl solution at desired pH and HA concentration. The pulp was then conditioned for 5 minutes, during which the solution pH was adjusted using KOH or HCl.

Thereafter, MIBC was added to achieve a concentration of 20 ppm, and the pulp was further conditioned for 1 minute. The conditioned slurry was transferred to the flotation tube and floated for 4 minutes using high purity compressed air. The gas flow rate during flotation was maintained at 20 $cm^3$/min.

In the single mineral flotation, the concentrate and tailings were filtered, dried and weighed to calculate the recovery of the single mineral, while in mixed mineral flotation tests, the concentrates were filtered, dried and weighed. The dried concentrates were added into piranha solution (3:1 mixture of concentrated sulfuric acid and hydrogen peroxide) and stirred for at least 72 hours until no molybdenite particles (black particles) can be observed in the residues. Since the molybdenite can readily dissolve in piranha solution while talc (white particles) is insoluble in this solution, the white residues can be considered to be talc. The piranha solution was then diluted and filtered; the obtained residues were dried and weighed to calculate the recoveries of talc and molybdenite.

2.2.2.2 Contact angle measurements

The contact angle of HA-treated mineral particles was determined using a Sigma 700/701 tensiometer (Biolin Scientific, Sweden) based on the Washburn method. Before contact angle measurements, the mineral particles (size: -150+74 μm) were pretreated with various concentrations (i.e. 0, 5, 10, 20 ppm) of HA solutions in 0.001 M KCl at pH 9. The treated mineral particles were filtered and washed three times with Milli-Q water to remove the non-adsorbed or weakly attached HA on minerals surfaces. After filtration and washing, the solids were dried in a vacuum drying oven and used in contact angle measurements. Two grams of the treated mineral particles were packed inside the close-ended stainless steel capillary tube with filter paper and connected to a balance. Afterwards, the tube was brought into contact with Milli-Q water. The weight of the tube was recorded against time until equilibrium was reached, and the contact angles of treated mineral particles were calculated based on the Washburn equation (equation 2.1). Ethanol was used as the reference liquid since it could fully wet the untreated molybdenite and talc surfaces (where the contact angles were considered to be 0),[52, 53] and was tested in the beginning to obtain the materials constant C of minerals in equation 2.1.

$$\frac{m^2}{t} = \frac{C \cdot \rho^2 \cdot \sigma \cdot \cos\theta}{\eta} \tag{2.1}$$

Where $m$ is the mass of adsorbed liquid, $t$ is the equilibrium time of the test, $C$ is materials constant for the mineral particles, $\rho$ is the density of the liquid, $\theta$ is contact angle, and $\eta$ is the viscosity of the wetting liquid.

2.2.2.3 Adsorption studies

The equilibrium adsorption isotherms of HA on talc and molybdenite were determined in 0.001 M KCl solution at pH 9. Adsorption tests were conducted in a series of conical flasks which were shaken on an orbital shaker at 295 K. Specifically, 0.5 g mineral samples (size: -37 μm) were added into conical flasks containing 40 mL 0.001 M KCl solutions with various concentrations of HA at pH 9, then the flasks were stoppered and continuously shaken for 30 minutes.[25]

Thereafter, a suspension sample was collected from the solution and centrifuged at a speed of 5752×g for 10 min, and the supernatant of the sample was then extracted and filtered through membranes (pore size 0.22 μm) to remove the fine solids.[45] An Evolution 300 UV-Vis Spectrophotometer was used to determine the concentration of residual HA in solution. The calibration curve of the HA solution concentration was established with various concentrations of HA (i.e., 0, 10, 25, 50, 100, 150, 250 ppm) present in 0.001 M KC1 solution at pH 9. The measurements were run in the wavelength range from 200 to 500 nm. It was found that the absorbance (Y) at 370 nm has the best linear relationship ($Y=0.010945X$, $R^2=0.999954$) with the change of HA concentration (X, ppm) under this solution condition. Hence, the concentration of residual HA in solution was determined at a wavelength of 370 nm based on the equation $X=Y/0.010945$. It is assumed that the HA depleted from solution has been all adsorbed onto the mineral surfaces.

2.2.2.4 Infrared spectroscopy

Diffuse reflectance infrared Fourier transform (DRIFT) spectroscopy was used to illustrate the structure of HA as well as to study the adsorption of HA onto mineral surfaces. The DRIFT spectroscopy tests were conducted using a Nicolet Nexus 670 FTIR spectrophotometer (Thermo Scientific, USA) instrument with a Smart Diffuse Reflectance accessory. A total of 128 scans per sample with a spectral resolution of 4 $cm^{-1}$ were collected in all experiments. FTIR grade potassium bromide KBr (ACROS Organics, USA) powder was used to obtain the background spectrum. To investigate HA adsorption onto minerals surfaces, 0.5 g of -37 μm minerals particles were ground to ~2 μm using an agate mortar/pestle, then added into 50 mL 500 ppm HA solution in 0.001 M KCl at pH 9. The mineral suspension was continuously shaken for 30 min. The treated mineral particles were then filtered and washed 3 times with Milli-Q water to eliminate the influence of non-adsorbed or weakly adsorbed HA. After filtration, the solids were dried in a vacuum drying oven. The HA samples, treated and untreated minerals powders, were hand mixed with KBr powder respectively with an agate mortar/pestle, and the DRIFT spectra of HA, untreated and treated minerals were obtained against the KBr background.

2.2.2.5 Electrokinetic studies

The zeta potentials of mineral particles under various solution conditions were determined using a Zetasizer Nano (Malvern Instruments Ltd., UK). In each test, 0.5 g of fine mineral particles (size fraction: -37 μm) were mixed with 50 mL 0.001 M KCl solution in a 100 mL polyethylene bottle, with or without HA at the desired

concentration.[22] The pH of the mineral suspension was adjusted using 0.1 M and 0.01 M KOH or HCl, and then ultrasonicated for 5 minutes. An equilibration time of 15 min was allowed before each measurement.

2.2.2.6 Atomic force microscope imaging

An Asylum MFP-3D atomic force microscope (Asylum Research, Santa Barbara, USA) was used for imaging the morphology of mineral surfaces[54-56] before and after HA treatment, which can provide information of HA adsorption on mineral surfaces such as polymer surface coverage and layer thickness.[57, 58] In each test, freshly cleaved talc or molybdenite surface was obtained by removing the top layers using sticky tape, and then immersed into 5 ppm HA in 0.001 M KCl solution at different pH for 30 minutes. After that, the mineral substrate was taken out from the solution and washed 3 times with Milli-Q water, then dried with high purity nitrogen gas prior to imaging.

## 2.3 Results and discussion

### 2.3.1 Flotation

2.3.1.1 Single mineral flotation

Flotation tests were carried out on single minerals in 0.001 M KCl solution at pH 9 under various concentrations of HA to determine the critical concentration of HA. As shown in **Figure 2.2**, very high flotation recovery was observed for both talc (~97%) and molybdenite (~92%) in the absence of HA. After the addition of 5 ppm HA, the flotation

recovery of molybdenite (black curve) was reduced dramatically from 92% to 12%, and further increasing the concentration of HA (up to 20 ppm) only slightly reduced the flotation recovery to 5%, which indicates that 5 ppm HA would be sufficient to depress the molybdenite flotation. In contrast, the addition of HA had a negligible influence on the flotation of talc (red curve), and the flotation recovery remained above 97% over the entire HA concentration range tested (up to 20 ppm). Hence, the critical concentration of HA was determined to be 5 ppm, which was used in the following flotation tests to investigate the influence of solution pH.

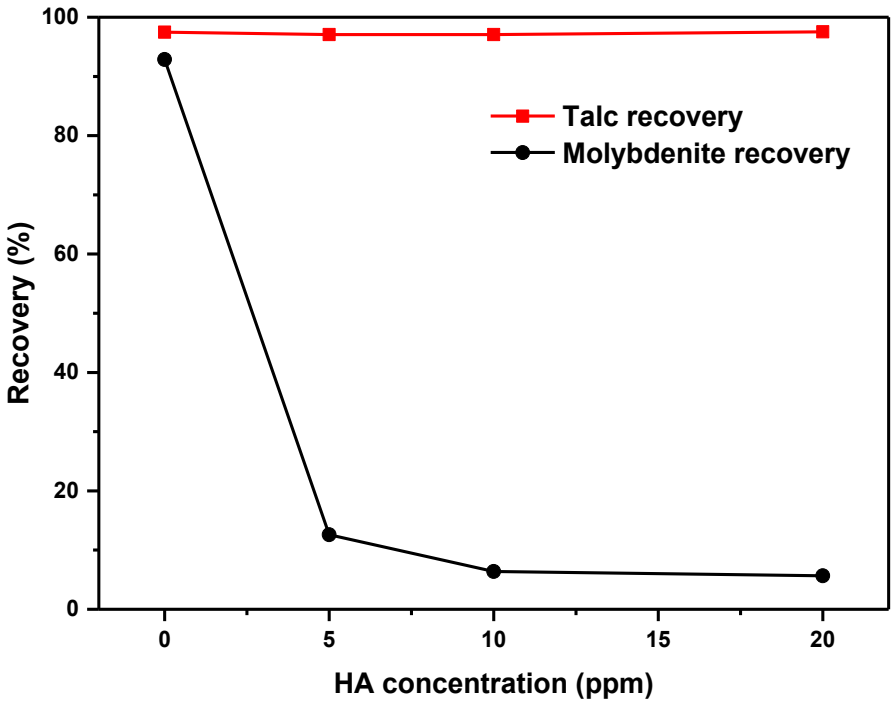


**Figure 2.2**. Recovery of talc and molybdenite in 0.001 M KCl solution at pH 9 with the addition of varying HA concentration (i.e., 0 to 20 ppm). Frother: 20 ppm MIBC.

**Figure 2.3** shows the talc and molybdenite flotation recovery in the absence and presence of 5 ppm HA as a function of pH. As can be seen, the talc and molybdenite flotation recovery is above 90% under most of the pH conditions tested without the addition of HA, except at pH 11 under which the recovery of molybdenite dropped to 66%. These results are consistent with the literature,[6, 14, 26, 28] which showed that the molybdenite flotation recovery could be reduced under alkaline conditions (pH > 9) while the talc recovery would be insensitive to solution pH.

At an electrolyte concentration of 0.001 M KCl, the anionic HA is an effective depressant for molybdenite over the entire pH range from 3 to 11, as its recovery remained below 17% in the presence of 5 ppm HA regardless of the change in pH. In comparison, the talc flotation was generally not affected in most pH tested and remained above 95% except for strong acid conditions (pH 3), where the recovery of talc was lowered to 43%. This may be caused by the increased adsorption density of HA on talc surfaces due to less electrostatic repulsion between HA and talc and increased hydrophobicity of HA molecules (based on hydrophilic-lipophilic balance definition) at the lower pH, as the carboxylate groups and phenolate groups etc. of HA are protonated. Therefore, a large separation window from pH 5 to 11 exists in which molybdenite is almost completely depressed while talc is almost completely floated.

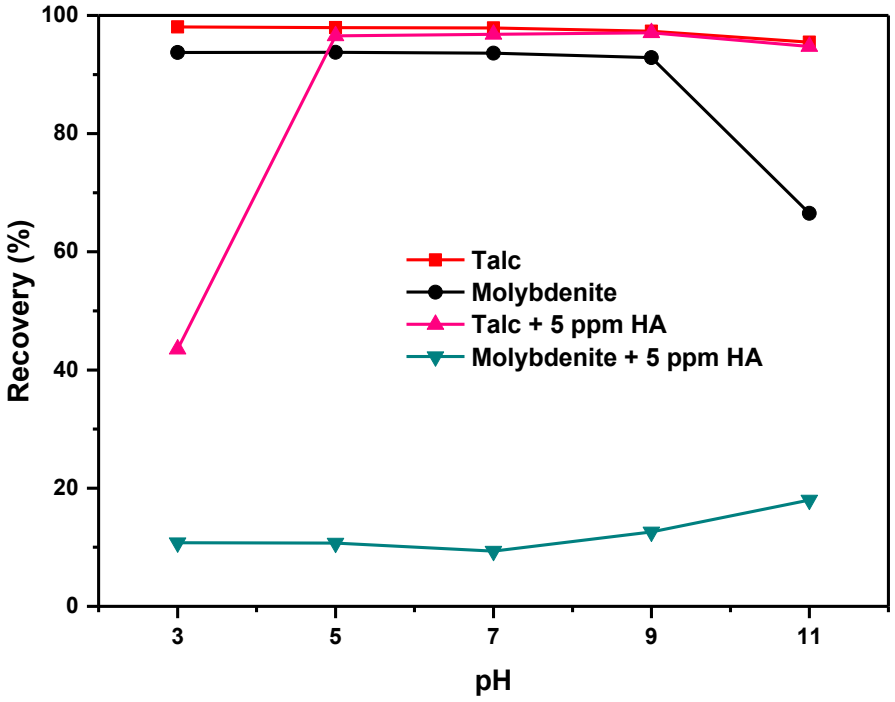


**Figure 2.3**. Recovery of talc and molybdenite with and without the addition of 5 ppm HA at varying pH in 0.001 M KCl solution. Frother: 20 ppm MIBC.

2.3.1.2 Mixed minerals flotation

The single mineral flotation tests with the presence of 5 ppm HA indicate a large separation window from pH 5 to 11. Hence, the mixed minerals flotation tests were carried out at varying pH in 0.001 M KCl solution with the addition of 5 ppm HA, to examine the possibility of using HA as a selective depressant in the flotation separation of talc-molybdenite mixtures.

**Figure 2.4** shows the molybdenite and talc recovery in the concentrates floated from the artificial mixtures of molybdenite and talc with a weight ratio of 1:1. As can be seen, talc was selectively separated from molybdenite in alkaline solutions, especially around

pH 11, where talc was almost completely floated with a flotation recovery of 90%, while molybdenite was effectively depressed with a recovery of 19%. Interestingly, the flotation recovery of talc in the mixed minerals flotation was lower than that in single mineral flotation tests, especially in the pH range 5 to 9, where the recovery of talc in the single mineral flotation was higher than 95% but when it was floated from the molybdenite-talc mixture, its recovery was lower than 60%. In comparison, the floatability of molybdenite was consistent with single mineral flotation tests over the entire pH range tested, and the recovery of molybdenite remained under 20% in single mineral flotation as well as in mixed minerals flotation tests. The reduced recovery of talc in the mixed minerals flotation from pH 5 to 9 indicates that heterocoagulation between talc and molybdenite may have occurred, possibly caused by the electrostatic interaction, although no direct evidence was observed. The zeta potential plots of talc and molybdenite in the presence and absence of HA are shown in **Figure 2.10**, which are the average values over all surface areas of the mineral particles including both basal planes and edges. It should be noted that the PZC of talc edges is around pH 9 while the talc basal planes are inherently negatively charged over a wide range of pH due to isomorphic substitution.[59] On the other hand, the basal planes of molybdenite were reported to carry negative charge over the entire investigated region from pH 3 to 11, while the PZC of molybdenite edges was found to be around pH 3. Therefore, the positively charged edges of talc could attach to the negatively charged edges and/or basal planes of molybdenite at pH < 9 as a result of electrostatic attraction, leading to the heterocoagulation or slime coating. It is worth

mentioning that less aggregation could be observed with increasing solution pH, which was consistent with the increased recovery of talc, most likely because the electrostatic attraction was weakened from pH 3 to 9. However, under strong alkaline conditions, e.g., pH 11, both the edges and basal planes of talc and molybdenite particles may have been strongly negatively charged, the heterocoagulation is eliminated as a result of electrostatic repulsion. The mineral particles are well-dispersed under this solution conditions; hence the selective separation was achieved.

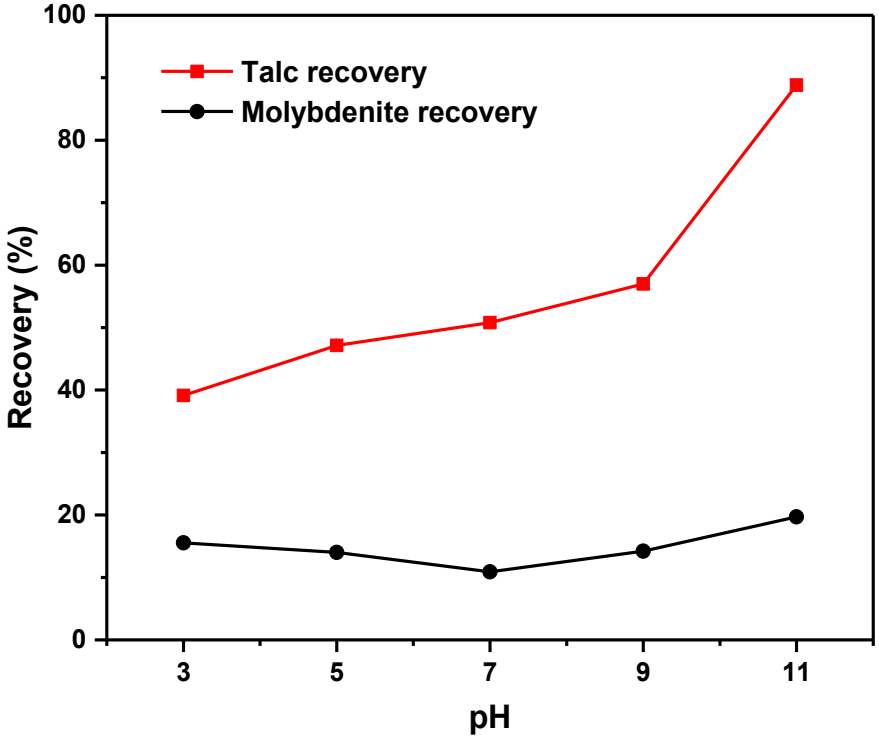


**Figure 2.4**. Flotation recovery of talc and molybdenite from a 1:1 artificial mixture with the addition of 5 ppm HA at varying pH in 0.001 M KCl solution. Frother: 20 ppm MIBC.

### 2.3.2 Contact angle measurements

**Figure 2.5** shows the water contact angles of molybdenite and talc particles before and after treatment with various concentrations of HA in 0.001 M KCl solution at pH 9. It can be seen that both talc and molybdenite exhibit inherent hydrophobicity with a relatively high water contact angle of 87º and 76º, respectively. However, after treatment with 5 ppm HA solution at pH 9, the contact angles of both molybdenite and talc decreased dramatically. Specifically, the contact angle of talc decreased from 87º to 77º while the contact angle of molybdenite decreased from 75º to 63º.

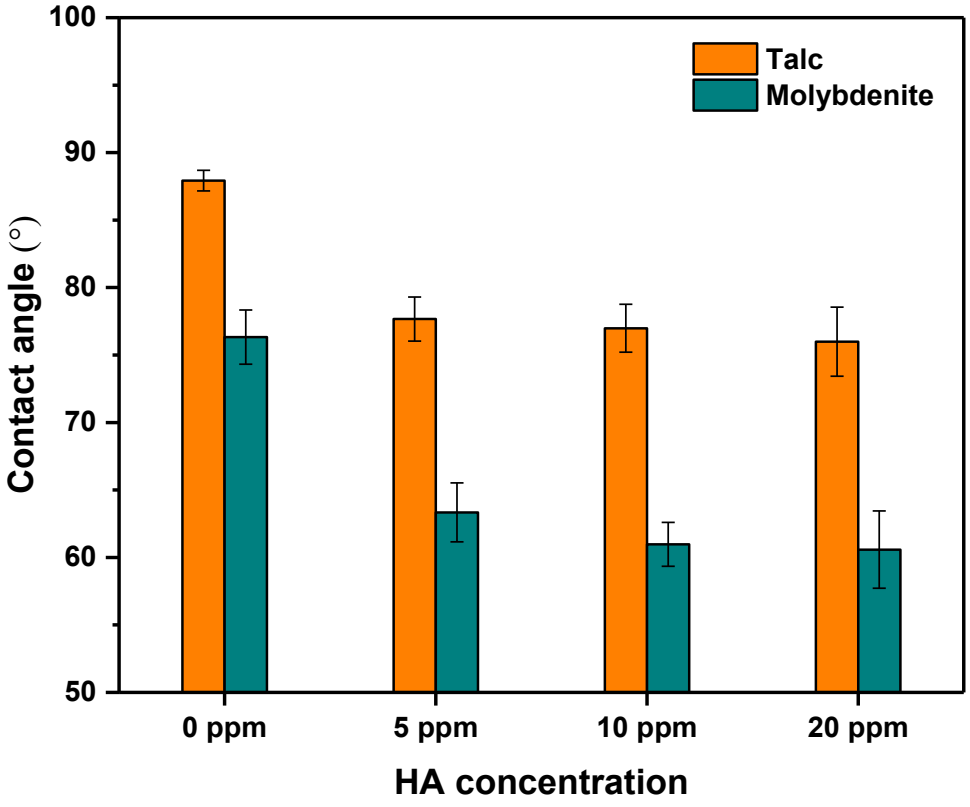


**Figure 2.5**. Contact angles of talc and molybdenite particles (size: -150+74 μm) pretreated with varying concentration of HA in 0.001 M KCl at pH 9.

At higher HA concentration, the contact angles of both molybdenite and talc only slightly decreased further. Overall, the contact angles of treated talc were still much higher than the treated molybdenite under the same solution condition. This trend is consistent with the results of flotation, showing that the treatment by HA increased the wettability of molybdenite much more than talc, and inhibited bubble attachment on molybdenite surfaces, lowering the recovery of molybdenite while not affecting the flotation of talc.

### 2.3.3 Adsorption isotherms

The equilibrium adsorption isotherms of HA on talc and molybdenite are shown in **Figure 2.6**. Generally, the adsorption density of HA on these two minerals increases with increasing HA concentration. However, the adsorption density of HA on molybdenite is much higher than that on talc at the same equilibrium concentration of HA. This result is in agreement with flotation and contact angle measurement. Specifically, when the HA solution equilibrium concentration is around 20 ppm, the adsorption density of HA on molybdenite is 1.6 $mg/m^2$, while the adsorption density of HA on talc is only around 0.13 $mg/m^2$, i.e., the adsorption density of HA on molybdenite is an order of magnitude higher than that on talc. Considering the edges of molybdenite/talc usually account for 10% of the total surface areas,[25, 60] the higher adsorption density of HA on molybdenite compared to talc are likely caused by the different adsorption sites. Specifically, the adsorption of

HA on talc most likely took place on talc edges due to the electrostatic interaction, while the adsorption of HA on molybdenite more likely occurred on basal planes.

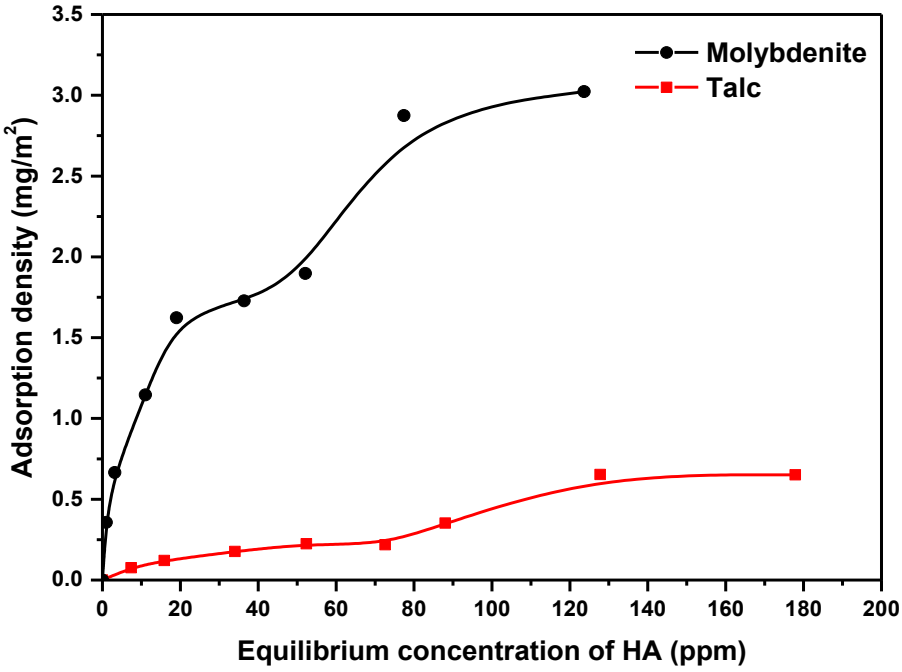


**Figure 2.6**. Adsorption isotherms of HA on talc and molybdenite in 0.001 M KCl at pH 9. (Initial HA concentration was 0, 10, 20, 40, 60, 80, 100, 150, 200 ppm)

To better illustrate the underlying adsorption mechanisms, the adsorption isotherms of HA on molybdenite and talc were fitted by the Langmuir-Freundlich adsorption model. According to the Langmuir-Freundlich equation, the equilibrium concentration $C_{eq}$ (mol/L) of HA in the bulk solution, and the adsorption density q (mg/m$^2$) of HA on mineral surface, are related through the equation 2.2:

$$q = \frac{Q_{sat} \cdot K \cdot C_{eq}^{\ n}}{\left(1 + K \cdot C_{eq}^{\ n}\right)} \tag{2.2}$$

Where $Q_{sat}$ is the maximum adsorption density of HA on mineral surfaces, and K is the Langmuir adsorption equilibrium constant. In order to calculate the free energy of adsorption, the Langmuir equilibrium constant K must have a unit of liters per mole. Hence, the unit of $C_{eq}$ in this equation must be moles per liter. Assuming the molecular weight of HA in this work is 10,000 g/mol, which is a typical value for HA molecules. The equilibrium concentration of HA can then be converted from ppm to mol/L, and **Figure 2.6** can be replotted as **Figure 2.7**.

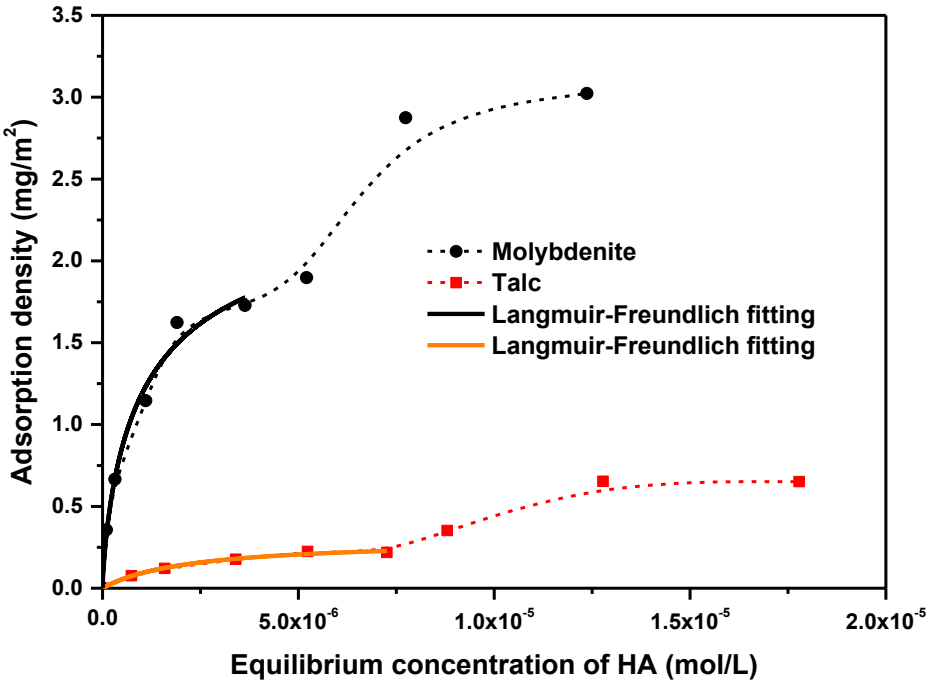


**Figure 2.7**. Fitted adsorption isotherms of HA on talc and molybdenite in 0.001 M KCl at pH 9.

It should be noted that the last three data points of each isotherm were not included during the fitting of the Langmuir-Freundlich equation. The primary consideration is that

only six suspension samples can be centrifuged each time during the adsorption study, thus the adsorption time of the other (last) three suspension samples is at least 10 min (centrifugation time, etc.) longer. Therefore, the apparent HA adsorption density of last three samples are unusually higher than the other six samples.

The parameters of Langmuir-Freundlich fitting are presented in **Table 2.1**. Based on the Langmuir equilibrium constant K, the standard free energy change (ΔG) during the adsorption can be calculated from equation 2.3:

$$\Delta G = -RT \cdot \ln K_a \approx -RT \cdot \ln K \tag{2.3}$$

Where R is the gas constant (8.314 $J \cdot mol^{-1} \cdot K^{-1}$). T is the temperature in kelvins, and $K_a$ is a dimensionless thermodynamic equilibrium constant. For a dilute solution, $K_a$ equal to the Langmuir equilibrium constant K.[61]

**Table 2.1**. Adsorption parameters of HA adsorption on molybdenite and talc at T=298.15K, as determined from fitting to Langmuir-Freundlich equation.

| | $Q_{sat}$ (mg/m$^2$) | K | n | $R^2$ | ΔG(KJ/mol) |
|---|---|---|---|---|---|
| **Molybdenite** | 2.48±0.76 | 44661 | 0.78±0.27 | 0.98 | -26.54 |
| **Talc** | 0.30±0.08 | 451306 | 1±0.46 | 0.98 | -32.27 |

As shown in **Table 2.1**, the maximum adsorption density ($Q_{sat}$) of HA on molybdenite is about seven times higher than that on talc. Again, considering the

face-to-edge ratio of molybdenite and talc particles, the adsorption of HA on molybdenite is likely to occur on its basal planes, while the adsorption of HA on talc more likely happens on its edges. Besides, since both adsorption isotherms are well described by the Langmuir-Freundlich equation, the adsorption of HA on molybdenite/talc is likely to be monolayer adsorption. In fact, the AFM images in **Figure 2.11** confirmed that the adsorption of HA at pH 9 is monolayer adsorption.

In addition, the changes of free energy during the adsorption of HA on molybdenite and talc were less than 50 KJ/mol, which indicates chemical interactions were not involved during the adsorption process. Therefore, the interactions between HA and molybdenite/talc are likely governed by weak physical interactions such as hydrophobic interaction and electrostatic interaction. Hydrogen bonding was not considered as a dominant adsorption mechanism since the formation of hydrogen bonds between HA and mineral surfaces requires the breakdown of existing hydrogen bonds between HA/mineral surfaces and water molecules. It is interesting to know that the calculated heat of adsorption of HA on talc is higher than that of molybdenite. The possible explanation is that the adsorption of HA on talc edges are mostly driven by electrostatic attraction, while the HA adsorption on molybdenite basal planes was not only governed by hydrophobic attraction but also strongly hindered by electrostatic repulsion, as demonstrated in the electrokinetic study (section 2.3.5).

### 2.3.4 Infrared spectroscopy

The DRIFT spectra of talc and molybdenite before and after treatment with 500 ppm HA in 0.001 M KCl solutions at pH 9 are shown in **Figure 2.8** and **Figure 2.9** respectively, together with the spectrum of HA. In the spectrum of HA, the characteristic peaks in the range of 1000-3000 $cm^{-1}$ were assigned based on Stevenson et al..[1] More specifically, the bands at 2920 $cm^{-1}$ and 2850 $cm^{1}$ were attributed to the stretching vibration of methyl and methylene groups ($–CH_3$ and $–CH_2–$), respectively. The peak at 1677 $cm^{-1}$ was possibly caused by the C=O stretching vibration of the amide groups (amide I band), quinone C=O and/or C=O of H-bonded conjugated ketones. The strong band at 1577 $cm^{-1}$ comes from the asymmetric stretching of $–COO^-$, N–H deformation and C=N stretching (amide II band). The peak at 1390 $cm^{-1}$ with a relatively high intensity belongs to the symmetric stretching of $–COO^-$, C–H deformation of $–CH_3$ and $–CH_2–$ groups, O–H deformation and C–O stretching of phenolic OH. The peaks at 1100, 1033, 1010 $cm^{-1}$ come from the C–O stretching and –C–O– vibration of polysaccharides or polysaccharides-like substances.[1, 62, 63]

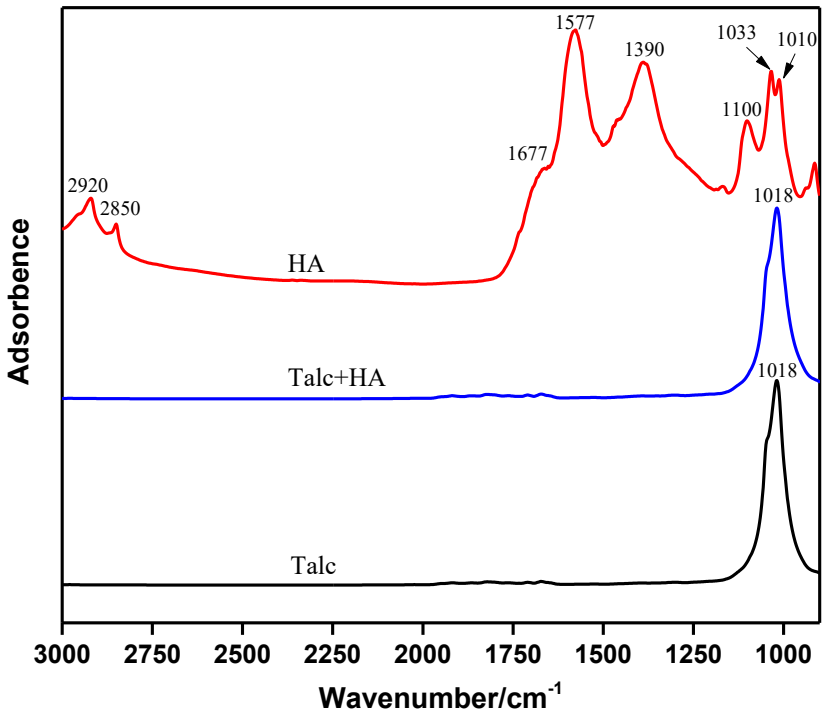


**Figure 2.8**. The DRIFT spectra of talc before and after treatment with 500 ppm HA at pH 9 in 0.001 M KCl.

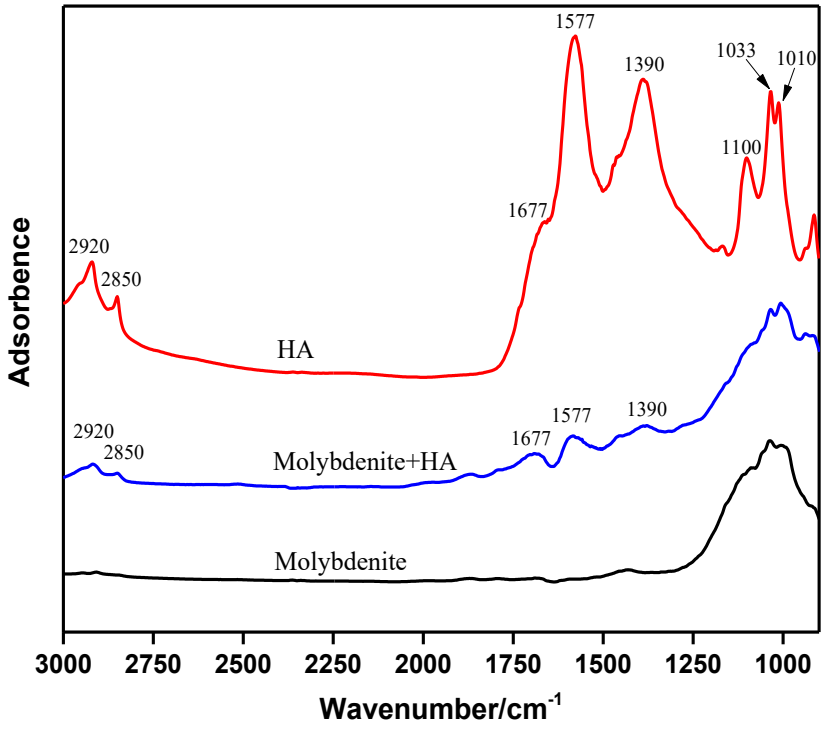

**Figure 2.9**. The DRIFT spectra of molybdenite before and after treatment with 500 ppm HA at pH 9 in 0.001 M KCl.

**Figure 2.8** shows the strong band near 1018 $cm^{-1}$ in the spectrum of talc which is caused by the stretching vibration of Si−O−Si.[25] The results also showed that the spectrum of talc treated with 500 ppm HA is the same as the untreated talc. It can be concluded that there were no detectable HA molecules on talc surfaces after being washed 3 times with Milli-Q water, suggesting that the interactions between talc and HA are relatively weak.

However, the results in **Figure 2.9** indicate that after treatment with HA, several new peaks appeared near 2920, 2850, 1677, 1577 and 1390 $cm^{-1}$ on the spectrum of treated molybdenite, corresponding to the stretching vibration of $–CH_3$ and $–CH_2–$, C=O stretching vibration of amide groups, asymmetric and symmetric stretching of $–COO^-$. This indicates that HA has been adsorbed on molybdenite surfaces, even after three times washing with Milli-Q water. Besides, the lack of peak shift indicates no strong chemical interactions were involved during the adsorption process.

### 2.3.5 Electrokinetic studies

To further understand the flotation results of molybdenite and talc and possible interaction mechanisms, the influence of pH on the zeta potential of treated and untreated minerals particles was measured and the results are shown in **Figure 2.10**. As the zeta

potential measurement in this work was based on electrophoresis technique, the measured zeta potential is an average of the apparent zeta potential of the talc and molybdenite particles without a detailed account to the actual charges carried by the basal or the edge surfaces. As can be seen, both talc and molybdenite particles are negatively charged over the entire pH (3 to 11) range tested, with an estimated iso-electric point (IEP) around pH 2 for talc and less than pH 2 for molybdenite, respectively. Besides, the zeta potential of molybdenite is more negative that talc from pH 3 to 10, especially in the low pH range, these results are consistent with the literature values.[6, 28]

In the presence of 20 ppm HA, the zeta potential of talc or molybdenite particles is more negative than in the absence of HA over the entire pH range. The possible explanation is that HA is strongly negatively charged, and the adsorption of HA rendered the mineral surface charges more negative. In addition, it can be seen that as the solution pH decreases, the zeta potential difference between treated talc and untreated talc increases, indicating that the adsorption density of HA on talc surfaces may increase at lower pH, possibly due to lower electrostatic repulsion. At pH 3, the zeta potential of untreated talc is -12.9 mV while the zeta potential of treated talc is -40.3 mV, showing that the adsorption of HA shifted the zeta potential of talc by 27.4 mV. This suggests that there is a relatively large amount of HA adsorbed onto talc surfaces at this pH. In fact, AFM imaging results in **Figure 2.11** also confirmed that at pH 3, the talc surfaces were fully covered with HA molecules. This phenomenon also explains why the floatability of talc is reduced dramatically at pH 3.

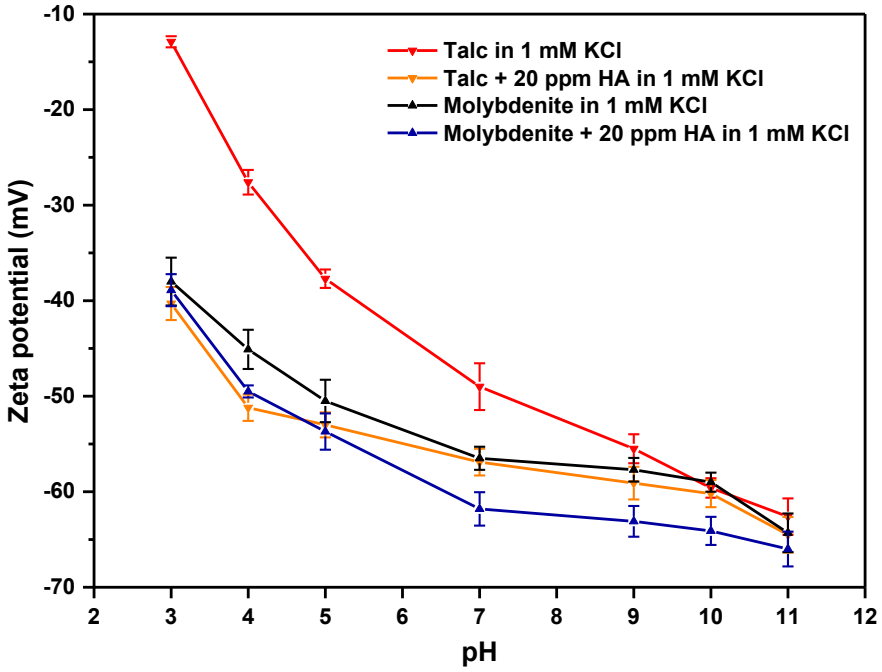


**Figure 2.10**. Zeta potential of talc, talc + HA, molybdenite and molybdenite + HA at varying pH in 0.001 M KCl solution.

Since the zeta potential values of molybdenite and talc particles determined by electrophoresis technique were averaged values over all surface areas, which includes both faces and edges. The surface charges of edges and faces of talc and molybdenite were also discussed independently based on the literature reports and the experimental results in this work.

Specifically, the talc basal plane is inherently negatively charged over a wide range of pH due to isomorphic substitution, possibly broken bonds and/or hydrolysis of siloxane bonds on the basal planes.[59] The negatively charged HA molecules barely adsorb onto talc basal planes at pH 9 (or more generally, pH>5) as a result of electrostatic

repulsion; hence the flotation of talc was not affected by HA over a wide range of pH except for pH<3. On the other hand, the edges of talc have a point of zero charge (PZC) around pH 9 based on the results of direct force measurements using atomic force microscopy.[59] Below the PZC, the edges of talc particles are positively charged, which could interact with the negatively charged HA molecules due to electrostatic attraction, rendering the talc particles more negatively charged at pH<9 compared to the untreated talc particles.

In comparison, the surface potential of molybdenite edges is negative over a wide range of pH with a PZC around pH 3,[64] while the basal planes of molybdenite are less negatively charged compared to its edges at pH above 4.[64] Thus, HA molecules adsorb more readily onto molybdenite basal plane as a result of hydrophobic interaction and less electrostatic repulsion.

### 2.3.6 AFM imaging

**Figure 2.11** shows the topographic AFM images of mineral surfaces before and after treatment by 5 ppm HA in 0.001 M KCl solution. As can be seen in **Figures 2.11 (a)** and **(b)**, both the bare molybdenite and talc showed molecularly smooth surfaces with root-mean-square (rms) roughness of ~0.3 nm. After treatment with 5 ppm HA at pH 9, the HA molecules covered a significant surface area (70-80%) of molybdenite basal plane as shown in **Figure 2.11 (c)**; whilst HA could not be detected on the cleaved surface of treated talc under the same pH as displayed in **Figure 2.11 (d)**. The AFM images

coincided with the results of DRIFT spectroscopy in **Figure 2.8** and **2.9**, which explained the preferential adsorption and strong depression effect of HA on molybdenite over talc. Besides, HA molecules tend to "spread" onto molybdenite surface rather than form aggregates at pH 9. This is possibly due to the relatively low ionic strength of the solution (0.001 M KCl) and the HA molecules are strongly negatively charged at pH 9, making HA more likely to have a stretched conformation on molybdenite surface instead of forming aggregates as a result of the strong inter/intramolecular electrostatic repulsion at pH 9.

However, when the molybdenite and talc surfaces were treated with 5 ppm HA at pH 3, both mineral surfaces were fully covered by the aggregates of HA molecules, as shown in **Figures 2.11 (e)** and **2.11 (f)**. The HA molecules would more readily form aggregates (via hydrophobic interaction, π–π stacking, etc.) and adsorb onto the mineral surfaces under the acidic condition. This is attributed to the reduced electrostatic repulsion among the HA molecules as well as between the HA molecules and mineral surfaces due to the relatively weak charges of HA molecules and mineral surfaces under the acidic condition.

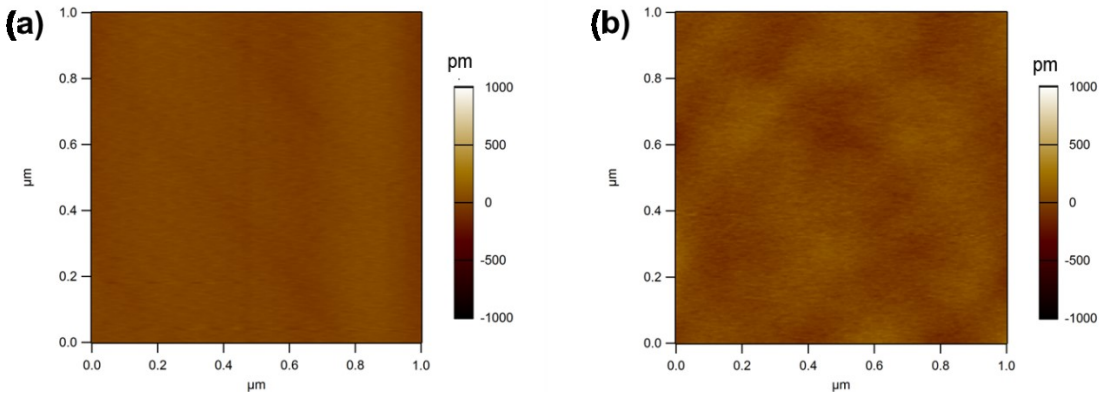

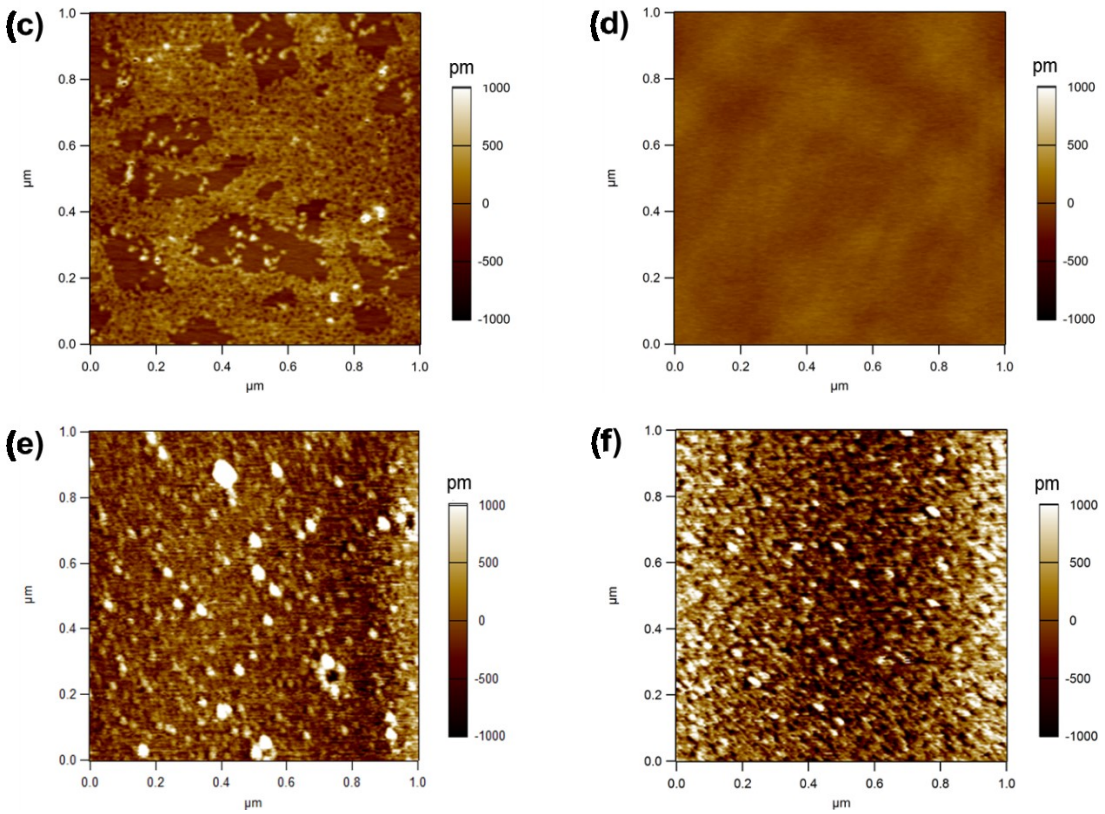


**Figure 2.11**. AFM height images of mineral substrates: (a) freshly cleaved molybdenite surface, (b) freshly cleaved talc surface, (c) molybdenite surface treated with 5 ppm HA in 0.001 M KCl solution at pH 9, (d) talc surface treated with 5 ppm HA in 0.001 M KCl solution at pH 9, (e) molybdenite surface treated with 5 ppm HA in 0.001 M KCl solution at pH 3, and (f) talc surface treated with 5 ppm HA in 0.001 M KCl solution at pH 3.

The AFM imaging results are in good agreement with the DRIFT spectroscopy results and further confirmed that the adsorption of HA on talc basal planes is strongly hindered by electrostatic repulsions, while the adsorption of HA on molybdenite basal planes is driven by hydrophobic interaction and partially hindered by electrostatic repulsion under alkaline conditions.

## 2.4 Conclusions

In this study, HA was explored as a potential depressant for molybdenite during mineral flotation. The results of flotation tests showed that both talc and molybdenite exhibit good natural floatability over a wide pH range (pH 3 to 9). The addition of HA could effectively depress the flotation recovery of molybdenite even at very low HA concentration (5 ppm). However, the addition of HA had no significant influence on the flotation of talc, and the recovery of talc remained above 97% over the entire HA concentration range tested (up to 20 ppm). Contact angle measurements demonstrated that both talc and molybdenite became more hydrophilic after the HA treatment, but HA adsorption has less impact on the hydrophobicity of talc than on molybdenite.

The results of adsorption isotherms revealed that HA had a much higher adsorption density on molybdenite over talc, indicating that HA adsorbs more onto molybdenite surfaces than onto talc. DRIFT spectroscopy and AFM imaging further demonstrated that HA had a much higher affinity for molybdenite than talc, and the adsorption of HA on talc basal planes could be easily affected by a change in solution pH while the adsorption of HA on molybdenite basal planes was not significantly affected by the solution pH. All of the above results suggest that humic acids could be used as a potential depressant for molybdenite during the flotation separation of molybdenite and talc in alkaline conditions, and the interactions between talc and HA are relatively weak physical interactions dominated by electrostatic interaction and hydrophobic interaction (at basal planes). In

comparison, the adsorption of HA onto molybdenite surfaces may be driven by a combination of interactions including hydrophobic interaction (at basal planes), electrostatic interaction, van der Waals force, sulfur-π interaction, etc., which will be further investigated in a separate study. It is noted that in this work both minerals were "fresh" and untreated by collectors etc. before they were treated by the depressant HA. It remains to be further explored whether selective separation can be achieved if both minerals are treated by oily collectors first and if molybdenite can restore its floatability after depressed by HA. It is also worth to mention that a significantly large percentage of Cu/Mo industrial flotation process where talc is problematic operate in high salinity waters (e.g., seawater) or in the presence of high concentrations of divalent ions such as $Ca^{2+}$ and $Mg^{2+}$ ions.[50] Future work is required to investigate the influence of common species such as divalent ions and oily collectors present in the practical flotation process, as well as better elucidate the interaction mechanisms between HA and these two minerals.

## 2.5 Acknowledgements

We acknowledge the financial support from the Natural Sciences and Engineering Research Council of Canada (NSERC) and the Canada Research Chairs Program (H. Zeng). Duowei Yuan gratefully appreciates the scholarship support from the China Scholarship Council (CSC). The authors also thank the Imerys Talc Group for providing the talc samples.

## 2.6 References

1. Stevenson, F. J., Humus chemistry: genesis, composition, reactions. 2nd ed.; Wiley: New York, 1994.

2. dos Santos, I. D.; Oliveira, J. F., Utilization of humic acid as a depressant for hematite in the reverse flotation of iron ore. *Minerals Engineering* **2007,** *20* (10), 1003-1007.

3. Lai, R. W. M.; Stone, L. C.; Rimmasch, B. E., Effect of humus organics on the flotation recovery of molybdenite. *International Journal of Mineral Processing* **1984,** *12* (1-3), 163-172.

4. Hoover, M., Water Chemistry Effects in the Flotation of Sulfide Ores-- a Review and Discussion for Molybdenite. *Complex Sulphide Ores* **1980**, 100-112.

5. Laskowski, J.; Yu, Z. In *The effect of humic acids on the emulsion flotation of inherently hydrophobic minerals*, III Latin American Congress on Froth Flotation. Universidad de Concepción, Concepción-Chile, 1994; pp 397-411.

6. Castro, S.; Lopez-Valdivieso, A.; Laskowski, J. S., Review of the flotation of molybdenite. Part I: Surface properties and floatability. *International Journal of Mineral Processing* **2016,** *148*, 48-58.

7. Firth, B. A.; Nicol, S. K., The influence of humic materials on the flotation of coal. *International Journal of Mineral Processing* **1981,** *8* (3), 239-248.

8. Laskowski, J. S.; Sirois, L. L.; Moon, K. S., Effect of Humic Acids on Coal Flotation Part I. Coal Flotation Selectivity in the Presence of Humic Acids. *Coal Preparation* **1986,** *3* (3), 133-154.

9. Lalvani, S. B.; Kang, J.-C., Coal Flotation in the Presence of Humic Acids. *Fuel Science and Technology International* **1992,** *10* (8), 1291-1312.

10. Pawlik, M.; Laskowski, J. S., Coal Reverse Flotation. Part II. Batch Flotation Tests. *Coal Preparation* **2003,** *23* (3), 113-127.

11. Turrer, H. D. G.; Peres, A. E. C., Investigation on alternative depressants for iron ore flotation. *Minerals Engineering* **2010,** *23* (11-13), 1066-1069.

12. Gomes, L.; Oliveira, J. In *The control of natural floatability of talc with carboxymethyl cellulose and aluminium chloride*, Fine Particles Processing Flotation, Proceedings of the 17th Int. Miner. Process. Congress, 1991; pp 353-364.

13. Beattie, D. A.; Huynh, L.; Kaggwa, G. B.; Ralston, J., Influence of adsorbed polysaccharides and polyacrylamides on talc flotation. *International Journal of Mineral Processing* **2006,** *78* (4), 238-249.

14. Braga, P. F. A.; Chaves, A. P.; Luz, A. B.; França, S. C. A., The use of dextrin in purification by flotation of molybdenite concentrates. *International Journal of Mineral Processing* **2014,** *127*, 23-27.

15. Zhao, K. L.; Gu, G. H.; Wang, H.; Wang, C. L.; Wang, X. H.; Luo, C., Influence of depressant foenum-graecum on the flotation of a sulfide ore which contains hydrophobic gangue. *International Journal of Mineral Processing* **2015,** *141*, 68-76.

16. Mhlanga, S. S.; O'Connor, C. T.; McFadzean, B., A study of the relative adsorption of guar onto pure minerals. *Minerals Engineering* **2012,** *36-38*, 172-178.

17. Allison, S. A.; O'Connor, C. T., An investigation into the flotation behaviour of pyrrhotite. *International Journal of Mineral Processing* **2011,** *98* (3-4), 202-207.

18. Quast, K.; Addai-Mensah, J.; Skinner, W., Preconcentration strategies in the processing of nickel laterite ores Part 5: Effect of mineralogy. *Minerals Engineering* **2017,** *110*, 31-39.

19. Xu, M., Ore Evaluation at Vale Base Metals. In *Separation Technologies for Minerals, Coal, and Earth Resources*, Young, C. A.; Luttrell, G. H., Eds. Society for Mining, Metallurgy, and Exploration (SME): 2013; Vol. 27, pp 521-537.

20. Fuerstenau, M. C.; Lopezvaldivieso, A.; Fuerstenau, D. W., Role of Hydrolyzed Cations in the Natural Hydrophobicity of Talc. *International Journal of Mineral Processing* **1988,** *23* (3-4), 161-170.

21. Kusaka, E.; Amano, N.; Nakahiro, Y., Effect of hydrolysed aluminum(III) and chromium(III) cations on the lipophilicity of talc. *International Journal of Mineral Processing* **1997,** *50*, 243-253.

22. Huang, P.; Fuerstenau, D. W., The effect of the adsorption of lead and cadmium ions on the interfacial behavior of quartz and talc. *Colloids and Surfaces A: Physicochemical and Engineering Aspects* **2001,** *177* (2-3), 147-156.

23. Parolis, L. A. S.; van der Merwe, R.; Groenmeyer, G. V.; Harris, P. J., The influence of metal cations on the behaviour of carboxymethyl celluloses as talc depressants.

*Colloids and Surfaces A: Physicochemical and Engineering Aspects* **2008,** *317* (1-3), 109-115.

24. Steenberg, E.; Harris, P., Adsorption of carboxymethylcellulose, guar gum, and starch onto talc, sulfides, oxides, and salt-type minerals. *South African Journal of Chemistry* **1984,** *37* (3), 85-90.

25. Morris, G. E. The adsorption characteristics of polymeric depressants at the talc-water interface. Ph.D. thesis, University of South Australia, 1996.

26. Rath, R. K.; Subramanian, S.; Laskowski, J. S., Adsorption of Dextrin and Guar Gum onto Talc. A Comparative Study. *Langmuir: the ACS journal of surfaces and colloids* **1997,** *13*, 6260-6266.

27. Shortridge, P. G.; Harris, P. J.; Bradshaw, D. J.; Koopal, L. K., The effect of chemical composition and molecular weight of polysaccharide depressants on the flotation of talc. *International Journal of Mineral Processing* **2000,** *59*, 215-224.

28. Morris, G. E.; Fornasiero, D.; Ralston, J., Polymer depressants at the talc–water interface: adsorption isotherm, microflotation and electrokinetic studies. *International Journal of Mineral Processing* **2002,** *67*, 211-227.

29. Laskowski, J. S.; Liu, Q.; O'Connor, C. T., Current understanding of the mechanism of polysaccharide adsorption at the mineral/aqueous solution interface. *International Journal of Mineral Processing* **2007,** *84* (1-4), 59-68.

30. Pugh, R. J., Macromolecular organic depressants in sulphide flotation—A review, 1. Principles, types and applications. *International Journal of Mineral Processing* **1989,** *25* (1-2), 101-130.

31. Rhodes, M. In *The effects of the physical variables of carboxymethyl cellulose reagents on the depression of magnesia bearing minerals in Western Australian nickel sulphide ores*, INTERNATIONAL MINERAL PROCESING CONGRESS, 1979; pp 346-366.

32. Cuba-Chiem, L. T.; Huynh, L.; Ralston, J.; Beattie, D. A., In situ particle film ATR FTIR spectroscopy of carboxymethyl cellulose adsorption on talc: binding mechanism, pH effects, and adsorption kinetics. *Langmuir: the ACS journal of surfaces and colloids* **2008,** *24* (15), 8036-44.

33. Mierczynska-Vasilev, A.; Beattie, D. A., Adsorption of tailored carboxymethyl cellulose polymers on talc and chalcopyrite: Correlation between coverage, wettability, and flotation. *Minerals Engineering* **2010,** *23* (11-13), 985-993.

34. Kor, M.; Korczyk, P. M.; Addai-Mensah, J.; Krasowska, M.; Beattie, D. A., Carboxymethylcellulose adsorption on molybdenite: the effect of electrolyte composition on adsorption, bubble-surface collisions, and flotation. *Langmuir: the ACS journal of surfaces and colloids* **2014,** *30* (40), 11975-84.

35. Wu, J.; Delcheva, I.; Ngothai, Y.; Krasowska, M.; Beattie, D. A., Bubble–surface interactions with graphite in the presence of adsorbed carboxymethylcellulose. *Soft matter* **2015,** *11* (3), 587-599.

36. Wang, J.; Somasundaran, P.; Nagaraj, D. R., Adsorption mechanism of guar gum at solid–liquid interfaces. *Minerals Engineering* **2005,** *18* (1), 77-81.

37. Vidal, C. A. G.; Pawlik, M., Molecular weight effects in interactions of guar gum with talc. *International Journal of Mineral Processing* **2015,** *138*, 38-43.

38. Rath, R. K.; Subramanian, S.; Laskowski, J. S., Adsorption of Dextrin and Guar Gum onto Talc. A Comparative Study. *Langmuir: the ACS journal of surfaces and colloids* **1997,** *13* (23), 6260-6266.

39. Mierczynska-Vasilev, A.; Ralston, J.; Beattie, D. A., Adsorption of modified dextrins on talc: effect of surface coverage and hydration water on hydrophobicity reduction. *Langmuir: the ACS journal of surfaces and colloids* **2008,** *24* (12), 6121-7.

40. Beaussart, A.; Mierczynska-Vasilev, A.; Beattie, D. A., Adsorption of dextrin on hydrophobic minerals. *Langmuir: the ACS journal of surfaces and colloids* **2009,** *25* (17), 9913-21.

41. Mierczynska-Vasilev, A.; Beattie, D. A., In situ atomic force microscopy of modified dextrin adsorption on hydrophobic and hydrophilic layered silicate minerals. *Journal of colloid and interface science* **2010,** *344* (2), 429-37.

42. Beaussart, A.; Parkinson, L.; Mierczynska-Vasilev, A.; Beattie, D. A., Adsorption of modified dextrins on molybdenite: AFM imaging, contact angle, and flotation studies. *Journal of colloid and interface science* **2012,** *368* (1), 608-15.

43. Chiem, L. T.; Huynh, L.; Ralston, J.; Beattie, D. A., An in situ ATR-FTIR study of polyacrylamide adsorption at the talc surface. *Journal of colloid and interface science* **2006,** *297* (1), 54-61.

44. Sedeva, I. G.; Fornasiero, D.; Ralston, J.; Beattie, D. A., The influence of surface hydrophobicity on polyacrylamide adsorption. *Langmuir: the ACS journal of surfaces and colloids* **2009,** *25* (8), 4514-21.

45. Khraisheh, M.; Holland, C.; Creany, C.; Harris, P.; Parolis, L., Effect of molecular weight and concentration on the adsorption of CMC onto talc at different ionic strengths. *International Journal of Mineral Processing* **2005,** *75* (3-4), 197-206.

46. Fuerstenau, D. W.; Huang, P., Interfacial phenomena involved in talc flotation and depression. In *XXII International Mineral Processing Congress*, Cape Town, 2003; pp 1034-1043.

47. Burdukova, E.; Becker, M.; Bradshaw, D. J.; Laskowski, J. S., Presence of negative charge on the basal planes of New York talc. *Journal of colloid and interface science* **2007,** *315* (1), 337-42.

48. Du, H.; Miller, J. D., A molecular dynamics simulation study of water structure and adsorption states at talc surfaces. *International Journal of Mineral Processing* **2007,** *84* (1-4), 172-184.

49. Du, H.; Miller, J. D., Adsorption states of amphipatic solutes at the surface of naturally hydrophobic minerals: a molecular dynamics simulation study. *Langmuir: the ACS journal of surfaces and colloids* **2007,** *23* (23), 11587-96.

50. Zanin, M.; Ametov, I.; Grano, S.; Zhou, L.; Skinner, W., A study of mechanisms affecting molybdenite recovery in a bulk copper/molybdenum flotation circuit. *International Journal of Mineral Processing* **2009,** *93* (3-4), 256-266.

51. Cao, M.; Liu, Q., Reexamining the functions of zinc sulfate as a selective depressant in differential sulfide flotation--the role of coagulation. *Journal of colloid and interface science* **2006,** *301* (2), 523-31.

52. Mu, Y.; Peng, Y.; Lauten, R. A., The mechanism of pyrite depression at acidic pH by lignosulfonate-based biopolymers with different molecular compositions. *Minerals Engineering* **2016,** *92*, 37-46.

53. Yang, B.; Song, S.; Lopez-Valdivieso, A., Effect of Particle Size on the Contact Angle of Molybdenite Powders. *Mineral Processing and Extractive Metallurgy Review* **2014,** *35* (3), 208-215.

54. Wang, J.; Liu, Q.; Zeng, H., Understanding Copper Activation and Xanthate Adsorption on Sphalerite by Time-of-Flight Secondary Ion Mass Spectrometry, X-ray Photoelectron Spectroscopy, and in Situ Scanning Electrochemical Microscopy. *The Journal of Physical Chemistry C* **2013,** *117* (39), 20089-20097.

55. Xie, L.; Wang, J.; Shi, C.; Huang, J.; Zhang, H.; Liu, Q.; Liu, Q.; Zeng, H., Probing Surface Interactions of Electrochemically Active Galena Mineral Surface Using Atomic Force Microscopy. *The Journal of Physical Chemistry C* **2016,** *120* (39), 22433-22442.

56. Xie, L.; Wang, J.; Shi, C.; Cui, X.; Huang, J.; Zhang, H.; Liu, Q.; Liu, Q.; Zeng, H., Mapping the Nanoscale Heterogeneity of Surface Hydrophobicity on the Sphalerite Mineral. *The Journal of Physical Chemistry C* **2017,** *121* (10), 5620-5628.

57. Wu, J.; Delcheva, I.; Ngothai, Y.; Krasowska, M.; Beattie, D. A., Bubble-surface interactions with graphite in the presence of adsorbed carboxymethylcellulose. *Soft Matter* **2015,** *11* (3), 587-99.

58. Xie, L.; Wang, J.; Yuan, D.; Shi, C.; Cui, X.; Zhang, H.; Liu, Q.; Liu, Q.; Zeng, H., Interaction Mechanisms between Air Bubble and Molybdenite Surface: Impact of Solution Salinity and Polymer Adsorption. *Langmuir: the ACS journal of surfaces and colloids* **2017,** *33* (9), 2353-2361.

59. Yan, L.; Englert, A. H.; Masliyah, J. H.; Xu, Z., Determination of anisotropic surface characteristics of different phyllosilicates by direct force measurements. *Langmuir: the ACS journal of surfaces and colloids* **2011,** *27* (21), 12996-3007.

60. Lobato, E. M. d. C., Determination of Surface Free Energies and Aspect Ratio of Talc. VT: 2004.

61. Liu, Y., Is the Free Energy Change of Adsorption Correctly Calculated? *Journal of Chemical & Engineering Data* **2009,** *54* (7), 1981-1985.

62. Stevenson, F. J.; Goh, K. M., Infrared spectra of humic acids and related substances. *Geochimica et Cosmochimica Acta* **1971,** *35* (5), 471-483.

63. Piccolo, A.; Stevenson, F. J., Infrared spectra of Cu2+ Pb2+ and Ca2+ complexes of soil humic substances. *Geoderma* **1982,** *27* (3), 195-208.

64. Lu, Z.; Liu, Q.; Xu, Z.; Zeng, H., Probing Anisotropic Surface Properties of Molybdenite by Direct Force Measurements. *Langmuir: the ACS journal of surfaces and colloids* **2015,** *31* (42), 11409-18.

# Chapter 3. Selective separation of copper-molybdenum sulfides using humic acids

## 3.1 Introduction

The flotation separation of copper-molybdenum sulfides generally relies on the use of toxic and hazardous depressants such as cyanides, sodium sulfide/hydrosulfide, Noke's reagents,[1-4] and thioglycolic acid and its salts.[1, 5] It is desired to replace these aggressive chemicals with more environmentally benign reagents. Humic acids (HA), as a major organic constituents of and soil one of the most abundant naturally occurring organic macromolecules, has a wide range of applications owing to its abundance, low-cost, and biocompatibility.[6, 7] HA and its analogues have been examined in the mineral industry and were found to have a detrimental effect on molybdenite flotation.[8-11] Our previous work has also shown that humic acids can selectively depress molybdenite during the molybdenite-talc flotation separation. Therefore, in the present work, HA was investigated as a depressant for molybdenite during the molybdenite-chalcopyrite separation. Microflotation tests on single minerals and mineral mixtures were conducted to study the flotation response of molybdenite and chalcopyrite in the presence of HA and xanthate collector under various solution conditions. Adsorption study, electrokinetic study, diffuse reflectance infrared Fourier transform (DRIFT) spectroscopy, X-ray photoelectron spectroscopy (XPS) and time-of-flight secondary ion mass spectrometry (ToF-SIMS) measurements were also performed to study the adsorption characteristics of

HA onto molybdenite and chalcopyrite surfaces, as well as elucidate the possible interaction mechanisms between HA and these two minerals.

## 3.2 Materials and methods

### 3.2.1 Materials

3.2.1.1 Minerals

The high purity chalcopyrite (Ward's Science, NY, USA) and molybdenite (Dayu, Jiangxi, China) lumps were first hand-picked, crushed and sorted manually, then dry ground. The ground samples were dry screened through a series of Tyler standard sieves (Fisher Scientific, USA) to obtain the desired size fractions. The -150+74 μm size fraction was used for single and mixed mineral flotation tests, while the -37 μm mineral particles were used for adsorption study, electrokinetic study, DRIFT spectroscopy, and ToF-SIMS analysis. The Brunauer–Emmett–Teller (BET) specific surface areas of the -37 μm chalcopyrite and molybdenite particles were determined by an Autosorb Quantachrome 1MP (Quantachrome, USA), and were found to be 0.66 $m^2/g$ and 2.02 $m^2/g$ for chalcopyrite and molybdenite, respectively.

The mineralogical and elemental composition of the chalcopyrite and molybdenite samples were analyzed by X-ray diffraction using a Rigaku Ultimate IV XRD and atomic absorption spectrometry (AAS). The XRD patterns of chalcopyrite and molybdenite samples are shown in **Figure 3.1** (a) and (b), respectively. The purity of chalcopyrite was over 90%, with a minor amount of pyrite ($FeS_2$) and quartz ($SiO_2$), while the purity of

molybdenite was over 96% with quartz (< 4%) as the major impurity. Hence, the mineral samples were used after hand sorting.

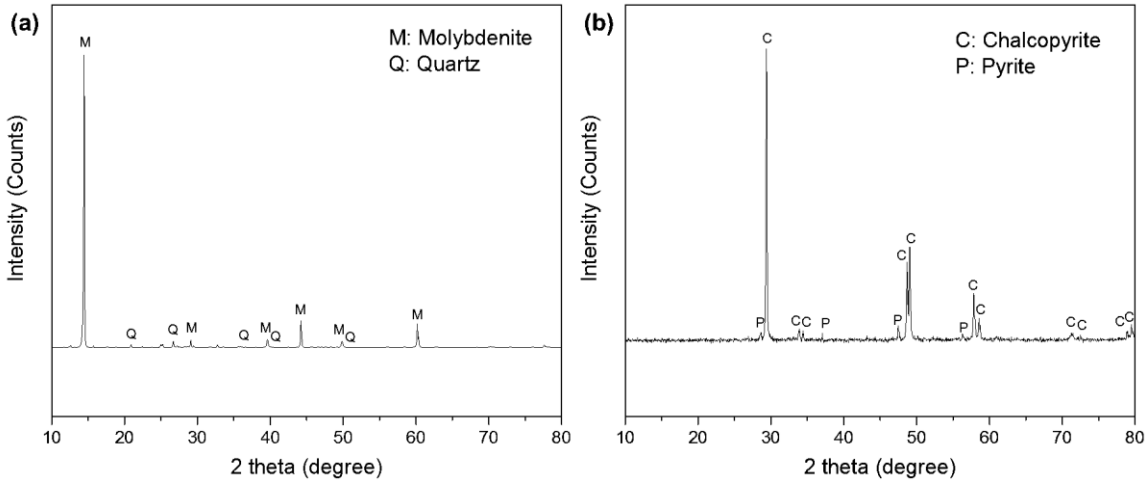


**Figure 3.1**. XRD pattern of (a) Molybdenite sample (b) Chalcopyrite sample.

3.2.1.2 Reagents

Humic acids sodium salt or HA (Sigma-Aldrich, USA) was investigated as a depressant in this study. Potassium isobutyl xanthate or KIBX ($C_4H_7OS_2K$, Prospec Chemicals Ltd., Canada) was employed as the collector during the flotation. The KIBX was purified by dissolving in acetone at 40°C in a water bath, followed by precipitation using ether as described in our previous reports.[12-15] The precipitates (purified KIBX) were collected by filtration and dried in a vacuum oven. 4-Methyl-2-pentanol or MIBC (99+%, Acros Organics) was employed as a frother in microflotation. All solutions were prepared using Milli-Q water (Millipore deionized) with a resistivity of 18.2 MΩ·cm at 295K, and the pH of all solutions was adjusted by dilute HCl and KOH solutions.

### 3.2.2 Methods

3.2.2.1 Flotation

The flotation tests were performed in a custom-made Hallimond flotation tube with a Siwek top.[16] In single mineral flotation tests, 1.5 g chalcopyrite or molybdenite particles (size fraction: −150+74 μm) were added into 150 mL 0.001 M KCl solution with or without HA at a desired concentration and pH. In mixed minerals flotation tests, 1.5 g artificial mixture of molybdenite and chalcopyrite particles (size fraction: −150+74 μm) with a weight ratio of 1:1 was mixed with 150 mL 0.001 M KCl solution at desired pH and HA concentration. The pulp pH was adjusted by KOH or HCl again and then stirred for 5 min.

Thereafter, KIBX was added to obtain a concentration of 20 ppm and the suspension was conditioned for 3 minutes. Then MIBC was injected to reach a concentration of 20 ppm and the slurry was further conditioned for 2 minutes. The conditioned pulp was then transferred to the Hallimond flotation tube and floated for 2 minutes using compressed air at a flow rate of 20 $cm^3$/min. In single mineral flotation tests, the recovery of each mineral was calculated based on the dry weight of concentrate and tailings. In flotation experiments on mineral mixtures, the concentrates and tailings were filtered, dried and weighed. The recovery of chalcopyrite and molybdenite was calculated based on the chemical assays of the copper and molybdenum contents in the concentrates and tailings, and the average values were reported.

3.2.2.2 Adsorption study

Adsorption isotherm measurements were performed at 295 K in a series of conical flasks that shaken on an orbital shaker. Specifically, 0.5 g -37 μm mineral particles were added into a series of conical flasks with 40 mL 0.001 M KCl solutions at pH 9 and varying concentration (0, 10, 20, 40, 60, 80, 100, 150, 200, 250 ppm) of HA, respectively. The flasks were then stoppered and shaken at 500 rpm for 30 minutes.

The supernatants of the suspensions were then extracted and filtered separately through a series of polyvinylidene difluoride membranes with a reported pore size of 0.22 μm to remove any fine particles. The residual HA concentration in solution was determined by an Evolution 300 UV-Vis Spectrophotometer (Thermo Scientific, USA). The calibration curve for the HA concentration determination was established with various known concentrations (i.e., 0, 10, 20, 40, 80, 150, 250 ppm) of HA in 0.001 M KC1 solution at pH 9. It was discovered that the absorbance at 370 nm has a satisfying linear relationship with the HA concentration in this solution condition.[17] Therefore, the concentration of residual HA in the suspension was calculated from the absorbance of 370 nm. It was assumed that all the HA depleted from solution had been adsorbed completely onto the mineral surfaces.

3.2.2.3 Electrokinetic studies

Zeta potential measurements were conducted to investigate the adsorption behaviors of HA onto mineral particles at different pH. A Zetasizer Nano (Malvern Instruments Ltd.,

UK) was used to record the zeta potentials of mineral particles under different solution conditions. In each measurement, 0.5 g of fresh mineral particles (size fraction: -37 μm) were added into 50 mL 0.001 M KCl solution at desired pH, with or without 20 ppm HA. The pH of mineral suspensions was adjusted again using KOH or HCl, and then ultrasonicated for 5 minutes. Prior to each measurement, an equilibration time of 15 min was allowed, and each measurement was repeated three times and the average value was presented.

3.2.2.4 Infrared spectroscopy

In each test, 0.5 g of mineral particles (size fraction: −37 μm) were ground to ~2 μm by agate mortar/pestle, then conditioned in 50 mL 0.001 M KCl solution with 500 ppm HA at pH 9 for 30 min. Thereafter, the conditioned mineral particles were filtered and washed three times with Milli-Q water, and dried prior to measurements. The as-received HA powder, HA-treated and untreated minerals particles, were mixed with potassium bromide (IR grade, ACROS Organics, USA) powder respectively. The DRIFT spectra of HA, untreated and treated mineral particles were then recorded against the KBr background using a Nicolet iS50 FT-IR spectrophotometer (Thermo Scientific, USA).

3.2.2.5 X-ray photoelectron spectroscopy (XPS)

The XPS was performed on freshly exfoliated and HA-treated molybdenite basal planes. The HA-treated molybdenite was prepared by immersing the freshly exfoliated

molybdenite basal plane into a 0.001 M KCl solution with 20 ppm HA at pH 9 for 10 min. The treated molybdenite was then taken out, rinsed by Milli-Q water, and purge dried with high purity $N_2$ gas before XPS measurements. The binding energy peak intensities and positions of HA-treated and untreated substrates were compared to detect any possible chemical interactions between HA and molybdenite surfaces.

3.2.2.6 ToF-SIMS measurements

The HA distribution on the mineral surfaces was mapped by Time-of-Flight Secondary Ion Mass Spectrometry (ToF-SIMS), to demonstrate the possible preferential adsorption of HA on mineral surfaces and the interaction mechanisms. Specifically, 1.5 g artificial mixture of chalcopyrite and molybdenite particles (size fraction: -37 μm) with a weight ratio 1:1 was added into 150 mL 0.001 M KCl solution with 20 ppm HA at pH 9. The suspension was then magnetically stirred for 30 min and filtered. The filter cake was washed three times with Milli-Q water, and dried in a vacuum oven at 298K prior to ToF-SIMS analysis. The ToF-SIMS measurements were carried out within 12 h after sample preparation to minimize surface oxidation and contamination.

## 3.3 Results and discussion

### 3.3.1 Single mineral flotation

The single minerals flotation tests were firstly performed in 0.001 M KCl solution at pH 9 with 20 ppm KIBX and 20 ppm MIBC under various concentrations of HA, to

determine the proper HA concentration for efficient chalcopyrite-molybdenite separation. **Figure 3.2** shows that molybdenite flotation was evidently depressed with the addition of HA, as its recovery dropped sharply from 98% to 14% at 20 ppm HA, and then remained around 10% at higher HA concentrations. In comparison, the chalcopyrite recovery was not affected in the presence of HA after the addition of 20 ppm KIBX, and remained around 97% in the entire HA concentration range tested (up to 40 ppm). Therefore, the proper concentration of HA for Cu-Mo separation was determined to be 20 ppm, and was tested in the following flotation tests to study the influence of solution pH on the flotation performance of each mineral.

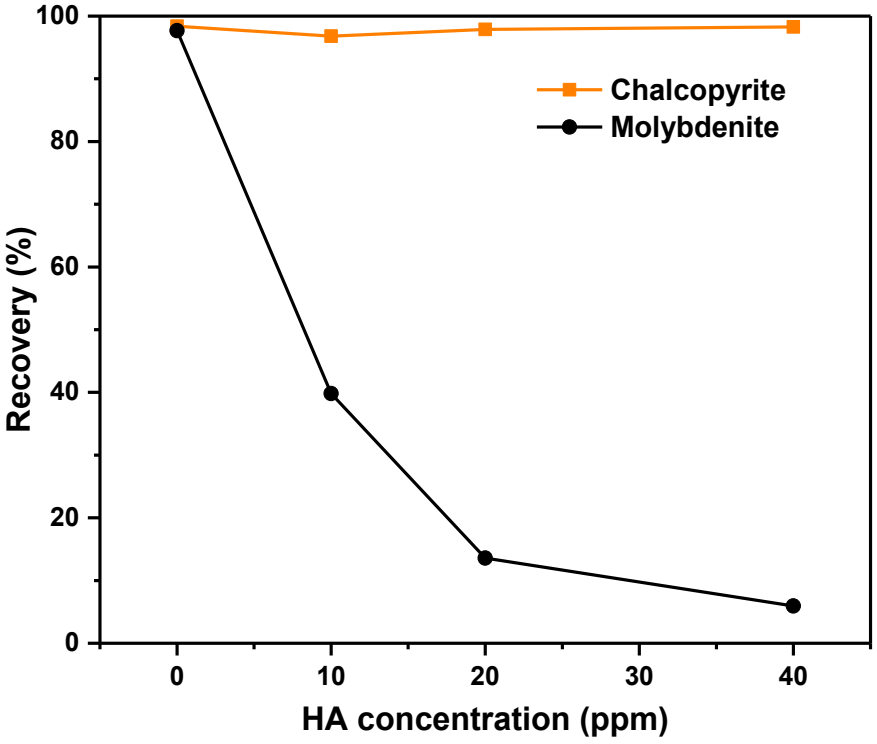


**Figure 3.2**. Flotation recovery of chalcopyrite and molybdenite in 0.001 M KCl solution with various concentration (0 to 40 ppm) of HA at pH 9. Collector: 20 ppm KIBX. Frother: 20 ppm MIBC.

The flotation response of molybdenite and chalcopyrite was then tested individually without and with 20 ppm HA at different pH. As can be seen in **Figure 3.3**, in the absence of HA and the presence of 20 ppm KIBX, the recovery of chalcopyrite remained above 97% regardless of the change in solution pH. On the other hand, molybdenite flotation recovery was above 95% in the pH range of 3-9 without HA and dropped to 82% at pH 11. These results agree well with the literature reports[11, 18] and our previous work,[17] which reported that molybdenite recovery is reduced under strong alkaline conditions (pH 11) while the chalcopyrite recovery was not affected by the variations of pH.

However, after the addition of 20 ppm HA, the molybdenite recovery remained below 14% in the entire pH range tested. While the flotation of chalcopyrite was not affected by the addition of HA and remained above 95% under all pH conditions. Hence, a large separation window from pH 3 to 11 can be observed in which molybdenite was effectively depressed by 20 ppm HA while chalcopyrite was completely floated with the addition of 20 ppm KIBX.

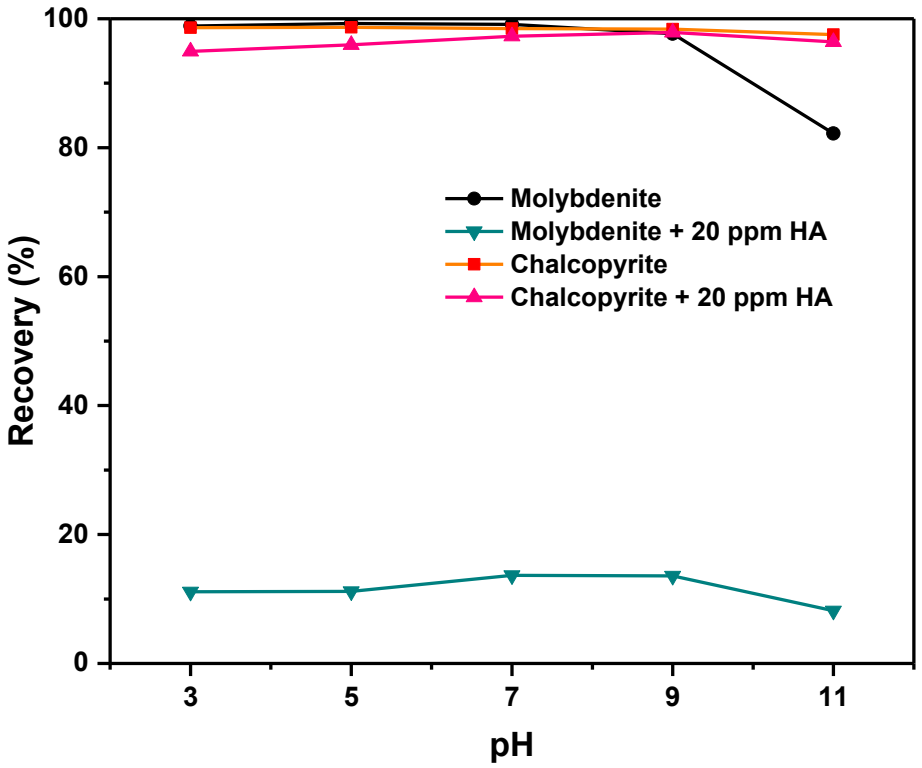


**Figure 3.3**. Flotation recovery of chalcopyrite and molybdenite in 0.001 M KCl solution with and without 20 ppm HA at varying pH. Collector: 20 ppm KIBX. Frother: 20 ppm MIBC.

### 3.3.2 Mixed minerals flotation

The flotation tests on single minerals with 20 ppm HA at varying pH revealed a large separation window from pH 3 to 11. Therefore, flotation tests were carried out for the artificial mixtures of chalcopyrite and molybdenite with 1:1 weight ratio in the presence of HA, to verify the possibility of employing HA as a selective depressant in the separation of molybdenite-chalcopyrite mixtures.

**Figure 3.4** shows the recovery of molybdenite and chalcopyrite in the concentrates floated from the molybdenite-chalcopyrite mixtures with 1:1 weight ratio. As can be seen, chalcopyrite was separated from molybdenite in the entire pH range tested, where chalcopyrite recovery was over 80% in most pH range except for pH 11. Meanwhile, molybdenite flotation was effectively depressed with a recovery of around 20% except pH 3. Therefore, even at a concentration of 10 ppm, HA could depress molybdenite flotation well and only slightly depressed chalcopyrite and the selectivity of HA was not influenced by pH. It can be concluded that HA is an effective depressant in separating the two sulfide minerals.

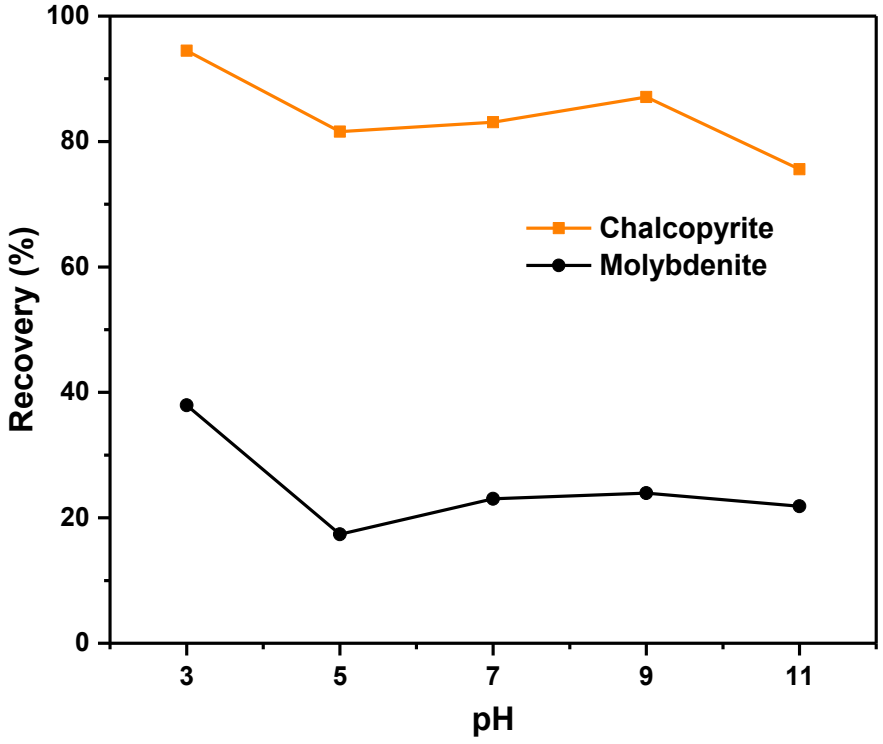


**Figure 3.4**. Flotation recovery of molybdenite and chalcopyrite from a 1:1 artificial mixture in 0.001 M KCl solution with 10 ppm HA at varying pH. Collector: 20 ppm KIBX. Frother: 20 ppm MIBC.

### 3.3.3 Adsorption isotherms

The adsorption isotherms of HA on chalcopyrite and molybdenite at 295 K are presented in **Figure 3.5**. Overall, the adsorption density of HA on both minerals increases with increasing HA concentration. However, it can be noticed that the adsorption density of HA on chalcopyrite was higher than that on molybdenite under the same equilibrium concentration of HA, especially in the low HA concentration region. The adsorption result is contradictory to the flotation results if HA is considered to be a selective depressant for molybdenite during the molybdenite-chalcopyrite separation. However, it should be noted that the "apparent" higher adsorption density of HA on chalcopyrite compared to molybdenite could be caused by the different adsorption mechanisms. The "apparent" adsorption density of HA on chalcopyrite may seem higher, but the interactions between HA and chalcopyrite could be weaker physical interactions such as electrostatic interaction. In fact, the HA could interact with the surface oxidation products (metal ions, metal oxides, and metal hydroxides, etc.) of chalcopyrite (or pyrite, the major impurity), and depleted or precipitated from the solution,[19, 20] thereby resulting in the apparent higher adsorption density of HA on chalcopyrite sample. However, after the addition of collector xanthate, the adsorption of xanthate on chalcopyrite surface will compete with the adsorption of HA, leading to the desorption of HA due to the stronger chemical interaction between xanthate and chalcopyrite surfaces; thus the flotation of chalcopyrite was not affected by HA. In contrast, no such a strong chemical interaction

was reported between xanthate and molybdenite basal planes, and the interaction between HA and molybdenite are dictated by hydrophobic interaction. Hence, the adsorbed HA on molybdenite basal planes, as observed in the AFM imaging of our previous work,[17] could not be easily displaced by xanthate.

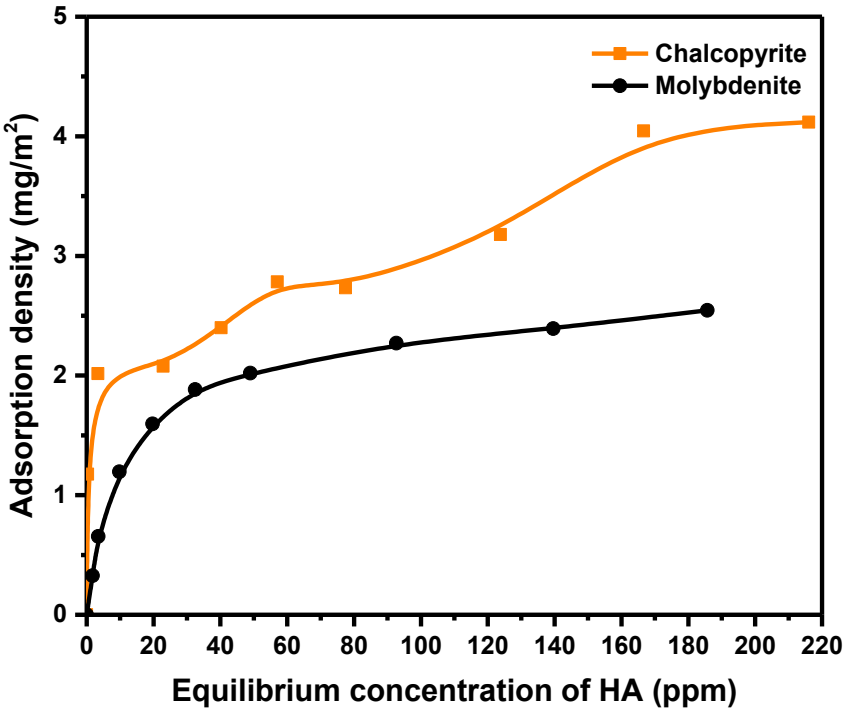


**Figure 3.5**. Adsorption isotherms of HA on chalcopyrite and molybdenite in 0.001 M KCl at pH 9 (Initial HA concentration was 0, 10, 20, 40, 60, 80, 100, 150, 200, 250 ppm).

To better understand the adsorption mechanisms, the adsorption isotherm of HA on molybdenite was fitted to the Langmuir-Freundlich adsorption equation (equation 2.2) as shown in section 2.3.3 of chapter 2, while the adsorption isotherm of HA on chalcopyrite was not modelled owing to its irregular shape. The equilibrium concentration ($C_{eq}$) of HA and the adsorption density (q) are related by the equation 2.2 (or equation 3.1) as follows:

$$q = \frac{Q_{sat} \cdot K \cdot C_{eq}^{\ n}}{\left(1 + K \cdot C_{eq}^{\ n}\right)} \tag{3.1}$$

All the parameters are already introduced in the section 2.3.3 of chapter 2. Again, the unit of Langmuir equilibrium constant (K) must be liters per mole in order to calculate the free energy change of adsorption ($\Delta G = -RT \cdot \ln K$). Hence, the $C_{eq}$ must have a unit of moles per liter. Assuming the HA has a molecular weight of 10,000 g/mol, **Figure 3.5** can then be replotted as **Figure 3.6**.

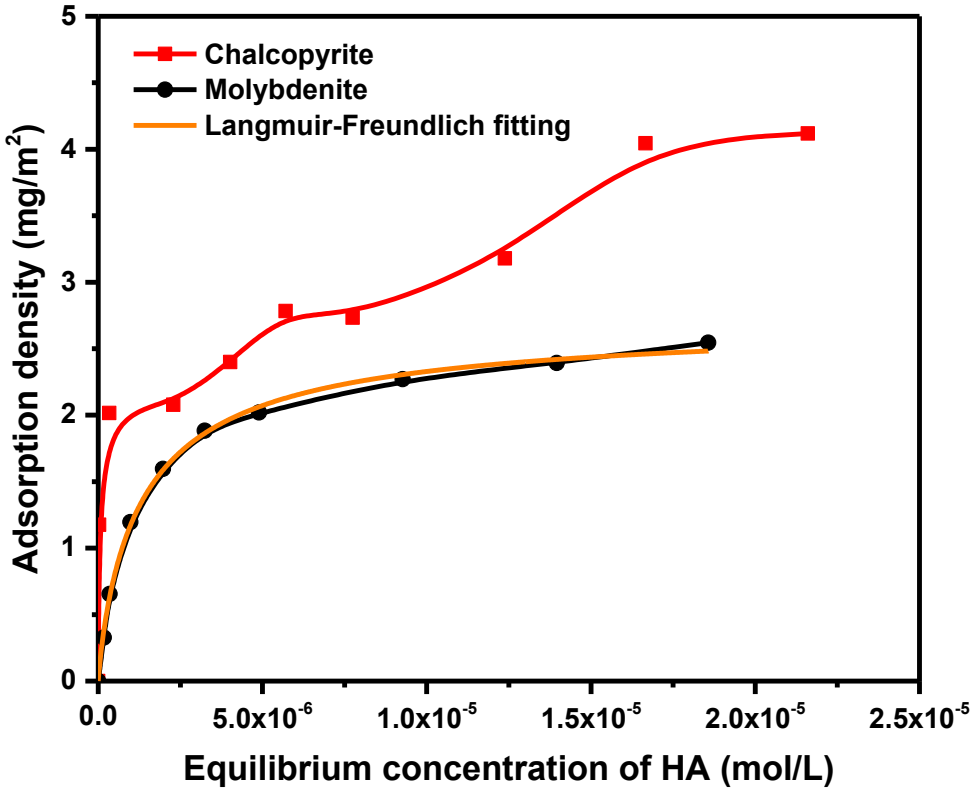


**Figure 3.6**. Fitted adsorption isotherms of HA on chalcopyrite and molybdenite in 0.001 M KCl at pH 9.

The parameters of Langmuir-Freundlich fitting are listed in **Table 3.1**, together with the results (molybdenite 1) from **Table 2.1**. As shown in **Table 3.1**, the maximum adsorption density ($Q_{sat}$) of HA on both samples (molybdenite 1 and 2) are close to each other. The slight differences in some parameters are likely attributed to the different sample preparation procedures. Specifically, the mineral suspensions (molybdenite 1) in chapter 2 were centrifuged before the determination of residual HA concentration, while the mineral suspensions (molybdenite 2) in this work (chapter 3) were not centrifuged and were filtered before the measurements of HA concentration.

**Table 3.1**. Adsorption parameters for the adsorption of HA on molybdenite 1 and 2 at T=298.15K, as determined from fitting to Langmuir-Freundlich equation.

| | $Q_{sat}$ (mg/m$^2$) | K | n | $R^2$ | ΔG(KJ/mol) |
|---|---|---|---|---|---|
| **Molybdenite 1** | 2.48±0.76 | 44661 | 0.78±0.27 | 0.98 | -26.54 |
| **Molybdenite 2** | 2.73±0.08 | 142794 | 0.88±0.06 | 0.99 | -29.42 |

It can be seen that the free energy changes during the adsorption of HA on both molybdenite samples were < 50 KJ/mol, which further confirmed that no strong chemical interactions were involved. Hence, the interactions between HA and molybdenite basal planes should be dictated by physical interactions such as hydrophobic attraction and electrostatic repulsion. Again, hydrogen bonding was ruled out as the primary interaction

mechanism since the formation of hydrogen bonds between molybdenite surfaces and HA would require the breakdown of hydrogen bonds between $H_2O$ and HA/mineral surfaces.

### 3.3.4 Electrokinetic studies

To explain the adsorption results of HA and possible interaction mechanisms between HA and these two minerals, the zeta potentials of treated and untreated mineral particles under various pH were collected and the results are shown in **Figure 3.7**. As can be seen, the chalcopyrite particles were positively charged at pH below 7 and became negatively charged at pH above 7, and more negatively charged at higher pH, with an estimated iso-electric point (IEP) around pH 7, which is within the range of literature values.[21] In fact, the IEP of chalcopyrite is not a fixed value due to the rapid oxidation of its surface, and in most cases, an "apparent" iso-electric point (IEP) is determined, which represent the oxidation extent of the chalcopyrite.[21] On the other hand, the molybdenite particles were negatively charged over the entire pH (3 to 11) range tested; with an estimated iso-electric point (IEP) lower than 2. Besides, the zeta potential of molybdenite was more negative that chalcopyrite in all pH range tested, which is in agreement with the previous report.[11]

In the presence of 20 ppm HA, the zeta potentials of chalcopyrite or molybdenite particles were more negative than that in the absence of HA over the entire pH range. This is because HA is strongly negatively charged in the pH range of 3-11, hence the adsorbed HA on mineral surfaces would render the mineral particles overall more

negatively charged. Besides, it can be seen that as the solution pH decreased, the zeta potential difference between HA-treated chalcopyrite and untreated chalcopyrite increased, indicating that the adsorption density of HA on chalcopyrite surfaces increased at lower pH, possibly due to the increased electrostatic attraction at pH < 7. At pH 3, the zeta potential of untreated chalcopyrite was 16.4 mV while the zeta potential of HA-treated chalcopyrite was -37.7 mV, indicating that the adsorption of HA shifted the zeta potential of chalcopyrite by 54.1 mV. The results suggest that there was a relatively large amount of HA adsorbed onto chalcopyrite surfaces at pH 3, because of the strong electrostatic attraction. In comparison, the molybdenite surfaces, both the basal planes and edges are strongly negatively charged under all pH tested, indicating there is strong electrostatic repulsion between HA molecules and molybdenite surfaces. Hence, the driving forces for HA adsorption onto molybdenite surface would be dominated by hydrophobic interaction between the hydrophobic moieties of HA and the molybdenite basal planes. In fact, our previous study also directly observed the adsorption of HA molecules onto molybdenite basal planes.

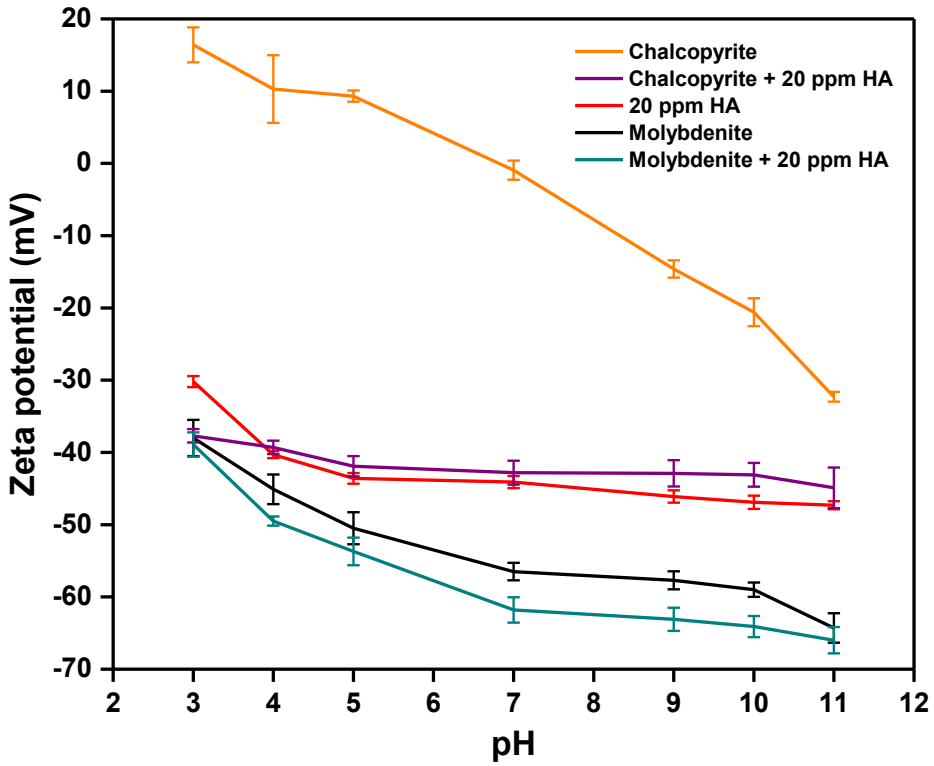


**Figure 3.7**. Zeta potential of chalcopyrite, chalcopyrite + HA, HA, molybdenite and molybdenite + HA at varying pH in 0.001 M KCl. The zeta potential results of molybdenite and molybdenite + HA are from our previous work.[17]

### 3.3.5 Infrared spectroscopy

The DRIFT spectra of chalcopyrite and molybdenite before and after conditioning in 0.001 M KCl solutions with 500 ppm HA at pH 9 are shown in **Figure 3.8** and **Figure 3.9**, respectively, together with the HA spectrum in the range of 900-3000 $cm^{-1}$. In the HA spectrum, the peaks at 2920 $cm^{-1}$ and 2850 $cm^{-1}$, 1677 $cm^{-1}$,1577 $cm^{-1}$, 1390 $cm^{-1}$ were attributed to the stretching vibration of $–CH_3$ and $–CH_2–$ groups, C=O stretching vibration (amide I), asymmetric stretching of $–COO^-$, symmetric stretching of $–COO^-$,

respectively. The bands at 1100, 1033, 1010 $cm^{-1}$ originate from the –C–O– vibration and C–O stretching of polysaccharides.[6, 22, 23]

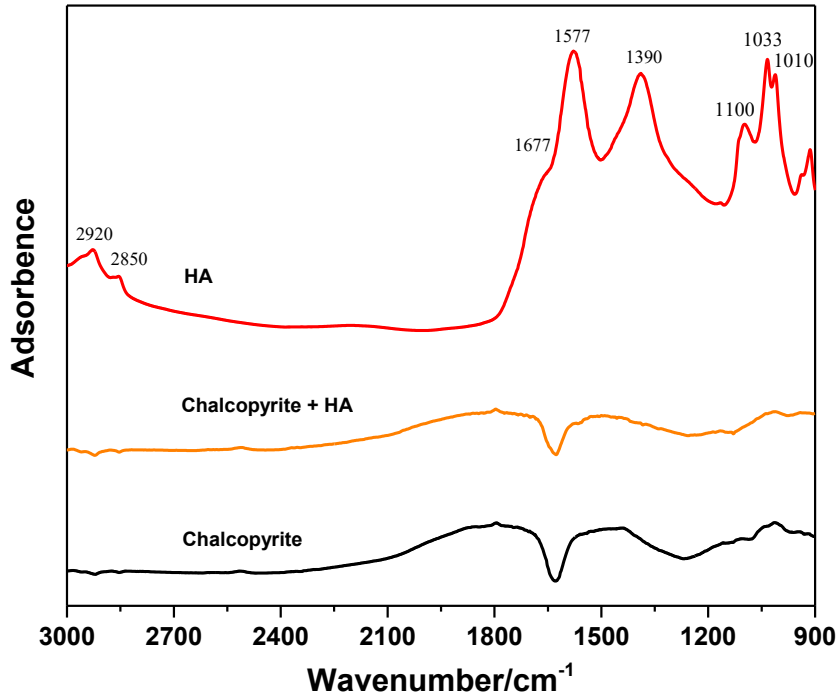


**Figure 3.8**. The DRIFT spectra of chalcopyrite before and after conditioning in 0.001 M KCl with 500 ppm HA at pH 9.

**Figure 3.8** demonstrates that the spectrum of chalcopyrite conditioned with 500 ppm HA was almost identical to that of the bare chalcopyrite. Hence, it can be inferred that no HA molecules were detected on chalcopyrite surfaces after being washed thoroughly with water, indicating that the interactions between chalcopyrite and HA are relatively weak and were mainly physical interactions such as electrostatic interaction, etc., as suggested by zeta potential measurements. However, **Figure 3.9** indicates that after conditioning with HA, several new bands near 2920, 2850, 1677, 1577 and 1390

$cm^{-1}$ appeared on the spectrum of HA-treated molybdenite, as a result of HA adsorption. This indicates that HA molecules could strongly adsorb onto molybdenite surfaces, and cannot be easily removed by Milli-Q water.

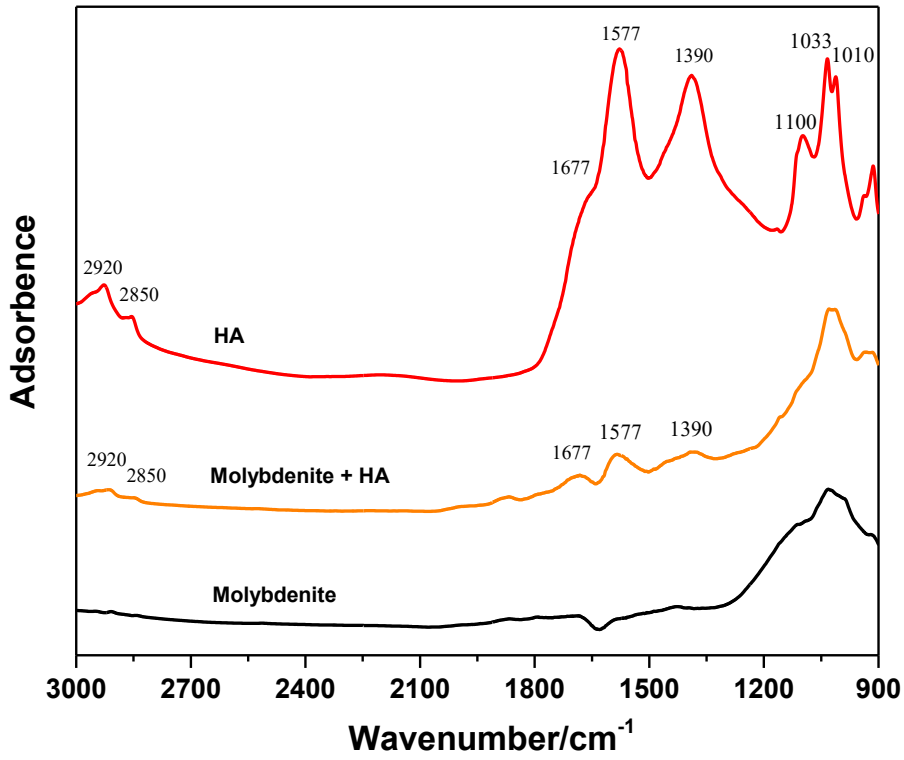


**Figure 3.9**. The DRIFT spectra of molybdenite before and after conditioning in 0.001 M KCl with 500 ppm HA at pH 9.

### 3.3.5 XPS measurements

Since HA is a group of complex anionic polyelectrolytes and the composition or molecular structure of HA has not been well defined,[6] the XPS spectra of humic acids have not been well understood.[24-26] Therefore, the XPS spectra of HA-treated mineral surfaces could not be well fitted or analyzed.

The high-resolution XPS spectra of molybdenite basal planes before and after treatment with 20 ppm HA in 0.001 M KCl solution at pH 9 were shown in **Figure 3.10** and **Figure 3.11**. As can be seen, no binding energy shift (or chemical shift) was observed for the Mo 3d and S 2p peaks before and after HA treatment, which implies that chemical interactions are absent between HA and molybdenite basal planes. Since both HA molecules and molybdenite basal planes carry strong negative charges from pH 3 to 11, as shown in the zeta potential measurements and previous reports,[27, 28] the only possible interaction between HA and molybdenite that could overcome the electrostatic repulsion is the hydrophobic interaction between the hydrophobic moieties of HA and molybdenite basal planes.

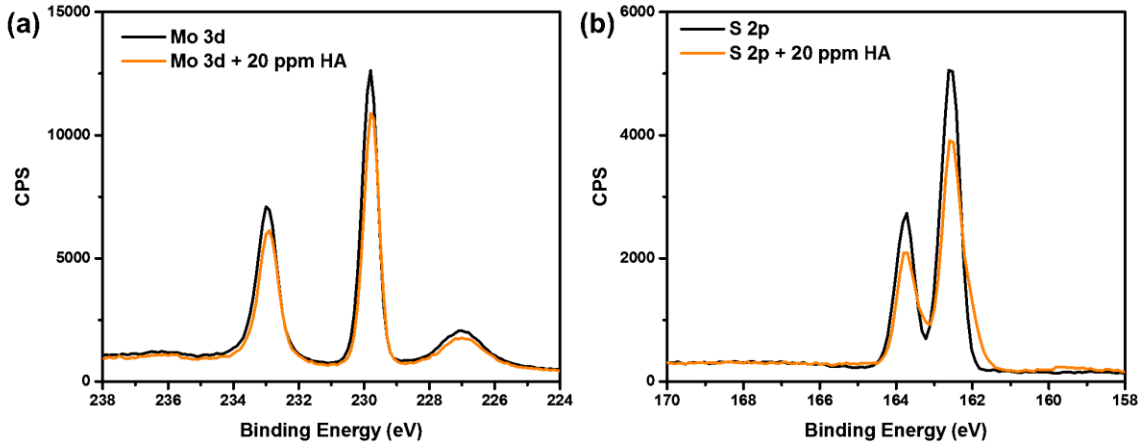


**Figure 3.10**. High-resolution XPS spectra of (a) Mo 3d and (b) S 2p of molybdenite before and after treatment by 20 ppm HA in 0.001 M KCl solution at pH 9.

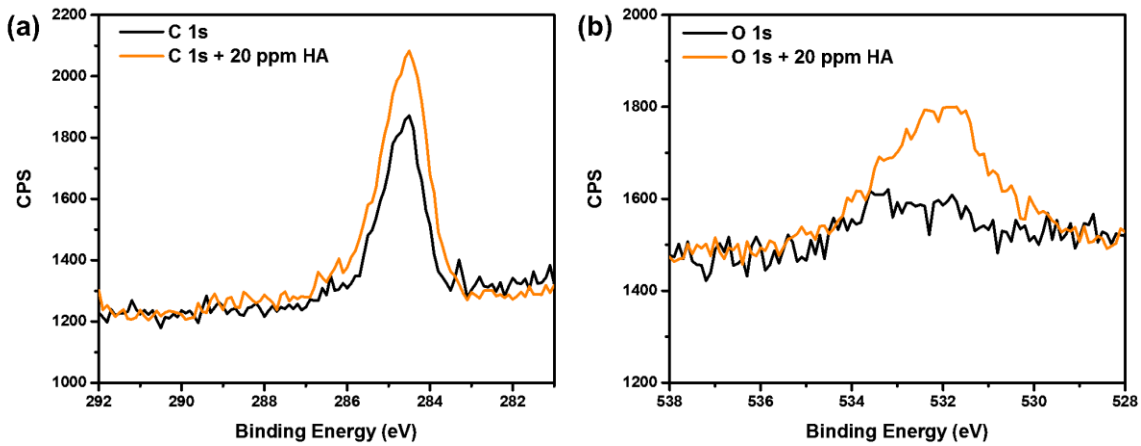


**Figure 3.11**. High-resolution XPS spectra of (a) C 1s and (b) O 1s of molybdenite before and after treatment by 20 ppm HA in 0.001 M KCl solution at pH 9.

However, from the high-resolution C 1s and O 1s spectra as shown in **Figure 3.11**, it could not determine whether there is any binding energy shift or not before and after HA treatment. The C 1s and O 1s peaks of molybdenite basal planes before HA treatment originate from the airborne hydrocarbon contamination. After HA treatment, the peak intensity of C 1s increased slightly, and no apparent binding energy shift was observed, which further confirmed the absence of strong chemical interaction. In comparison, the O 1s peak of the HA-treated molybdenite increased significantly, which largely comes from the oxygen in the HA molecules. Again, due to the complexity of HA structures and the low signal-to-noise ratio, the O 1s peak could not be well analyzed.

The XPS analysis on chalcopyrite is much more complicated due to the rapid oxidation of chalcopyrite surfaces,[29, 30] especially before and after treatment in aqueous

solutions.[31] Since chalcopyrite is not depressed during the flotation, the XPS measurements were not performed on chalcopyrite before and after HA treatment.

### 3.3.6 ToF-SIMS measurements

ToF-SIMS measurement was employed to directly detect the possible selective adsorption of HA on molybdenite and chalcopyrite surfaces. On the chalcopyrite-molybdenite mixture surface, the distribution of $Cu^+$, $Fe^+$, and $Mo^+$ were chosen to outline the molybdenite and chalcopyrite particles in the mixture treated with HA. Similarly, the $C_3H_7^+$ and $C_4H_7^+$ ions, as fragments of HA, were selected to represent the distribution of HA on the mineral mixture surface. The distributions of HA, chalcopyrite, and molybdenite on a scan area of 86 × 86 $\mu m^2$ are shown in **Figure 3.12** (a)-(e). By comparing the images in **Figure 3.12**, it was observed that the distribution of HA matched well with the $Mo^+$ distribution and partially overlapped the $Fe^+$ distribution, but does not match well with the distribution of $Cu^+$. The ToF-SIMS images indicate that the HA has preferentially adsorbed onto the molybdenite surfaces and certain iron sites of chalcopyrite (or pyrite) surfaces. In fact, it has been reported that HA could interact with the oxidation species of Fe due to the electrostatic attraction between the $–COO^-$ groups and the $Fe^{2+}$, $Fe(OH)^+$ etc.[20, 32]

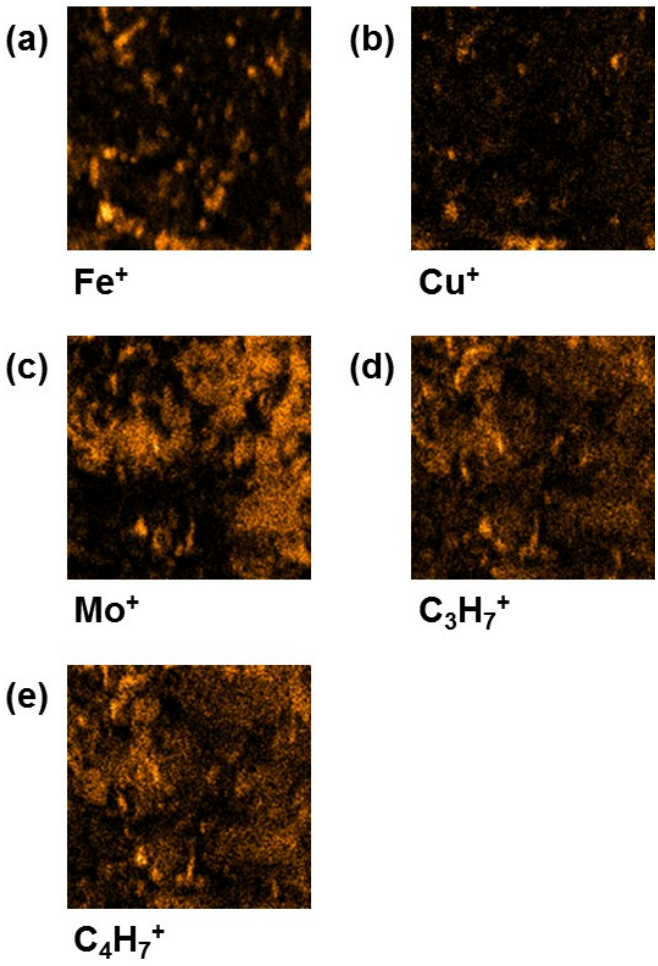


**Figure 3.12**. Positive-ion images of 86 × 86 μm$^2$ of the surface of chalcopyrite–molybdenite mixture (weight ratio of 1:1) treated with 20 ppm HA in 0.001 M KCl solution at pH 9. (a) Image of $Fe^+$ distribution; (b) Image of $Cu^+$ distribution; (c) Image of $Mo^+$ distribution; (d) Image of $C_3H_7^+$ distribution; (e) Image of $C_4H_7^+$ distribution.

To further interpret the possible adsorption characteristics of HA on chalcopyrite and molybdenite surfaces, the positive ion spectra of chalcopyrite–molybdenite mixture treated with 20 ppm HA at pH 9 is shown in **Figure 3.13**. It should be noted that HA is a group of anionic polyelectrolytes and the structure of HA is unknown. As a result, the

ToF-SIMS spectra are full of ionized fragments of HA and minerals, and could not provide much useful information about the interaction mechanisms. However, according to the atomic mass of elements (Mo, Cu, Fe, C, O, and H) in the minerals and HA, the peaks in positive ion spectra can be roughly assigned to different ionized fragments. The assignments of different peaks are presented in **Figure 3.13**. As can be seen, the ToF-SIMS spectra revealed that HA does adsorb on molybdenite surfaces and the iron-rich sites of chalcopyrite.

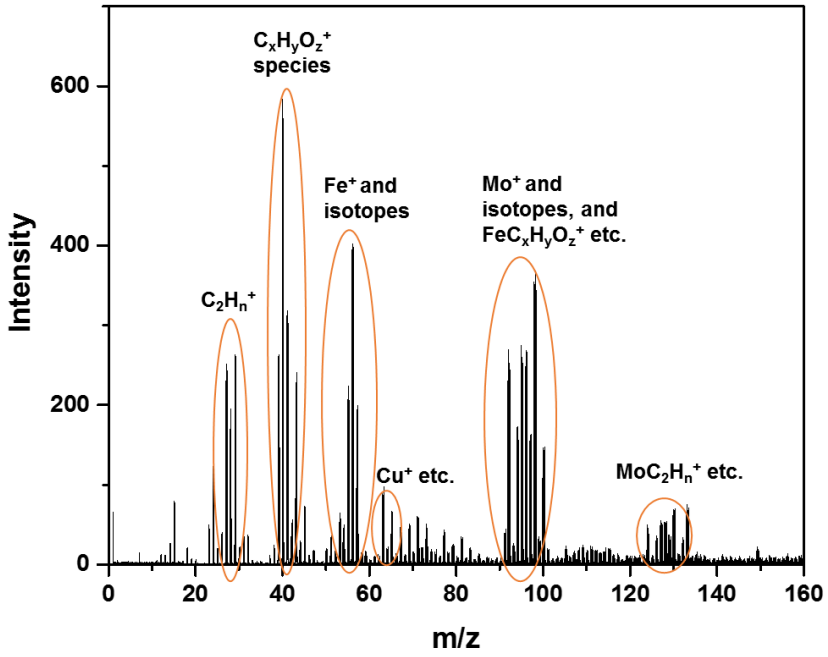


**Figure 3.13**. Positive ion ToF-SIMS spectra of chalcopyrite–molybdenite mixture (weight ratio 1:1) treated with 20 ppm HA in 0.001 M KCl solution at pH 9.

Since only the particles in the outermost layer of a sample have sufficient energy to escape from the sample, the sampling depth of ToF-SIMS analysis (without sputtering or itching) is typically around 1 to 2 nm. Therefore, the ToF-SIMS only reveals the surface

chemistry of the outmost layers of minerals. As shown in **Figure 3.12** and **3.13**, the stronger intensity of $Fe^{+}$ and its isotopes as compared with $Cu^{+}$ indicates that the chalcopyrite surface is partially covered by patches of iron oxides/hydroxides with a typical thickness of few nanometers (depending on oxidation degree). This phenomenon was confirmed by the XPS analysis of chalcopyrite by many other researchers.[29-31] Upon oxidation, patches of iron oxides/hydroxides will form on the chalcopyrite surface as shown in **Figure 3.14**. The iron oxides/hydroxides are typically positively charged with a relatively high IEP around pH 9,[21, 33] and these positively charged iron species would shift the overall zeta potential of chalcopyrite towards positive direction and provide possible adsorption sites for HA. The adsorption of HA on chalcopyrite is most likely due to the electrostatic interaction between the negatively charged carboxyl groups of HA and the positively charged iron oxides/hydroxides.[32] As a result, the apparent adsorption density of HA on chalcopyrite is higher than that of molybdenite. However, after the addition of xanthate, the competitive adsorption of HA will possibly desorb or partially desorb the adsorbed HA due to the stronger chemical interaction between xanthate and chalcopyrite surfaces.

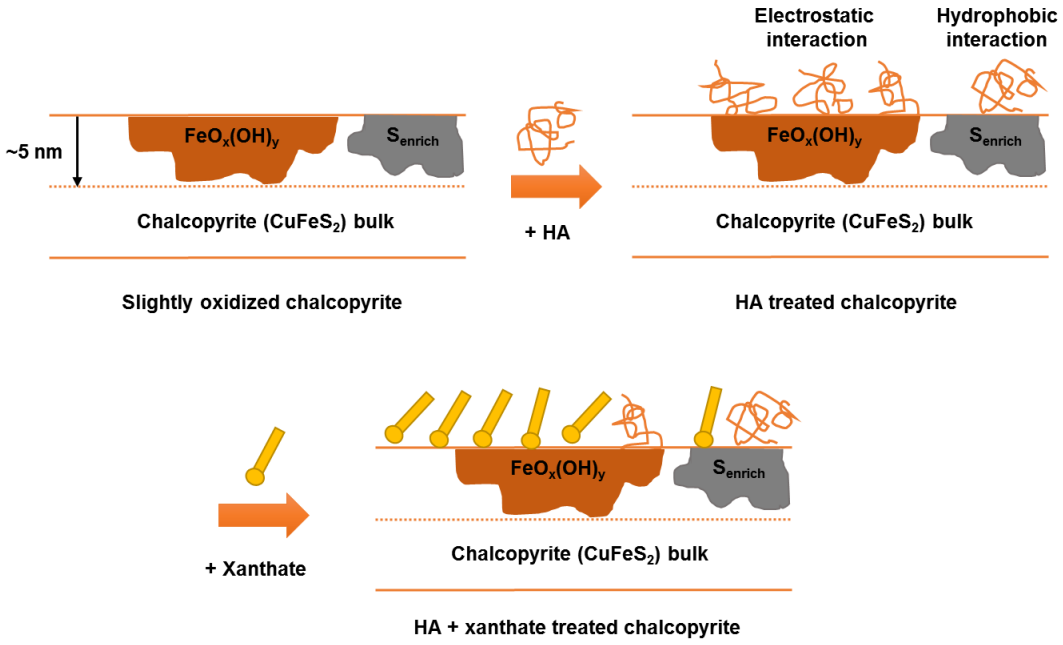


**Figure 3.14**. A simplified schematic diagram of the surface layer composition of chalcopyrite before and after treatment with HA and xanthate.

### 3.4 Conclusions

The influence of humic acids (HA) on the flotation response of molybdenite and chalcopyrite was investigated in this work. The microflotation tests on single minerals revealed that both chalcopyrite and molybdenite have good floatability with the addition of xanthate collector over a wide range of pH (3 to 9). Besides, the addition of HA had a negligible impact on the flotation of chalcopyrite in the presence of xanthate collector, and the chalcopyrite recovery remained above 95% over the entire HA concentration range tested (up to 40 ppm) and the entire pH range (3 to 11) tested. However, the addition of HA could dramatically reduce the molybdenite flotation recovery even at a very low concentration (20 ppm), regardless of the change in solution pH. Microflotation

tests on the artificial chalcopyrite-molybdenite mixtures further confirmed that HA could selectively depress molybdenite flotation during the copper-molybdenum sulfides separation in the pH range of 3-11.

The adsorption study and electrokinetic study revealed that the HA could adsorb on both chalcopyrite and molybdenite surfaces, and the interaction mechanisms between HA and these two minerals are different. It is concluded that chemical interaction is absent between HA molecules and molybdenite basal planes, as indicated in the high-resolution XPS analysis. Since both molybdenite basal planes and HA molecules are strongly negatively charged in the pH range of 3-11, the adsorption of HA on molybdenite basal planes (as confirmed in AFM imaging in **Figure 2.11**) is mainly attributed to the hydrophobic interaction between the hydrophobic moieties of HA and the molybdenite basal planes. On the other hand, the interactions between HA and chalcopyrite should be dominated by weak interactions such as electrostatic interaction and hydrophobic interaction (on the hydrophobic region or sulfur-enriched areas), due to the hydrophilic nature of fresh chalcopyrite surfaces and the surface oxides/hydroxides of chalcopyrite. In addition, the chalcopyrite flotation was not affected by HA after the addition of xanthate, indicating that HA may desorb or partially desorb from chalcopyrite surface upon xanthate addition.

DRIFT spectroscopy, XPS and ToF-SIMS analysis further confirmed the different interaction mechanisms between HA and these two minerals, as the adsorbed HA on chalcopyrite surfaces could be easily washed away by Milli-Q water while the adsorbed

HA on molybdenite surfaces could not be easily removed by rinsing or washing. All of the above results showed that HA could be employed as a cost-effective depressant for molybdenite during the flotation separation of molybdenite and chalcopyrite over a wide range of pH, and the stronger interaction between HA and molybdenite as compared to chalcopyrite is responsible for the selective separation. It worth to mention that no oily collectors such as kerosene or diesel oil[34] were added in this work. Future work is required to explore whether selective Cu-Mo separation can be achieved by HA if oily collectors were introduced. It is anticipated that the molybdenite flotation would still be depressed by HA even with the presence of oily collectors, and the chalcopyrite recovery will be slightly reduced, due to the hydrophobic interaction between HA and oil films on molybdenite and chalcopyrite surfaces. The adsorption of HA on oil/water interface was also observed in the oil sands flotation, where the bitumen is sometimes coated by layers of asphaltenes and humic acids.[35, 36] which could drastically decrease the hydrophobicity of bitumen and lower its recovery.

### 3.5 Acknowledgements

The XPS and ToF-SIMS measurements were conducted at the Alberta Centre for Surface Engineering and Science (ACSES), University of Alberta. This work is supported by the Natural Sciences and Engineering Research Council (NSERC) of Canada. Duowei Yuan appreciates the scholarship support from the China Scholarship Council (CSC).

## 3.6 References


1. Bulatovic, S. M., *Handbook of flotation reagents: chemistry, theory and practice: Volume 1: flotation of sulfide ores*. Elsevier: 2007.

2. Pearse, M. J., An overview of the use of chemical reagents in mineral processing. *Minerals Engineering* **2005,** *18* (2), 139-149.

3. Prasad, M. S., Reagents in the mineral industry — recent trends and applications. *Minerals Engineering* **1992,** *5* (3-5), 279-294.

4. Li, M.; Wei, D.; Liu, Q.; Liu, W.; Zheng, J.; Sun, H., Flotation separation of copper–molybdenum sulfides using chitosan as a selective depressant. *Minerals Engineering* **2015,** *83*, 217-222.

5. Poling, G.; Liu, Q., Flotation depression of chalcopyrite with thioglycolic acid. *TRANSACTIONS OF THE INSTITUTION OF MINING AND METALLURGY SECTION C-MINERAL PROCESSING AND EXTRACTIVE METALLURGY* **1987,** *96*, C7-C12.

6. Stevenson, F. J., Humus chemistry: genesis, composition, reactions. 2nd ed.; Wiley: New York, 1994.

7. dos Santos, I. D.; Oliveira, J. F., Utilization of humic acid as a depressant for hematite in the reverse flotation of iron ore. *Minerals Engineering* **2007,** *20* (10), 1003-1007.

8. Hoover, M., Water Chemistry Effects in the Flotation of Sulfide Ores-- a Review and Discussion for Molybdenite. *Complex Sulphide Ores* **1980**, 100-112.

9. Lai, R. W. M.; Stone, L. C.; Rimmasch, B. E., Effect of humus organics on the flotation recovery of molybdenite. *International Journal of Mineral Processing* **1984,** *12* (1-3), 163-172.

10. Laskowski, J.; Yu, Z. In *The effect of humic acids on the emulsion flotation of inherently hydrophobic minerals*, III Latin American Congress on Froth Flotation. Universidad de Concepción, Concepción-Chile, 1994; pp 397-411.

11. Castro, S.; Lopez-Valdivieso, A.; Laskowski, J. S., Review of the flotation of molybdenite. Part I: Surface properties and floatability. *International Journal of Mineral Processing* **2016,** *148*, 48-58.

12. Wang, J.; Liu, Q.; Zeng, H., Understanding Copper Activation and Xanthate Adsorption on Sphalerite by Time-of-Flight Secondary Ion Mass Spectrometry, X-ray Photoelectron Spectroscopy, and in Situ Scanning Electrochemical Microscopy. *The Journal of Physical Chemistry C* **2013,** *117* (39), 20089-20097.

13. Xie, L.; Shi, C.; Wang, J.; Huang, J.; Lu, Q.; Liu, Q.; Zeng, H., Probing the interaction between air bubble and sphalerite mineral surface using atomic force microscope. *Langmuir: the ACS journal of surfaces and colloids* **2015,** *31* (8), 2438-46.

14. Xie, L.; Wang, J.; Shi, C.; Cui, X.; Huang, J.; Zhang, H.; Liu, Q.; Liu, Q.; Zeng, H., Mapping the Nanoscale Heterogeneity of Surface Hydrophobicity on the Sphalerite Mineral. *The Journal of Physical Chemistry C* **2017,** *121* (10), 5620-5628.

15. Wang, J.; Xie, L.; Liu, Q.; Zeng, H., Effects of salinity on xanthate adsorption on sphalerite and bubble–sphalerite interactions. *Minerals Engineering* **2015,** *77*, 34-41.

16. Cao, M.; Liu, Q., Reexamining the functions of zinc sulfate as a selective depressant in differential sulfide flotation--the role of coagulation. *Journal of colloid and interface science* **2006,** *301* (2), 523-31.

17. Yuan, D.; Xie, L.; Shi, X.; Yi, L.; Zhang, G.; Zhang, H.; Liu, Q.; Zeng, H., Selective flotation separation of molybdenite and talc by humic substances. *Minerals Engineering* **2018,** *117*, 34-41.

18. Braga, P. F. A.; Chaves, A. P.; Luz, A. B.; França, S. C. A., The use of dextrin in purification by flotation of molybdenite concentrates. *International Journal of Mineral Processing* **2014,** *127*, 23-27.

19. Park, S.-j.; Yoon, T.-i., Effects of iron species and inert minerals on coagulation and direct filtration for humic acid removal. *Desalination* **2009,** *239* (1-3), 146-158.

20. Mahiuddin, S.; Suryanarayan, I.; Dutta, N. N.; Borthakur, P. C., Adsorption studies of sodium humate on Indian iron ore fines. *Colloids and Surfaces* **1992,** *64* (3-4), 177-184.

21. Fuerstenau, M. C.; Jameson, G. J.; Yoon, R.-H., *Froth flotation: a century of innovation*. SME: 2007.

22. Stevenson, F. J.; Goh, K. M., Infrared spectra of humic acids and related substances. *Geochimica et Cosmochimica Acta* **1971,** *35* (5), 471-483.

23. Piccolo, A.; Stevenson, F. J., Infrared spectra of Cu2+ Pb2+ and Ca2+ complexes of soil humic substances. *Geoderma* **1982,** *27* (3), 195-208.

24. Monteil-Rivera, F.; Brouwer, E. B.; Masset, S.; Deslandes, Y.; Dumonceau, J., Combination of X-ray photoelectron and solid-state 13C nuclear magnetic resonance

spectroscopy in the structural characterisation of humic acids. *Analytica Chimica Acta* **2000,** *424* (2), 243-255.

25. Bubert, H.; Lambert, J.; Burba, P., Structural and elemental investigations of isolated aquatic humic substances using X-ray photoelectron spectroscopy. *Fresenius' Journal of Analytical Chemistry* **2000,** *368* (2-3), 274-280.

26. Desbene, P.-L.; Silly, L.; Morizur, J.-P.; Delamar, M., Xps Analysis of Humic and Fulvic Acids. *Analytical Letters* **1986,** *19* (21-22), 2131-2140.

27. Lu, Z.; Liu, Q.; Xu, Z.; Zeng, H., Probing Anisotropic Surface Properties of Molybdenite by Direct Force Measurements. *Langmuir: the ACS journal of surfaces and colloids* **2015,** *31* (42), 11409-18.

28. Jada, A.; Ait Akbour, R.; Douch, J., Surface charge and adsorption from water onto quartz sand of humic acid. *Chemosphere* **2006,** *64* (8), 1287-95.

29. Buckley, A. N.; Woods, R., An X-ray photoelectron spectroscopic study of the oxidation of chalcopyrite. *Australian Journal of Chemistry* **1984,** *37* (12), 2403.

30. Fairthorne, G.; Fornasiero, D.; Ralston, J., Effect of oxidation on the collectorless flotation of chalcopyrite. *International Journal of Mineral Processing* **1997,** *49* (1-2), 31-48.

31. Mielczarski, J. A.; Cases, J. M.; Alnot, M.; Ehrhardt, J. J., XPS Characterization of Chalcopyrite, Tetrahedrite, and Tennantite Surface Products after Different Conditioning. 1. Aqueous Solution at pH 10. *Langmuir: the ACS journal of surfaces and colloids* **1996,** *12* (10), 2519-2530.

32. Vermeer, A. W. P.; van Riemsdijk, W. H.; Koopal, L. K., Adsorption of Humic Acid to Mineral Particles. 1. Specific and Electrostatic Interactions. *Langmuir: the ACS journal of surfaces and colloids* **1998,** *14* (10), 2810-2819.

33. Rao, S. R.; Leja, J., *Surface chemistry of froth flotation*. New York: Kluwer Academic/Plenum Publishers, 2nd ed. : 2004.

34. Zanin, M.; Ametov, I.; Grano, S.; Zhou, L.; Skinner, W., A study of mechanisms affecting molybdenite recovery in a bulk copper/molybdenum flotation circuit. *International Journal of Mineral Processing* **2009,** *93* (3-4), 256-266.

35. Gutierrez, L.; Pawlik, M., Influence of humic acids on oil sand processing. Part I: Detection and quantification of humic acids in oil sand ores and their effect on bitumen wettability. *International Journal of Mineral Processing* **2014,** *126*, 117-125.

36. Gutierrez, L.; Pawlik, M., Influence of humic acids on oil sand processing. Part II: Relationship between bitumen extraction, humic acids concentration and power draw measurements on oil sand slurries. *International Journal of Mineral Processing* **2014,** *126*, 126-135.

# Chapter 4. Impact of surface hydrophobicity and salinity on the adsorption of humic acids

## 4.1 Introduction

Humic acids (HA) are major constituents of humic substances or humus (soil), and they are produced by the microbial decomposition of vegetation, animals and microorganisms and subsequent polymerization and condensation of the biodegradation products.[1] As one of the most abundant naturally occurring organic macromolecules in the earth crust, humic acids and its analogues contribute to 60-70% of natural organic matter in soil, and 30-50% of dissolved organic constituents in aquatic systems depending on the source,[2-4] and widely exist in rivers, dystrophic lakes, groundwater, and even seawater.[1, 5] Understanding the adsorption kinetics and characteristics of humic acids onto surfaces with varying hydrophobicity and salinity is of both fundamental and practical importance. Which could provide important implications to various natural and engineering processes, such as the clay-humic interactions in soil,[6, 7] transportation of nutrients (N, P) and pollutants/contaminants (e.g. heavy metal ions) in soil and natural water environment,[1, 7, 8] water treatment and purification,[9] mineral processing industry,[10-12] oil sands industry and tailing management,[13] pharmaceutical and cosmetic areas etc.[14] However, to our knowledge, limited reports are available on the influence of surface hydrophobicity and solution salinity on the adsorption kinetics and characteristics of humic acids.

Herein, the influence of surface hydrophobicity and solution salinity on the adsorption of humic acids was studied, and the ability of humic acids to alter the surface hydrophobicity under different ionic strength and pH was also investigated. Long chain thiols terminated with varying functional groups (e.g., $-CH_3$, $-OH$, etc.) were used to produce surfaces with a broad range of hydrophobicities by changing the initial molar fraction of the thiols terminated with different functional groups.[15] Thiols terminated with $-CH_3$ and $-OH$ groups were chosen for this work to eliminate the possibility of specific chemical interactions between the humic acids and the substrate as well as alter the surface hydrophobicity. QCM-D measurements were performed to examine how humic acids adsorb onto gold surfaces coated with various long chain thiols. Contact angle measurements were also conducted immediately after QCM-D study to record the surface hydrophobicity of gold surfaces after HA treatment under various solution conditions.

## 4.2 Experimental section

### 4.2.1 Materials

Two long-chain thiols: 1-undecanethiol (98%, Sigma Aldrich, USA) and 11-mercapto-1-undecanol (97%, Sigma Aldrich, USA) were employed for the surface modification of gold substrates. Humic acids sodium salt or HA (Sigma-Aldrich, USA) was investigated in this study, and the molecular weight of HA ranges from 2 to 500 KDa. Potassium chloride (KCl, ACS reagent grade, Fisher Scientific) was introduced as the background electrolyte (0.001 M and 0.1 M KCl) for all the experiments. Milli-Q water

(Thermo Scientific, USA) with a resistivity of 18.2 MΩ·cm at 295K was used for the preparation of all aqueous solutions. The pH of all solutions was adjusted by small quantities of 0.1 M and 0.01 M KOH/HCl.

Since humic acids are a group of natural organic macromolecules, the exact molecular structure of HA cannot be determined. Hence, a theoretical molecular structure of HA is shown in **Figure 4.1**. As can be seen, HA contains both aromatic rings and aliphatic chains (hydrophobic moieties), in which –COOH groups, phenolic –OH groups and –O–, –N– bridging units (hydrophilic moieties) randomly distributed. As a result, HA is strongly negatively charged over a wide range of pH.[1] The aromatic rings and the hydrocarbon chain of HA originate from the lignin and microbial degradation, which contribute to its hydrophobic characteristics under certain pH range.[1]

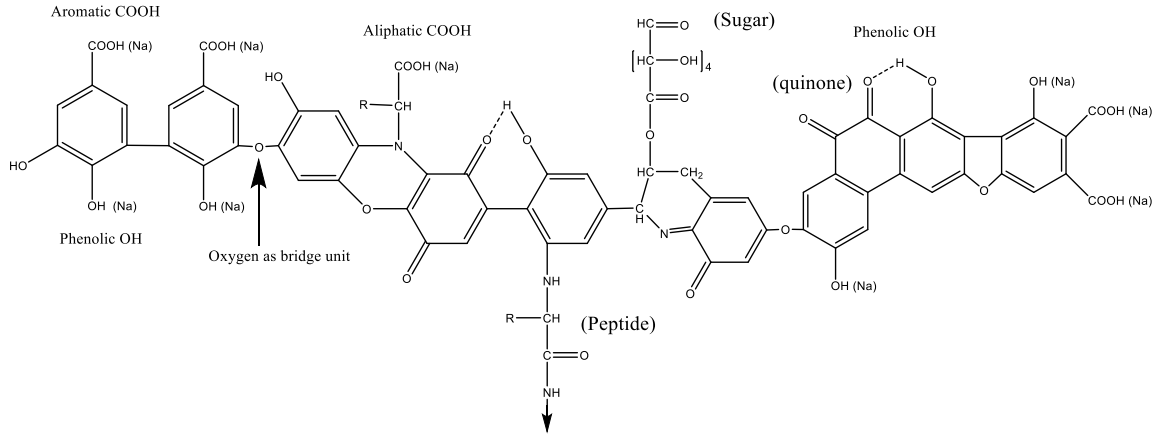


**Figure 4.1**. A theoretical structure of humic acids sodium salts (HA).[1]

As a polyelectrolyte with strong anionic characteristics, the zeta potential of HA used in this study was determined by a Zetasizer Nano (Malvern Instruments Ltd., UK). The Zetasizer Nano utilizes the technique of electrophoretic light scattering to determine the zeta potential of macromolecules. HA stock solution with 0.001 M KCl was diluted with 0.001 M KCl solution to reach a concentration of 20 ppm prior to measurements. Each measurement was repeated at least three times and the average value and standard deviation were reported. The zeta potential of HA in 0.001 M KCl solution as a function of pH is plotted in **Figure 4.2**. The HA has a significant negative zeta potential at high pH, becoming less negatively charged and more protonated with decreasing pH. Overall, the HA molecules are negatively charged in the entire pH range tested (3 to 11).

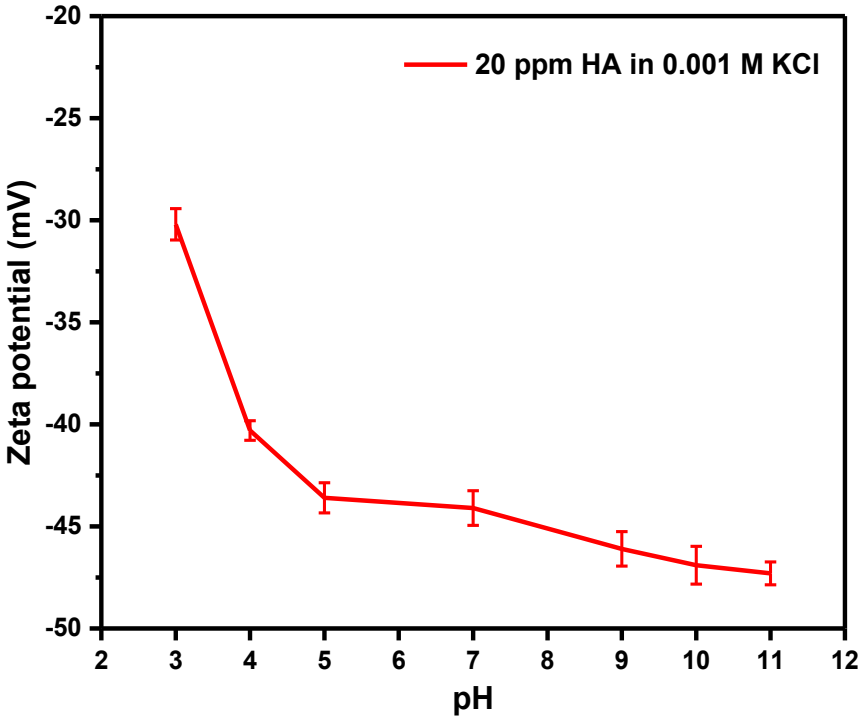


**Figure 4.2**. Zeta potential of 20 ppm HA in 0.001 M KCl solution at varying pH.

### 4.2.2 Surface modification

The gold QCM-D sensors were cleaned following the standard cleaning protocols prior to surface modification by thiols. The thiol-coated gold surfaces of QCM-D sensors with varying hydrophobicity were prepared by procedures reported previously.[16] Two long-chain thiols, 1-undecanethiol (98%, Sigma Aldrich, USA) and 11-mercapto-1-undecanol (97%, Sigma Aldrich, USA) were used for the surface modification of gold substrates. The thiol layers on gold substrates were formed by immersing the sensors into 0.005 M single or mixed anhydrous ethanol solutions of thiols (molar ratios $M_{OH}$ : $M_{CH3}$ = 1:0, 0.5:0.5, 0:1, where the first number is molar fraction of 11-mercapto-1-undecanol, and the second number is the molar fraction of 1-undecanethiol) for 16 hours. The sensors were then taken out and washed thoroughly with high purity ethanol followed by Milli-Q water, and dried with high purity nitrogen gas prior to further measurements.

### 4.2.3 Methods

#### 4.2.3.1 QCM-D experiments

The QCM-D experiments were performed using a Q-sense E1 QCM-D instrument (Biolin Scientific, Sweden). The instrument contains one flow cell in which a QCM-D sensor or crystal is placed, which serves as the substrate for the adsorption experiments. The QCM-D sensors are AT-cut and have a fundamental resonance frequency of ~5 MHz, with a diameter of 14 mm and a root-mean-square (rms) roughness of <1 nm. The

temperature was maintained at 293.15K throughout the experiments. During the adsorption process, the resonance frequency of the crystal $f_0$ will decrease to a lower value f due to the adsorption of molecules from solution onto the sensor surface, and the change in the resonance frequency $\Delta f=f_0-f$ is recorded by the instrument. Besides, the change in the dissipation energy loss of the crystal ($\Delta D$), which reflects the viscoelastic properties of the adsorbed layer, is also recorded simultaneously.[16]

For a rigid adsorbed layer with only a small change to the dissipation energy loss ($\Delta D < 5\times10^{-6}$),[17, 18] the change in resonance frequency ($\Delta f$) of the crystal is proportional to the adsorbed mass ($\Delta m$). In this circumstance, the adsorbed mass ($\Delta m$) can be calculated from the Sauerbrey equation as follows:

$$\Delta m = -C \cdot \Delta f = -C \cdot \frac{\Delta f_n}{n} \tag{4.1}$$

Where C is the mass sensitivity constant (17.7 $ng \cdot cm^{-2} \cdot Hz^{-1}$ at 5 MHz, the fundamental resonance frequency) that describes the mass sensitivity of the device, $\Delta f$ is the change in the crystal frequency (Hz). The adsorbed mass also can be determined from the change of the frequencies ($\Delta f_n$) at different overtone numbers (n), while n is the vibrational resonance overtone numbers (equal to 1, 3, 5, 7, 9 ...).[16, 17] Since the noise at 5 MHz (fundamental overtone, n=1) was particularly large, we followed the practice of literature reports,[19, 20] i.e., neglected these data and only focused on the overtones larger than one (n=3, 5, 7, 9). The adsorbed mass ($\Delta m$) values obtained from these overtone

numbers (3, 5, 7, 9) were compared, and the average values of adsorbed mass and standard deviation were also presented.

In addition, energy losses occur in the crystal during the adsorption of materials, leads to a damping of the crystal oscillation when the driving voltage is turned off. From the decay of the crystal oscillations, the energy dissipation can be monitored simultaneously and the dissipation factor D can be calculated using the following equation,[17] which reflects the viscoelastic properties of the adsorbed material.

$$D = \frac{E_{dissipated}}{2\pi E_{stored}} \tag{4.2}$$

Where $E_{dissipated}$ is the energy dissipated in one oscillation cycle, and $E_{stored}$ is the stored energy in one oscillating circuit. The change in dissipation $\Delta D = D - D_0$, where $D_0$ is the dissipation when the QCM-D sensor is just immersed into solution and before the adsorption progress, and D denotes the dissipation at any given time during the measurement.[17] For an adsorbed film with high rigidity, no significant change in dissipation will be observed as the adsorption progress. However, for a soft and/or viscoelastic layer, the energy dissipation will increase through the layer. Hence, by monitoring the change in dissipation (ΔD), the relative rigidity or stiffness of an adsorbed layer may be semi-quantitative determined,[17, 21] and an adsorbed layer with a high dissipation energy loss (ΔD) can be considered to be soft, while one with a low ΔD is recognized to be rigid.[22]

The thiol-coated gold sensors (with average water contact angles of 22°, 79°, and 106° respectively) were tested in 20 ppm HA solution with 0.1 or 0.001 M KCl at pH 3 or 9. In a typical test, the freshly prepared sensor was installed in the instrument chamber first. The background solution, i.e., 0.001 M or 0.1 M KCl at desired pH, was flowed through the chamber for approximately 10 min to establish a stable baseline (where $\Delta f$ and $\Delta D = 0$ ). Then HA solution at a concentration of 20 ppm and desired pH and KCl concentration was pumped into the chamber continuously for about 60 minutes (which is sufficient to reach adsorption equilibrium in most cases) at a flow rate of 100 μL/min. Finally, the background KCl solution was injected into the chamber again to flush away the HA solution as well as remove the non-adsorbed or weakly attached HA molecules.

4.2.3.2 Contact angle determination

The contact angle measurements on gold substrates before and after surface modification were performed using a Ramé-Hart Model 250 Standard Goniometer/Tensiometer (Ramé-Hart Instrument Co., USA) by the sessile drop method. The gold sensor was placed on a clean glass slide and fixed on a holder; a water drop was then deposited onto the sensor surface through a needle. The shape of the sessile drop was captured with a CCD camera, and the contact angle was determined by the image analysis software. Multiple measurements were taken on each surface at three different locations and the average values were reported.

4.2.3.3 PeakForce QNM AFM Imaging

A Dimension Icon Atomic force microscope (Bruker, Santa Barbara, CA) under the PeakForce Quantitative Nanoscale Mechanical (QNM) imaging mode was utilized to acquire the surface topography of gold surfaces before and after thiol-functionalization. Prior to the thiol modification, the topography of clean gold surfaces was obtained using PeakForce QNM mode in air. After thiol treatment, the topography of gold surfaces was recorded again and the contact angle measurements were also carried out. The AFM imaging and contact angle measurements were conducted on at least three different locations of gold surfaces and the representative results are presented.

## 4.3 Results and discussion

### 4.3.1 Substrate Characterization

The surface topography of gold surfaces before and after thiols modification is shown in **Figure 4.3**. As indicated in **Figure 4.3** (a), the clean gold surface exhibits hemispherical gold grains (~0.1 μm) with a root-mean-square (rms) roughness of ~0.4 nm, which is consistent with the literature reports.[23-25] After treatment with thiols solutions, the surface morphology of gold substrate is similar to that of the untreated gold surface, and the root-mean-square (rms) roughnesses of gold surfaces in **Figure 4.3** (b), (c) and (d) remain around 0.4 nm. The AFM imaging confirmed that the surface roughness of gold surfaces is unchanged before and after thiols treatment; hence the influence of surface roughness was ruled out/excluded in this study. However, the contact

angles of thiol-treated gold surfaces are significantly different from each other, and the average contact angles of gold surfaces in **Figure 4.3** (b), (c), and (d) are 106, 79, and 22°, respectively. The contact angle differences between thiol-modified gold surfaces revealed the successful self-assembling of thiol monolayers on the gold substrates.

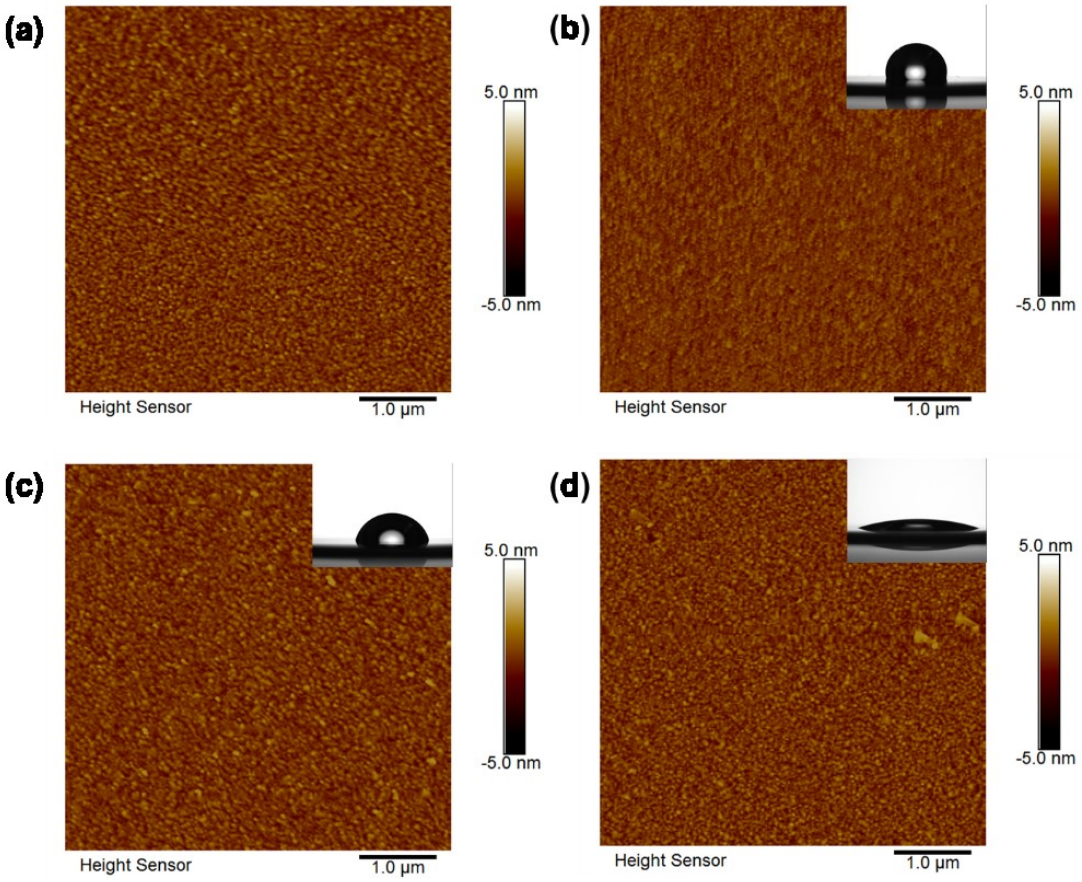


**Figure 4.3**. AFM height images and corresponding water contact angles of (a) Bare gold surface (b) $M_{OH}$ =0 gold surface with a contact angle θ =106°; (c) $M_{OH}$ =0.5 gold surface with a contact angle θ =79°; (d) $M_{OH}$ =1 gold surface with a contact angle θ =22°.

### 4.3.2 QCM-D Studies

4.3.2.1 Adsorption studies

(a) HA in 0.001 M KCl solution at pH 9

The adsorption isotherms of HA on three surfaces with varying hydrophobicity from a 0.001 M KCl solution at pH 9, in terms of sensed mass and dissipation, are shown in **Figure 4.4**. As can be seen, no significant changes in the crystal frequencies and dissipations were observed in all three cases, and only minor frequency reduction was observed on the most hydrophobic surface ($M_{OH}$=0, θ=106°). The slight frequency increase (less than 1 Hz per hour) in **Figure 4.4** (a) and (b) is most likely caused by the drift during the QCM-D experiments, which is normal and within the error range of QCM-D instrument, as even a clean and stable system would show a 1 Hz variation per hour.

However, slight HA adsorption or contamination (by HA molecules) may have taken place on the most hydrophilic gold surface ($M_{OH}$=1, θ =22°), as its contact angle increased from 22° to 48° after treatment by 20 ppm HA in 0.001 M KCl solution at pH 9. Overall, the experimental results demonstrate that at pH 9 and low ionic strength conditions, HA molecules could not adsorb onto hydrophilic (θ =22°) and mildly hydrophobic (θ =79°) surfaces, most likely due to the strong electrostatic repulsion between HA molecules and thiol-coated gold surfaces. It should be noted that all the gold surfaces are coated by thiols terminated with −OH and $-CH_3$ groups, and should not produce any negative charge themselves. However, it is well known that hydrophobic

surfaces, such as silane monolayers, oil droplets, and air bubbles, may carry strong negative charge over a wide range of pH simply due to the preferential adsorption of hydroxide ions from the aqueous solution.[26-29]

In comparison, a small proportion of HA molecules had adsorbed onto the most hydrophobic surface (θ =106°) because of the strong hydrophobic interaction. In all three cases, the change to the dissipation energy loss was less than $0.5\times10^{-6}$, which allows the use of the Sauerbrey equation for the determination of adsorbed mass. The adsorbed mass calculated from four overtone numbers (3, 5, 7, and 9), along with the standard deviation, are presented in **Figure 4.4** (d).

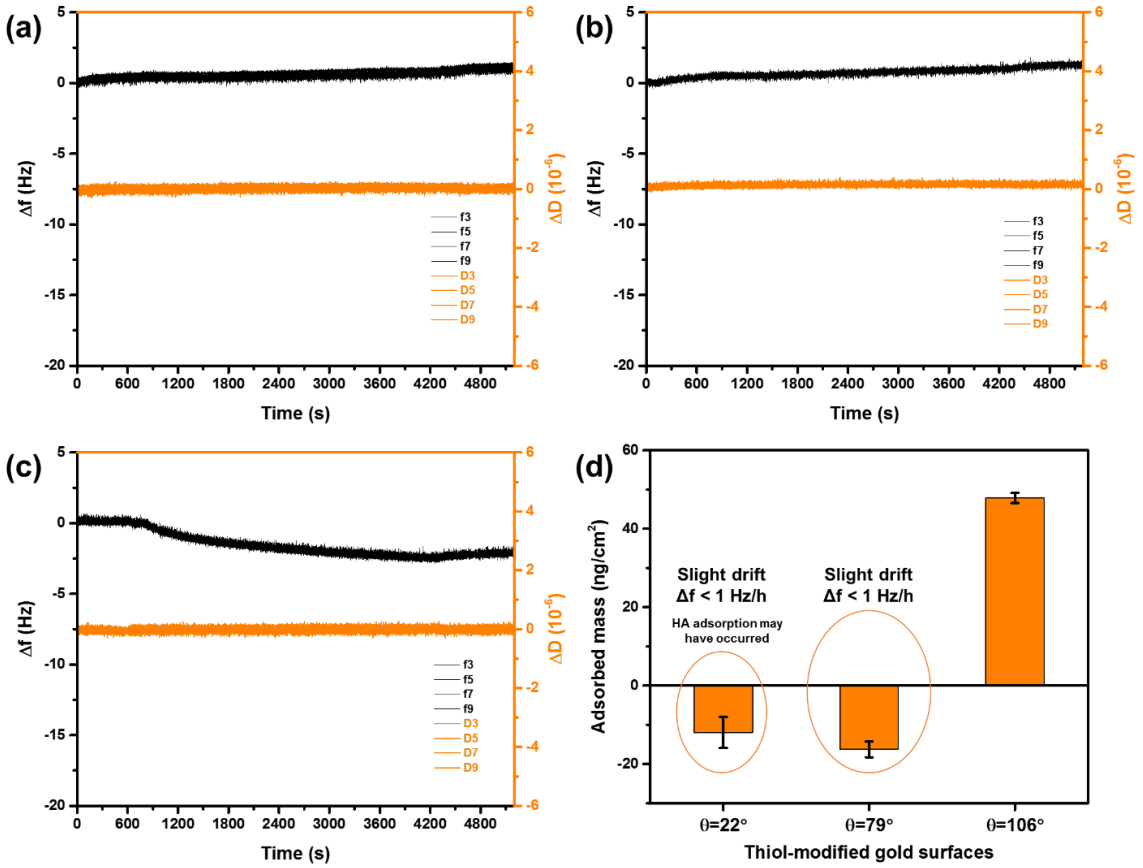

**Figure 4.4**. Influence of surface hydrophobicity on HA adsorption onto thiol-functionalized gold surfaces in 0.001 M KCl solution at pH 9 (a) $M_{OH}$ =1 gold surface with a contact angle θ =22°; (b) $M_{OH}$ =0.5 gold surface with a contact angle θ =79°; (c) $M_{OH}$ =0 gold surface with a contact angle θ =106°. Frequency change (Δf) and energy dissipation shift (ΔD) recorded at four different overtone number (3, 5, 7, and 9). (d) Summary of the adsorbed mass (at 4200s) of HA layers on gold surfaces; the error bar represents the standard deviation calculated from four different overtone numbers (3, 5, 7, and 9).

(b) HA in 0.001 M KCl solution at pH 3

The adsorption isotherms of HA on surfaces with varying hydrophobicities from 0.001 M KCl solutions at pH 3, plotted as the changes in crystal frequency and dissipation, are shown in **Figure 4.5**. As indicated in **Figure 4.5** (a), (b) and (c), HA adsorption occurred in all three cases and caused significant reductions to the crystal frequency. In addition, for all three cases, the HA molecules first adsorb rapidly onto the substrate surfaces at the beginning of the adsorption process, then the adsorption rate gradually decreases until reach adsorption equilibrium at ~4200 seconds. Therefore, the adsorption of HA can be best described by the Langmuir-Freundlich adsorption model and is most likely to be monolayer adsorption. It is proposed that the gold surfaces with varying hydrophobicities were first rapidly covered by a layer of HA molecules/aggregates at the initial stage of adsorption. Then the strong intermolecular

electrostatic repulsion between adsorbed HA layers and HA molecules in solution, as indicated in zeta potential results, prevents the HA molecules in solution from further adsorption.

As for the adsorption isotherms, the largest changes to frequency ($\Delta f$) or highest adsorption amount of HA are seen for the mildly hydrophobic surface ($\theta$ =79°), and the smallest changes of $\Delta f$ are observed for the most hydrophilic surface ($\theta$ =22°). While for the most hydrophobic surface ($\theta$ =106°), the mass of adsorbed HA is close to but lower than that of the mildly hydrophobic surface ($\theta$ =79°). The most likely explanation is that the adsorption of HA is not only governed by hydrophobic interaction, but also strongly influenced by the electrostatic interaction (attraction or repulsion). The most hydrophobic surface may still carry a strong negative charge at pH 3 due to the preferential uptake of hydroxide ions, while the mildly hydrophobic surface may be less negatively charged (or even positively charged) compared with the most hydrophobic surface. Consequently, the adsorption amount of HA on the mildly hydrophobic surface is the highest among all three cases.

Despite that the adsorption isotherms do not show a clear trend in the influence of the surface hydrophobicity on adsorption of the HA, the adsorbed amounts of HA (as shown in **Figure 4.5**(d)) on hydrophobic surfaces is still considerably higher than that of the hydrophilic surface, which further confirmed the importance of hydrophobic interaction during the adsorption process. Additional insights into the conformation of the adsorbed HA layers were obtained from the changes in the dissipation. In all three cases,

the dissipation energy loss was less than $1\times10^{-6}$, suggesting that the adsorbed HA layers on all three substrates are quite thin and rigid, and most likely to be monolayer adsorption. The desorption of HA during the flush of KCl background solution is weak and the amount of desorbed HA is similar in all three cases. It is likely that the removed material is loosely attached HA molecules or aggregates on the adsorbed films.

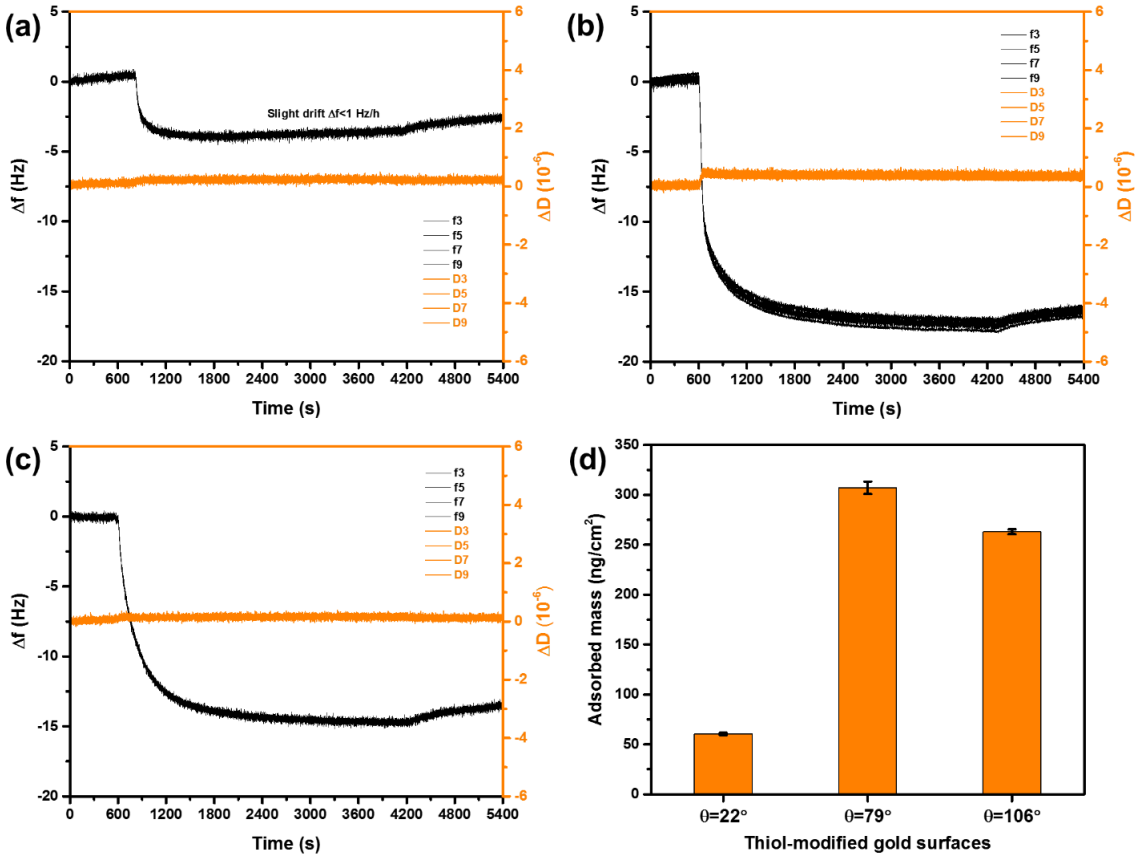


**Figure 4.5**. Influence of surface hydrophobicity on HA adsorption onto thiol-functionalized gold surfaces in 0.001 M KCl solution at pH 3 (a) $M_{OH}$ =1 gold surface with a contact angle θ =22°; (b) $M_{OH}$ =0.5 gold surface with a contact angle θ =79°; (c) $M_{OH}$ =0 gold surface with a contact angle θ =106°. Frequency change (Δf) and energy dissipation shift (ΔD) recorded at four different overtone number (3, 5, 7, and 9).

(d) Summary of the adsorbed mass (at 4200s) of HA layers on gold sensors; the error bar represents the standard deviation calculated from four overtone numbers (3, 5, 7, and 9).

(c) HA in 0.1 M KCl solution at pH 9

The adsorption of HA on thiol-coated gold surfaces was also studied for the solution condition of 0.1 M KCl and pH 9. The plots of Δf and ΔD versus time are shown in **Figure 4.6**. As indicated in **Figure 4.6** (a), (b) and (c), adsorption of HA occurred in all three cases and resulted in significant frequency change. The largest changes of frequency for adsorption are seen for the most hydrophobic surface (θ =106°), and the smallest changes to frequency are observed on the least hydrophobic surface (θ =22°). Besides, the change to the dissipation energy loss was still less than $2\times10^{-6}$ in all three cases, which enable the use of the Sauerbrey equation to calculate the adsorbed mass. The adsorbed masses of HA on the three substrates at 4200s are shown in **Figure 4.6** (d), and generally increases with increasing surface hydrophobicity.

At an ionic strength of 0.1 M KCl, the electric double layers of HA molecules and thiol-coated gold surfaces are significantly compressed. The calculated Debye length of the electric double layers is only ~0.96 nm, and the electrostatic interaction is significantly screened and can be neglected under such a circumstance.[30, 31] In addition, other interactions, such as van der Waals force, etc., also start to play important roles when the electrostatic interaction is negligible. Thus, the observed HA adsorption was primarily induced by the hydrophobic interaction at the initial stage of adsorption,

followed or more accurately, accompanied by a “stacking” or “precipitation” of HA molecules/aggregates on the substrate surfaces. However, it should be noted that the adsorption is “precipitation-like” rather than real precipitation, since the real precipitation is typically driven by gravity force and more suitable for large particles. While in this study, the HA solution is very dilute (20 ppm) and the molecular weight of HA is relatively small, the HA adsorption is driven by the attractive interactions between HA molecules/aggregates in the solution and adsorbed HA layers on the surface rather than gravity force.

As a consequence, the adsorption of HA on three substrates in 0.1 M KCl solution could not reach equilibrium, at least for an adsorption time of 100 minutes, due to the continuous deposition of HA molecules/aggregates. In addition, the HA molecules in the solution are more readily to form aggregates in the absence of electrostatic repulsion. Larger HA aggregates will form in the solution and adsorb onto the substrate surface as the adsorption progresses, forming less rigid extend layers with loose and open structures.

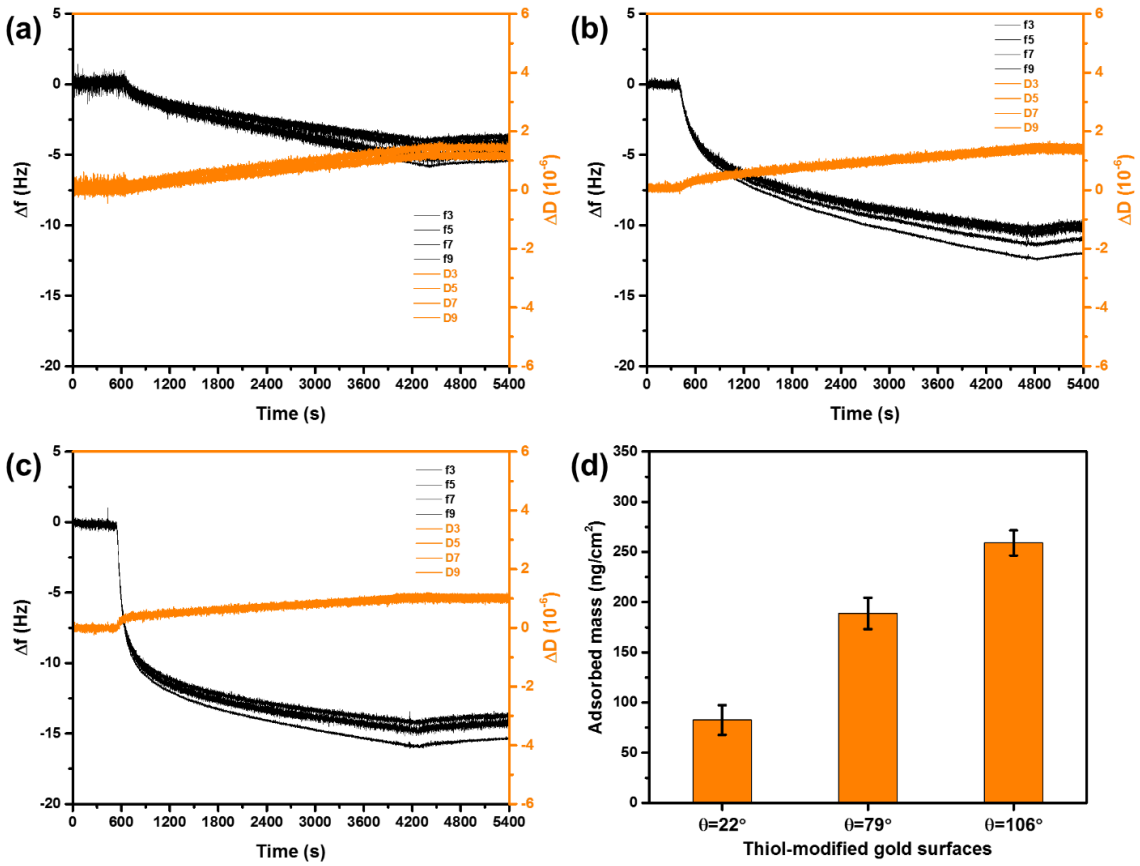


**Figure 4.6**. Influence of surface hydrophobicity on HA adsorption onto thiol-functionalized gold surfaces in 0.1 M KCl solution at pH 9 (a) $M_{OH}$ =1 gold surface with a contact angle θ =22°; (b) $M_{OH}$ =0.5 gold surface with a contact angle θ =79°; (c) $M_{OH}$ =0 gold surface with a contact angle θ =106°. Frequency change (Δf) and energy dissipation shift (ΔD) recorded at four different overtone number (3, 5, 7, and 9). (d) Summary of the adsorbed mass (at 4200s) of HA layers on gold sensors; the error bar represents the standard deviation calculated from four overtone numbers (3, 5, 7, and 9).

4.3.2.2 Adsorption kinetic analysis

The QCM-D data also enables the kinetic analysis of the adsorption isotherms. The adsorption isotherms were also plotted as adsorbed mass versus adsorption time, by applying the Sauerbrey equation to convert the change in frequency (Δf) to adsorbed mass. Since the adsorption of HA on the three surfaces from 0.001 M KCl solutions at pH 9 is negligible, only the adsorption kinetics of HA from 0.001 M KCl solution at pH 3 and 0.1 M KCl solution at pH 9 were analyzed and discussed.

(a) HA in 0.001 M KCl solution at pH 3

The adsorption data for the adsorption of 20ppm HA onto surfaces with varying hydrophobicities in 0.001 M KCl solution at pH 3 were fitted to Langmuir-Freundlich adsorption model as shown in equation 4.3, which is also known as Sips equation,[32, 33] using the fitting tool in Origin 2015.

$$m = \frac{m_{sat} \cdot k \cdot t^n}{(1 + k \cdot t^n)} \tag{4.3}$$

Where m is the adsorbed mass at any given time t during the adsorption process, and $m_{sat}$ is the maximum adsorbed mass. The variable k is a constant related to the binding affinity, and n is the heterogeneity index, which ranges from 0 to 1.[34] For a homogeneous surface, n =1, and the Langmuir-Freundlich equation becomes the Langmuir equation. When n < 1, the material is heterogeneous, and when n=0, the Langmuir-Freundlich isotherm reduces to Freundlich isotherm. Compared with the Langmuir and Freundlich isotherms, the Langmuir-Freundlich isotherm is capable of modeling the monolayer

single-solute adsorption from dilute solutions on both homogeneous and heterogeneous surfaces.[34]

As indicated in **Figure 4.7**, the adsorption isotherms are well described by the Langmuir-Freundlich model, with $R^2$ values larger than 0.98 in all three cases except the $M_{OH}$=1 surface. The deviation/discrepancy for the fitting of the adsorption isotherm on $M_{OH}$=1 surface is owing to the slight frequency drift during the measurements. However, the $R^2$ value of the fitting for the adsorption isotherm on $M_{OH}$=1 surface is still around 0.923 in the first 1200s of adsorption.

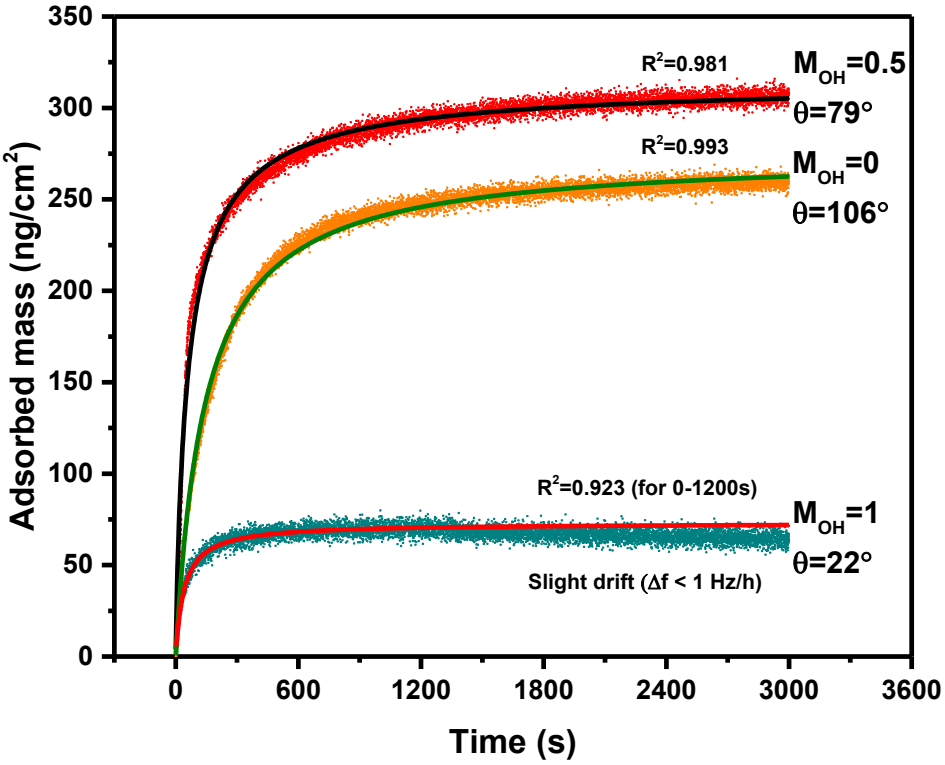


**Figure 4.7**. Adsorption isotherms (mass versus time) of 20 ppm HA on surfaces with varying hydrophobicity in 0.001 M KCl solution at pH 3. Solid lines represent fits to

Langmuir-Freundlich model. The $R^2$ values for the fits are as follows: 0.993 for $M_{OH}$= 0; 0.981 for $M_{OH}$= 0.5; 0.923 for $M_{OH}$= 1 in the first 1200s of adsorption.

The parameters of the fit are presented in **Table 4.1**. As can be seen, the three isotherms are accurately described by the Langmuir-Freundlich equation, and the standard deviations in the values of $m_{sat}$, k, and n are quite small. Besides, the values of heterogeneity index (n) of the three isotherms determined from Langmuir-Freundlich equation are equal or close to one. Therefore, it can be concluded that the $M_{OH}$ =0 and $M_{OH}$ =1 gold surfaces can be considered to be homogenous under this solution condition. However, slight heterogeneity may exist on the $M_{OH}$=0.5 gold surface, which is understandable as it is coated by a mixture of thiols terminated with −OH and $-CH_3$ groups.

**Table 4.1**. Adsorption kinetic parameters for HA adsorption on thiol-coated gold surfaces with varying hydrophobicity, as determined from fitting to Langmuir-Freundlich equation.

| **$M_{OH}$ and θ** | **$m_{sat}$ (ng/cm$^2$)** | **k** | **n** | **$R^2$** |
|---|---|---|---|---|
| **0 and 106°** | 275.02±0.16 | 0.0070±0.0001 | 1±0.0026 | 0.993 |
| **0.5 and 79°** | 314.88±0.21 | 0.0249±0.0004 | 0.893±0.0035 | 0.981 |
| **1 and 22°** | 72.88±0.17 | 0.0242±0.0013 | 1±0.0132 | 0.923 |

(b) HA in 0.1 M KCl solution at pH 9

The adsorption isotherms (adsorbed mass versus time) of 20ppm HA onto surfaces with varying hydrophobicity in 0.1 M KCl solution at pH 9 were fitted to the Langmuir-Freundlich adsorption model first. However, it was observed that the Langmuir-Freundlich adsorption model underestimates the adsorption rate of HA after 1800 seconds and hence does not fit well with the latter section of the adsorption isotherms. After repeated experiments and analysis, it was found that the adsorbed mass is in a linear relationship with the adsorption time after 1800 seconds, and could never reach adsorption equilibrium (as mentioned before in **Figure 4.6**). Therefore, we proposed an extension of the Langmuir-Freundlich adsorption model and named it as Langmuir-Freundlich-Linear (LFL) model, which is a summation function of the Langmuir-Freundlich equation and a linear equation as shown in equation 4.4.

$$m = \frac{m_{sat} \cdot k \cdot t^n}{(1 + k \cdot t^n)} + b \cdot t \tag{4.4}$$

All the parameters except for $m_{sat}$ and b are already defined in equation 4.3, here $m_{sat}$ is not the maximum adsorbed mass and is just a parameter in the Langmuir-Freundlich adsorption region, and b is the slope or the adsorption rate of the latter section (or linear region) of the adsorption isotherm. The variable b in here describes the “precipitation” rate of HA molecules on the substrates, and should be independent of the surface

properties of the substrates and only reflects the interactions between HA molecules/aggregates in the solution and the adsorbed HA films on the surfaces.

As shown in **Figure 4.8**, the fit to the LFL model is exceptionally good, with the $R^2$ values larger than 0.982 in all three cases. The adsorption isotherms can be divided into two distinct sections. The first part of adsorption is dominated by hydrophobic interaction and more resembles the Langmuir-Freundlich isotherm, although it already incorporated a linear adsorption isotherm. After the substrate surface is fully covered by a layer of HA molecules, the adsorption process is dictated by the interactions between HA molecules/aggregates in the solution and the adsorbed HA layers. Therefore, the later section of isotherms reflect the "precipitation" or stacking of HA molecules/aggregates on the substrates, and the adsorbed mass in this region is proportional to the adsorption time.

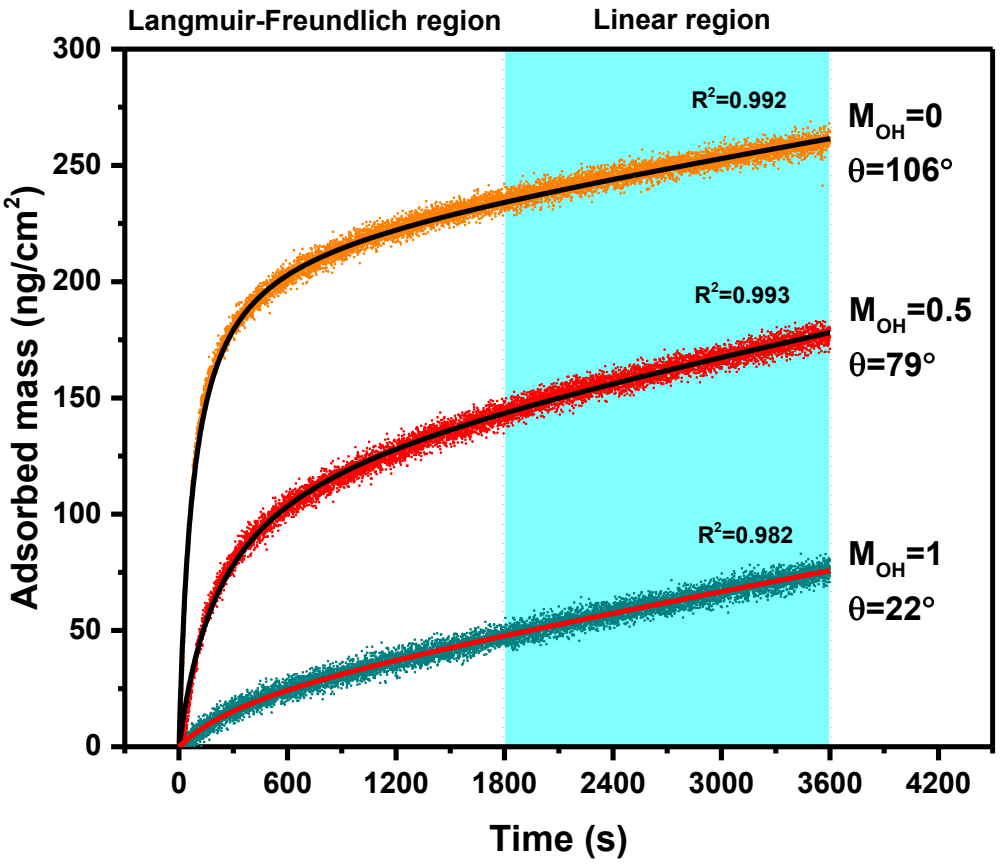


**Figure 4.8**. Adsorption kinetic data for 20 ppm HA adsorption on gold surfaces with varying hydrophobicity in 0.1 M KCl solution at pH 9. Solid lines represent fits to a summation of Langmuir-Freundlich equation and linear equation. The $R^2$ values for the fits are as follows: 0.992 for $M_{OH}$= 0; 0.993 for $M_{OH}$= 0.5; 0.982 for $M_{OH}$= 1.

The parameters of the fit are presented in **Table 4.2**. It can be seen that the errors in the values of $m_{sat}$, k, n, and b are actually quite small, in spite of the fact that the errors are a result of an unconstrained four-parameter fit. Besides, the values of heterogeneity index (n) of the three isotherms determined from LFL equation are equal to one. Therefore, the three gold surfaces with varying hydrophobicity can be regarded as

homogenous in this circumstance, most likely because of the absence of electrostatic repulsion. In addition, the values of b of three isotherms determined from the LFL equation are quite close to each other, which further confirmed that the parameter b is independent of the surface properties of the substrate and is an indication of the interactions between HA molecules/aggregates and the adsorbed HA films.

**Table 4.2**. Adsorption kinetic parameters for HA adsorption on thiol-coated gold surfaces of varying hydrophobicity, as determined from fitting to a summation of Langmuir-Freundlich equation and linear equation.

| $M_{OH}$ and θ | $m_{sat}$ (ng/cm$^2$) | k | n | b | $R^2$ |
|---|---|---|---|---|---|
| **0 and 106°** | 219.98±0.32 | 0.0131±0.0003 | 1±0.005 | 0.0128±0.0001 | 0.992 |
| **0.5 and 79°** | 130.63±0.61 | 0.0043±0.0001 | 1±0.007 | 0.0154±0.0001 | 0.993 |
| **1 and 22°** | 27.53±0.95 | 0.0022±0.0003 | 1±0.032 | 0.0143±0.0002 | 0.982 |

4.3.2.3 The ΔD–Δf plots of QCM-D

Additional information can be extracted from the raw Δf and ΔD data by plotting ΔD–Δf plots (ΔD versus Δf). The ΔD/Δf ratio can provide information on the viscoelastic properties of the adsorbed layer. In general, a high ΔD/Δf ratio indicates a relatively nonrigid and loose layer structure, whereas a low ratio reflects a stiffer and more compact structure where the adsorbed mass induces less energy dissipation. In addition, a change

in the slope of ΔD/Δf indicates structural changes in the adsorbed layer as the adsorption progresses, and an increase in the slope is an indication that the layer has become less rigid due to decreased packing density, while a decrease in the slope implying the layer has become more rigid.[19, 21, 35] Therefore, the ΔD–Δf plots essentially reflect the dissipation changes per unit adsorbed mass, pinpointing changes in polymer conformation and layer structure as the adsorption progress. If the ΔD and Δf have a linear relationship with a constant slope, then the adsorbed polymer does not undergo conformation changes during the adsorption process. In contrast, if the relationship between ΔD and Δf is non-linear, or has a discontinuity, then there is a change in the conformation of the adsorbed layer as the adsorption progress.[22, 36, 37]

(a) HA in 0.001 M KCl solution at pH 3

Figure 9 shows the ΔD–Δf plots for the adsorption of HA on thiol-coated gold surfaces with varying hydrophobicity in 0.001 M KCl solution at pH 3. Only slight changes in ΔD were observed in all three cases, suggesting the adsorbed layers are relatively rigid and compact. Besides, HA appears to adsorb without any significant change in its conformation, as the ΔD–Δf plots of all three cases show single slopes (excluded the desorption part) without any discontinuity. In other words, the relation between ΔD and Δf is linear, indicating that the adsorbed HA layer has a consistent layer conformation with increasing adsorbed mass.

The ΔD–Δf plots corroborated with the adsorption kinetic data and further support that the adsorbed HA films in 0.001 M KCl solution at pH 3 are relatively thin and rigid, and most likely to be monolayer adsorption.

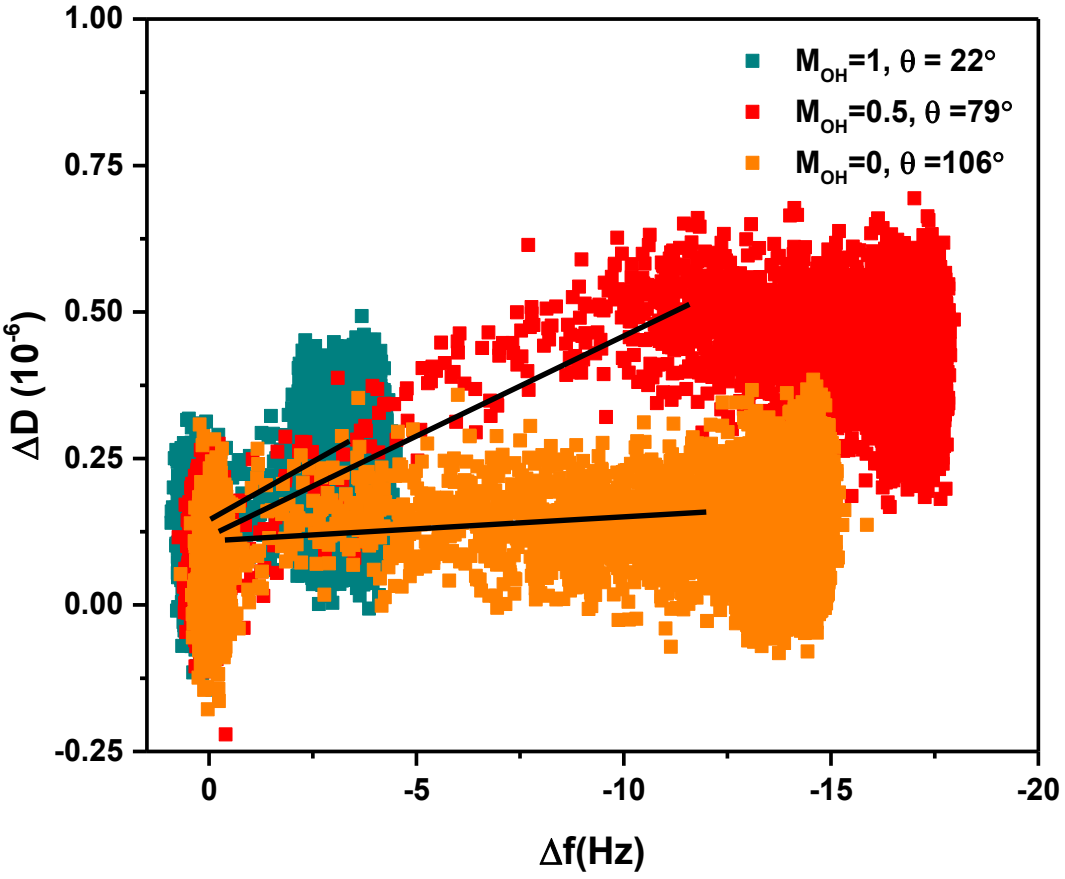


**Figure 4.9**. Influence of surface hydrophobicity on Δf/ΔD recorded at overtone number n=7 in 0.001 M KCl solution with 20 ppm HA at pH 3.

(b) HA in 0.1 M KCl solution at pH 9

**Figure 4.10** contains the Δf−ΔD plots for the adsorption of HA on three substrates in 0.1 M KCl solution at pH 9. As can be seen, there are two distinct regions with

different slopes in the Δf−ΔD plots for all three substrates. The discontinuity in the slope reflects a change in conformation of HA layer, and the change from a smaller to a larger slope implies that the conformation of adsorbed HA changed from a rigid layer to a more softer extended layer. In other words, softer films with loose and open structures were formed as the adsorption progresses.

The Δf−ΔD plots data further support the conclusion from the adsorption kinetic analysis. The observed HA adsorption was primarily induced by the hydrophobic interaction at the initial stage of adsorption, followed or accompanied by a "stacking" or "precipitation" of HA molecules/aggregates on the substrate surfaces. After the substrate surface is fully covered by a layer of HA molecules, the adsorption process is controlled by the interactions between HA molecules/aggregates in the solution and the adsorbed HA layers.

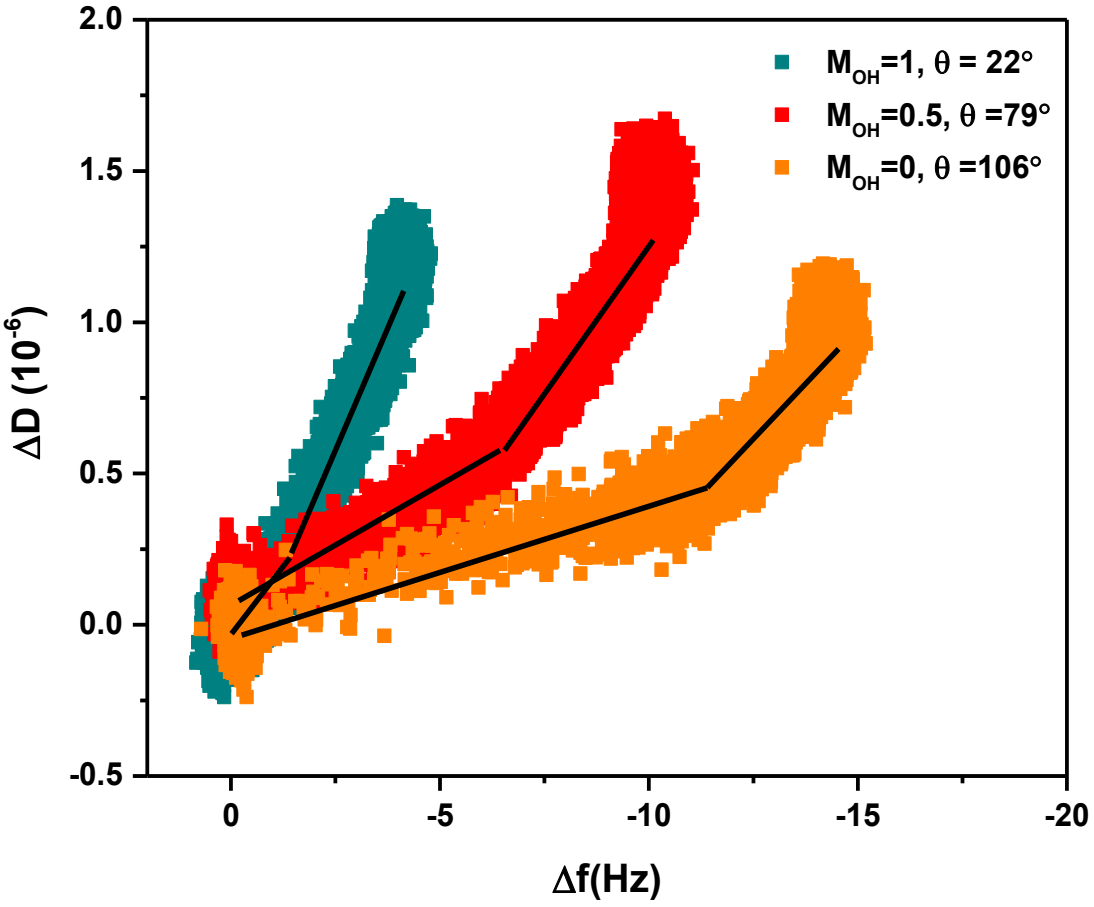


**Figure 4.10**. Influence of surface hydrophobicity on Δf/ΔD recorded at overtone number n=7 in 0.1 M KCl solution with 20 ppm HA at pH 9.

### 4.3.3 Adsorbed layer thickness and contact angles

The adsorbed HA layer thickness can be readily determined from the adsorbed mass and the density of the adsorbed layer. It is assumed that the density of adsorbed HA layer is 1.00 g/cm$^3$, which is in fact quite accurate for most of the polymer films since the water content in many adsorbed polysaccharides could range from 70 to 95%.[22, 38, 39] As shown in **Table 4.3**, the adsorbed HA layers are ultra-thin and less than 3 nm in most of

the cases, owing to the fact that HA is a group of low molecular weight polyelectrolytes. The ultrathin HA films also make the AFM imaging rather challenging to perform and would require atomically smooth substrates for AFM characterization of adsorbed species. However, the gold surface used in this study is full of hemispherical gold grains, making it complicated to distinguish the HA aggregates/molecules from the gold substrate features (gold grains).

**Table 4.3**. Adsorbed HA layer thickness (at 4200 s) of different surfaces after treatment with 20 ppm HA in 0.001 M or 0.1 M KCl solution at pH 3 or pH 9.

| | $M_{OH}$=1 | $M_{OH}$=0.5 | $M_{OH}$=0 |
|---|---|---|---|
| **0.001 M KCl at pH 9** | ~0 | ~0 | 0.48±0.01 nm |
| **0.001 M KCl at pH 3** | 0.60±0.01 nm | 3.07±0.06 nm | 2.63±0.02 nm |
| **0.1 M KCl at pH 9** | 0.83±0.15 nm | 1.89±0.16 nm | 2.59±0.12 nm |

Overall, the adsorbed HA layer thickness increases with increasing surface hydrophobicity under the same solution conditions. While for surfaces with the same initial hydrophobicity, the adsorbed layer thickness would increase at lower pH or higher ionic strength.

The contact angles of thiol-coated gold surfaces, before and after treatment with 20 ppm HA under different solution conditions, are presented in **Table 4.4**. Prior to HA

adsorption, the freshly prepared thiol-functionalized gold sensors have an average contact angle of 22, 79, and 106° for $M_{OH}$=1, $M_{OH}$=0.5, and $M_{OH}$=0 surfaces, respectively.

**Table 4.4**. Contact angles of thiol-coated gold surfaces before and after treatment with 20 ppm HA in 0.001 M or 0.1 M KCl solution at pH 3 or pH 9.

| | **$M_{OH}$=1** | **$M_{OH}$=0.5** | **$M_{OH}$=0** |
|---|---|---|---|
| **Fresh thiol-coated** | 22±7° | 79±4° | 106±4° |
| **0.001 M KCl at pH 9** | 48±3° | 80±3° | 90±4° |
| **0.001 M KCl at pH 3** | 42±3° | 46±3° | 53±4° |
| **0.1 M KCl at pH 9** | 28±3° | 67±3° | 69±3° |

After treatment by 20 ppm HA in 0.001 M solution at pH 9 for 60 minutes and flushed by 0.001 M KCl background solution at pH 9, the average contact angle of $M_{OH}$=1 gold surface increased from 22° to 48°, which may be caused by the slight uptake of HA molecules or contamination. In contrast, the contact angle $M_{OH}$=0.5 gold surface barely changed after HA treatment, indicating that no HA molecules had adsorbed onto the $M_{OH}$=0.5 gold surface under this solution condition because of the strong electrostatic repulsion. While the $M_{OH}$=0 gold surface show some contact angle reduction after HA treatment but remain strongly hydrophobic, suggesting that HA molecules have only

partially (instead of fully) covered the gold surface, which also correlates well with the QCM-D data.

The contact angles of three substrates treated with 20 ppm HA in 0.001 M solution at pH 3 are around 46° and quite close to each other, suggesting that the surfaces are possibly fully covered by HA molecules and hence show similar surface wettability. On the other hand, the contact angles of $M_{OH}$=0.5 and $M_{OH}$=0 surfaces treated in 0.1 M KCl solution with 20 ppm HA at pH 9 are also around 60°, which are close to that of substrates treated in 0.001 M KCl at pH 3 but with slight differences. These results indicate that surfaces treated with HA in 0.1 M KCl at pH 9 may also fully covered by HA, and the slight contact angle differences are probably caused by the differences in adsorbed layer conformation and layer thickness.

Despite the experimental results do not show a clear trend in the influence of the adsorbed layer thickness (or adsorbed amount) on the contact angles of HA-treated surfaces, it was observed that surfaces with the same initial hydrophobicity tend to have a smaller contact angle when the adsorbed HA layer is thicker. Since the adsorbed layer thickness is increased at lower pH and/or higher KCl concentration, the influence of the HA adsorption on the contact angles of the surfaces was seen to be greatest when adsorbed at low pH and/or higher ionic strength.

## 4.4 Conclusions

The adsorption characteristics and kinetics of HA onto three surfaces with varying hydrophobicity have been studied as a function of solution pH and ionic strength, using QCM-D and contact angle measurements. The possible adsorption mechanisms of HA onto various surfaces under different solution conditions were also illustrated.

The QCM-D data indicates that the HA molecules could not effectively adsorb onto all three surfaces at a low ionic strength and high pH (0.001 M KCl and pH 9) condition, possibly due to the strong electrostatic repulsion between HA molecules and thiol-coated gold surfaces. However, HA adsorption occurred and reached adsorption equilibrium on all three surfaces in 0.001 M KCl solution at pH 3, owing to the reduced electrostatic repulsion. Besides, the QCM-D dissipation data indicates that the HA molecules form relatively rigid and thin layers when adsorbing onto surfaces at low ionic strength. While at high ionic strength conditions (0.1 M KCl and pH 9), the QCM-D crystal frequency continued to decrease with increasing adsorption time, implying that the adsorption of HA could never reach equilibrium, most likely due to the lack of electrostatic repulsion. In addition, the $\Delta D$-$\Delta f$ plots indicate that HA molecules undergo conformational changes when adsorbing onto surfaces at high ionic strength, forming softer extended layers as the adsorption progresses. This conclusion is also supported by the kinetic analysis of the HA adsorption process, which shows that the HA adsorption was primarily induced by the hydrophobic interaction at the initial stage of adsorption, followed or more accurately,

accompanied by a “stacking” or “precipitation” of HA molecules/aggregates on the substrate surfaces.

Contact angle measurements illustrate that the surfaces hydrophobicity of substrates were reduced to different extents by HA under different solution conditions, and the influence of the HA adsorption on the contact angle of the surface was seen to be greatest when adsorbed at low pH or at higher ionic strength.

In conclusion, HA molecules adsorb faster and in larger amounts on the more hydrophobic surfaces under the same solution conditions, which signify the importance of hydrophobic interaction during the adsorption process. Besides, the reduction in solution pH and/or increasing in ionic strength will result in enhanced adsorption of HA because of reduced electrostatic repulsion between HA molecules and substrate surfaces. The results pointed to a new type of adsorption isotherm for HA adsorption at conditions of high ionic strength.

## 4.5 Acknowledgements

The financial support from the Natural Sciences and Engineering Research Council of Canada (NSERC) is gratefully acknowledged. Duowei Yuan also deeply appreciate a state scholarship support from the China Scholarship Council (CSC).

## 4.6 References


1. Stevenson, F. J., Humus chemistry: genesis, composition, reactions. 2nd ed.; Wiley: New York, 1994.

2. Jones, M. N.; Bryan, N. D., Colloidal properties of humic substances. *Advances in colloid and interface science* **1998,** *78* (1), 1-48.

3. Hur, J.; Schlautman, M. A., Effects of pH and phosphate on the adsorptive fractionation of purified Aldrich humic acid on kaolinite and hematite. *Journal of colloid and interface science* **2004,** *277* (2), 264-70.

4. Woodwell, G. M.; Whittaker, R. H.; Reiners, W. A.; Likens, G. E.; Delwiche, C. C.; Botkin, D. B., The biota and the world carbon budget. *Science* **1978,** *199* (4325), 141-6.

5. Thurman, E. M., Aquatic Humic Substances. In *Organic Geochemistry of Natural Waters*, Springer Netherlands: Dordrecht, 1985; pp 273-361.

6. Wang, K.; Xing, B., Structural and sorption characteristics of adsorbed humic acid on clay minerals. *Journal of Environmental Quality* **2005,** *34* (1), 342-349.

7. Kang, S.; Xing, B., Humic acid fractionation upon sequential adsorption onto goethite. *Langmuir: the ACS journal of surfaces and colloids* **2008,** *24* (6), 2525-31.

8. Zhou, P.; Yan, H.; Gu, B., Competitive complexation of metal ions with humic substances. *Chemosphere* **2005,** *58* (10), 1327-37.

9. Yuan, W.; Zydney, A. L., Humic Acid Fouling during Ultrafiltration. *Environmental Science & Technology* **2000,** *34* (23), 5043-5050.

10. dos Santos, I. D.; Oliveira, J. F., Utilization of humic acid as a depressant for hematite in the reverse flotation of iron ore. *Minerals Engineering* **2007,** *20* (10), 1003-1007.

11. Pawlik, M.; Laskowski, J. S., Coal Reverse Flotation. Part I. Adsorption of Dodecyltrimethyl Ammonium Bromide and Humic Acids onto Coal and Silica. *Coal Preparation* **2003,** *23* (3), 91-112.

12. Yuan, D.; Xie, L.; Shi, X.; Yi, L.; Zhang, G.; Zhang, H.; Liu, Q.; Zeng, H., Selective flotation separation of molybdenite and talc by humic substances. *Minerals Engineering* **2018,** *117*, 34-41.

13. Tamiz Bakhtiari, M.; Harbottle, D.; Curran, M.; Ng, S.; Spence, J.; Siy, R.; Liu, Q.; Masliyah, J.; Xu, Z., Role of Caustic Addition in Bitumen–Clay Interactions. *Energy & Fuels* **2015,** *29* (1), 58-69.

14. de Melo, B. A.; Motta, F. L.; Santana, M. H., Humic acids: Structural properties and multiple functionalities for novel technological developments. *Materials science & engineering. C, Materials for biological applications* **2016,** *62*, 967-74.

15. Bain, C. D.; Evall, J.; Whitesides, G. M., Formation of monolayers by the coadsorption of thiols on gold: variation in the head group, tail group, and solvent. *Journal of the American Chemical Society* **1989,** *111* (18), 7155-7164.

16. Sedeva, I. G.; Fornasiero, D.; Ralston, J.; Beattie, D. A., The influence of surface hydrophobicity on polyacrylamide adsorption. *Langmuir: the ACS journal of surfaces and colloids* **2009,** *25* (8), 4514-21.

17. Naderi, A.; Claesson, P. M., Adsorption properties of polyelectrolyte-surfactant complexes on hydrophobic surfaces studied by QCM-D. *Langmuir: the ACS journal of surfaces and colloids* **2006,** *22* (18), 7639-45.

18. Hemmersam, A. G.; Foss, M.; Chevallier, J.; Besenbacher, F., Adsorption of fibrinogen on tantalum oxide, titanium oxide and gold studied by the QCM-D technique. *Colloids and surfaces. B, Biointerfaces* **2005,** *43* (3-4), 208-15.

19. Dutta, A. K.; Belfort, G., Adsorbed gels versus brushes: viscoelastic differences. *Langmuir: the ACS journal of surfaces and colloids* **2007,** *23* (6), 3088-94.

20. Sedeva, I. G.; Fornasiero, D.; Ralston, J.; Beattie, D. A., Reduction of surface hydrophobicity using a stimulus-responsive polysaccharide. *Langmuir: the ACS journal of surfaces and colloids* **2010,** *26* (20), 15865-74.

21. Yan, M.; Liu, C.; Wang, D.; Ni, J.; Cheng, J., Characterization of adsorption of humic acid onto alumina using quartz crystal microbalance with dissipation. *Langmuir: the ACS journal of surfaces and colloids* **2011,** *27* (16), 9860-5.

22. Sedeva, I. G.; Fetzer, R.; Fornasiero, D.; Ralston, J.; Beattie, D. A., Adsorption of modified dextrins to a hydrophobic surface: QCM-D studies, AFM imaging, and dynamic contact angle measurements. *Journal of colloid and interface science* **2010,** *345* (2), 417-26.

23. Chai, L.; Klein, J., Large area, molecularly smooth (0.2 nm rms) gold films for surface forces and other studies. *Langmuir: the ACS journal of surfaces and colloids* **2007,** *23* (14), 7777-83.

24. Rost, M. J.; Quist, D. A.; Frenken, J. W., Grains, growth, and grooving. *Physical review letters* **2003,** *91* (2), 026101.

25. Nogues, C.; Wanunu, M., A rapid approach to reproducible, atomically flat gold films on mica. *Surface Science* **2004,** *573* (3), L383-L389.

26. Kudin, K. N.; Car, R., Why are water-hydrophobic interfaces charged? *Journal of the American Chemical Society* **2008,** *130* (12), 3915-9.

27. Marinova, K. G.; Alargova, R. G.; Denkov, N. D.; Velev, O. D.; Petsev, D. N.; Ivanov, I. B.; Borwankar, R. P., Charging of Oil−Water Interfaces Due to Spontaneous Adsorption of Hydroxyl Ions. *Langmuir: the ACS journal of surfaces and colloids* **1996,** *12* (8), 2045-2051.

28. Tian, C. S.; Shen, Y. R., Structure and charging of hydrophobic material/water interfaces studied by phase-sensitive sum-frequency vibrational spectroscopy. *Proceedings of the National Academy of Sciences of the United States of America* **2009,** *106* (36), 15148-53.

29. Beattie, J. K.; Djerdjev, A. M., The pristine oil/water interface: surfactant-free hydroxide-charged emulsions. *Angew Chem Int Ed Engl* **2004,** *43* (27), 3568-71.

30. Xie, L.; Wang, J.; Yuan, D.; Shi, C.; Cui, X.; Zhang, H.; Liu, Q.; Liu, Q.; Zeng, H., Interaction Mechanisms between Air Bubble and Molybdenite Surface: Impact of Solution Salinity and Polymer Adsorption. *Langmuir: the ACS journal of surfaces and colloids* **2017,** *33* (9), 2353-2361.

31. Israelachvili, J. N., *Intermolecular and surface forces: revised third edition*. Academic press: 2011.

32. Sips, R., On the Structure of a Catalyst Surface. II. *The Journal of Chemical Physics* **1950,** *18* (8), 1024-1026.

33. Sips, R., On the Structure of a Catalyst Surface. *The Journal of Chemical Physics* **1948,** *16* (5), 490-495.

34. Umpleby, R. J.; Baxter, S. C.; Chen, Y.; Shah, R. N.; Shimizu, K. D., Characterization of Molecularly Imprinted Polymers with the Langmuir−Freundlich Isotherm. *Analytical Chemistry* **2001,** *73* (19), 4584-4591.

35. Notley, S. M.; Eriksson, M.; Wagberg, L., Visco-elastic and adhesive properties of adsorbed polyelectrolyte multilayers determined in situ with QCM-D and AFM measurements. *Journal of colloid and interface science* **2005,** *292* (1), 29-37.

36. Höök, F.; Rodahl, M.; Brzezinski, P.; Kasemo, B., Energy Dissipation Kinetics for Protein and Antibody−Antigen Adsorption under Shear Oscillation on a Quartz Crystal Microbalance. *Langmuir: the ACS journal of surfaces and colloids* **1998,** *14* (4), 729-734.

37. Monkawa, A.; Ikoma, T.; Yunoki, S.; Yoshioka, T.; Tanaka, J.; Chakarov, D.; Kasemo, B., Fabrication of hydroxyapatite ultra-thin layer on gold surface and its application for quartz crystal microbalance technique. *Biomaterials* **2006,** *27* (33), 5748-54.

38. Malmstrom, J.; Agheli, H.; Kingshott, P.; Sutherland, D. S., Viscoelastic modeling of highly hydrated laminin layers at homogeneous and nanostructured surfaces:

quantification of protein layer properties using QCM-D and SPR. *Langmuir: the ACS journal of surfaces and colloids* **2007,** *23* (19), 9760-8.

39. Hedin, J.; Lofroth, J. E.; Nyden, M., Adsorption behavior and cross-linking of EHEC and HM-EHEC at hydrophilic and hydrophobic modified surfaces monitored by SPR and QCM-D. *Langmuir: the ACS journal of surfaces and colloids* **2007,** *23* (11), 6148-55.

# Chapter 5. Flotation separation of Cu-Mo sulfides by O-Carboxymethyl chitosan and the associated mechanisms

## 5.1 Introduction

With excellent electronic, optical and mechanical properties, molybdenum disulfide ($MoS_2$) has attracted intense research interest in a broad range of engineering and technological applications, including but not limited to catalysts,[1, 2] photovoltaics,[3, 4] batteries,[5, 6] electronics,[7, 8] and lubrication.[9] Molybdenite, the natural mineral form of molybdenum disulfide, is the most important source of molybdenum and the only commercially viable mineral from which molybdenum is extracted.[10] Naturally occurring molybdenite ores are typically associated with copper sulfide minerals such as chalcopyrite, and approximately 50% of the world's molybdenum production comes from molybdenite that is recovered as a by-product with chalcopyrite through bulk flotation.[10-12] The molybdenite in the bulk concentrate is then separated from chalcopyrite by differential flotation through the depression of chalcopyrite or molybdenite based on the molybdenite mass ratio in the bulk concentrate. The conventional practice in the mineral industry is to depress chalcopyrite from the Cu−Mo bulk concentrate using inorganic depressants, such as cyanides (KCN, NaCN, $Ca(CN)_2$, $NH_4CN$), sodium sulfide ($Na_2S$), sodium hydrosulfide (NaHS), ammonium sulfide ($(NH_4)_2S$), Noke's reagent (thiophosphorus or thioarsenic compounds), ferricyanide ($K_3Fe(CN)_6$, $Na_3Fe(CN)_6$), ferrocyanide ($K_4Fe(CN)_6$, $Na_4Fe(CN)_6$),[11, 13-16] and low molecular weight organic

compounds including thioglycolic acid ($HSCH_2COOH$), sodium thioglycollate ($HSCH_2COONa$) etc.[11, 17] However, these routinely used depressants all suffer from a variety of drawbacks including toxicity, volatility, large dosage, and environmental hazards.

Chitosan, a nontoxic and biodegradable linear cationic copolymer of D-glucosamine and N-acetyl-D-glucosamine, is produced by the deacetylation of a natural polysaccharide chitin.[18-21] Chitin, as the second most abundant natural polymer in the world after cellulose, can be easily obtained from crab or shrimp shells and fungal mycelia.[19, 22] Recently, chitosan has been proposed as a selective depressant for the mineral flotation industry. For example, chitosan has been studied as a depressant in galena-sphalerite flotation separation[22] and chalcopyrite-galena flotation separation.[23] However, as a cationic polymer with the presence of a large number of amino groups, chitosan is generally lack of selectivity towards negatively charged mineral particles. In addition, chitosan is only soluble in acidic conditions, while industrial flotation processes are typically performed under alkaline conditions around pH 9,[10, 24] which largely restrained its applications in the mineral industry. Hence, proper modification of chitosan would be necessary to enhance its water solubility as well as selectivity under alkaline conditions.

O-Carboxymethyl chitosan (O-CMC), a derivative of the natural polysaccharide chitosan, has been used in a wide range of technological and engineering applications such biomedical and food industry due to its nontoxic, biodegradable and cost-effective

properties.[25-28] In addition, the water solubility of O-CMC is significantly improved compared with chitosan.[28, 29] Therefore, in this work, O-carboxymethyl chitosan was proposed and investigated as a selective depressant for molybdenite during the flotation separation of copper-molybdenum sulfides, and the adsorption mechanisms of O-CMC on copper and molybdenum sulfides were studied.

## 5.2 Materials and methods

### 5.2.1 Materials

5.2.1.1 Mineral samples

The mineral samples used for flotation are high purity molybdenite (Dayu, Jiangxi, China) and chalcopyrite lumps (Ward's Science, NY, USA). While the mineral samples used for surface analysis are high purity molybdenite flakes (Research grade, Ward's Science, NY, USA), and chalcopyrite crystals (Good grade, Ward's Science, NY, USA). The chemical and mineralogical composition of chalcopyrite and molybdenite samples were analyzed by atomic absorption spectrometry (AAS) and X-ray powder diffraction (XRD) using a Rigaku Ultimate IV XRD. The purity of chalcopyrite used for flotation was identified to be > 90% with pyrite (< 10%) and quartz as the major impurities, and the purity of chalcopyrite crystals was identified to be > 95% with pyrite as the major impurity. While the purity of molybdenite used for flotation was confirmed to be > 96% with quartz (< 4%) as the major impurity and the purity of molybdenite flakes was

confirmed to be > 99%. Hence, the mineral samples were handpicked and used without any further treatment.

The lumps of chalcopyrite and molybdenite used for flotation were hammer crushed, sorted and then dry ground. The ground products were dry screened by Tyler standard sieves (Fisher Scientific, USA), and the -150+74 μm size fraction was collected and used for the flotation experiments. While several high purity molybdenite flakes and chalcopyrite crystals used for surface analysis were crushed and dry ground by an agate mortar/pestle. The ground products were dry screened by Tyler standard sieves (Fisher Scientific, USA), and the -37 μm portion was used for electrokinetic studies, infrared spectroscopy, and ToF-SIMS analysis. A few high purity molybdenite flakes were exfoliated for AFM imaging and XPS measurements, while several chalcopyrite crystals were cleaved and hand-polished and used for XPS measurements and AFM imaging, respectively.

5.2.1.2 Reagents

Potassium isobutyl xanthate or KIBX ($C_4H_7OS_2K$, Prospec Chemicals Ltd., Canada) was added as the collector for both minerals during the flotation. Prior to use, the KIBX was purified by adding 50 g of xanthate to 500 mL of acetone at 40 °C and continuously stirred for 5 minutes, then precipitated by ether following our previous reports.[30-33] The precipitates were collected by filtration and dried in a vacuum oven at 295 K, then sealed and stored in a freezer for future use.

O-Carboxymethyl Chitosan (O-CMC, Santa Cruz Biotechnology, USA), with a degree of deacetylation of 90.78% and a degree of substitution of ~95%, was investigated as a selective depressant during the flotation separation of copper-molybdenum sulfides. The molecular weight of the O-CMC is reported in the range of 100 to 300 KDa, and the molecular structure of O-CMC is shown in **Figure 5.1**.

4-Methyl-2-pentanol (MIBC, 99+%, Acros Organics) was introduced as a frothing agent in flotation tests. All aqueous solutions were prepared using Milli-Q water (Thermo Scientific, USA) with a resistivity of 18.2 MΩ·cm at 295 K. Potassium chloride was employed as the background electrolyte for the solutions. The pH of all solutions was adjusted using 0.1 M and 0.01 M KOH and HCl.

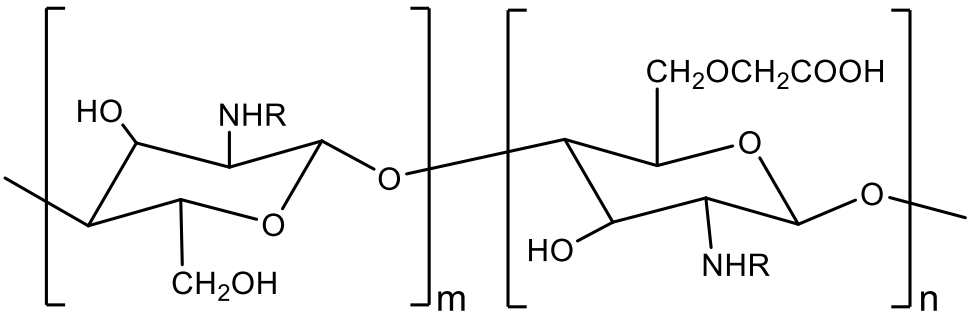


**Figure 5.1**. The molecular structure of O-Carboxymethyl chitosan (O-CMC).

### 5.2.2 Methods

5.2.2.1 Flotation

The flotation experiments were conducted in a customized Hallimond tube with a Siwek top.[34] In the flotation tests on individual minerals, 1.50 g chalcopyrite or molybdenite mineral particles were added into 150 mL 0.001 M KCl solution at the desired pH and concentration of O-CMC. In the flotation tests on artificial mineral mixtures, 3.00 g of molybdenite-chalcopyrite (weight ratio 1:1) mineral mixtures were added into 150 mL 0.001 M KCl solution at the desired pH and O-CMC concentration. The mineral suspension was stirred for 5 min while the pH was adjusted by KOH or HCl. Prior to the flotation, KIBX solution was injected into the slurry to reach a concentration of 20 ppm and the slurry was stirred for 3 min. Then the MIBC solution was introduced to obtain a concentration of 20 ppm and the suspension was further stirred for 2 min. The conditioned suspension was then transferred to the Hallimond flotation tube and floated for 2 min using high purity compressed air at a flowrate of 20 $cm^3$/min.

In flotation tests on single minerals, the recovery of molybdenite or chalcopyrite was obtained from the dry weight of the concentrates and tailings. While in flotation tests on artificial mineral mixtures, the concentrates and tailings were filtered, dried, weighed and sent for elemental analysis. The chalcopyrite and molybdenite recovery were then calculated based on the elemental content of Cu and Mo in the concentrates and tailings.

5.2.2.2 Electrokinetic studies

Electrokinetic measurements were performed to investigate the adsorption characteristics and mechanisms of O-CMC on the mineral particles at varying pH, as

slight changes in adsorption may lead to significant variations in the electrokinetic potentials of particles.[35] The electrokinetic potentials of mineral particles under various solution conditions were recorded using a Zetasizer Nano (Malvern Instruments Ltd., UK). In each test, 0.5 g of ground mineral particles (size fraction: -37 μm) were mixed with 50 mL 0.001 M KCl solution with or without 150 ppm O-CMC at the desired pH in a 100 mL polyethylene bottle. The pH of the mineral suspensions was adjusted using 0.1 M and 0.01 M KOH or HCl, and then ultrasonicated for 5 minutes. An equilibrium time of 15 min was allowed prior to each measurement. Each measurement was repeated at least three times and the average value was reported.

5.2.2.3 Infrared spectroscopy

Diffuse reflectance infrared Fourier transform (DRIFT) spectroscopy was employed to analyze the structure of O-CMC and investigate the adsorption of O-CMC on both mineral surfaces. The DRIFT spectra were recorded by a Nicolet iS50 FTIR spectrophotometer (Thermo Scientific, USA) with a Smart Diffuse Reflectance accessory. The number of scans for each spectrum was 128 with a spectral resolution of 4 $cm^{-1}$. The background spectrum was acquired using potassium bromide (KBr, FTIR grade, ACROS Organics) powder. To examine the adsorption of O-CMC onto mineral surfaces, 0.5 g mineral particles (size fraction: -37 μm) were ground to approximately 2 μm, the ground products were then added into 50 mL 0.001 M KCl solution with 150 ppm O-CMC at pH 9. The mineral suspensions were continuously shaken on an orbital shaker at 500 rpm for

30 min. Thereafter, the mineral particles were filtered and washed three times with Milli-Q water to remove the non-adsorbed or weakly attached O-CMC, then dried in a vacuum drying oven. The O-CMC powders, O-CMC treated and untreated minerals particles, were mixed with KBr powder respectively, and the spectra of O-CMC, untreated and O-CMC treated mineral particles were obtained by subtracting the spectrum of KBr background, respectively.

5.2.2.4 Atomic force microscope imaging

The morphology of the mineral surfaces, before and after O-CMC treatment, was characterized by an Asylum MFP-3D atomic force microscope (Santa Barbara, USA) using acoustic tapping mode. The surface topography of freshly cleaved molybdenite or polished chalcopyrite surface was obtained first. Thereafter, the mineral surfaces were immersed in 0.001 M KCl solution with 150 ppm O-CMC at pH 9 for 10 minutes, then taken out from the solution and rinsed thoroughly by Milli-Q water. The mineral substrates were dried with high purity nitrogen gas prior to imaging. The AFM imaging tests were performed immediately after sample preparation to minimize the surface oxidation and contamination.

5.2.2.5 XPS measurements

The XPS characterization was conducted on a Kratos AXIS Ultra X-ray photoelectron spectrometer (Kratos Analytical, USA) equipped with a monochromatic Al

Kα X-ray source (hv=1486.69 eV). The sampling area of XPS measurements on the sample surface is 400 μm × 700 μm, while the sampling depth was around 10 nm. Therefore, the recorded spectra can reveal the surface composition and chemistry of the samples. All of the XPS spectra were processed and analyzed by the CasaXPS software (Version 2.3.18).

The XPS measurements were performed on five samples: O-carboxymethyl chitosan (O-CMC) powder, freshly exfoliated molybdenite surface, freshly cleaved chalcopyrite surface, O-CMC treated molybdenite, and O-CMC treated chalcopyrite. The O-CMC treated mineral samples were prepared by immersing the freshly exfoliated molybdenite surface or cleaved chalcopyrite surface into 0.001 M KCl solution with 150 ppm O-CMC at pH 9 for 10 min. The treated mineral substrates were then taken out, without Milli-Q water rinsing, and dried with high purity nitrogen gas prior to XPS analysis. The binding energy peak intensities and positions of these samples were compared to investigate the possible chemical interactions between O-CMC and mineral surfaces. All of the XPS measurements were carried out within 1 h of sample preparation to minimize surface oxidation and contamination.

5.2.2.6 ToF-SIMS analysis

Time-of-Flight Secondary Ion Mass Spectrometry (ToF-SIMS) was employed to determine the metal ions and O-CMC distribution on the mineral surfaces, to illustrate the

possible selective adsorption of O-CMC on molybdenite and chalcopyrite surfaces and the underlying interaction mechanisms.

The sample was prepared by adding 1.5 g artificial chalcopyrite-molybdenite mixture (size fraction: -37 μm), with a weight ratio 1:1, to 150 mL 0.001 M KCl solution with 150 ppm O-CMC at pH 9. The mineral suspension was continuously stirred by a magnetic stirring bar for 30 min and then filtered. The collected solids were washed three times with Milli-Q water, and then dried in a vacuum oven at 298 K before ToF-SIMS measurements. To minimize the sample oxidation and contamination, the ToF-SIMS characterization was performed within 12 h of sample preparation.

## 5.3 Results and discussion

### 5.3.1 Flotation

5.3.1.1 Single mineral flotation

To determine the proper O-CMC concentration for effective Cu-Mo separation, flotation tests were first carried out on single minerals in 0.001 M KCl solutions at pH 9 with varying O-CMC concentrations. As shown in **Figure 5.2**, both chalcopyrite and molybdenite have superior floatability with the addition of collector KIBX at pH 9 in the absence of O-CMC, with the recovery of both minerals at approximately 97%. After adding 150 ppm O-CMC, the flotation recovery of molybdenite was reduced from 97% to 11%. As the dosage of O-CMC increases, the molybdenite recovery decreases further, but only to a small extent, and further increasing the concentration of O-CMC from 150 ppm

to 200 ppm only slightly reduced the flotation recovery from 11% to 3%, which demonstrates that 150 ppm O-CMC can efficiently suppress the molybdenite flotation. In comparison, the addition of O-CMC has no significant impact on the flotation of chalcopyrite, and the recovery of chalcopyrite remained above 94% over the entire O-CMC concentration range tested (up to 200 ppm). Therefore, 150 ppm was selected as the O-CMC concentration for Cu-Mo separations and this concentration was used for all subsequent flotation tests, to study the influence of solution pH on the Cu-Mo flotation and separation.

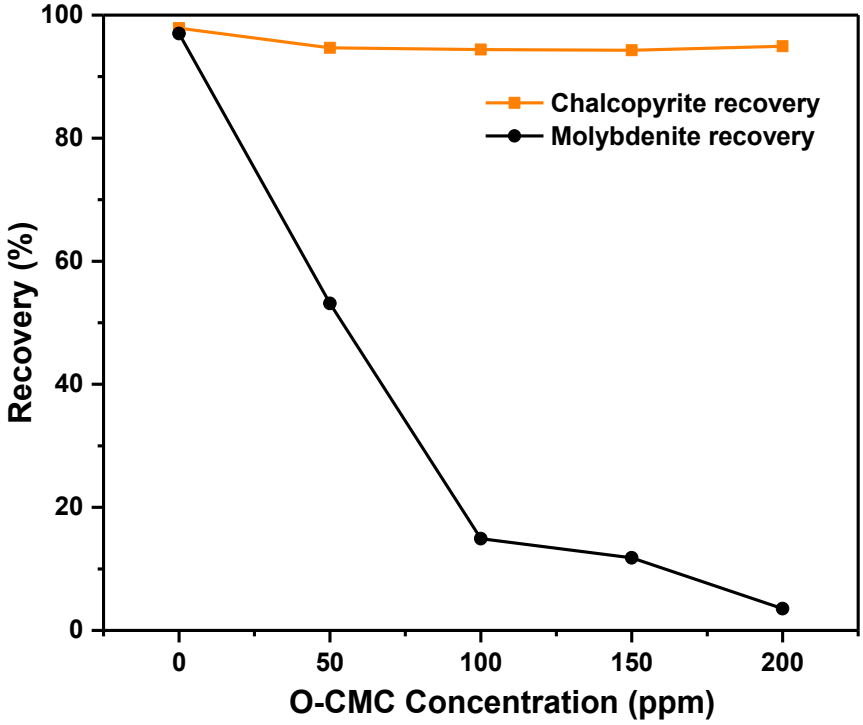


**Figure 5.2**. Recovery of chalcopyrite and molybdenite in 0.001 M KCl solution at pH 9 under various concentrations (i.e., 0 to 200 ppm) of O-CMC. Collector: 20 ppm KIBX. Frother: 20 ppm MIBC.

The flotation recovery of chalcopyrite and molybdenite with and without 150 ppm O-CMC at varying pH is shown in **Figure 5.3**. In the absence of O-CMC, the chalcopyrite and molybdenite flotation recoveries are above 95% for most of the pH range, except that at pH 11 where the recovery of molybdenite is reduced to 82%. This is owing to both the molybdenite and air bubble surfaces are strongly negatively charged at pH 11, which significantly lowers the probability of bubble-molybdenite attachment because of the strong electrostatic repulsion. It is worth to mention that these flotation results are consistent with the literature[36, 37] and our previous report,[38] which showed that the molybdenite flotation recovery is reduced under alkaline conditions (pH > 9). While the chalcopyrite recovery would not be affected by solution pH with the addition of xanthate collectors.[23]

However, after the addition of 150 ppm O-CMC, the flotation of molybdenite is strongly depressed over a wide pH range (3 to 11), and its recovery remained below 12% regardless of the change in the pulp pH. In contrast, the chalcopyrite flotation was not affected by the addition of O-CMC and solution pH, and its recovery remained above 93% except at pH 3, where the recovery of chalcopyrite was lowered to 82%. This is primarily caused by the increased adsorption density of O-CMC on chalcopyrite surfaces due to less electrostatic repulsion and even electrostatic attraction between O-CMC and chalcopyrite at lower pH, as the carboxylate groups of O-CMC are protonated at this pH. Overall, a large separation window from pH 3 to 11 exists in which O-CMC can be seen to depress molybdenite and also have a negligible impact on the chalcopyrite recovery.

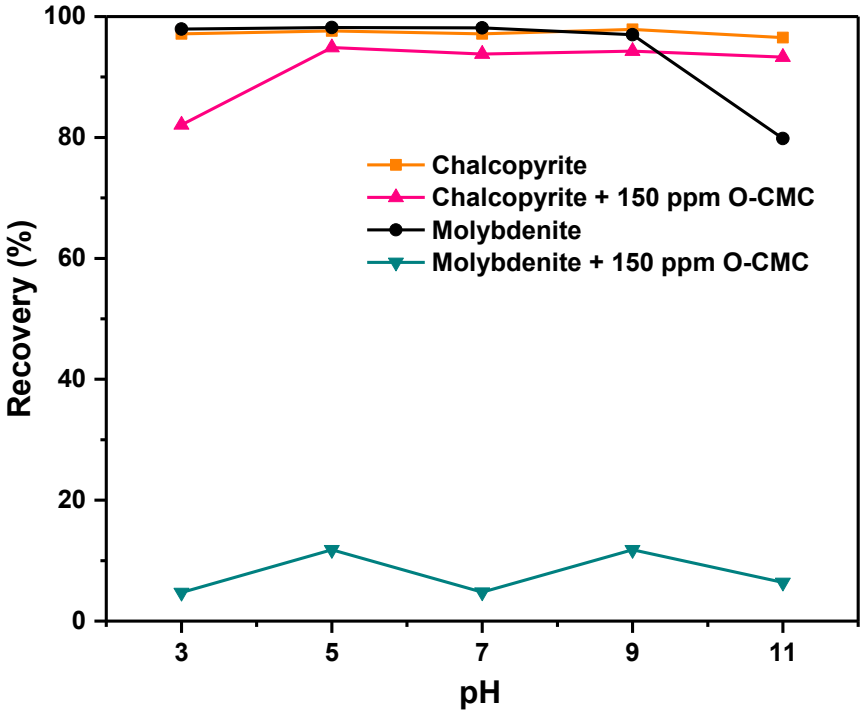


**Figure 5.3**. Recovery of chalcopyrite and molybdenite with and without the addition of 150 ppm O-CMC at varying pH in 0.001 M KCl solution. Collector: 20 ppm KIBX. Frother: 20 ppm MIBC.

5.3.1.2 Mixed minerals flotation

Given the large separation window over a wide pH range (3 to 11) for molybdenite and chalcopyrite during the single mineral flotation tests with 150 ppm O-CMC. Flotation tests on chalcopyrite-molybdenite mixtures were carried out in 0.001 M KCl solutions with 150 ppm O-CMC at varying pH, to examine the selectivity of O-CMC during the flotation separation of chalcopyrite-molybdenite mixtures, as well as to investigate the influence of pH on the flotation separation efficiency of O-CMC as a depressant.

**Figure 5.4** shows the molybdenite and chalcopyrite recovery in the concentrates floated from the artificial mixtures of molybdenite and chalcopyrite (weight ratio of 1:1). As can be seen, chalcopyrite was selectively floated from molybdenite-chalcopyrite mixtures over the entire pH range tested, with flotation recovery over 80% in most pH range. Meanwhile, molybdenite was effectively suppressed, with recovery less than 10%, for most of the pH range. Hence, O-CMC acts as a selective depressant for molybdenite during the Cu-Mo sulfides separation, and solution pH does not significantly affect the separation efficiency of O-CMC.

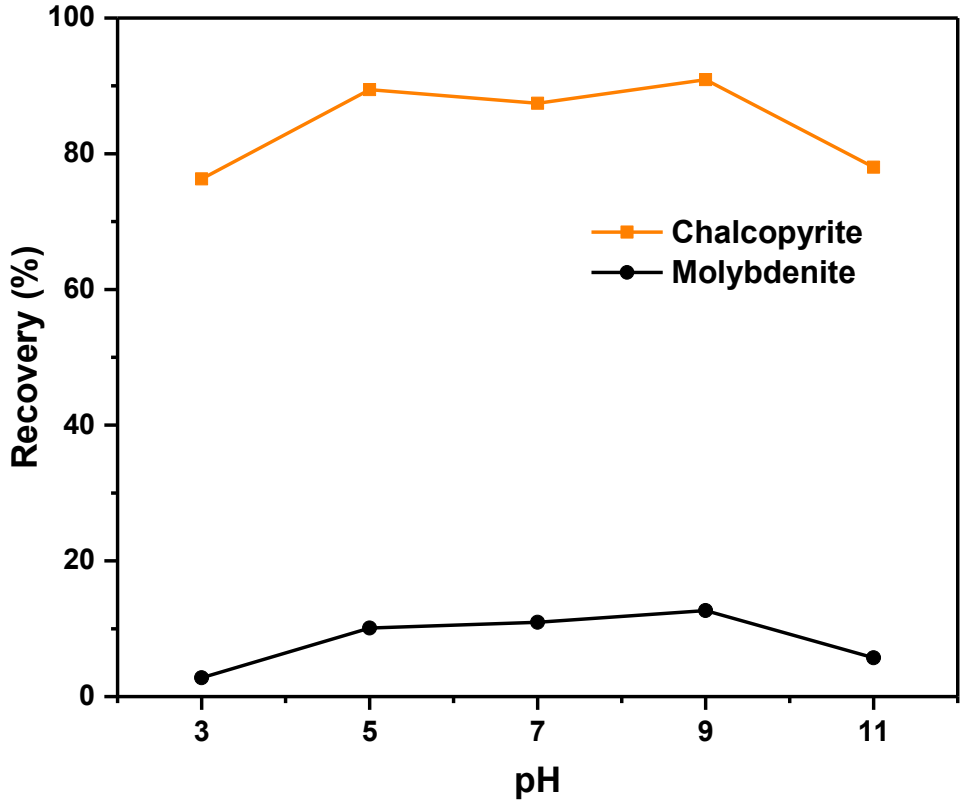


**Figure 5.4**. Flotation recovery of chalcopyrite and molybdenite from artificial molybdenite-chalcopyrite mixtures (weight ratio: 1:1) in 0.001 M KCl solution with the

addition of 150 ppm O-CMC at varying pH. Collector: 20 ppm KIBX. Frother: 20 ppm MIBC.

### 5.3.2 Electrokinetic studies

To elucidate the flotation results of molybdenite and chalcopyrite and the underlying interaction mechanisms between O-CMC and these two minerals, the zeta potentials of O-CMC treated and untreated mineral particles at varying pH were studied and the results are plotted in **Figure 5.5**. In addition, as an organic macromolecule, the zeta potential of polymer O-CMC could be readily determined and the results are also presented in **Figure 5.5**, which indicates that O-CMC is strongly negatively charged at pH > 4 with an iso-electric point (IEP) around pH 3.5. At pH below 3.5, the carboxyl groups of O-CMC are expected to be mostly protonated, and the positive charge originates from the protonated amino groups ($-NH_3^+$) of O-CMC, while at pH above 3.5, the amino groups ($-NH_3^+$ at pH < 7 or $-NH_2$ at pH > 7) of O-CMC would interact with its carboxylate groups ($-COO^-$) due to the intramolecular electrostatic attraction.[39] The strong anionic characteristic of O-CMC at pH > 4 comes from the excess carboxylate groups that not bounded to the amino groups, since the degree of substitution of O-CMC in this work is ~ 95% while the degree of deacetylation is only 90.78%.

The zeta potential of freshly ground chalcopyrite particles was positive at pH below 4 and became negative at pH above 5, and more negative at higher pH, with an iso-electric point (IEP) around pH 4.5, which is within the range of reported values.[40]

However, due to the rapid oxidation of chalcopyrite surfaces, the iso-electric point (IEP) of chalcopyrite is not a fixed value, and usually falls between the IEP (~ pH 1.6) of sulfur groups (–SH) and the IEP of corresponding metal oxide/hydroxide species (~ pH 9.0).[40, 41] Hence, in most cases, an "apparent" iso-electric point (IEP) is determined, which is an indication of the oxidation extent of the chalcopyrite surface.[40] The zeta potential of aged chalcopyrite particles (exposed in ambient air for ~ 30 min after grinding) was also determined and the results are shown in **Figure 5.5**. As can be seen, the aged chalcopyrite particles are more positively charged compared with the freshly ground chalcopyrite samples, because of the increased amount of metal oxide/hydroxide species formed on aged chalcopyrite surfaces.

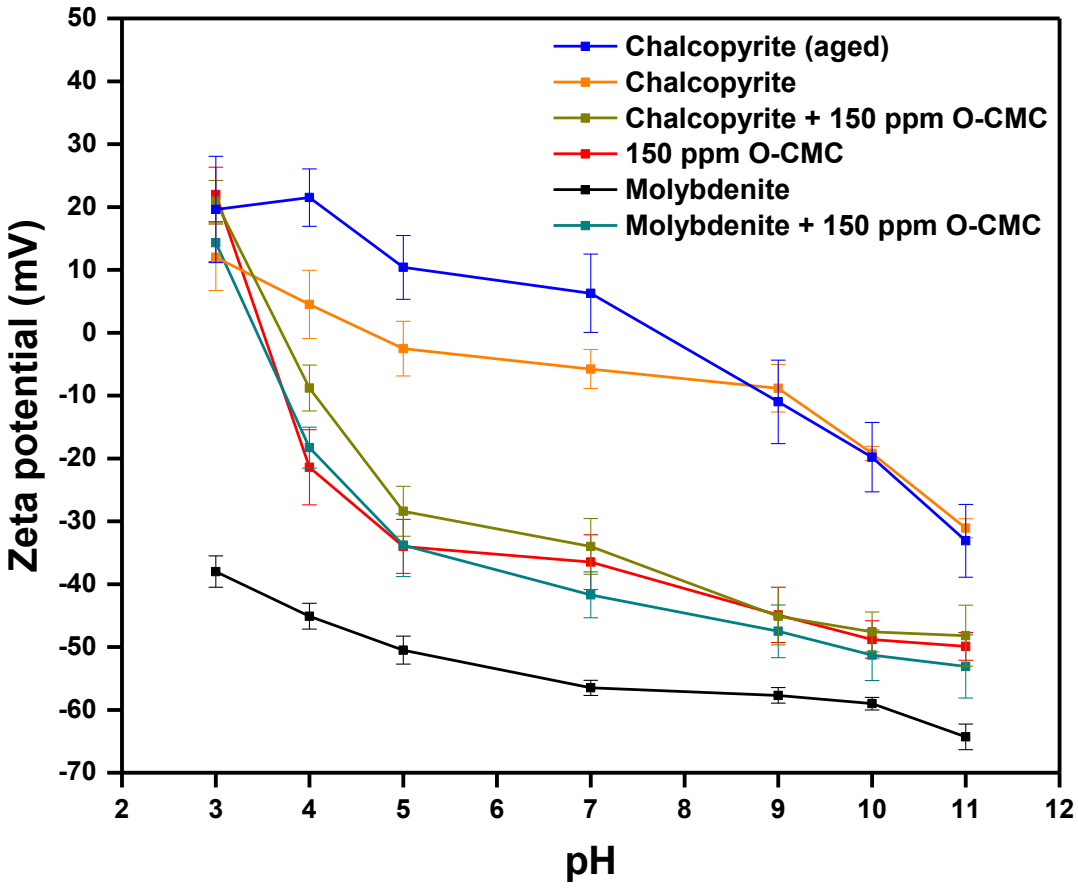


**Figure 5.5**. Zeta potential of aged chalcopyrite (exposed in air for ~30 minutes after grinding), fresh ground chalcopyrite, chalcopyrite + O-CMC, O-CMC, molybdenite (data from our previous work[38]), and molybdenite + O-CMC at varying pH in 0.001 M KCl solution.

To better illustrate the oxidation process of chalcopyrite, a schematic depiction of the oxidation process of the chalcopyrite surface is shown in **Figure 5.6**. As can be seen, the surface of chalcopyrite is not homogeneous upon oxidation and is heterogeneous with patch-wise structures. Upon slight oxidation, patches of metal oxides/hydroxides will form on chalcopyrite surface, which serve as the cathode of the galvanic cell.[42] The metal

oxides/hydroxides are hydrophilic and typically positively charged over a wide range of pH, with a relatively high IEP around pH 9.[40, 41] These positively charged species would shift the overall zeta potential of chalcopyrite towards positive direction upon oxidation and provide possible adsorption sites for O-CMC. As shown in **Figure 5.5**, the zeta potential of O-CMC treated chalcopyrite particles become more negative and close to that of O-CMC, suggesting that O-CMC molecules have adsorbed onto the chalcopyrite surfaces, rendering the surface potential of chalcopyrite similar to that of O-CMC.

The adsorption of O-CMC on chalcopyrite is likely attributed to the electrostatic interaction between the negatively charged carboxyl groups of O-CMC and the positively charged metal oxide/hydroxide species. However, in the flotation tests, chalcopyrite flotation was barely affected by O-CMC after the addition of collector (potassium isobutyl xanthate). The possible explanation is that the competitive adsorption of xanthate will desorb most of the adsorbed O-CMC molecules due to the stronger chemical interaction between xanthate and chalcopyrite surface, thereby the flotation of chalcopyrite was not affected by O-CMC.

On the other hand, sulfur-rich region (metal-deficient sulfides and polysulfides, etc.) that act as anode will also form on chalcopyrite surface, as shown in **Figure 5.6**. The sulfur-rich areas are generally considered to be hydrophobic and provide chalcopyrite self-induced hydrophobicity or collector-less flotation behavior upon oxidation.[41-44] The sulfide groups (–SH) in the sulfide-rich region can either lose a proton and become negatively charged ($–S^-$) for pH above their IEP of 1.6, or gain a proton and become

positively charged ($-SH_2^+$) at pH below 1.6.[40] Hence, in the pH range 3 to 11, these sulfur-rich patches are negatively charged. These negatively charged sulfur species may interact with the amino groups of O-CMC under certain pH conditions (pH 1.6 to 3.5), by electrostatic interaction and hydrophobic interaction, etc. At pH above 3.5, the hydrophobic sulfur-rich region may interact with O-CMC through hydrophobic interaction.

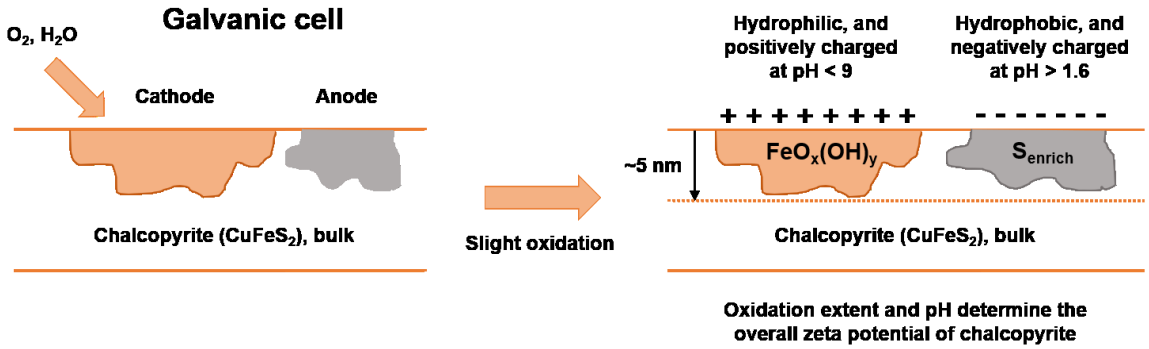


**Figure 5.6**. A simplified depiction of the surface layer composition of chalcopyrite upon slight oxidation.

Overall, the surface reaction of chalcopyrite upon slight oxidation[42, 43] as shown in **Figure 5.6** is recognized as:

$$CuFeS_2 + 0.75 \cdot n \cdot O_2 + 1.5 \cdot n \cdot H_2O = CuFe_{1-n}S_2 + n \cdot Fe(OH)_3$$

Where the $CuFe_{1-n}S_2$ represents the sulfur-enriched surface species such as metal deficient sulfides and polysulfides etc., and $Fe(OH)_3$ represents all iron (ferrous and ferric) oxide/hydroxide species.[42]

In comparison, the zeta potential of molybdenite particles is always negative in the pH range of 3 to 11, with an estimated iso-electric point (IEP) lower than pH 2. Besides, the molybdenite particles are more negatively charged than chalcopyrite particles over the entire pH range, which is consistent with the literature.[37, 40]

After conditioning with 150 ppm O-CMC in 0.001 M KCl solution, the zeta potential curve of O-CMC treated molybdenite particles shifted towards positive direction and close to that of O-CMC over the entire pH range. At pH below 5, the zeta potential curve of treated molybdenite essentially overlaps the zeta potential curve of O-CMC, indicating the strong adsorption of O-CMC at molybdenite surfaces in this pH range. In addition, as the solution pH decreased, the zeta potential difference between treated molybdenite and untreated molybdenite increased, which implies that the adsorption density of O-CMC on molybdenite surfaces may have increased at lower pH, because of the reduced electrostatic repulsion and even electrostatic attraction at pH < 3.5.

Based on the results of zeta potential measurements and literature reports, it is suggested that interactions between O-CMC and chalcopyrite are mostly electrostatic and hydrophobic interaction due to the positively charged species presented on chalcopyrite surface and the self-induced hydrophobicity in certain surface areas of chalcopyrite. Similarly, since molybdenite is an anisotropic mineral with distinct basal planes and edges, the adsorption of O-CMC on molybdenite basal planes (faces) and edges was also discussed independently. The molybdenite basal planes are generated by the exfoliation

of van der Waals force linked S–Mo–S layers, hence the outmost layer of molybdenite basal plane is a layer of S atoms and are recognized to be hydrophobic. The adsorption of O-CMC onto molybdenite basal planes should be driven by hydrophobic attraction and partially hindered by electrostatic repulsion at pH above 3.5, since the molybdenite basal planes are hydrophobic and strongly negatively charged over a broad pH range from pH 3 to 11[45] and O-CMC is also negatively charged at pH > 3.5. On the other hand, the edges of molybdenite are created by the broken of strong Mo-S covalent bonds within the S–Mo–S layers, and are hydrophilic. The molybdenite edges typically account for less than 10% of the total surface areas of molybdenite particles depending on particle size, similar to that of talc;[46, 47] and the edges generally do not affect the natural floatability of molybdenite. Nevertheless, the possible adsorption of O-CMC on molybdenite edges was discussed in this study.

Molybdenite edges are typically strongly negatively charged at pH above 3 due to the presence of $HMoO_4^-$ and $MoO_4^{2-}$ species.[45] As a result, strong electrostatic repulsion is expected between O-CMC and molybdenite edges at pH > 3.5, and the adsorption of O-CMC on molybdenite edges should be negligible and strongly hindered by electrostatic repulsion, as observed in the case of carboxymethyl cellulose (CMC) on molybdenite edges.[48] In fact, O-CMC and CMC have similar molecular structures, and O-CMC can be regarded as CMC with hydroxyl groups on C-2 replaced by amino groups; however, the amino groups of O-CMC should interact with its carboxylate groups at pH above 3.5 (IEP of O-CMC).[39] Therefore, the adsorption mechanisms of O-CMC on molybdenite surfaces

are expected to be similar to that of CMC, and the adsorption of O-CMC on molybdenite edges should also be negligible and hindered by electrostatic repulsion at pH above 3.5.

Hydrogen bonding is not considered as an important adsorption mechanism of O-CMC on molybdenite or chalcopyrite. The primary consideration is that O-CMC and mineral surfaces could also form hydrogen bonds with surrounding water molecules. Therefore, the formation of one hydrogen bond between O-CMC and mineral surfaces requires the breakdown of at least two existing hydrogen bonds between O-CMC/mineral surfaces and water molecules.[21, 49] In addition, the amino groups (possible groups for hydrogen bonding formation) of O-CMC should also interact with its own carboxylate groups at pH above 3.5.[39] Therefore, it is questionable to consider hydrogen bonding as an important adsorption mechanism of O-CMC in aqueous solutions. However, at this stage, it is unknown that if chemical interactions were involved during the adsorption process of O-CMC. To further reveal the adsorption mechanisms, infrared spectroscopy, AFM imaging, and ToF-SIMS measurements were performed.

### 5.3.3 Infrared spectroscopy

The DRIFT spectra of chalcopyrite and molybdenite particles, before and after conditioning with 150 ppm O-CMC in 0.001 M KCl solutions at pH 9 then washed thoroughly with Milli-Q water, are presented in **Figure 5.7** and **Figure 5.8** respectively, together with the spectrum of O-CMC. In the spectrum of O-CMC, the characteristic peaks in the range of 900-3000 $cm^{-1}$ were assigned based on literature reports.[20-22, 50]

Specifically, the broad band at 2907 $cm^{-1}$ comes from the stretching vibration of methyl - and methylene groups (–$CH_3$ and –$CH_2$–). The strong band at 1584 $cm^{-1}$ is attributed to the asymmetric stretching of –$COO^-$, N–H deformation. The peak at 1417 $cm^{-1}$, with a strong intensity, belongs to the symmetric stretching of –$COO^-$, C–N stretching, and N–H deformation. The peak at 1324 $cm^{-1}$ originates from the O–H deformation of –CH–OH. The broad peak at 1057 $cm^{-1}$ originates from the –C–O– vibration and C–O stretching of polysaccharides and its analogues.[20, 38, 51]

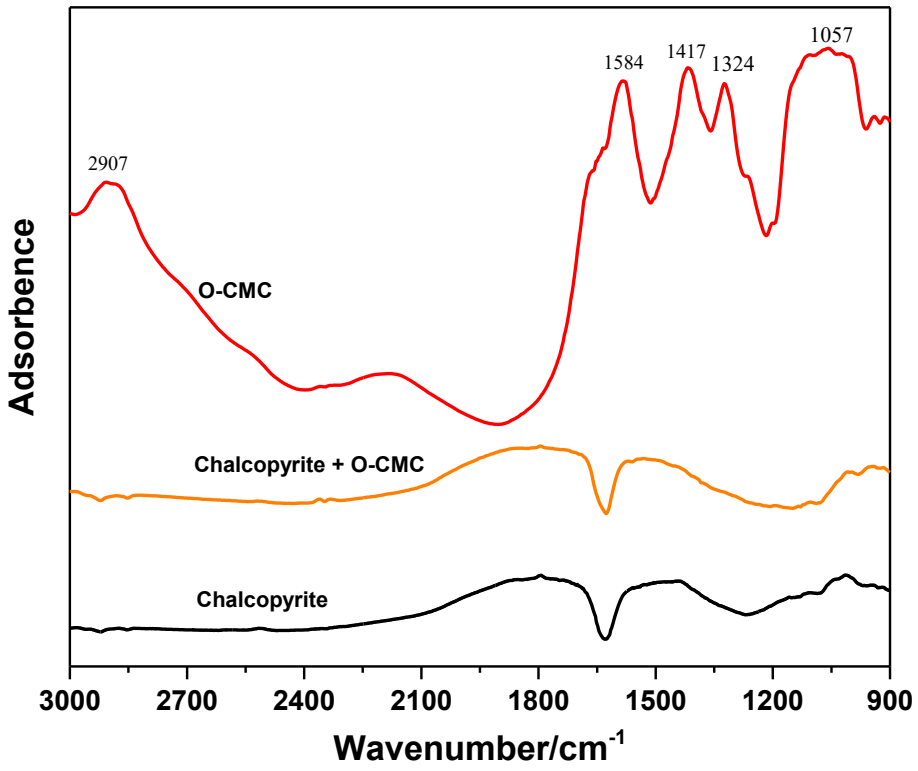


**Figure 5.7**. The DRIFT spectra of O-CMC, O-CMC treated chalcopyrite, and chalcopyrite (chalcopyrite spectrum data from our previous work[38]).

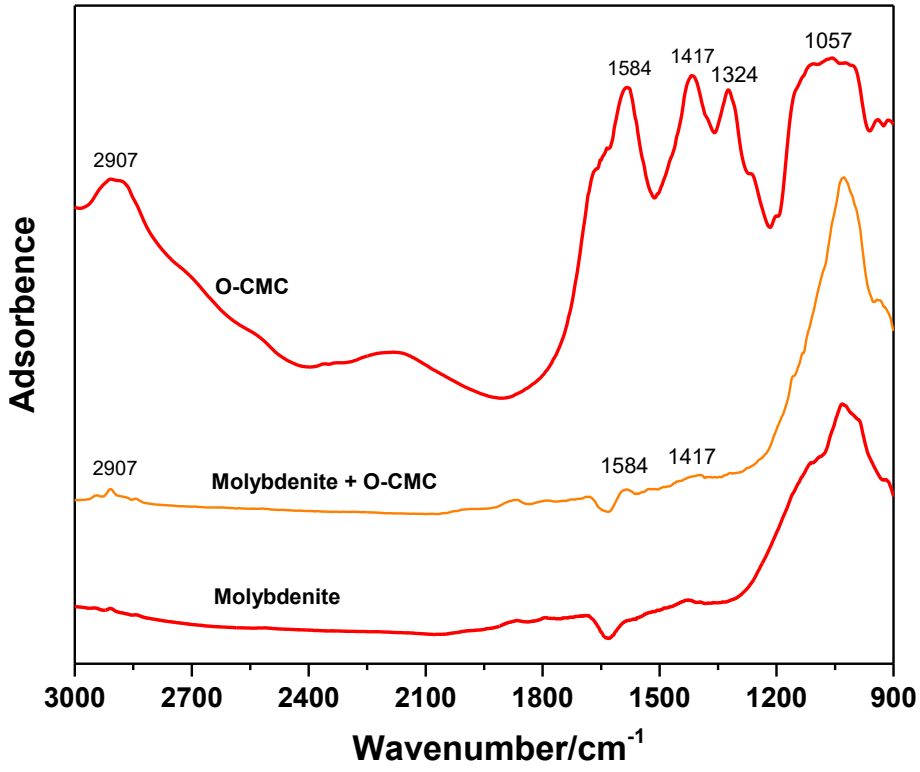


**Figure 5.8**. The DRIFT spectra of O-CMC, O-CMC treated molybdenite, and molybdenite (molybdenite spectrum data from our previous work[38]).

**Figure 5.6** illustrates that the spectrum of chalcopyrite treated with 150 ppm O-CMC then washed with Milli-Q water is almost identical to that of untreated chalcopyrite. It can be inferred that there were no detectable O-CMC molecules on chalcopyrite surfaces after being washed three times with Milli-Q water, suggesting that the adhered O-CMC on chalcopyrite surfaces, as indicated in the electrokinetic study, are likely removed by rinsing, and the adsorption of O-CMC onto chalcopyrite surfaces are likely to be weak and reversible.

However, the results in **Figure 5.7** indicate that molybdenite, after treatment with O-CMC, had several new DRIFT peaks appearing near 2907, 1584 and 1417 $cm^{-1}$ which corresponded to the stretching vibration of $–CH_3$ and $–CH_2–$, asymmetric and symmetric stretching of $–COO^-$ etc. These spectra indicate that O-CMC has been strongly adsorbed on molybdenite surfaces, and washing the O-CMC treated molybdenite particles with Milli-Q water could not completely remove the adsorbed O-CMC.

### 5.3.4 AFM imaging

Constrained by the detection limits of DRIFT spectroscopy, the presence of trace amounts of O-CMC on chalcopyrite surfaces may not be detectable. AFM imaging was applied to further investigate the adsorption of O-CMC on freshly prepared mineral surfaces after washing thoroughly with Milli-Q water, as well as support our hypothesis. Compared to DRIFT spectroscopy, AFM is a much more surface sensitive technique with much lower detection limits. The topographic AFM images of molybdenite surfaces before and after conditioning with 150 ppm O-CMC in 0.001 M KCl solution at pH 9 are presented in **Figure 5.9**. As a layer structure mineral, molybdenite can be readily exfoliated using sticky tape along the van der Waals force linked basal planes to generate atomically smooth surfaces, which shows a root-mean-square (rms) roughness of ~0.14 nm as indicated in **Figures 5.9** A and B.

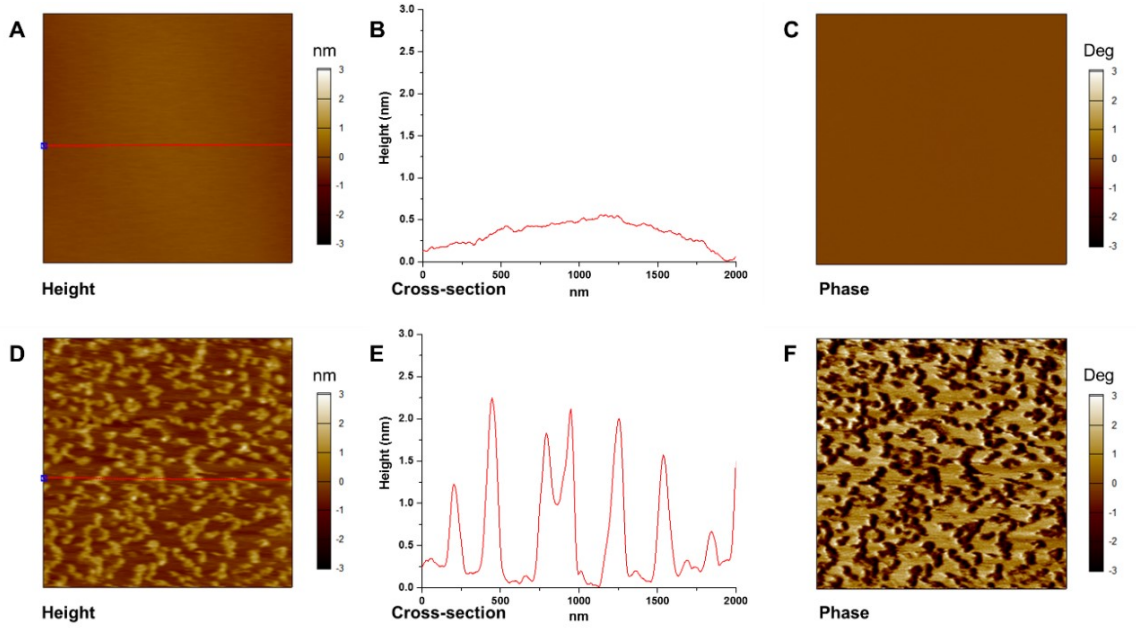


**Figure 5.9**. AFM height, cross-section and phase images (2 × 2 μm$^2$) of molybdenite basal planes before and after treatment with 150 ppm O-CMC in 0.001 M KCl solution at pH 9. (A) freshly exfoliated molybdenite surface; (B) cross-section line profile of fresh molybdenite surface; (C) phase image of fresh molybdenite surface; (D) molybdenite surface treated with O-CMC; (E) cross-section line profile of molybdenite surface treated with O-CMC; (F) phase image of molybdenite surface treated with O-CMC.

After treatment with 150 ppm O-CMC in 0.001 M KCl solution at pH 9, a significant change of the surface morphology of molybdenite was observed in the height image in **Figure 5.9** D. The treated molybdenite surface exhibited randomly and sparsely distributed aggregates with an average diameter of ~200 nm and height up to ~2 nm as demonstrated in **Figure 5.9** E. The aggregates are sparsely distributed rather than

uniformly coating the molybdenite surface. This possible explanation is that the ionic strength of the solution is relatively low (0.001 M KCl) and the O-CMC molecules are strongly negatively charged at pH 9, making the O-CMC molecules more likely to form isolated "islands" instead of uniform coatings on the molybdenite surface due to the strong intermolecular electrostatic repulsion. The apparent phase difference between the formed aggregates (dark spots in **Figure 5.9** F) and the surrounding areas further demonstrates that these aggregates are O-CMC adsorbed on the molybdenite surface, while the surrounding areas are molybdenite surface that not covered by O-CMC.

**Figure 5.10** shows the surface morphology of chalcopyrite before and after conditioning with 150 ppm O-CMC in 0.001 M KCl at pH 9. The freshly polished chalcopyrite surface shows a root-mean-square (rms) roughness of ~0.4 nm in the height image of **Figure 5.10** A and B. After treatment with O-CMC, no significant variations in surface morphology of chalcopyrite was observed in **Figure 5.10** D, and the root-mean-square (rms) roughness of the chalcopyrite surface remains around 0.4 nm, as indicated in **Figure 5.10** D and **Figure 5.10** E. The phase images in **Figure 5.10** C and Figure 9F also confirmed that no apparent adsorption of O-CMC was detected on the chalcopyrite surface after rinsing. However, after conditioned in O-CMC solution, several "white" particles appeared on the chalcopyrite surface, as shown in the height and phase images in **Figure 5.10** D and **Figure 5.10** F, respectively. These particles are less likely to be the residual O-CMC molecules and are more likely to be the surface oxidation products (such as polysulfide, metal-deficient sulfide, elemental sulfur, and even metal

oxides/hydroxides) of chalcopyrite,[41] as initially no or only a few white particles were observed on the fresh chalcopyrite surface. After exposure to air, an increasing number of particles appeared during the repeating AFM scan of the same region of chalcopyrite surface.

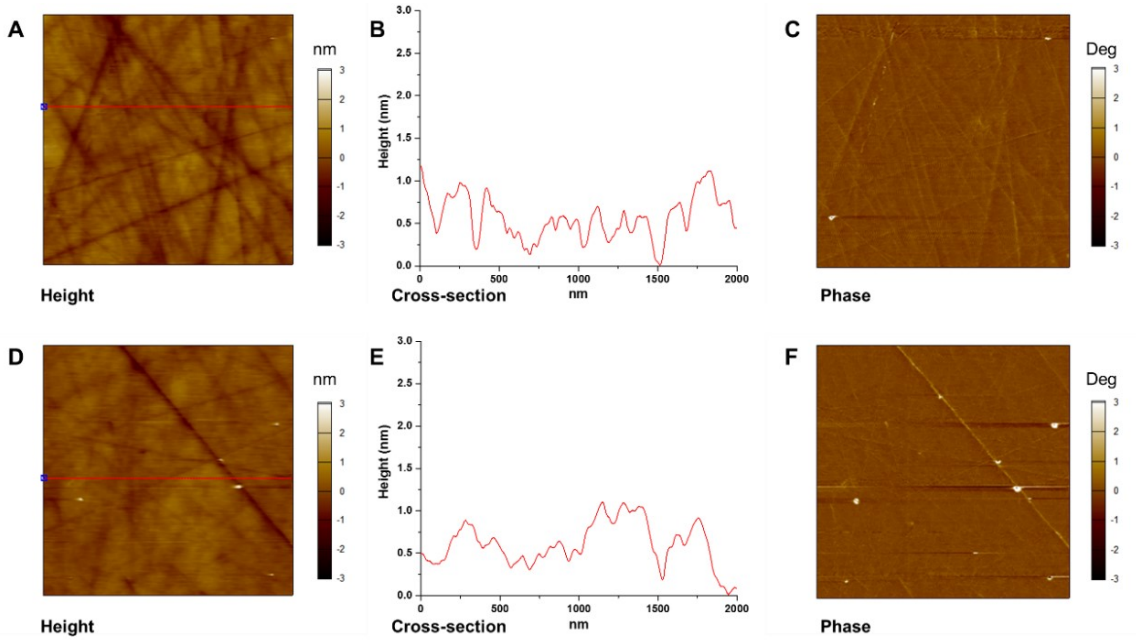


**Figure 5.10**. AFM height, cross-section and phase images (2 × 2 μm$^2$) of chalcopyrite surfaces before and after treatment with 150 ppm O-CMC in 0.001 M KCl solution at pH 9. (A) freshly polished chalcopyrite surface; (B) cross-section line profile of fresh chalcopyrite surface; (C) phase image of fresh chalcopyrite surface; (D) chalcopyrite surface treated with O-CMC; (E) cross-section line profile of chalcopyrite surface treated with O-CMC; (F) phase image of chalcopyrite surface treated with O-CMC.

The AFM images further revealed that the adsorption of O-CMC onto fresh chalcopyrite surface is likely to be a reversible process, and the weakly attached O-CMC on chalcopyrite surface (as indicated in the electrokinetic study) could be readily removed by Milli-Q water washing. In comparison, the adsorption O-CMC onto molybdenite basal plane is more irreversible and could not be easily washed away by water, indicating that the adsorption may be dictated by stronger interaction such as hydrophobic interaction.

### 5.3.5. XPS analyses

5.3.5.1 XPS spectra of O-CMC

The XPS spectra of as-received O-carboxymethyl chitosan (O-CMC) powder was recorded first. The presence of carbon, oxygen, and nitrogen peaks was confirmed by the XPS survey scan of O-CMC, in accordance with the molecular structure of O-CMC, and no significant contamination was observed in the XPS survey spectrum of O-CMC. The high-resolution C 1s, N 1s, and O 1s spectra of O-CMC were recorded and analyzed, and the results are presented in **Figure 5.11**.

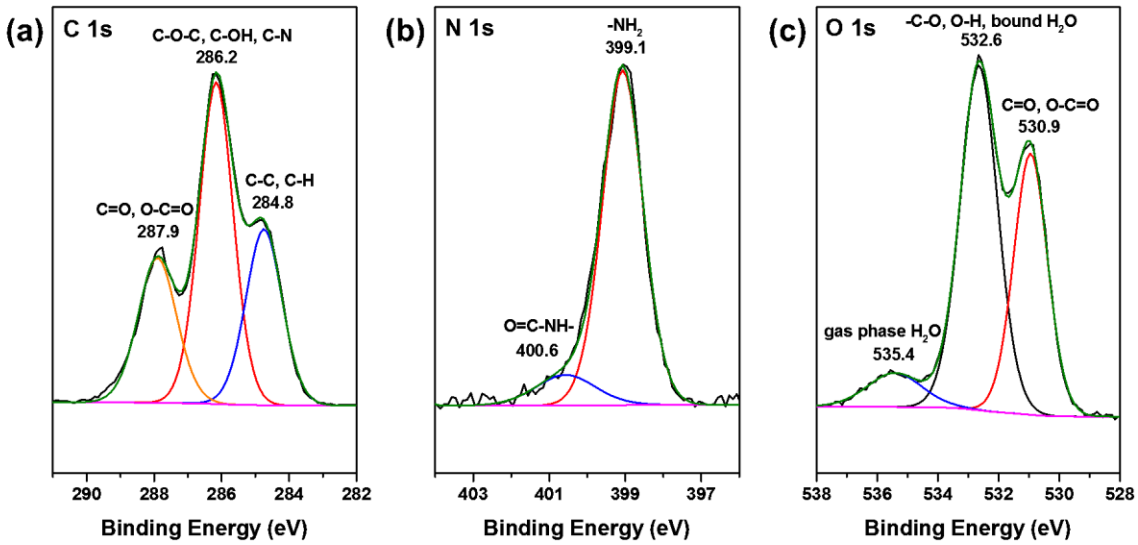


**Figure 5.11**. High-resolution (a) C 1s (b) N 1s (c) O 1s XPS spectrum of as-received O-CMC.

As can be seen from **Figure 5.11** (a), the high-resolution C 1s line could be deconvoluted into three individual peaks. Specifically, the peak at 284.8 eV is originated from the C–C and C–H. The peak at 286.2 eV with the strongest intensity comes from the C–N and C–O in the O-CMC, and the peak at 287.9 eV is attributed to the carboxylic groups (O–C=O) of O-CMC and the C=O existed in the undeacetylated amide groups of O-CMC.[52-54] In **Figure 5.11** (b), two peaks can be resolved on the high-resolution N 1s spectrum of O-CMC. The strong peak at 399.1 eV is attributed to the $–NH_2$ groups of O-CMC,[50, 55, 56] while the peak with a relatively weak intensity at 400.6 eV comes from the O=C–NH– groups, i.e., the undeacetylated amide groups of O-CMC.[50, 56] It should be

noted that the degree of deacetylation of O-CMC used in this study is 90.78%, which correlate well with the XPS peak intensity.

The high-resolution O 1s spectrum of O-CMC is shown in **Figure 5.11** (c), at least three species can be resolved from the O 1s line. The broad peak at 535.4 eV is caused by the photoemission from gas phase $H_2O$[57] that vaporized from the polymer powder. The peak at 532.6 eV with the highest intensity comes from the C–O, O–H and bound $H_2O$ in O-CMC.[52-54] The peak at 530.9 eV is assigned to the carbonyl oxygen of the C=O, O–C=O groups in the O-CMC.[52, 53, 58]

5.3.5.2 XPS spectra of molybdenite

The high-resolution C 1s, N 1s, and O 1s spectra of molybdenite before and after O-CMC treatment are shown in **Figure 5.12**. Before treatment by O-CMC, the molybdenite surface exist a C 1s peak at 284.8 eV, which is well known from the adventitious carbon. In comparison, no significant amount of oxygen and nitrogen species were detected on the freshly exfoliated molybdenite surface.

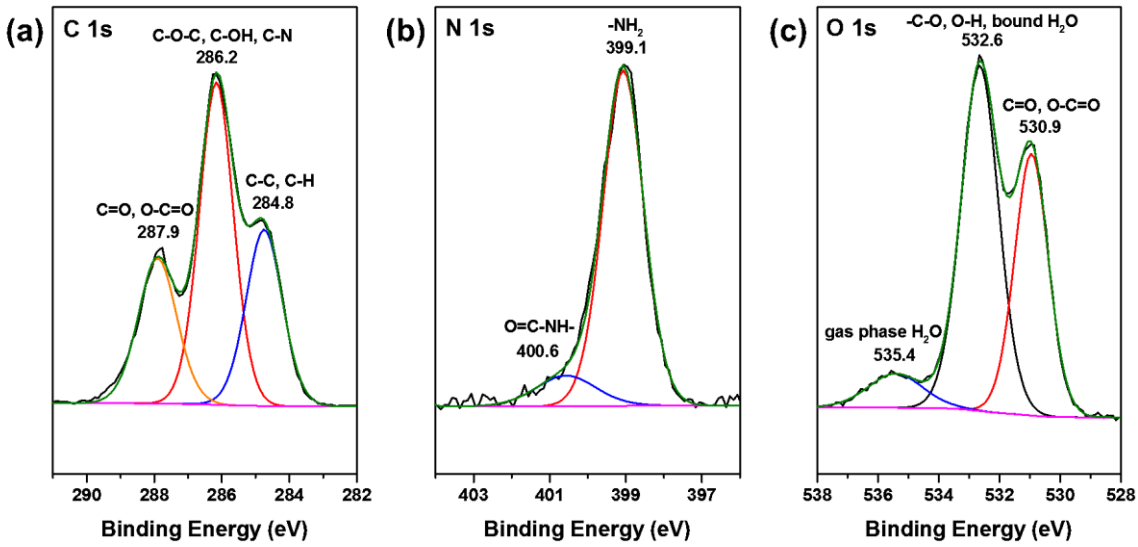


**Figure 5.12**. High-resolution (a) C 1s (b) N 1s (c) O 1s XPS spectra of molybdenite before (bottom) and after O-CMC treatment (top).

After treatment with the O-CMC solution, two new peaks near 287.8 eV (O–C=O, C=O) and 286.1 eV (C–O, C–N) arise in the C 1s spectrum of treated molybdenite, as a result of the O-CMC adsorption. Besides, the peak intensities and the peak-to-peak ratio are similar to that of O-CMC powder, indicating the O-CMC is the primary carbon species on O-CMC treated molybdenite surface. In other words, the adventitious carbon only accounts for a small percentage of carbon on the O-CMC treated molybdenite surface. Otherwise, if adventitious carbon is the dominant carbon species, then the C 1s peak at 284.8 eV should be the highest peak among all three C 1s peaks.

In addition, the N 1s and O 1s spectra of treated molybdenite also confirmed that O-CMC had adsorbed onto molybdenite surface, and the peak positions, peak intensities,

and peak-to-peak ratios correlate well with that of O-CMC powder. Since there were no obvious binding energy shifts of C 1s, N 1s and O 1s peaks, the adsorption of O-CMC on molybdenite basal planes could not be attributed to the chemical interactions. Herein, the physical interactions, most likely the hydrophobic interaction, was suggested to be the adsorption mechanisms of O-CMC onto molybdenite surface.

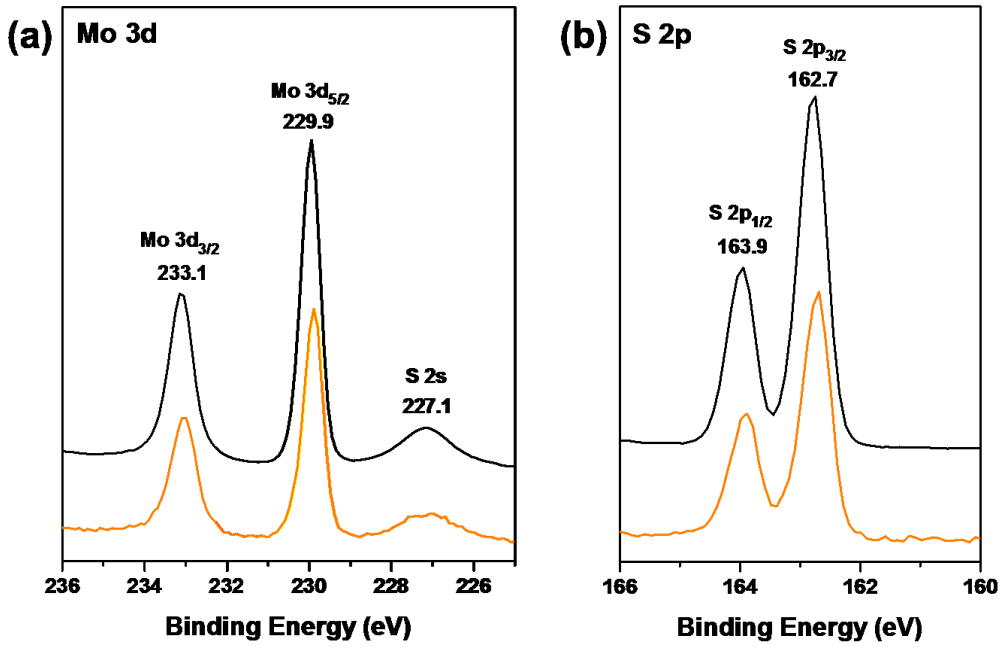


**Figure 5.13**. High-resolution (a) Mo 3d (b) S 2p XPS spectra of Molybdenum disulfide before (top) and after O-CMC treatment (bottom).

To further confirm the absence of chemical interactions between molybdenite and O-CMC, the high-resolution Mo 3d and S 2p spectra of molybdenite before and after O-CMC treatment were also recorded and the results are presented in **Figure 5.13**. As can be seen, no binding energy shifts or new peaks were observed in the high-resolution Mo

3d and S 2p spectra of molybdenite before and after O-CMC treatment, which further confirmed that no strong chemical interactions were involved during the adsorption process of O-CMC onto molybdenite basal planes. Since both O-CMC molecules and molybdenite surfaces are strongly negatively charged at pH > 4, as indicated in the zeta potential measurements and literature,[45] the most likely strong interaction between O-CMC and molybdenite surfaces that could overcome the electrostatic repulsion is the hydrophobic interaction between the hydrophobic moieties of O-CMC and the molybdenite basal planes.

5.3.5.3 XPS spectra of chalcopyrite

The high-resolution C 1s, N 1s, and O 1s spectra of chalcopyrite before and after O-CMC treatment are presented in **Figure 5.14**. Before treatment by O-CMC, the chalcopyrite surface exist several C 1s peaks at 288.5 eV (C=O, O–C=O), 286.5 eV (C–OH, C–O–C) and 284.8 eV (C–C, C–H), which is known from the adventitious carbon. Meanwhile, no N 1s peaks were observed on the high-resolution N 1s line of chalcopyrite before O-CMC treatment. The high-resolution O 1s spectrum of chalcopyrite before O-CMC treatment, of relatively weak intensity and very broad, consists at least three components, which could be assigned to the adsorbed water and sulfate (532.9 eV), hydroxides (531.4 eV) and oxides (529.7 eV).[42, 59]

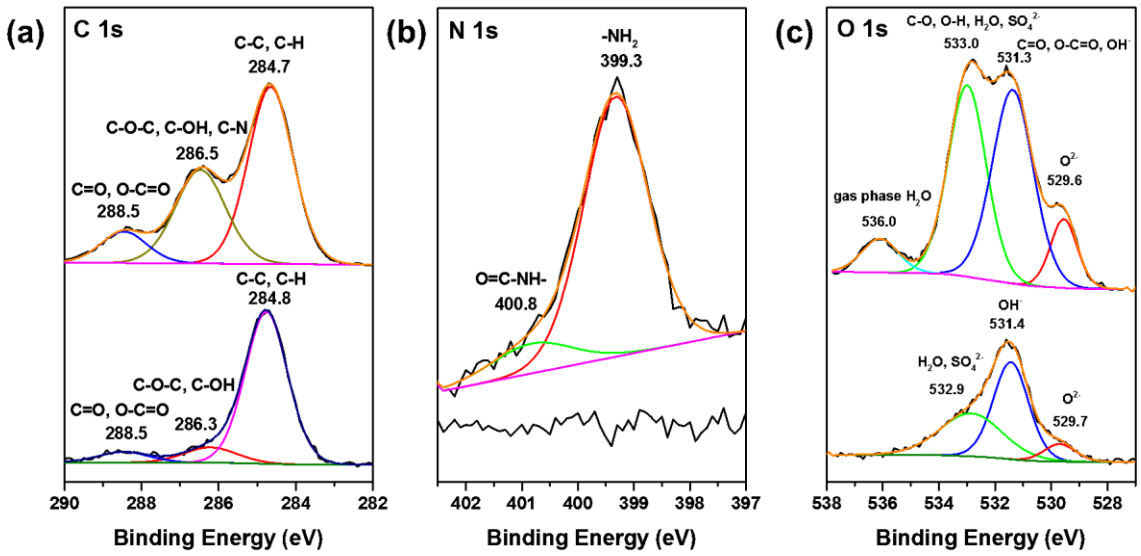


**Figure 5.14**. High-resolution (a) C 1s (b) N 1s (c) O 1s XPS spectra of chalcopyrite before (bottom) and after O-CMC treatment (top).

However, after immersion in O-CMC solution and dried without Milli-Q water rinsing, the peak intensity of C=O/O–C=O (288.5 eV) and C–O/C–N (286.3 eV) increased significantly as compared with that of C–C/C–H. According to the C 1s spectrum of O-CMC, the C 1s peak at 286.5 eV (C–O/C–N) is the highest among all three C 1s peaks. However, in the C 1s spectrum of O-CMC treated chalcopyrite, the C–O/C–N peak is not the highest peak among all three peaks. Therefore, it can be concluded that O-CMC is not the dominant carbon species on chalcopyrite surface, and the adventitious carbon may contribute to a significant proportion of the carbon on the chalcopyrite surface. The C 1s spectrum of O-CMC treated chalcopyrite and zeta potential measurements revealed that a small quantity of O-CMC has attached to

chalcopyrite surface before Milli-Q water rinsing; however, the attached O-CMC can be mostly removed by washing with water, as indicated by AFM imaging.

The N 1s line of chalcopyrite before and after O-CMC treatment are shown in **Figure 5.14** (b). Before O-CMC treatment, no nitrogen species were observed on the chalcopyrite surface. After conditioned in O-CMC solution, an N 1s peak with a relatively low intensity appeared on chalcopyrite surface, suggesting that O-CMC has been attached or deposited onto chalcopyrite surface before rinsing by water, and the increase of C 1s peak intensity is not solely caused by the adventitious carbon. Besides, the two peaks of N 1s line have shifted from 399.1 and 400.6 eV to 399.3 and 400.8 eV, respectively; which is mostly like caused by the charging effect during the XPS measurements or errors (fitting and measurements).

The O 1s line of chalcopyrite before and after O-CMC solution treatment is a much more complicated due to the rapid oxidation of chalcopyrite surface. However, at least four components can be resolved from the O 1s line. In addition to the three O 1s peaks already existed on chalcopyrite surface, a new peak at 536.0 eV appeared on the O 1s line of treated chalcopyrite, which is attributed to the gas phase $H_2O$ (vaporized from the polymer film on chalcopyrite surface) as mentioned in **Figure 5.11**. The two O 1s peaks at 532.9 eV ($H_2O$, $SO_4^{2-}$) and 531.4 eV ($OH^-$) on chalcopyrite surface merged with the C–O/O–H peak (532.6 eV) and C=O peak (530.9 eV) of the O-CMC, respectively; and formed two strong and broad peaks around 533.0 eV and 531.3 eV. Again, the slight binding energy shifts are most likely due to the charging effect during the XPS

measurements or errors (fitting and measurements). Besides, the electrostatic attraction between the carboxylic groups of O-CMC and the surface oxidation species of chalcopyrite surface may also result in the slight binding energy shifts.

Since no significant binding energy shifts were observed on the C 1s, N 1s and O 1s electrons, the interactions between O-CMC and chalcopyrite are unlikely to be strong chemical interactions. Considering the surface charge properties and self-induced hydrophobicity in certain region of chalcopyrite surface, the interactions between O-CMC and chalcopyrite should be relatively weak physical interactions such as electrostatic interaction and hydrophobic interaction, as indicated in the zeta potential measurements.

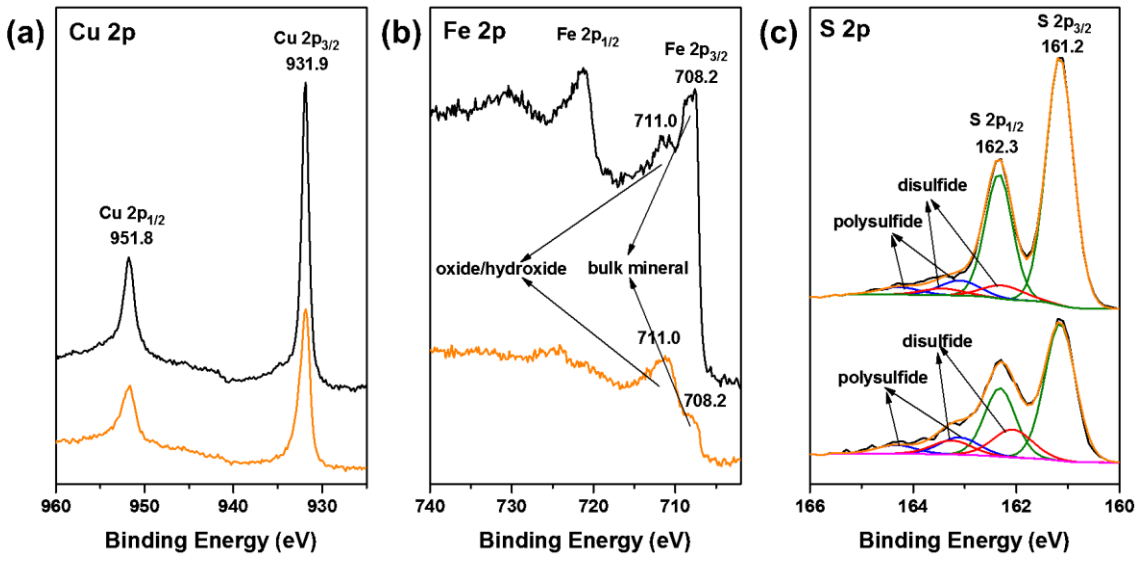


**Figure 5.15**. High-resolution (a) Cu 2p (b) Fe 2p (c) S 2p XPS spectra of chalcopyrite before (top) and after O-CMC treatment (bottom).

The Cu 2p spectra of chalcopyrite are presented in **Figure 5.15** (a), as can be seen, no binding energy shift was observed for the Cu 2p peaks of chalcopyrite before and after O-CMC treatment, which further confirmed the absence of chemical interactions between O-CMC and chalcopyrite.

As indicated in **Figure 5.15** (b), the broad Fe 2p line of chalcopyrite before O-CMC treatment consists of at least two components. The broad band at about 711.0 eV comes from the ferric and ferrous oxide/hydroxide species such as FeOOH, $Fe(OH)_2$, $Fe_2O_4$, $Fe_3O_4$ on the chalcopyrite surface, while the Fe 2p peak at 708.2 eV is attributed to the iron in the bulk mineral structure.[42, 60, 61] After treatment with the O-CMC solution, the peak intensity of iron oxide/hydroxide species increased significantly due to the rapid oxidation of chalcopyrite surface, while the peak intensity of iron in the bulk chalcopyrite decreased dramatically. The line shape and peak position etc. of Fe 2p spectrum after O-CMC treatment are highly consistent with the literature reports,[42, 60, 61] and indicate that the change of Fe 2p line shape is irrelevant to the O-CMC adsorption, and is mainly caused by the surface oxidation.

In addition, the S 2p spectra of chalcopyrite before and after O-CMC treatment were also shown in **Figure 5.15** (c), and three groups of S 2p doublets can be resolved from the S 2p line. The strongest doublet at 161.2 and 162.3 eV comes from the metal sulfide ($S^{2-}$) in the bulk of chalcopyrite. The doublet at 162.2 and 163.4 eV originated from the metal-deficient disulfide ($S_2^{2-}$) on the chalcopyrite surface, The weakest doublet at 163.1 and 164.3 eV is assigned to the polysulfide ($S_n^{2-}$, $n>2$) on chalcopyrite surface.[59, 62] The

notable reduction of the bulk S intensity and the increasing of disulfides and polysulfides intensity suggest that the chalcopyrite surface is more oxidized after immersion in the O-CMC solution, while the lack of binding energy shifts of S 2p peaks reveals the absence of chemical interactions.

### 5.3.6 ToF-SIMS analysis

To directly demonstrate the possible selective adsorption of O-CMC on the molybdenite and chalcopyrite surfaces, ToF-SIMS measurement was employed to determine metal ions and O-CMC distribution on the treated chalcopyrite-molybdenite mixture. On the surface of the mixture, positive ion maps of $Fe^+$, $Cu^+$, $Mo^+$, and their dominant isotopes were selected to outline the molybdenite and chalcopyrite surfaces in the artificial chalcopyrite-molybdenite mixture treated with O-CMC, since molybdenite and chalcopyrite are the only source of $Mo^+$, $Cu^+$ and $Fe^+$, respectively. Similarly, the $CH_4N^+$ and $NH_4^+$ ions, as fragments of O-CMC, were chosen to represent the distribution of O-CMC on the surface of the mineral mixture. The distributions of O-CMC, molybdenite, and chalcopyrite on a sample area of 86 × 86 $\mu m^2$ are shown in **Figure 5.16** A-H. It can be noticed that molybdenite and chalcopyrite complemented each other in the scanned area. By comparing **Figure 5.16** A-H, it can be seen that the distribution of O-CMC overlapped the $Mo^+$ and $Cu^+$ distribution, and does not match well with the distribution of $Fe^+$, indicating that the O-CMC has preferentially adsorbed on the

molybdenite surfaces and the sulfur-rich areas of chalcopyrite surfaces after washing thoroughly with Milli-Q water.

It should be noted that the typical sampling depth of ToF-SIMS measurements (without continuous sputtering or itching) is about 1 to 2 nm. Hence, the ToF-SIMS only reveals the surface chemistry of the topmost layers of minerals. As shown in **Figure 5.16**, the stronger intensity of $Fe^{+}$ in certain region as compared with $Cu^{+}$ and its isotopes further confirmed that the chalcopyrite surface is actually heterogeneous and consists of patches of iron oxides/hydroxides with a typical thickness of few nanometers (depending on oxidation degree), which is consistent with the literature reports.[42-44] Upon oxidation, the chalcopyrite surface would form patches of iron oxides/hydroxides as mentioned earlier in **Figure 5.6**. The iron oxides/hydroxides are one of the possible adsorption sites for O-CMC, due to electrostatic interaction, as mentioned in the zeta potential measurements.

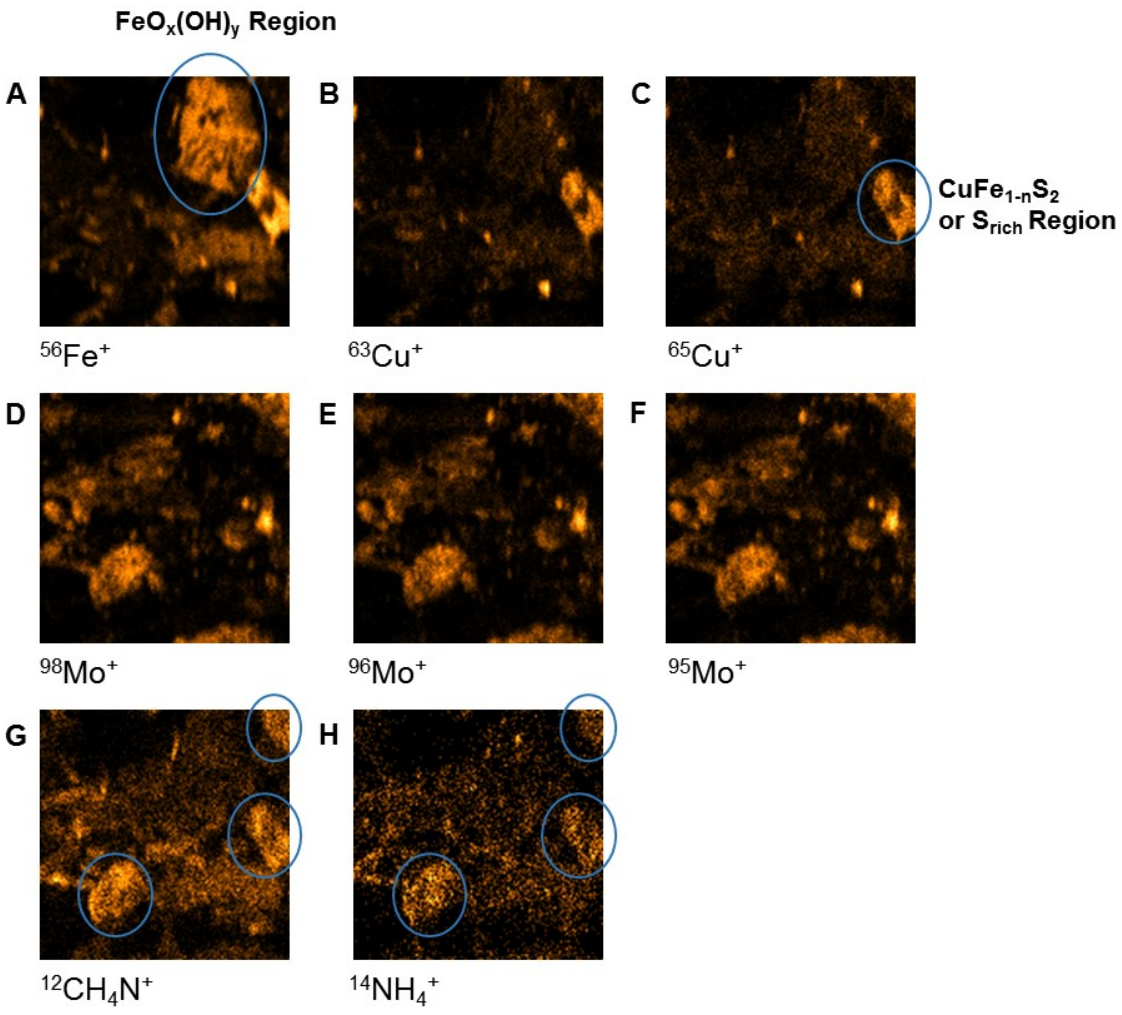


**Figure 5.16**. Positive-ion images of 86 × 86 μm$^2$ of the surface of chalcopyrite–molybdenite mixture (weight ratio of 1:1) treated with 150 ppm O-CMC in 0.001 M KCl solution at pH 9. (A) Image of $^{56}Fe^+$ distribution; (B) Image of $^{63}Cu^+$ distribution; (C) Image of $^{65}Cu^+$ distribution; (D) Image of $^{98}Mo^+$ distribution; (E) Image of $^{96}Mo^+$ distribution; (F) Image of $^{95}Mo^+$ distribution; (G) Image of $^{12}CH_4N^+$ distribution; (H) Image of $^{14}NH_4^+$ distribution.

However, **Figure 5.16** shows that O-CMC was not detected in the iron oxides/hydroxides region of chalcopyrite after washing. The possible explanation is that the thin layer of iron oxides/hydroxides (together with the adsorbed O-CMC) could be easily peeled off or removed mechanically from the chalcopyrite surface,[42, 43] as shown in **Figure 5.17**. Hence, O-CMC was not observed in the iron oxides/hydroxides region of chalcopyrite in the ToF-SIMS imaging in **Figure 16**. However, the interactions between O-CMC and the sulfur-rich areas of chalcopyrite surface are likely to be hydrophobic interaction, etc. As a result, the O-CMC could not be easily washed away from the sulfur-enriched areas or $CuFe_{1-n}S_2$ region of chalcopyrite, and was detected in the $Cu^+$ site of the ToF-SIMS images.

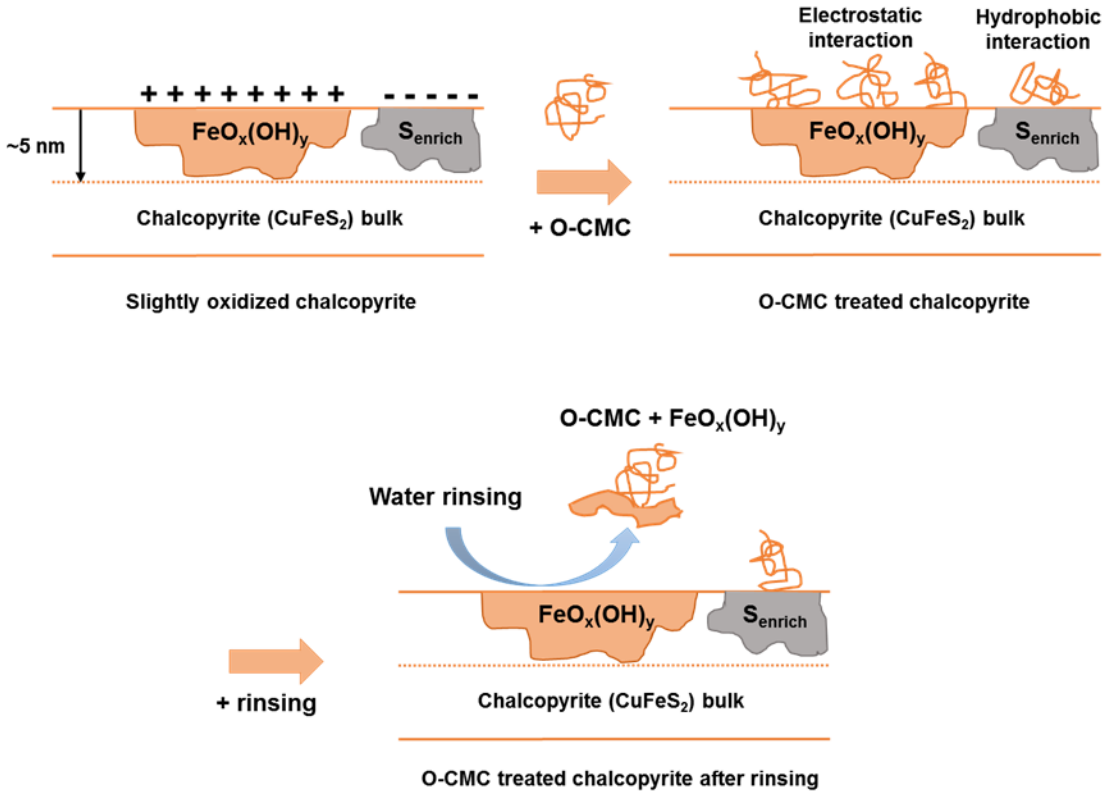

**Figure 5.17**. A simplified schematic diagram of the surface layer composition of chalcopyrite after treatment with O-CMC and water rinsing.

## 5.4 Conclusions

In this work, O-Carboxymethyl chitosan (O-CMC), a nontoxic, biodegradable and cost-effective derivative of the naturally occurring polysaccharide chitosan, was exploited as an efficient and selective depressant for molybdenite in the Cu-Mo separation, to replace the current toxic and hazardous depressants. In single mineral flotation tests, O-CMC demonstrated good molybdenite depression ability over the entire pH range tested (3-11), while the floatability of chalcopyrite was only slightly affected by O-CMC under strong acidic condition (pH 3). In the mixed minerals flotation, O-CMC is selective and efficient in depressing molybdenite flotation while not significantly affecting the recovery of chalcopyrite over the entire pH range tested.

The flotation results were explained by the higher adsorption density of O-CMC on molybdenite than chalcopyrite, and the adsorption characteristics of O-Carboxymethyl chitosan (O-CMC) on chalcopyrite and molybdenite surfaces were analyzed by a range of different techniques. The results showed that O-CMC strongly adsorbs on molybdenite surfaces, while no apparent adsorption of O-CMC was identified on chalcopyrite surfaces by AFM or DRIFT spectroscopy after rinsing thoroughly with Milli-Q water. The higher adsorption density of O-CMC on molybdenite than chalcopyrite successfully explained the selective separation of chalcopyrite and molybdenite during the flotation process.

The results of electrokinetic studies and XPS measurements indicate that interactions between O-CMC and chalcopyrite are mostly weak physical interactions such as electrostatic interaction and hydrophobic interaction due to the absence of significant binding energy shift. In addition, the adsorption of O-CMC on chalcopyrite is reversible and most of the adsorbed O-CMC could be removed mechanically (e.g., washing), as indicated in DRIFT spectroscopy, AFM and ToF-SIMS imaging. In contrast, the adsorption O-CMC onto molybdenite is more irreversible and should be dictated by hydrophobic interaction, owing to the natural hydrophobicity of the molybdenite basal planes. The bubble-molybdenite attachment and the dewetting process during the flotation process was hindered by the adsorbed polymer layer,[63, 64] thereby resulting in the strong depression of molybdenite. In addition, the preferential adsorption of O-CMC onto molybdenite over chalcopyrite from a mixture was verified by ToF-SIMS analysis, which further demonstrated that O-CMC adsorbs strongly on molybdenite surface over chalcopyrite surface, and also correlate well with AFM results and successfully explained the selective separation of chalcopyrite and molybdenite from the mixture.

In conclusion, the adsorption characteristics of a biodegradable, non-toxic, and cost-effective depressant O-CMC on molybdenite/chalcopyrite were systematically studied, and the associated interaction mechanisms between O-CMC and two mineral surfaces were successfully explained. Besides, it was observed the water solubility and selectivity of O-CMC were significantly enhanced compared with the recently found polymeric depressant—chitosan.[15, 22] Moreover, compared to the conventional polymer

depressants such as carboxymethyl cellulose.[65] O-CMC is stimulus or pH responsive and becomes insoluble and precipitates at its iso-electric point around pH 3.5, which provides a potential approach to remove, recycle and reuse it from the tailings water; and to our knowledge, this approach has not been reported. The precipitation of O-CMC could also facilitate the settling and removal of fine particles in the slurry and purify the tailings water. However, it should be noted that the IEP of O-CMC may not be a fixed value and is likely affected by the degree of substitution and deacetylation of O-CMC. Additional research is required to investigate how to efficiently remove or recycle the O-CMC from the tailings water. This work also provides important implications and guidance for the development of novel polymeric depressants or flocculants, and separation of many other mineral systems and related engineering processes such as wastewater treatment.

## 5.5 Acknowledgements

The financial support from the Natural Sciences and Engineering Research Council of Canada (NSERC) is gratefully acknowledged. The XPS and ToF-SIMS characterizations were conducted at the Alberta Centre for Surface Engineering and Science (ACSES), University of Alberta. The authors thank Dr. Shihong Xu and Dr. Anqiang He for their assistance in XPS and ToF-SIMS measurements. Duowei Yuan also gratefully appreciates the scholarship support from the China Scholarship Council (CSC).

## 5.6 References


1. Karunadasa, H. I.; Montalvo, E.; Sun, Y.; Majda, M.; Long, J. R.; Chang, C. J., A molecular $MoS_2$ edge site mimic for catalytic hydrogen generation. *Science* **2012,** *335* (6069), 698-702.

2. Gao, M. R.; Liang, J. X.; Zheng, Y. R.; Xu, Y. F.; Jiang, J.; Gao, Q.; Li, J.; Yu, S. H., An efficient molybdenum disulfide/cobalt diselenide hybrid catalyst for electrochemical hydrogen generation. *Nature communications* **2015,** *6*, 5982.

3. Fontana, M.; Deppe, T.; Boyd, A. K.; Rinzan, M.; Liu, A. Y.; Paranjape, M.; Barbara, P., Electron-hole transport and photovoltaic effect in gated MoS2 Schottky junctions. *Scientific reports* **2013,** *3*, 1634.

4. Bernardi, M.; Palummo, M.; Grossman, J. C., Extraordinary sunlight absorption and one nanometer thick photovoltaics using two-dimensional monolayer materials. *Nano letters* **2013,** *13* (8), 3664-70.

5. Liu, H.; Su, D.; Zhou, R.; Sun, B.; Wang, G.; Qiao, S. Z., Highly Ordered Mesoporous MoS2 with Expanded Spacing of the (002) Crystal Plane for Ultrafast Lithium Ion Storage. *Advanced Energy Materials* **2012,** *2* (8), 970-975.

6. Zhang, C.; Wang, Z.; Guo, Z.; Lou, X. W., Synthesis of MoS(2)-C one-dimensional nanostructures with improved lithium storage properties. *ACS applied materials & interfaces* **2012,** *4* (7), 3765-8.

7. Cheng, R.; Jiang, S.; Chen, Y.; Liu, Y.; Weiss, N.; Cheng, H. C.; Wu, H.; Huang, Y.; Duan, X., Few-layer molybdenum disulfide transistors and circuits for high-speed flexible electronics. *Nature communications* **2014,** *5*, 5143.

8. Zhu, W.; Low, T.; Lee, Y. H.; Wang, H.; Farmer, D. B.; Kong, J.; Xia, F.; Avouris, P., Electronic transport and device prospects of monolayer molybdenum disulphide grown by chemical vapour deposition. *Nature communications* **2014,** *5*, 3087.

9. Winer, W. O., Molybdenum disulfide as a lubricant: A review of the fundamental knowledge. *Wear* **1967,** *10* (6), 422-452.

10. Wills, B. A., *Wills' mineral processing technology: an introduction to the practical aspects of ore treatment and mineral recovery*. Butterworth-Heinemann: 2011.

11. Bulatovic, S. M., *Handbook of flotation reagents: chemistry, theory and practice: Volume 1: flotation of sulfide ores*. Elsevier: 2007.

12. Zanin, M.; Ametov, I.; Grano, S.; Zhou, L.; Skinner, W., A study of mechanisms affecting molybdenite recovery in a bulk copper/molybdenum flotation circuit. *International Journal of Mineral Processing* **2009,** *93* (3-4), 256-266.

13. Pearse, M. J., An overview of the use of chemical reagents in mineral processing. *Minerals Engineering* **2005,** *18* (2), 139-149.

14. Prasad, M. S., Reagents in the mineral industry — recent trends and applications. *Minerals Engineering* **1992,** *5* (3-5), 279-294.

15. Li, M.; Wei, D.; Liu, Q.; Liu, W.; Zheng, J.; Sun, H., Flotation separation of copper–molybdenum sulfides using chitosan as a selective depressant. *Minerals Engineering* **2015,** *83*, 217-222.

16. Ansari, A.; Pawlik, M., Floatability of chalcopyrite and molybdenite in the presence of lignosulfonates. Part II. Hallimond tube flotation. *Minerals Engineering* **2007,** *20* (6), 609-616.

17. Poling, G.; Liu, Q., Flotation depression of chalcopyrite with thioglycolic acid. *TRANSACTIONS OF THE INSTITUTION OF MINING AND METALLURGY SECTION C-MINERAL PROCESSING AND EXTRACTIVE METALLURGY* **1987,** *96*, C7-C12.

18. Rinaudo, M., Chitin and chitosan: Properties and applications. *Progress in Polymer Science* **2006,** *31* (7), 603-632.

19. Pillai, C. K. S.; Paul, W.; Sharma, C. P., Chitin and chitosan polymers: Chemistry, solubility and fiber formation. *Progress in Polymer Science* **2009,** *34* (7), 641-678.

20. Mourya, V. K.; Inamdar, N. N.; Tiwari, A., Carboxymethyl chitosan and its applications. *Advanced Materials Letters* **2010,** *1* (1), 11-33.

21. Xiang, Y. Carboxymethyl Chitosan as a Selective Depressant in Differential Flotation of Galena and Chalcopyrite. University of Alberta, 2015.

22. Huang, P. Chitosan in Differential Flotation of Base Metal Sulfides. University of Alberta, 2013.

23. Huang, P.; Cao, M.; Liu, Q., Using chitosan as a selective depressant in the differential flotation of Cu–Pb sulfides. *International Journal of Mineral Processing* **2012,** *106-109*, 8-15.

24. Wu, J.; Delcheva, I.; Ngothai, Y.; Krasowska, M.; Beattie, D. A., Bubble–surface interactions with graphite in the presence of adsorbed carboxymethylcellulose. *Soft matter* **2015,** *11* (3), 587-599.

25. Dutta, P. K.; Tripathi, S.; Mehrotra, G. K.; Dutta, J., Perspectives for chitosan based antimicrobial films in food applications. *Food Chemistry* **2009,** *114* (4), 1173-1182.

26. Berger, J.; Reist, M.; Mayer, J. M.; Felt, O.; Peppas, N. A.; Gurny, R., Structure and interactions in covalently and ionically crosslinked chitosan hydrogels for biomedical applications. *European Journal of Pharmaceutics and Biopharmaceutics* **2004,** *57* (1), 19-34.

27. Periayah, M. H.; Halim, A. S.; Mat Saad, A. Z.; Yaacob, N. S.; Hussein, A. R.; Abdul Karim, F.; Abdul Rashid, A. H.; Ujang, Z., Effect of the Novel Biodegradable N, O-Carboxymethylchitosan and Oligo-Chitosan on the Platelet Thrombogenicity Cascade in von Willebrand Disease. *Thrombosis research* **2015,** *136* (3), 625-33.

28. Anitha, A.; Maya, S.; Deepa, N.; Chennazhi, K. P.; Nair, S. V.; Tamura, H.; Jayakumar, R., Efficient water soluble O-carboxymethyl chitosan nanocarrier for the delivery of curcumin to cancer cells. *Carbohydrate polymers* **2011,** *83* (2), 452-461.

29. Chen, X.-G.; Park, H.-J., Chemical characteristics of O-carboxymethyl chitosans related to the preparation conditions. *Carbohydrate polymers* **2003,** *53* (4), 355-359.

30. Wang, J.; Liu, Q.; Zeng, H., Understanding Copper Activation and Xanthate Adsorption on Sphalerite by Time-of-Flight Secondary Ion Mass Spectrometry, X-ray Photoelectron Spectroscopy, and in Situ Scanning Electrochemical Microscopy. *The Journal of Physical Chemistry C* **2013,** *117* (39), 20089-20097.

31. Xie, L.; Shi, C.; Wang, J.; Huang, J.; Lu, Q.; Liu, Q.; Zeng, H., Probing the interaction between air bubble and sphalerite mineral surface using atomic force microscope. *Langmuir: the ACS journal of surfaces and colloids* **2015,** *31* (8), 2438-46.

32. Xie, L.; Wang, J.; Shi, C.; Cui, X.; Huang, J.; Zhang, H.; Liu, Q.; Liu, Q.; Zeng, H., Mapping the Nanoscale Heterogeneity of Surface Hydrophobicity on the Sphalerite Mineral. *The Journal of Physical Chemistry C* **2017,** *121* (10), 5620-5628.

33. Wang, J.; Xie, L.; Liu, Q.; Zeng, H., Effects of salinity on xanthate adsorption on sphalerite and bubble–sphalerite interactions. *Minerals Engineering* **2015,** *77*, 34-41.

34. Siwek, B.; Zembala, M.; Pomianowski, A., A method for determination of fine-particle flotability. *International Journal of Mineral Processing* **1981,** *8* (1), 85-88.

35. Fuerstenau, D. W.; Pradip, Zeta potentials in the flotation of oxide and silicate minerals. *Advances in colloid and interface science* **2005,** *114-115*, 9-26.

36. Braga, P. F. A.; Chaves, A. P.; Luz, A. B.; França, S. C. A., The use of dextrin in purification by flotation of molybdenite concentrates. *International Journal of Mineral Processing* **2014,** *127*, 23-27.

37. Castro, S.; Lopez-Valdivieso, A.; Laskowski, J. S., Review of the flotation of molybdenite. Part I: Surface properties and floatability. *International Journal of Mineral Processing* **2016,** *148*, 48-58.

38. Yuan, D.; Xie, L.; Shi, X.; Yi, L.; Zhang, G.; Zhang, H.; Liu, Q.; Zeng, H., Selective flotation separation of molybdenite and talc by humic substances. *Minerals Engineering* **2018,** *117*, 34-41.

39. Muzzarelli, R. A. A., Carboxymethylated chitins and chitosans. *Carbohydrate polymers* **1988,** *8* (1), 1-21.

40. Fuerstenau, M. C.; Jameson, G. J.; Yoon, R.-H., *Froth flotation: a century of innovation*. SME: 2007.

41. Rao, S. R.; Leja, J., *Surface chemistry of froth flotation*. New York: Kluwer Academic/Plenum Publishers, 2nd ed. : 2004.

42. Mielczarski, J. A.; Cases, J. M.; Alnot, M.; Ehrhardt, J. J., XPS Characterization of Chalcopyrite, Tetrahedrite, and Tennantite Surface Products after Different Conditioning. 1. Aqueous Solution at pH 10. *Langmuir: the ACS journal of surfaces and colloids* **1996,** *12* (10), 2519-2530.

43. Zachwieja, J. B.; McCarron, J. J.; Walker, G. W.; Buckley, A. N., Correlation between the surface composition and collectorless flotation of chalcopyrite. *Journal of colloid and interface science* **1989,** *132* (2), 462-468.

44. Fairthorne, G.; Fornasiero, D.; Ralston, J., Effect of oxidation on the collectorless flotation of chalcopyrite. *International Journal of Mineral Processing* **1997,** *49* (1-2), 31-48.

45. Lu, Z.; Liu, Q.; Xu, Z.; Zeng, H., Probing Anisotropic Surface Properties of Molybdenite by Direct Force Measurements. *Langmuir: the ACS journal of surfaces and colloids* **2015,** *31* (42), 11409-18.

46. Morris, G. E. The adsorption characteristics of polymeric depressants at the talc-water interface. Ph.D. thesis, University of South Australia, 1996.

47. Lobato, E. M. d. C., Determination of Surface Free Energies and Aspect Ratio of Talc. VT: 2004.

48. Xie, L.; Wang, J.; Huang, J.; Cui, X.; Wang, X.; Liu, Q.; Zhang, H.; Liu, Q.; Zeng, H., Anisotropic Polymer Adsorption on Molybdenite Basal and Edge Surfaces and Interaction Mechanism With Air Bubbles. *Frontiers in chemistry* **2018,** *6*, 361.

49. Liu, Q.; Zhang, Y.; Laskowski, J. S., The adsorption of polysaccharides onto mineral surfaces: an acid/base interaction. *International Journal of Mineral Processing* **2000,** *60* (3-4), 229-245.

50. Huang, P.; Cao, M.; Liu, Q., Adsorption of chitosan on chalcopyrite and galena from aqueous suspensions. *Colloids and Surfaces A: Physicochemical and Engineering Aspects* **2012,** *409*, 167-175.

51. Stevenson, F. J., Humus chemistry: genesis, composition, reactions. 2nd ed.; Wiley: New York, 1994.

52. Kang, J.; Liu, H.; Zheng, Y. M.; Qu, J.; Chen, J. P., Systematic study of synergistic and antagonistic effects on adsorption of tetracycline and copper onto a chitosan. *Journal of colloid and interface science* **2010,** *344* (1), 117-25.

53. Dambies, L.; Guimon, C.; Yiacoumi, S.; Guibal, E., Characterization of metal ion interactions with chitosan by X-ray photoelectron spectroscopy. *Colloids and Surfaces A: Physicochemical and Engineering Aspects* **2001,** *177* (2-3), 203-214.

54. Vieira, R. S.; Oliveira, M. L. M.; Guibal, E.; Rodríguez-Castellón, E.; Beppu, M. M., Copper, mercury and chromium adsorption on natural and crosslinked chitosan films: An XPS investigation of mechanism. *Colloids and Surfaces A: Physicochemical and Engineering Aspects* **2011,** *374* (1-3), 108-114.

55. Amaral, I. F.; Granja, P. L.; Barbosa, M. A., Chemical modification of chitosan by phosphorylation: an XPS, FT-IR and SEM study. *Journal of Biomaterials Science, Polymer Edition* **2005,** *16* (12), 1575-1593.

56. Lawrie, G.; Keen, I.; Drew, B.; Chandler-Temple, A.; Rintoul, L.; Fredericks, P.; Grondahl, L., Interactions between alginate and chitosan biopolymers characterized using FTIR and XPS. *Biomacromolecules* **2007,** *8* (8), 2533-41.

57. Wagstaffe, M.; Hussain, H.; Acres, M. J.; Jones, R.; Syres, K. L.; Thomas, A. G., Structure and Reactivity of a Model Oxide Supported Silver Nanocluster Catalyst Studied by Near Ambient Pressure X-ray Photoelectron Spectroscopy. *The Journal of Physical Chemistry C* **2017,** *121* (39), 21383-21389.

58. Ettedgui, E.; Hsieh, B. R.; Gao, Y., Interface formation of metals and poly(p-phenylene vinylene): surface species and band bending. *Polymers for Advanced Technologies* **1997,** *8* (7), 408-416.

59. Ghahremaninezhad, A.; Dixon, D. G.; Asselin, E., Electrochemical and XPS analysis of chalcopyrite (CuFeS2) dissolution in sulfuric acid solution. *Electrochimica Acta* **2013,** *87*, 97-112.

60. Suyantara, G. P. W.; Hirajima, T.; Miki, H.; Sasaki, K.; Yamane, M.; Takida, E.; Kuroiwa, S.; Imaizumi, Y., Selective flotation of chalcopyrite and molybdenite using H 2 O 2 oxidation method with the addition of ferrous sulfate. *Minerals Engineering* **2018,** *122*, 312-326.

61. Buckley, A. N.; Woods, R., An X-ray photoelectron spectroscopic study of the oxidation of chalcopyrite. *Australian Journal of Chemistry* **1984,** *37* (12), 2403.

62. Liu, G.; Qiu, Z.; Wang, J.; Liu, Q.; Xiao, J.; Zeng, H.; Zhong, H.; Xu, Z., Study of N-isopropoxypropyl-N'-ethoxycarbonyl thiourea adsorption on chalcopyrite using in situ SECM, ToF-SIMS and XPS. *Journal of colloid and interface science* **2015,** *437*, 42-49.

63. Sedeva, I. G.; Fetzer, R.; Fornasiero, D.; Ralston, J.; Beattie, D. A., Adsorption of modified dextrins to a hydrophobic surface: QCM-D studies, AFM imaging, and dynamic contact angle measurements. *Journal of colloid and interface science* **2010,** *345* (2), 417-26.

64. Xie, L.; Wang, J.; Yuan, D.; Shi, C.; Cui, X.; Zhang, H.; Liu, Q.; Liu, Q.; Zeng, H., Interaction Mechanisms between Air Bubble and Molybdenite Surface: Impact of

Solution Salinity and Polymer Adsorption. *Langmuir: the ACS journal of surfaces and colloids* **2017,** *33* (9), 2353-2361.

65. Beaussart, A.; Mierczynska-Vasilev, A.; Beattie, D. A., Evolution of carboxymethyl cellulose layer morphology on hydrophobic mineral surfaces: variation of polymer concentration and ionic strength. *Journal of colloid and interface science* **2010,** *346* (2), 303-10.

# Chapter 6. Summary and Future Work

## 6.1 Conclusions

### 6.1.1 Conclusions about HA

Humic acids (HA), an organic fraction of soil and one of the most abundant natural organic macromolecules in the earth's crust, was exploited as a selective depressant for molybdenite during the molybdenite-talc separation and molybdenite-chalcopyrite separation. The adsorption characteristics and kinetics of HA on model hydrophobic/hydrophilic surfaces under different solution conditions (e.g., pH and ionic strength) were also studied by QCM-D measurements.

6.1.1.1. HA in molybdenite-talc separation

(1) Single mineral flotation tests revealed that the addition of HA strongly depresses the molybdenite flotation even at a concentration of 5 ppm. However, the presence of HA has no significant impact on the talc recovery, especially under alkaline conditions, the recovery of talc stay above 97% over the entire HA concentration range (0-20 ppm) tested. Mixed mineral flotation tests confirmed that HA could be utilized as a selective and efficient depressant for molybdenite-talc separation under alkaline conditions.

(2) Contact angle measurements confirmed that the wettability of both talc and molybdenite were enhanced after treated with HA. However, the addition of HA has less influence on the hydrophobicity of talc than on molybdenite.

(3) The adsorption isotherms revealed that the adsorption density of HA on molybdenite is higher than that of talc. Zeta potential measurements and literature reports imply the adsorption HA mostly occurred on talc edges, while the adsorption of HA on molybdenite mainly took place on its basal planes.

(4) DRIFT spectroscopy and AFM imaging further confirmed that the adsorption density of HA on molybdenite is much higher than that of talc, and the adsorption of HA on talc can be easily influenced by the solution pH, while the adsorption of HA on molybdenite was less sensitive to the variations of solution pH. The research results also suggest that the interactions between HA and molybdenite/talc are dictated by hydrophobic interaction and electrostatic interaction, and the hydrophobic attraction and electrostatic repulsion determine whether or not the adsorption of HA will occur on molybdenite/talc basal planes.

6.1.1.2. HA in molybdenite-chalcopyrite separation

(1) Single flotation tests indicate that the addition of HA had no significant influence on the flotation of chalcopyrite, and the recovery of chalcopyrite remained above 97% in the entire HA concentration range (0-40 ppm) tested. In contrast, the presence of HA could drastically reduce molybdenite recovery. Flotation tests on the chalcopyrite-molybdenite mixtures further demonstrated that HA selectively depresses molybdenite flotation during the Cu-Mo sulfides separation from pH 3 to 11.

(2) Adsorption study revealed that HA has a higher adsorption density on chalcopyrite over molybdenite, which may seem contradictory to the flotation results. However, it should be noted that the interaction mechanisms between HA and molybdenite/chalcopyrite are different. DRIFT spectroscopy, XPS, and zeta potential measurements demonstrated that the interactions between HA molybdenite are governed by hydrophobic interaction. In comparison, the interactions between HA and chalcopyrite are mainly electrostatic in nature, and the adsorbed HA on chalcopyrite are likely replaced by xanthate. The above experimental results indicated that HA is a cost-efficient depressant for molybdenite in the Cu-Mo sulfides separation over a broad range of pH, and the stronger interaction between HA and molybdenite than that of chalcopyrite lead to the selective separation.

6.1.1.3. Adsorption of HA on model hydrophobic/hydrophilic surfaces

(1) The adsorption of HA on the model hydrophobic surfaces and hydrophilic surfaces was characterized by QCM-D experiments. The adsorption data reveal that the surface hydrophobicity has a significant influence on the uptake of HA, and in general, the adsorption of HA on thiol-coated gold surfaces increases with increasing surface hydrophobicity under the same solution conditions, which signify the importance of hydrophobic interaction during the HA adsorption process.

(2) In addition, electrostatic interaction also plays a vital role during the adsorption process, as the adsorption of HA on model substrates is faster and increased at lower pH and/or higher ionic strength, attributed to the reduced electrostatic repulsion.

(3) Contact angle determination illustrates that the hydrophobicity of substrates was reduced to different extents by HA under different solution conditions, and HA has a more significant impact on the surface hydrophobicity of substrates when the adsorption occurred at lower pH or at higher salinity conditions.

### 6.1.2 Conclusions about O-CMC

O-Carboxymethyl chitosan (O-CMC), a nontoxic and cost-effective derivative of the natural polysaccharide—chitin, was also studied as a depressant for molybdenite during the Cu-Mo sulfides separation, to replace the current toxic depressants.

(1) The flotation experiments on single minerals revealed that O-CMC strongly depresses molybdenite from pH 3 to 11, while the floatability of chalcopyrite is not affected by the addition of O-CMC except for pH 3. The flotation experiments on mineral mixtures revealed O-CMC could effectively depress the molybdenite without significantly reducing chalcopyrite recovery and selective Cu-Mo was achieved from pH 3 to 11.

(2) The infrared spectroscopy and AFM imaging demonstrated the stronger interaction between O-CMC and molybdenite compared with chalcopyrite lead to the depression of molybdenite and selective separation of two minerals in mineral flotation.

(3) The electrokinetic study, XPS and ToF-SIMS results revealed that the interactions between chalcopyrite and O-CMC are mostly weak physical interactions such as electrostatic interaction. In comparison, the adsorption of O-CMC on molybdenite is induced by hydrophobic interaction and partially hindered by electrostatic repulsion. In addition, infrared spectroscopy and XPS analysis revealed that chemical interactions are absent between O-CMC and molybdenite/chalcopyrite surfaces.

## 6.2 Original contributions

In this work, one of the most abundant natural macromolecules, humic acids or HA, was discovered to be a promising depressant in the flotation separation of molybdenite, chalcopyrite, and talc. It was observed that molybdenite flotation was depressed by HA during molybdenite-talc separation and molybdenite-chalcopyrite separation, while chalcopyrite and talc flotation was barely affected by HA.

The adsorption of HA on molybdenite basal planes was analyzed by AFM imaging, XPS, and other related techniques. Besides, the adsorption of HA on model hydrophobic surfaces (thiol-coated gold surfaces) was also studied by QCM-D measurements. The experimental results indicated that the adsorption of HA on molybdenite basal planes is governed by hydrophobic interaction, while electrostatic repulsion partially hindered the adsorption of HA under alkaline conditions.

In addition, O-Carboxymethyl chitosan (O-CMC), a nontoxic and biodegradable derivative of the second most abundant naturally occurring polysaccharide—chitosan, was also found to be a cost-efficient depressant for molybdenite in the Cu-Mo separation.

The adsorption characteristics and interaction mechanisms of O-CMC on molybdenite were also investigated by AFM imaging, XPS analyses, and zeta potential measurements, etc. The results revealed that the adsorption of O-CMC on molybdenite basal planes was also induced by hydrophobic interaction while chemical interaction was not involved. In comparison, the adsorption of O-CMC on chalcopyrite is mainly driven by electrostatic interaction. In addition, it was observed that O-CMC becomes insoluble and precipitates at its iso-electric point around pH 3.5, which provides a potential approach to recycle and reuse it from the tailings water.

### 6.3 Future work

(1) The adsorption HA on molybdenite and talc surfaces were only investigated on basal planes and under relatively simple solution conditions. The adsorption characteristics of HA on molybdenite and talc edges/basal planes under complex aqueous media (e.g., various ion species and concentration) need to be investigated.

(2) In this work, all minerals are “fresh” (untreated by collectors, etc.) before the treatment of HA or O-CMC. It remains to be explored whether selective separation would occur if the minerals are treated by collectors first and if molybdenite can restore its floatability after depressed by HA or O-CMC. It is also worth mentioning that divalent

ions and high salinity water such as seawater also have a significant impact on the flotation process. Future research is required to study the influence of divalent ions and oily collectors etc. presented in the practical flotation process.

(3) O-carboxymethyl chitosan (O-CMC) was found to be a selective depressant for molybdenite during the copper-molybdenum sulfides separation. However, additional work is required to verify if O-CMC is a viable depressant for the industrial flotation process, which requires multifactorial experiments with real copper-molybdenum concentrates.

(4) It was observed that O-CMC becomes insoluble and precipitates at its iso-electric point (IEP) around pH 3.5. However, the IEP of O-CMC may not be a fixed value and is likely affected by the degree of substitution and deacetylation of O-CMC. Additional research is required to modify the IEP of O-CMC, and efficiently recycle and reuse it from the tailings water.

# Bibliography

1. Allison, S. A.; O'Connor, C. T., An investigation into the flotation behaviour of pyrrhotite. *International Journal of Mineral Processing* **2011,** *98* (3-4), 202-207.

2. Amaral, I. F.; Granja, P. L.; Barbosa, M. A., Chemical modification of chitosan by phosphorylation: an XPS, FT-IR and SEM study. *Journal of Biomaterials Science, Polymer Edition* **2005,** *16* (12), 1575-1593.

3. Anitha, A.; Maya, S.; Deepa, N.; Chennazhi, K. P.; Nair, S. V.; Tamura, H.; Jayakumar, R., Efficient water soluble O-carboxymethyl chitosan nanocarrier for the delivery of curcumin to cancer cells. *Carbohydrate polymers* **2011,** *83* (2), 452-461.

4. Ansari, A.; Pawlik, M., Floatability of chalcopyrite and molybdenite in the presence of lignosulfonates. Part II. Hallimond tube flotation. *Minerals Engineering* **2007,** *20* (6), 609-616.

5. Attia, Y. A., Chapter 9 - Flocculation. In *Developments in Mineral Processing*, Laskowski, J. S.; Ralston, J., Eds. Elsevier: 1992; Vol. Volume 12, pp 277-308.

6. Bain, C. D.; Evall, J.; Whitesides, G. M., Formation of monolayers by the coadsorption of thiols on gold: variation in the head group, tail group, and solvent. *Journal of the American Chemical Society* **1989,** *111* (18), 7155-7164.

7. Bakinov, K.; Vaneev, I.; Gorlovsky, S.; Eropkin, U.; Zashikhin, N.; Konev, A., New methods of sulphide concentrate upgrading. In *7th Int. Miner. Process. Congr.*, Gordon And Breach New York: 1964; pp 227-238.

8. Beattie, D. A.; Huynh, L.; Kaggwa, G. B.; Ralston, J., Influence of adsorbed polysaccharides and polyacrylamides on talc flotation. *International Journal of Mineral Processing* **2006,** *78* (4), 238-249.

9. Beattie, J. K.; Djerdjev, A. M., The pristine oil/water interface: surfactant-free hydroxide-charged emulsions. *Angew Chem Int Ed Engl* **2004,** *43* (27), 3568-71.

10. Beaussart, A.; Mierczynska-Vasilev, A.; Beattie, D. A., Adsorption of dextrin on hydrophobic minerals. *Langmuir: the ACS journal of surfaces and colloids* **2009,** *25* (17), 9913-21.

11. Beaussart, A.; Mierczynska-Vasilev, A.; Beattie, D. A., Evolution of carboxymethyl cellulose layer morphology on hydrophobic mineral surfaces: variation of polymer concentration and ionic strength. *Journal of colloid and interface science* **2010,** *346* (2), 303-10.

12. Beaussart, A.; Parkinson, L.; Mierczynska-Vasilev, A.; Beattie, D. A., Adsorption of modified dextrins on molybdenite: AFM imaging, contact angle, and flotation studies. *Journal of colloid and interface science* **2012,** *368* (1), 608-15.

13. Berger, J.; Reist, M.; Mayer, J. M.; Felt, O.; Peppas, N. A.; Gurny, R., Structure and interactions in covalently and ionically crosslinked chitosan hydrogels for biomedical applications. *European Journal of Pharmaceutics and Biopharmaceutics* **2004,** *57* (1), 19-34.

14. Bernardi, M.; Palummo, M.; Grossman, J. C., Extraordinary sunlight absorption and one nanometer thick photovoltaics using two-dimensional monolayer materials. *Nano letters* **2013,** *13* (8), 3664-70.

15. Bradshaw, D. J.; Oostendorp, B.; Harris, P. J., Development of methodologies to improve the assessment of reagent behaviour in flotation with particular reference to collectors and depressants. *Minerals Engineering* **2005,** *18* (2), 239-246.

16. Braga, P. F. A.; Chaves, A. P.; Luz, A. B.; França, S. C. A., The use of dextrin in purification by flotation of molybdenite concentrates. *International Journal of Mineral Processing* **2014,** *127*, 23-27.

17. Bubert, H.; Lambert, J.; Burba, P., Structural and elemental investigations of isolated aquatic humic substances using X-ray photoelectron spectroscopy. *Fresenius' Journal of Analytical Chemistry* **2000,** *368* (2-3), 274-280.

18. Buckley, A. N.; Woods, R., An X-ray photoelectron spectroscopic study of the oxidation of chalcopyrite. *Australian Journal of Chemistry* **1984,** *37* (12), 2403.

19. Bulatovic, S. M., *Handbook of flotation reagents: chemistry, theory and practice: Volume 1: flotation of sulfide ores*. Elsevier: 2007.

20. Burdukova, E.; Becker, M.; Bradshaw, D. J.; Laskowski, J. S., Presence of negative charge on the basal planes of New York talc. *Journal of colloid and interface science* **2007,** *315* (1), 337-42.

21. Cao, M.; Liu, Q., Reexamining the functions of zinc sulfate as a selective depressant in differential sulfide flotation--the role of coagulation. *Journal of colloid and interface science* **2006,** *301* (2), 523-31.

22. Castro, S.; Lopez-Valdivieso, A.; Laskowski, J. S., Review of the flotation of molybdenite. Part I: Surface properties and floatability. *International Journal of Mineral Processing* **2016,** *148*, 48-58.

23. Chai, L.; Klein, J., Large area, molecularly smooth (0.2 nm rms) gold films for surface forces and other studies. *Langmuir : the ACS journal of surfaces and colloids* **2007,** *23* (14), 7777-83.

24. Chen, X.-G.; Park, H.-J., Chemical characteristics of O-carboxymethyl chitosans related to the preparation conditions. *Carbohydrate polymers* **2003,** *53* (4), 355-359.

25. Cheng, R.; Jiang, S.; Chen, Y.; Liu, Y.; Weiss, N.; Cheng, H. C.; Wu, H.; Huang, Y.; Duan, X., Few-layer molybdenum disulfide transistors and circuits for high-speed flexible electronics. *Nature communications* **2014,** *5*, 5143.

26. Chiem, L. T.; Huynh, L.; Ralston, J.; Beattie, D. A., An in situ ATR-FTIR study of polyacrylamide adsorption at the talc surface. *Journal of colloid and interface science* **2006,** *297* (1), 54-61.

27. Cuba-Chiem, L. T.; Huynh, L.; Ralston, J.; Beattie, D. A., In situ particle film ATR FTIR spectroscopy of carboxymethyl cellulose adsorption on talc: binding mechanism, pH effects, and adsorption kinetics. *Langmuir: the ACS journal of surfaces and colloids* **2008,** *24* (15), 8036-44.

28. Dambies, L.; Guimon, C.; Yiacoumi, S.; Guibal, E., Characterization of metal ion interactions with chitosan by X-ray photoelectron spectroscopy. *Colloids and Surfaces A: Physicochemical and Engineering Aspects* **2001,** *177* (2-3), 203-214.

29. de Melo, B. A.; Motta, F. L.; Santana, M. H., Humic acids: Structural properties and multiple functionalities for novel technological developments. *Materials science & engineering. C, Materials for biological applications* **2016,** *62*, 967-74.

30. Desbene, P.-L.; Silly, L.; Morizur, J.-P.; Delamar, M., Xps Analysis of Humic and Fulvic Acids. *Analytical Letters* **1986,** *19* (21-22), 2131-2140.

31. dos Santos, I. D.; Oliveira, J. F., Utilization of humic acid as a depressant for hematite in the reverse flotation of iron ore. *Minerals Engineering* **2007,** *20* (10), 1003-1007.

32. Du, H.; Miller, J. D., A molecular dynamics simulation study of water structure and adsorption states at talc surfaces. *International Journal of Mineral Processing* **2007,** *84* (1-4), 172-184.

33. Du, H.; Miller, J. D., Adsorption states of amphipatic solutes at the surface of naturally hydrophobic minerals: a molecular dynamics simulation study. *Langmuir: the ACS journal of surfaces and colloids* **2007,** *23* (23), 11587-96.

34. Dutta, A. K.; Belfort, G., Adsorbed gels versus brushes: viscoelastic differences. *Langmuir: the ACS journal of surfaces and colloids* **2007,** *23* (6), 3088-94.

35. Dutta, P. K.; Dutta, J.; Tripathi, V., Chitin and chitosan: Chemistry, properties and applications. *Journal of Scientific and Industrial Research* **2004,** *63* (1), 20-31.

36. Dutta, P. K.; Tripathi, S.; Mehrotra, G. K.; Dutta, J., Perspectives for chitosan based antimicrobial films in food applications. *Food Chemistry* **2009,** *114* (4), 1173-1182.

37. Elmahdy, A. M.; Mirnezami, M.; Finch, J. A., Zeta potential of air bubbles in presence of frothers. *International Journal of Mineral Processing* **2008,** *89* (1-4), 40-43.

38. Ettedgui, E.; Hsieh, B. R.; Gao, Y., Interface formation of metals and poly(p-phenylene vinylene): surface species and band bending. *Polymers for Advanced Technologies* **1997,** *8* (7), 408-416.

39. Fairthorne, G.; Fornasiero, D.; Ralston, J., Effect of oxidation on the collectorless flotation of chalcopyrite. *International Journal of Mineral Processing* **1997,** *49* (1-2), 31-48.

40. Firth, B. A.; Nicol, S. K., The influence of humic materials on the flotation of coal. *International Journal of Mineral Processing* **1981,** *8* (3), 239-248.

41. Fontana, M.; Deppe, T.; Boyd, A. K.; Rinzan, M.; Liu, A. Y.; Paranjape, M.; Barbara, P., Electron-hole transport and photovoltaic effect in gated MoS2 Schottky junctions. *Scientific reports* **2013,** *3*, 1634.

42. Fuerstenau, D. W.; Huang, P., Interfacial phenomena involved in talc flotation and depression. In *XXII International Mineral Processing Congress*, Cape Town, 2003; pp 1034-1043.

43. Fuerstenau, D. W.; Pradip, Zeta potentials in the flotation of oxide and silicate minerals. *Advances in colloid and interface science* **2005,** *114-115*, 9-26.

44. Fuerstenau, M. C., *Principles of mineral processing*. SME: 2003.

45. Fuerstenau, M. C.; Jameson, G. J.; Yoon, R.-H., *Froth flotation: a century of innovation*. SME: 2007.

46. Fuerstenau, M. C.; Lopezvaldivieso, A.; Fuerstenau, D. W., Role of Hydrolyzed Cations in the Natural Hydrophobicity of Talc. *International Journal of Mineral Processing* **1988,** *23* (3-4), 161-170.

47. Fuerstenau, M. C.; Miller, J. D.; Kuhn, M. C., *Chemistry of flotation*. Society for Mining Metallurgy: 1985.

48. Gao, M. R.; Liang, J. X.; Zheng, Y. R.; Xu, Y. F.; Jiang, J.; Gao, Q.; Li, J.; Yu, S. H., An efficient molybdenum disulfide/cobalt diselenide hybrid catalyst for electrochemical hydrogen generation. *Nature communications* **2015,** *6*, 5982.

49. Ghahremaninezhad, A.; Dixon, D. G.; Asselin, E., Electrochemical and XPS analysis of chalcopyrite (CuFeS2) dissolution in sulfuric acid solution. *Electrochimica Acta* **2013,** *87*, 97-112.

50. Giles, C. H.; D'Silva, A. P.; Easton, I. A., A general treatment and classification of the solute adsorption isotherm part. II. Experimental interpretation. *Journal of colloid and interface science* **1974,** *47* (3), 766-778.

51. Giles, C. H.; MacEwan, T.; Nakhwa, S.; Smith, D., Studies in adsorption. Part XI. A system of classification of solution adsorption isotherms, and its use in diagnosis of adsorption mechanisms and in measurement of specific surface areas of solids. *Journal of the Chemical Society (Resumed)* **1960**, 3973-3993.

52. Giles, C. H.; Smith, D.; Huitson, A., A general treatment and classification of the solute adsorption isotherm. I. Theoretical. *Journal of colloid and interface science* **1974,** *47* (3), 755-765.

53. Gomes, L.; Oliveira, J. In *The control of natural floatability of talc with carboxymethyl cellulose and aluminium chloride*, Fine Particles Processing Flotation, Proceedings of the 17th Int. Miner. Process. Congress, 1991; pp 353-364.

54. Gutierrez, L.; Pawlik, M., Influence of humic acids on oil sand processing. Part I: Detection and quantification of humic acids in oil sand ores and their effect on bitumen wettability. *International Journal of Mineral Processing* **2014,** *126*, 117-125.

55. Gutierrez, L.; Pawlik, M., Influence of humic acids on oil sand processing. Part II: Relationship between bitumen extraction, humic acids concentration and power draw measurements on oil sand slurries. *International Journal of Mineral Processing* **2014,** *126*, 126-135.

56. Hedin, J.; Lofroth, J. E.; Nyden, M., Adsorption behavior and cross-linking of EHEC and HM-EHEC at hydrophilic and hydrophobic modified surfaces monitored by SPR and QCM-D. *Langmuir: the ACS journal of surfaces and colloids* **2007,** *23* (11), 6148-55.

57. Hemmersam, A. G.; Foss, M.; Chevallier, J.; Besenbacher, F., Adsorption of fibrinogen on tantalum oxide, titanium oxide and gold studied by the QCM-D technique. *Colloids and surfaces. B, Biointerfaces* **2005,** *43* (3-4), 208-15.

58. Höök, F.; Rodahl, M.; Brzezinski, P.; Kasemo, B., Energy Dissipation Kinetics for Protein and Antibody−Antigen Adsorption under Shear Oscillation on a Quartz Crystal Microbalance. *Langmuir: the ACS journal of surfaces and colloids* **1998,** *14* (4), 729-734.

59. Hoover, M., Water Chemistry Effects in the Flotation of Sulfide Ores-- a Review and Discussion for Molybdenite. *Complex Sulphide Ores* **1980**, 100-112.

60. Huang, P. Chitosan in Differential Flotation of Base Metal Sulfides. University of Alberta, 2013.

61. Huang, P.; Cao, M.; Liu, Q., Using chitosan as a selective depressant in the differential flotation of Cu–Pb sulfides. *International Journal of Mineral Processing* **2012,** *106-109*, 8-15.

62. Huang, P.; Cao, M.; Liu, Q., Adsorption of chitosan on chalcopyrite and galena from aqueous suspensions. *Colloids and Surfaces A: Physicochemical and Engineering Aspects* **2012,** *409*, 167-175.

63. Huang, P.; Fuerstenau, D. W., The effect of the adsorption of lead and cadmium ions on the interfacial behavior of quartz and talc. *Colloids and Surfaces A: Physicochemical and Engineering Aspects* **2001,** *177* (2-3), 147-156.

64. Huch, R. O.; Valles, P. Talc-molybdenite separation. 1975.

65. Hur, J.; Schlautman, M. A., Effects of pH and phosphate on the adsorptive fractionation of purified Aldrich humic acid on kaolinite and hematite. *Journal of colloid and interface science* **2004,** *277* (2), 264-70.

66. Israelachvili, J. N., *Intermolecular and surface forces: revised third edition*. Academic press: 2011.

67. Jada, A.; Ait Akbour, R.; Douch, J., Surface charge and adsorption from water onto quartz sand of humic acid. *Chemosphere* **2006,** *64* (8), 1287-95.

68. Jones, M. N.; Bryan, N. D., Colloidal properties of humic substances. *Advances in colloid and interface science* **1998,** *78* (1), 1-48.

69. Kang, J.; Liu, H.; Zheng, Y. M.; Qu, J.; Chen, J. P., Systematic study of synergistic and antagonistic effects on adsorption of tetracycline and copper onto a chitosan. *Journal of colloid and interface science* **2010,** *344* (1), 117-25.

70. Kang, S.; Xing, B., Humic acid fractionation upon sequential adsorption onto goethite. *Langmuir: the ACS journal of surfaces and colloids* **2008,** *24* (6), 2525-31.

71. Karunadasa, H. I.; Montalvo, E.; Sun, Y.; Majda, M.; Long, J. R.; Chang, C. J., A molecular $MoS_2$ edge site mimic for catalytic hydrogen generation. *Science* **2012,** *335* (6069), 698-702.

72. Kelebek, S.; Yoruk, S.; Smith, G. W., Wetting Behavior of Molybdenite and Talc in Lignosulphonate/Mibc Solutions and Their Separation by Flotation. *Separation Science and Technology* **2001,** *36* (2), 145-157.

73. Khraisheh, M.; Holland, C.; Creany, C.; Harris, P.; Parolis, L., Effect of molecular weight and concentration on the adsorption of CMC onto talc at different ionic strengths. *International Journal of Mineral Processing* **2005,** *75* (3-4), 197-206.

74. Klassen, V. I.; Mokrousov, V. A., *An introduction to the theory of flotation*. Butterworths: 1963.

75. Kor, M.; Korczyk, P. M.; Addai-Mensah, J.; Krasowska, M.; Beattie, D. A., Carboxymethylcellulose adsorption on molybdenite: the effect of electrolyte composition on adsorption, bubble-surface collisions, and flotation. *Langmuir: the ACS journal of surfaces and colloids* **2014,** *30* (40), 11975-84.

76. Kudin, K. N.; Car, R., Why are water-hydrophobic interfaces charged? *Journal of the American Chemical Society* **2008,** *130* (12), 3915-9.

77. Kusaka, E.; Amano, N.; Nakahiro, Y., Effect of hydrolysed aluminum(III) and chromium(III) cations on the lipophilicity of talc. *International Journal of Mineral Processing* **1997,** *50*, 243-253.

78. Lai, R. W. M.; Stone, L. C.; Rimmasch, B. E., Effect of humus organics on the flotation recovery of molybdenite. *International Journal of Mineral Processing* **1984,** *12* (1-3), 163-172.

79. Lalvani, S. B.; Kang, J.-C., Coal Flotation in the Presence of Humic Acids. *Fuel Science and Technology International* **1992,** *10* (8), 1291-1312.

80. Laskowski, J.; Yu, Z. In *The effect of humic acids on the emulsion flotation of inherently hydrophobic minerals*, III Latin American Congress on Froth Flotation. Universidad de Concepción, Concepción-Chile, 1994; pp 397-411.

81. Laskowski, J. S.; Liu, Q.; O'Connor, C. T., Current understanding of the mechanism of polysaccharide adsorption at the mineral/aqueous solution interface. *International Journal of Mineral Processing* **2007,** *84* (1-4), 59-68.

82. Laskowski, J. S.; Sirois, L. L.; Moon, K. S., Effect of Humic Acids on Coal Flotation Part I. Coal Flotation Selectivity in the Presence of Humic Acids. *Coal Preparation* **1986,** *3* (3), 133-154.

83. Lawrie, G.; Keen, I.; Drew, B.; Chandler-Temple, A.; Rintoul, L.; Fredericks, P.; Grondahl, L., Interactions between alginate and chitosan biopolymers characterized using FTIR and XPS. *Biomacromolecules* **2007,** *8* (8), 2533-41.

84. Li, M.; Wei, D.; Liu, Q.; Liu, W.; Zheng, J.; Sun, H., Flotation separation of copper–molybdenum sulfides using chitosan as a selective depressant. *Minerals Engineering* **2015,** *83*, 217-222.

85. Liu, G.; Qiu, Z.; Wang, J.; Liu, Q.; Xiao, J.; Zeng, H.; Zhong, H.; Xu, Z., Study of N-isopropoxypropyl-N'-ethoxycarbonyl thiourea adsorption on chalcopyrite using in situ SECM, ToF-SIMS and XPS. *Journal of colloid and interface science* **2015,** *437*, 42-49.

86. Liu, H.; Su, D.; Zhou, R.; Sun, B.; Wang, G.; Qiao, S. Z., Highly Ordered Mesoporous MoS2 with Expanded Spacing of the (002) Crystal Plane for Ultrafast Lithium Ion Storage. *Advanced Energy Materials* **2012,** *2* (8), 970-975.

87. Liu, Q.; Laskowski, J. S., The interactions between dextrin and metal hydroxides in aqueous solutions. *Journal of colloid and interface science* **1989,** *130* (1), 101-111.

88. Liu, Q.; Laskowski, J. S., The role of metal hydroxides at mineral surfaces in dextrin adsorption, II. Chalcopyrite-galena separations in the presence of dextrin. *International Journal of Mineral Processing* **1989,** *27* (1-2), 147-155.

89. Liu, Q.; Laskowski, J. S., The role of metal hydroxides at mineral surfaces in dextrin adsorption, I. Studies on modified quartz samples. *International Journal of Mineral Processing* **1989,** *26* (3-4), 297-316.

90. Liu, Q.; Zhang, Y.; Laskowski, J. S., The adsorption of polysaccharides onto mineral surfaces: an acid/base interaction. *International Journal of Mineral Processing* **2000,** *60* (3-4), 229-245.

91. Liu, Y., Is the Free Energy Change of Adsorption Correctly Calculated? *Journal of Chemical & Engineering Data* **2009,** *54* (7), 1981-1985.

92. Lobato, E. M. d. C., Determination of Surface Free Energies and Aspect Ratio of Talc. VT: 2004.

93. Lu, Z.; Liu, Q.; Xu, Z.; Zeng, H., Probing Anisotropic Surface Properties of Molybdenite by Direct Force Measurements. *Langmuir: the ACS journal of surfaces and colloids* **2015,** *31* (42), 11409-18.

94. Mahiuddin, S.; Suryanarayan, I.; Dutta, N. N.; Borthakur, P. C., Adsorption studies of sodium humate on Indian iron ore fines. *Colloids and Surfaces* **1992,** *64* (3-4), 177-184.

95. Malmstrom, J.; Agheli, H.; Kingshott, P.; Sutherland, D. S., Viscoelastic modeling of highly hydrated laminin layers at homogeneous and nanostructured surfaces:

quantification of protein layer properties using QCM-D and SPR. *Langmuir: the ACS journal of surfaces and colloids* **2007,** *23* (19), 9760-8.

96. Marinova, K. G.; Alargova, R. G.; Denkov, N. D.; Velev, O. D.; Petsev, D. N.; Ivanov, I. B.; Borwankar, R. P., Charging of Oil−Water Interfaces Due to Spontaneous Adsorption of Hydroxyl Ions. *Langmuir: the ACS journal of surfaces and colloids* **1996,** *12* (8), 2045-2051.

97. Mhlanga, S. S.; O'Connor, C. T.; McFadzean, B., A study of the relative adsorption of guar onto pure minerals. *Minerals Engineering* **2012,** *36-38*, 172-178.

98. Mielczarski, J. A.; Cases, J. M.; Alnot, M.; Ehrhardt, J. J., XPS Characterization of Chalcopyrite, Tetrahedrite, and Tennantite Surface Products after Different Conditioning. 1. Aqueous Solution at pH 10. *Langmuir: the ACS journal of surfaces and colloids* **1996,** *12* (10), 2519-2530.

99. Mierczynska-Vasilev, A.; Beattie, D. A., Adsorption of tailored carboxymethyl cellulose polymers on talc and chalcopyrite: Correlation between coverage, wettability, and flotation. *Minerals Engineering* **2010,** *23* (11-13), 985-993.

100. Mierczynska-Vasilev, A.; Beattie, D. A., In situ atomic force microscopy of modified dextrin adsorption on hydrophobic and hydrophilic layered silicate minerals. *Journal of colloid and interface science* **2010,** *344* (2), 429-37.

101. Mierczynska-Vasilev, A.; Ralston, J.; Beattie, D. A., Adsorption of modified dextrins on talc: effect of surface coverage and hydration water on hydrophobicity reduction. *Langmuir: the ACS journal of surfaces and colloids* **2008,** *24* (12), 6121-7.

102. Monkawa, A.; Ikoma, T.; Yunoki, S.; Yoshioka, T.; Tanaka, J.; Chakarov, D.; Kasemo, B., Fabrication of hydroxyapatite ultra-thin layer on gold surface and its application for quartz crystal microbalance technique. *Biomaterials* **2006,** *27* (33), 5748-54.

103. Monteil-Rivera, F.; Brouwer, E. B.; Masset, S.; Deslandes, Y.; Dumonceau, J., Combination of X-ray photoelectron and solid-state 13C nuclear magnetic resonance spectroscopy in the structural characterisation of humic acids. *Analytica Chimica Acta* **2000,** *424* (2), 243-255.

104. Morris, G. E. The adsorption characteristics of polymeric depressants at the talc-water interface. PhD thesis, University of South Australia, 1996.

105. Morris, G. E.; Fornasiero, D.; Ralston, J., Polymer depressants at the talc–water interface: adsorption isotherm, microflotation and electrokinetic studies. *International Journal of Mineral Processing* **2002,** *67*, 211-227.

106. Mourya, V. K.; Inamdar, N. N.; Tiwari, A., Carboxymethyl chitosan and its applications. *Advanced Materials Letters* **2010,** *1* (1), 11-33.

107. Mu, Y.; Peng, Y.; Lauten, R. A., The mechanism of pyrite depression at acidic pH by lignosulfonate-based biopolymers with different molecular compositions. *Minerals Engineering* **2016,** *92*, 37-46.

108. Muzzarelli, R. A. A., Carboxymethylated chitins and chitosans. *Carbohydrate polymers* **1988,** *8* (1), 1-21.

109. Naderi, A.; Claesson, P. M., Adsorption properties of polyelectrolyte-surfactant complexes on hydrophobic surfaces studied by QCM-D. *Langmuir: the ACS journal of surfaces and colloids* **2006,** *22* (18), 7639-45.

110. Nogues, C.; Wanunu, M., A rapid approach to reproducible, atomically flat gold films on mica. *Surface Science* **2004,** *573* (3), L383-L389.

111. Notley, S. M.; Eriksson, M.; Wagberg, L., Visco-elastic and adhesive properties of adsorbed polyelectrolyte multilayers determined in situ with QCM-D and AFM measurements. *Journal of colloid and interface science* **2005,** *292* (1), 29-37.

112. Park, S.-j.; Yoon, T.-i., Effects of iron species and inert minerals on coagulation and direct filtration for humic acid removal. *Desalination* **2009,** *239* (1-3), 146-158.

113. Parolis, L. A. S.; van der Merwe, R.; Groenmeyer, G. V.; Harris, P. J., The influence of metal cations on the behaviour of carboxymethyl celluloses as talc depressants. *Colloids and Surfaces A: Physicochemical and Engineering Aspects* **2008,** *317* (1-3), 109-115.

114. Pawlik, M.; Laskowski, J. S., Coal Reverse Flotation. Part I. Adsorption of Dodecyltrimethyl Ammonium Bromide and Humic Acids onto Coal and Silica. *Coal Preparation* **2003,** *23* (3), 91-112.

115. Pawlik, M.; Laskowski, J. S., Coal Reverse Flotation. Part II. Batch Flotation Tests. *Coal Preparation* **2003,** *23* (3), 113-127.

116. Pearse, M. J., An overview of the use of chemical reagents in mineral processing. *Minerals Engineering* **2005,** *18* (2), 139-149.

117. Periayah, M. H.; Halim, A. S.; Mat Saad, A. Z.; Yaacob, N. S.; Hussein, A. R.; Abdul Karim, F.; Abdul Rashid, A. H.; Ujang, Z., Effect of the Novel Biodegradable N, O-Carboxymethylchitosan and Oligo-Chitosan on the Platelet Thrombogenicity Cascade in von Willebrand Disease. *Thrombosis research* **2015,** *136* (3), 625-33.

118. Piccolo, A.; Stevenson, F. J., Infrared spectra of Cu2+ Pb2+ and Ca2+ complexes of soil humic substances. *Geoderma* **1982,** *27* (3), 195-208.

119. Pillai, C. K. S.; Paul, W.; Sharma, C. P., Chitin and chitosan polymers: Chemistry, solubility and fiber formation. *Progress in Polymer Science* **2009,** *34* (7), 641-678.

120. Poling, G.; Liu, Q., Flotation depression of chalcopyrite with thioglycolic acid. *TRANSACTIONS OF THE INSTITUTION OF MINING AND METALLURGY SECTION C-MINERAL PROCESSING AND EXTRACTIVE METALLURGY* **1987,** *96*, C7-C12.

121. Prasad, M. S., Reagents in the mineral industry — recent trends and applications. *Minerals Engineering* **1992,** *5* (3-5), 279-294.

122. Pugh, R. J., Macromolecular organic depressants in sulphide flotation—A review, 1. Principles, types and applications. *International Journal of Mineral Processing* **1989,** *25* (1-2), 101-130.

123. Quast, K.; Addai-Mensah, J.; Skinner, W., Preconcentration strategies in the processing of nickel laterite ores Part 5: Effect of mineralogy. *Minerals Engineering* **2017,** *110*, 31-39.

124. Rao, S. R.; Leja, J., *Surface chemistry of froth flotation*. New York : Kluwer Academic/Plenum Publishers, 2nd ed. : 2004.

125. Rath, R. K.; Subramanian, S.; Laskowski, J. S., Adsorption of Dextrin and Guar Gum onto Talc. A Comparative Study. *Langmuir: the ACS journal of surfaces and colloids* **1997,** *13*, 6260-6266.

126. Ravi Kumar, M. N. V., A review of chitin and chitosan applications. *Reactive and Functional Polymers* **2000,** *46* (1), 1-27.

127. Rhodes, M. In *The effects of the physical variables of carboxymethyl cellulose reagents on the depression of magnesia bearing minerals in Western Australian nickel sulphide ores*, INTERNATIONAL MINERAL PROCESING CONGRESS, 1979; pp 346-366.

128. Rinaudo, M., Chitin and chitosan: Properties and applications. *Progress in Polymer Science* **2006,** *31* (7), 603-632.

129. Rost, M. J.; Quist, D. A.; Frenken, J. W., Grains, growth, and grooving. *Physical review letters* **2003,** *91* (2), 026101.

130. Scheutjens, J. M. H. M.; Fleer, G. J., Statistical theory of the adsorption of interacting chain molecules. 2. Train, loop, and tail size distribution. *The Journal of Physical Chemistry* **1980,** *84* (2), 178-190.

131. Sedeva, I. G.; Fetzer, R.; Fornasiero, D.; Ralston, J.; Beattie, D. A., Adsorption of modified dextrins to a hydrophobic surface: QCM-D studies, AFM imaging, and dynamic contact angle measurements. *Journal of colloid and interface science* **2010,** *345* (2), 417-26.

132. Sedeva, I. G.; Fornasiero, D.; Ralston, J.; Beattie, D. A., The influence of surface hydrophobicity on polyacrylamide adsorption. *Langmuir: the ACS journal of surfaces and colloids* **2009,** *25* (8), 4514-21.

133. Sedeva, I. G.; Fornasiero, D.; Ralston, J.; Beattie, D. A., Reduction of surface hydrophobicity using a stimulus-responsive polysaccharide. *Langmuir: the ACS journal of surfaces and colloids* **2010,** *26* (20), 15865-74.

134. Shortridge, P.; Harris, P.; Bradshaw, D., The influence of ions on the effectiveness of polysaccharide depressants in the flotation of talc. *Polymers in Mineral Processing, JS Laskowski, Met Soc, Quebec* **1999**, 155-170.

135. Shortridge, P. G.; Harris, P. J.; Bradshaw, D. J.; Koopal, L. K., The effect of chemical composition and molecular weight of polysaccharide depressants on the flotation of talc. *International Journal of Mineral Processing* **2000,** *59*, 215-224.

136. Sips, R., On the Structure of a Catalyst Surface. *The Journal of Chemical Physics* **1948,** *16* (5), 490-495.

137. Sips, R., On the Structure of a Catalyst Surface. II. *The Journal of Chemical Physics* **1950,** *18* (8), 1024-1026.

138. Siwek, B.; Zembala, M.; Pomianowski, A., A method for determination of fine-particle flotability. *International Journal of Mineral Processing* **1981,** *8* (1), 85-88.

139. Smith, J. M., *Chemical engineering kinetics*. 1981.

140. Somasundaran, P.; Wang, D., *Solution chemistry: minerals and reagents*. Elsevier: 2006; Vol. 17.

141. Steenberg, E.; Harris, P., Adsorption of carboxymethylcellulose, guar gum, and starch onto talc, sulfides, oxides, and salt-type minerals. *South African Journal of Chemistry* **1984,** *37* (3), 85-90.

142. Stevenson, F. J., Humus chemistry : genesis, composition, reactions. 2nd ed.; Wiley: New York, 1994.

143. Stevenson, F. J.; Goh, K. M., Infrared spectra of humic acids and related substances. *Geochimica et Cosmochimica Acta* **1971,** *35* (5), 471-483.

144. Suyantara, G. P. W.; Hirajima, T.; Miki, H.; Sasaki, K.; Yamane, M.; Takida, E.; Kuroiwa, S.; Imaizumi, Y., Selective flotation of chalcopyrite and molybdenite using H 2 O 2 oxidation method with the addition of ferrous sulfate. *Minerals Engineering* **2018,** *122*, 312-326.

145. Tamiz Bakhtiari, M.; Harbottle, D.; Curran, M.; Ng, S.; Spence, J.; Siy, R.; Liu, Q.; Masliyah, J.; Xu, Z., Role of Caustic Addition in Bitumen–Clay Interactions. *Energy & Fuels* **2015,** *29* (1), 58-69.

146. Thurman, E. M., Aquatic Humic Substances. In *Organic Geochemistry of Natural Waters*, Springer Netherlands: Dordrecht, 1985; pp 273-361.

147. Tian, C. S.; Shen, Y. R., Structure and charging of hydrophobic material/water interfaces studied by phase-sensitive sum-frequency vibrational spectroscopy. *Proceedings of the National Academy of Sciences of the United States of America* **2009,** *106* (36), 15148-53.

148. Turrer, H. D. G.; Peres, A. E. C., Investigation on alternative depressants for iron ore flotation. *Minerals Engineering* **2010,** *23* (11-13), 1066-1069.

149. Umpleby, R. J.; Baxter, S. C.; Chen, Y.; Shah, R. N.; Shimizu, K. D., Characterization of Molecularly Imprinted Polymers with the Langmuir−Freundlich Isotherm. *Analytical Chemistry* **2001,** *73* (19), 4584-4591.

150. Vermeer, A. W. P.; van Riemsdijk, W. H.; Koopal, L. K., Adsorption of Humic Acid to Mineral Particles. 1. Specific and Electrostatic Interactions. *Langmuir: the ACS journal of surfaces and colloids* **1998,** *14* (10), 2810-2819.

151. Vidal, C. A. G.; Pawlik, M., Molecular weight effects in interactions of guar gum with talc. *International Journal of Mineral Processing* **2015,** *138*, 38-43.

152. Vieira, R. S.; Oliveira, M. L. M.; Guibal, E.; Rodríguez-Castellón, E.; Beppu, M. M., Copper, mercury and chromium adsorption on natural and crosslinked chitosan films: An XPS investigation of mechanism. *Colloids and Surfaces A: Physicochemical and Engineering Aspects* **2011,** *374* (1-3), 108-114.

153. Wagstaffe, M.; Hussain, H.; Acres, M. J.; Jones, R.; Syres, K. L.; Thomas, A. G., Structure and Reactivity of a Model Oxide Supported Silver Nanocluster Catalyst Studied by Near Ambient Pressure X-ray Photoelectron Spectroscopy. *The Journal of Physical Chemistry C* **2017,** *121* (39), 21383-21389.

154. Wang, J.; Liu, Q.; Zeng, H., Understanding Copper Activation and Xanthate Adsorption on Sphalerite by Time-of-Flight Secondary Ion Mass Spectrometry, X-ray

Photoelectron Spectroscopy, and in Situ Scanning Electrochemical Microscopy. *The Journal of Physical Chemistry C* **2013,** *117* (39), 20089-20097.

155. Wang, J.; Somasundaran, P.; Nagaraj, D. R., Adsorption mechanism of guar gum at solid–liquid interfaces. *Minerals Engineering* **2005,** *18* (1), 77-81.

156. Wang, J.; Xie, L.; Liu, Q.; Zeng, H., Effects of salinity on xanthate adsorption on sphalerite and bubble–sphalerite interactions. *Minerals Engineering* **2015,** *77*, 34-41.

157. Wang, K.; Xing, B., Structural and sorption characteristics of adsorbed humic acid on clay minerals. *Journal of Environmental Quality* **2005,** *34* (1), 342-349.

158. Wills, B. A., *Wills' mineral processing technology: an introduction to the practical aspects of ore treatment and mineral recovery*. Butterworth-Heinemann: 2011.

159. Winer, W. O., Molybdenum disulfide as a lubricant: A review of the fundamental knowledge. *Wear* **1967,** *10* (6), 422-452.

160. Woodwell, G. M.; Whittaker, R. H.; Reiners, W. A.; Likens, G. E.; Delwiche, C. C.; Botkin, D. B., The biota and the world carbon budget. *Science* **1978,** *199* (4325), 141-6.

161. Wu, J.; Delcheva, I.; Ngothai, Y.; Krasowska, M.; Beattie, D. A., Bubble–surface interactions with graphite in the presence of adsorbed carboxymethylcellulose. *Soft matter* **2015,** *11* (3), 587-599.

162. Wu, J.; Delcheva, I.; Ngothai, Y.; Krasowska, M.; Beattie, D. A., Bubble-surface interactions with graphite in the presence of adsorbed carboxymethylcellulose. *Soft Matter* **2015,** *11* (3), 587-99.

163. Xiang, Y. Carboxymethyl Chitosan as a Selective Depressant in Differential Flotation of Galena and Chalcopyrite. University of Alberta, 2015.

164. Xie, L.; Shi, C.; Wang, J.; Huang, J.; Lu, Q.; Liu, Q.; Zeng, H., Probing the interaction between air bubble and sphalerite mineral surface using atomic force microscope. *Langmuir: the ACS journal of surfaces and colloids* **2015,** *31* (8), 2438-46.

165. Xie, L.; Wang, J.; Huang, J.; Cui, X.; Wang, X.; Liu, Q.; Zhang, H.; Liu, Q.; Zeng, H., Anisotropic Polymer Adsorption on Molybdenite Basal and Edge Surfaces and Interaction Mechanism With Air Bubbles. *Frontiers in chemistry* **2018,** *6*, 361.

166. Xie, L.; Wang, J.; Shi, C.; Cui, X.; Huang, J.; Zhang, H.; Liu, Q.; Liu, Q.; Zeng, H., Mapping the Nanoscale Heterogeneity of Surface Hydrophobicity on the Sphalerite Mineral. *The Journal of Physical Chemistry C* **2017,** *121* (10), 5620-5628.

167. Xie, L.; Wang, J.; Shi, C.; Huang, J.; Zhang, H.; Liu, Q.; Liu, Q.; Zeng, H., Probing Surface Interactions of Electrochemically Active Galena Mineral Surface Using Atomic Force Microscopy. *The Journal of Physical Chemistry C* **2016,** *120* (39), 22433-22442.

168. Xie, L.; Wang, J.; Yuan, D.; Shi, C.; Cui, X.; Zhang, H.; Liu, Q.; Liu, Q.; Zeng, H., Interaction Mechanisms between Air Bubble and Molybdenite Surface: Impact of Solution Salinity and Polymer Adsorption. *Langmuir: the ACS journal of surfaces and colloids* **2017,** *33* (9), 2353-2361.

169. Xu, M., Ore Evaluation at Vale Base Metals. In *Separation Technologies for Minerals, Coal, and Earth Resources*, Young, C. A.; Luttrell, G. H., Eds. Society for Mining, Metallurgy, and Exploration (SME): 2013; Vol. 27, pp 521-537.

170. Yan, L.; Englert, A. H.; Masliyah, J. H.; Xu, Z., Determination of anisotropic surface characteristics of different phyllosilicates by direct force measurements. *Langmuir: the ACS journal of surfaces and colloids* **2011,** *27* (21), 12996-3007.

171. Yan, M.; Liu, C.; Wang, D.; Ni, J.; Cheng, J., Characterization of adsorption of humic acid onto alumina using quartz crystal microbalance with dissipation. *Langmuir: the ACS journal of surfaces and colloids* **2011,** *27* (16), 9860-5.

172. Yang, B.; Song, S.; Lopez-Valdivieso, A., Effect of Particle Size on the Contact Angle of Molybdenite Powders. *Mineral Processing and Extractive Metallurgy Review* **2014,** *35* (3), 208-215.

173. Yuan, D.; Xie, L.; Shi, X.; Yi, L.; Zhang, G.; Zhang, H.; Liu, Q.; Zeng, H., Selective flotation separation of molybdenite and talc by humic substances. *Minerals Engineering* **2018,** *117*, 34-41.

174. Yuan, W.; Zydney, A. L., Humic Acid Fouling during Ultrafiltration. *Environmental Science & Technology* **2000,** *34* (23), 5043-5050.

175. Zachwieja, J. B.; McCarron, J. J.; Walker, G. W.; Buckley, A. N., Correlation between the surface composition and collectorless flotation of chalcopyrite. *Journal of colloid and interface science* **1989,** *132* (2), 462-468.

176. Zanin, M.; Ametov, I.; Grano, S.; Zhou, L.; Skinner, W., A study of mechanisms affecting molybdenite recovery in a bulk copper/molybdenum flotation circuit. *International Journal of Mineral Processing* **2009,** *93* (3-4), 256-266.

177. Zeng, D.; Wu, J.; Kennedy, J. F., Application of a chitosan flocculant to water treatment. *Carbohydrate polymers* **2008,** *71* (1), 135-139.

178. Zeng, H.; Shi, C.; Huang, J.; Li, L.; Liu, G.; Zhong, H., Recent experimental advances on hydrophobic interactions at solid/water and fluid/water interfaces. *Biointerphases* **2015,** *11* (1), 018903.

179. Zhang, C.; Wang, Z.; Guo, Z.; Lou, X. W., Synthesis of MoS(2)-C one-dimensional nanostructures with improved lithium storage properties. *ACS applied materials & interfaces* **2012,** *4* (7), 3765-8.

180. Zhao, K. L.; Gu, G. H.; Wang, H.; Wang, C. L.; Wang, X. H.; Luo, C., Influence of depressant foenum-graecum on the flotation of a sulfide ore which contains hydrophobic gangue. *International Journal of Mineral Processing* **2015,** *141*, 68-76.

181. Zhou, P.; Yan, H.; Gu, B., Competitive complexation of metal ions with humic substances. *Chemosphere* **2005,** *58* (10), 1327-37.

182. Zhu, W.; Low, T.; Lee, Y. H.; Wang, H.; Farmer, D. B.; Kong, J.; Xia, F.; Avouris, P., Electronic transport and device prospects of monolayer molybdenum disulphide grown by chemical vapour deposition. *Nature communications* **2014,** *5*, 3087.